# Stochastic growth models : universality and fragility

Thomas Gueudré

# Physique Statistique des systèmes désordonnés

## Stochastic Growth Models : Universality and Fragility

**Thomas Gueudré**

Paris 2013

# Physique Statistique des systèmes désordonnés

## Stochastic Growth Models : Universality and Fragility

**Thomas Gueudré**

Thèse de Doctorat
au Département de Physique
de l'Ecole Normale Supérieure
Paris

présenté par
Thomas Gueudré

Paris, le 30 septembre 2014

Directeur: Pierre Le Doussal
Codirecteur: Jean-Philippe Bouchaud

# Contents

# 1 Stochastic growth

Growth refers to a positive change over time, usually in size. Most objects in Nature go through an evolution process. From the stalactites to the humans, they follow a stage of maturation towards fullness or fulfilment. This evolution is particularly central to the notion of *emergence*, a process whereby larger entities, patterns, or regularities arise through interactions among smaller or simpler entities that themselves do not exhibit such properties. For example, this is a common strategy found in many animal groups, from the colonies of ants to the flocks of birds [1]. The notion of life, from the mass of cells and molecules to a living being, can as well be linked to this vast notion.

Of course, merely having numerous interactions is not enough to guarantee an emergent behaviour: many of the interactions may be negligible, irrelevant, or may cancel each other. In some cases, a large number of interactions can in fact work against the emergence of interesting behaviour, akin to a white-noise blurring the meaningful signal. One needs self-organization, distributed over all the components, with some form of global order or coordination spontaneously arising out of the interactions. This order is often triggered by random fluctuations and amplified by positive feedback.

Because of the scale and the complexity of the interacting systems, it is impossible to track the appearance of macroscopic collective behaviour from the microscopic details. There is even debate about the impossibility of closing that gap, an hypothesis coined *strong emergence*. An interesting example in [2] presents a class of physical systems that exhibits non-computable macroscopic properties. More precisely, computing such properties from microscopic considerations would be equivalent to solving computational problems known to be undecidable in computer science.

In that respect, the growth process is a good candidate to scrutinize the emergence phenomenon: the system is building its order in front of our eyes. During that process, it is very common to observe the occurrence of natural patterns: trees, spirals, meanders, waves, foams... They sometimes find explanations in chaos theory, fractals, logarithmic spirals, topology... Strikingly, roughness of the growing interface is observed in numerous experiments, triggering a large amount of statistical studies of those objects. Rough surfaces can occur under both in and ouf of equilibrium conditions but most rough surfaces are formed under conditions that are far from equilibrium. The interfaces may exhibit self-affinity over a significant range of length scales, their scaling properties be very similar from one process to another. These scaling and universal properties are central to statistical physics. The ultimate goal of identifying the main basins of attraction of these models (coined *universality classes*) would reduce the problem of describing and eventually understanding the structure of the enormous variety of rough surfaces to one of manageable proportions.

After this rather "grand" introduction, we will be interested in the statistical physics of stochastic growth, and more specifically growth with non-linear mechanisms, a class

of problem much associated to its paradigmatic representative, the *Kardar-Parisi-Zhang class*.

We first give a flavour of the physical problems considered by presenting some experiments, upon which we build the basic elements of the theoretical stochastic growth. After a rapid overview of the models developed to tackle some surprising features of those processes, we enter the main goal of this Thesis, that lays at the core of a well known mapping to an optimization problem, the *Directed Polymer* (DP). We state the elaborate results obtained recently that have triggered a renewed activity and how they might shed a new light on this mature field.

## 1.1 The experiments

Very often, growth processes can be described in terms of propagation of an "active zone", the growth front. After the front has passed, the structure left behind does not change anymore. For some simple growth models, this is an exact picture and (at least in principle) the internal structure can be understood completely in these terms. But actually, most systems expanding in time might be considered as growing interfaces, and this approximation holds in various experiments: dielectric breakdown, fluid displacement in porous media, fire fronts... To motivate the main object of that Thesis, the next section is devoted to some growth processes (either experiments or models) that arguably fall into the non-linear stochastic growth class, called the *KPZ class*. Two stringent difficulties when trying to observe that class are: i) ensuring that the growth mechanisms are local - for example, the interactions at the surface not being long-range. ii) avoiding the occurrence of quenched disorder, which leads to another universality class.

### 1.1.1 Growth of bacteria colonies

The material of this subsection is borrowed from [3].

Bacteria colonies exhibit a variety of patterns depending on both baterial species and environmental conditions. In [3], the migration of the wild-type strain *B. Subtilis*, with a rod-like cell form, was investigated. Their mobility or shape are affected by several factors, mainly the hardness of the agar medium and the surfactant they secrete. On a nutrient poor substrate, they turn into spores. The control parameter of the experiments is presently the agar medium. But, because in a soft agar medium, bacteria might scatter around the growing front of the colony, resulting in a fuzzy interface, one has to use a mutant of the bacteria in rich environment. This mutant does not produce any surfactant, resulting in a decrease of motility, and a sharply defined front of the colony.

Two regimes were explored:

- On a hard agar medium, the cells do not move actively on the surface, they mainly stretch. The colony interface consists on many chains of bacteria that lie almost side by side and advance forward by increasing their length along the interface and folding themselves (see Fig.1.1).

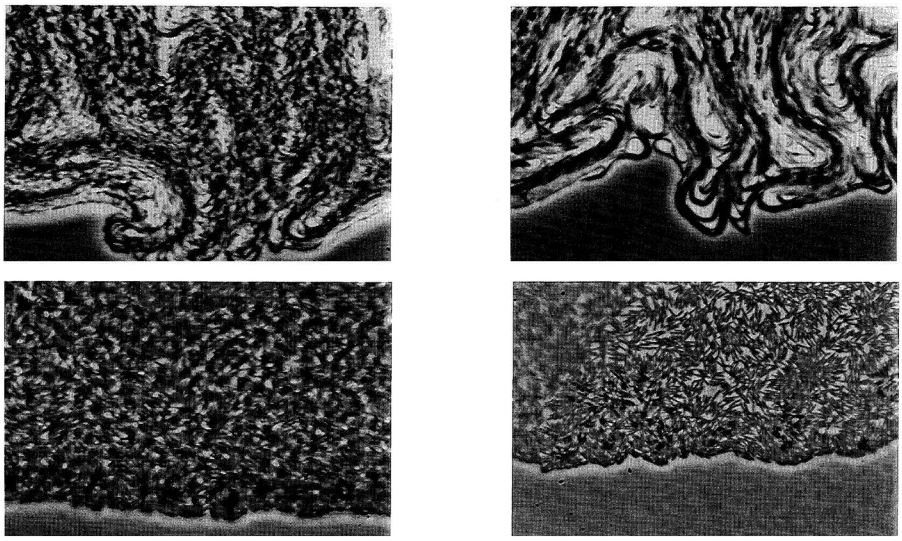

Figure 1.1: (Color online) Bacteria fronts in both regimes, for different magnifications (right and left): on top, the hard agar medium, leading to developing chains of cells stretching and foldin. At the bottom, a rich soft agar medium, with expanding cells colony due to a large motility.

- On a soft agar medium, the colony of mutants becomes compact and spreads homogeneously in every direction of the medium surface. This interface moves forward locally through random pushes due to active movement of individual cells inside the colony. Because of this activity, the interface advances much faster than in the former case (see Fig.1.1).

A considerable difference between both cases lies in the scale of the correlations in the height of the interface. The folding of bundles of long chains in the first case introduce long range correlations. Those chains align almost in parallel with the interface and statistically correlate a wide portion of the front. On the other hand, the growth in the second case looks very much local, the interface being driven by the forward move of independent bacteria. The measure of the front roughness in that case (see later for a definition) leads to an exponent $\chi = 0.5$.

### 1.1.2 Nematic crystal

The material of this subsection is borrowed from [4].

A liquid crystal is in a state enjoying properties between those of conventional liquid and those of solid crystal. It basically flows as a liquid, but its molecules may be oriented in a crystal-like way. The various liquid-crystal phases can be distinguished by their different optical properties (such as birefringence), for example by observing them under a microscope using a polarized light source: the contrasting areas in the textures correspond to domains where the liquid-crystal molecules are oriented in different directions.

In a beautiful set of experiments [4], the convection of nematic liquid crystal when confined in a thin container and driven by an electric field was studied. When subjected to an external voltage strong enough to trigger the Carr-Helfrich instability [5], turbulent

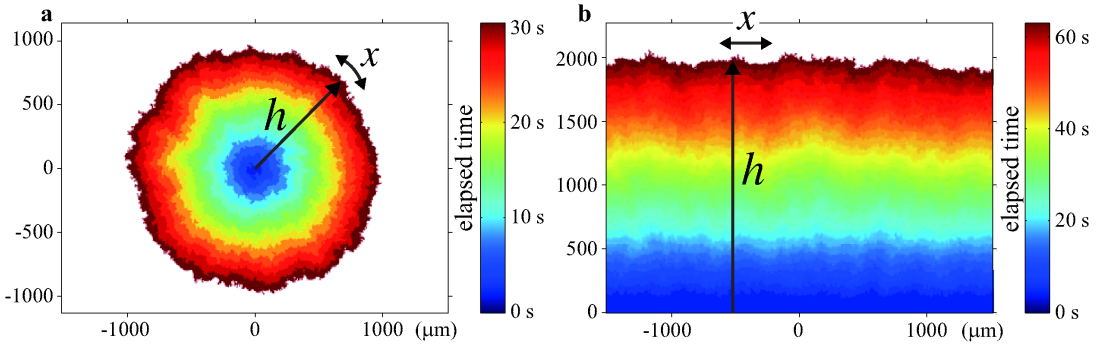


Figure 1.2: (Color online) Rough front in Takeuchi Sano experiment. (Left) Circular front growth corresponding to the so-called *droplet* geometry. (Right) Flat front growth corresponding to the *flat* geometry.

phases, called dynamic scattering modes 1 and 2 (DSM1 and DSM2) [6] are observed successively upon increasing the root-mean-square amplitude of the voltage at relatively low frequencies. The difference between DSM1 and DSM2 lies in their density of topological defects in the director field. In the DSM2 state, a large quantity of these defects, called disclinations, are present, a feature that can be very easily observed. The latter phase can be created by nucleating a defect with a ultraviolet laser pulse. It then starts growing constantly, forming a compact cluster bordered by a moving rough interface under voltage high enough.

In the experiment performed in [4, 7, 8], the mechanisms of the growth are carefully controlled. As the experiment can be easily repeated, it gives access to very clean statistics, and several initial geometries, droplet and flat (see Fig.1.2), can be tested. It was noticed (and expected before from theoretical considerations [9, 10, 11, 12]) that some characteristic scalings of the interface would exhibit universal behaviour, while the details of the fluctuations (most notably their full probability distribution) would be dependent on of the initial condition, even at very large time. More precisely, they measure:

$$h(t) = c_1 t + c_2 t^{1/3} \chi \tag{1.1}$$

with $c_1$ and $c_2$ non universal constants, and $\chi$ a probability distribution depending on the initial conditions.

### 1.1.3 Conductivity in Anderson Localization

To exhibit the large scope of stochastic interface growth, we now turn on a rather different example, whose notions will be useful in later chapters. The material of this subsection is borrowed from [13].

The distribution function of the conductance $g$ of disordered systems is very well understood in the metallic regime from the non-linear sigma model [14], but poorly understood in the localized phase. Provided that the degree of randomness of the impurities or defects is sufficiently large, the electronic waves might be localized rather than diffusing. The Anderson hopping model, simple yet phenomenologically rich, is described by the

Hamiltonian:

$$H = \sum \epsilon_i a_i^+ a_i + t \sum_{i,j} a_j^+ a_i \tag{1.2}$$

where the operator $a_i^+$ ($a_i$) creates (destroys) an electron at site $i$ and $\epsilon_i$ is the energy of this site chosen at random from a given distribution. The double sum runs over nearest neighbours. The conductivity $g$ can expressed through the Landauer formula as a sum of quantum amplitudes [15]. The amplitude between two sites $a$ and $b$ is expressed from Eq.1.2 in the Green formalism by:

$$\langle a|G(E)|b\rangle = \sum_{\Pi} \prod_{i \in \Pi} \frac{1}{E - \epsilon_i} \tag{1.3}$$

where the sum runs over the set $\Pi$ of all possible lattice paths connecting the two sites $a$ and $b$. In the strongly localized regime for distances much larger than the localization length, the previous sum is dominated by the forward-scattering paths [14].

$g$ now fluctuates depending on the realization of the disorder. It was realized in [13] that, in the strongly localized regime, $\ln g$ obeys the very same statistics than some well studied models of stochastic growth:

$$\ln g = c_0 L + c_1 L^{1/3} \chi \tag{1.4}$$

$\chi$ a probability distribution belonging to a family called Tracy-Widom.

Although baffling at first, the connection between them is drawn by a stylized model of glassy systems, the Directed Polymer, that we shall see later in this introduction.

## 1.2 The statistics of roughness

Because of the very different contexts of the above examples, a quantitative treatment of the characteristic features of the front is much needed. This goes along with the definition of scaling exponents, often with a geometrical interpretation much inspired by the theory of fractals.

At a mesoscopic scale, the height of a rough interface over a surface of size $L$[1] is well-defined and commonly enjoys a self-affine invariance property. After rescaling, the statistical properties of :

$$\tilde{h}(x,t) = b^{-\chi} h(bx, b^z t) \tag{1.5}$$

are the same than $h(x,t)$. Considering the average variations of height $W(x,t) = 1/L \int du |h(x+u,t) - h(u,t)|$, one obtains from Eq.1.5:

$$W(x,t) \sim x^{\chi} f\left(\frac{x}{t^{1/z}}\right) \tag{1.6}$$

[1] In higher dimensiosn, the statistical properties defined below are computed along a certain direction. If the system is isotropic, one can of course average over all directions.

with $\lim_{u\to 0} f(u) = \text{cste}$ and $\lim_{u\to\infty} f(u) \sim u^{-\chi}$ to ensure that two sites far apart are statistically uncorrelated. $z$ is a dynamical exponent: it measures how fast the fluctuations of $h(x,t)$ laterally spread over the front. $\chi$ is the rugosity exponent [16]: if $\chi = 1$ the surface is flat, while for $\chi > 0$ it exhibits roughness, up to $\chi = 1$ where it becomes purely fractal [17]. For $\chi < 1$, they are coined *self-affine fractals* and they look flat at large scales $L$.

One can define the more general height difference correlation functions:

$$C_q(x) = 1/L \left( \int du |h(x+u,t) - h(u,t)|^q \right)^{1/q} \tag{1.7}$$

The role of $q$ is to zoom on the contribution of different size populations of the increments $\delta h$. In many cases, one observes the scaling:

$$C_q(x) \sim x^{H_q} \tag{1.8}$$

If $H_q$ is independent of $q$, the rough surface is a statistically self-affine fractal over a corresponding range of length scales with a characteristic exponent (that we denote $\chi$, but often called the Hurst exponent, and denoted $H$ [18]). Therefore, over a space step $\delta x$:

$$\delta h \sim \delta x^{\chi} \tag{1.9}$$

The self-affinity property only holds over a finite range of $(\delta x, \delta h)$, bounded by vertical and horizontal scales $\delta x < \xi_{\parallel}$ and $\delta h < \xi_{\perp}$. Those scales are frequently found to grow algebraically with increasing time $t$, especially if growth occurs from a smooth surface.

Measuring $\chi$ poses less problem in computer simulations, where complete information about the front is available. A variety of methods exists, the most common one being to compute the scaling of the spatial variance $C_2(x)$, using Eq.1.8. Experimentally, the limit of accessible scales might lead to ambiguous results. A popular approach is the "slit island" method [19], where the rough surface is coated with a layer of a second material and carefully ground and polished parallel to the flat reference surface. As material is removed, "islands" of the surface material will appear in a "sea" of the coating material. As further material is removed these islands will grow and merge. It can be shown that the boundary between the two materials is a self-similar fractal boundary with a fractal dimensionality given by $D = d - \chi$. We refer to [20] for more details on the experimental methods.

## 1.3 The KPZ class and its equation

We now present the two best known continuum models used to describe stochastic growth processes.

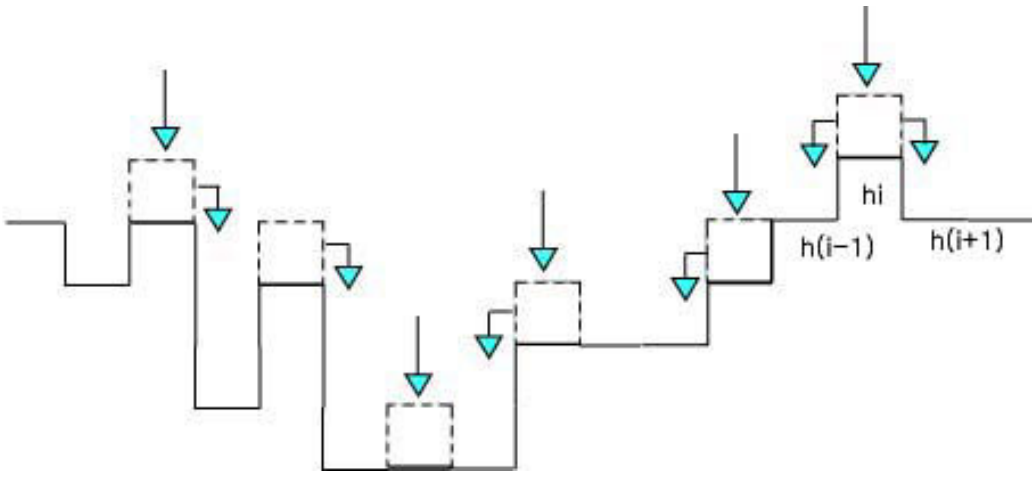


Figure 1.3: (Color online) A model of random deposition with surface relaxation. Each block fall in a random place at a random time. The deposited particle is allowed to diffuse along the surface up to a finite distance, settling when it finds the position with the locally lowest height. From [22].

### 1.3.1 Anatomy of the KPZ equation

The first step towards a description in the continuum of interface growth was made by Edwards and Wilkinson in [21]. They balance the competing effects of gravity (smoothing the interface) with random deposition. Starting from a pure random deposit model, they observe that a particle at the surface is more likely to fall in a local minimum around its landing point (see Fig.1.3). Such a local rearrangement is classically modelled by a Laplacian term, accounting for diffusion [2]. They finally obtained the Edwards-Wilkinson (EW) equation:

$$\partial_t h(x,t) = \nu \Delta h(x,t) + \eta(x,t) \tag{1.10}$$

where $h(x,t)$ defines the height of the interface, usually in a comoving frame chosen so that its average speed is set to 0, $\nu$ the diffusion coefficient and $\eta$ a space-time dependent noise of variance $\overline{\eta(x,t)\eta(x',t')} = 2D\delta(x-x')\delta(t-t')$. Eq.1.10 is linear and can be solved in Fourier space (for more details, see Section 2.2.1), giving the scaling exponents:

$$z = 2 \quad \text{and} \quad \chi = \frac{2-d}{2} \tag{1.11}$$

The interface is rough for $d = 1$, flat for $d > 2$ and shows logarithmic corrections for $d = 2$.

However, it was quickly realized that a broad variety of interfaces do not exhibit these scalings. If one assume that the growth speed only depends on local properties, the most general equation is:

$$\partial_t h = v(h, \nabla h, \nabla^2 h, (\nabla h)^2 \cdots), + \eta(x,t) \tag{1.12}$$

[2] It is already worthwhile to mention, as in [21], that the microscopic details of such a local smoothing of the interface are irrelevant in the continuum limit, a first step towards universality.

It would be rather unphysical to keep $h$ or $\nabla h$, as there is no preferential direction in the initial problem. Keeping the first relevant terms:

$$\partial_t h = \nu \Delta h + \frac{\lambda}{2}(\nabla h)^2 + \eta(x,t) \tag{1.13}$$

This equation is called the Kardar-Parisi-Zhang equation, first given in [23] and since then cited thousands of times in both the mathematics and physics literature. It is probably the most studied continuous model of stochastic growth. The occurrence of the non-linear term $(\nabla h)^2$ has a nice geometrical interpretation: when a random deposition occurs at $(x,t)$, the surface $h(x,t)$ grows in the direction normal to the tangent, and not vertically. Hence $\delta h \simeq (1 + (\nabla h)^2)$ at first order in $\nabla h$. Assuming self-affinity Eq.1.5 and plugging it into Eq.1.13, one obtains:

$$\partial_t \tilde{h} = b^{z-2}\nu \Delta \tilde{h} + b^{\chi+z-2}\frac{\lambda}{2}(\nabla \tilde{h})^2 + b^{(z-2\chi-d)/2}\nu \tag{1.14}$$

By comparing diffusion, noise and non-linearity in the limit $b \to \infty$, when $\chi < 0$ the non linearity can be neglected and we recover the same scaling exponents than in the EW model. On the other hand, for $\chi > 0$, so for $d \leq 2$ the non linear term dominates. A dynamical RG analaysis was performed in the seminal paper, and even before [23, 24]. A crucial parameter is the effective coupling constant $g = \lambda^2 D/\nu^3$. To the smallest order in $g$, the rescaled modes obey the flow equations:

$$d\nu/db = (z - 2 + K_d\, g^2(2-d)/4d)\nu \tag{1.15}$$

$$dD/db = (z - d - 2\chi + K_d\, g^2/4)D \tag{1.16}$$

$$d\lambda/db = (\chi + z - 2)\lambda \tag{1.17}$$

with $K_d = S_d/(2\pi)^d$. The Galilean invariance imposes $\chi + z - 2 = 0$ and the RG one-loop of $\lambda$ vanishes to first order. $g$ itself obeys the flow equation:

$$\frac{dg}{db} = \beta(g) = (2-d)g + \frac{2d-3}{2d}g^2 + O(g^3) \tag{1.18}$$

One can solve Eq.1.18 for the RG fixed points: if $d < 2$, the system always flows in the strong disorder regime[3], while for $d > 2$, there exists a critical transition at $g_c$, above which the system flows to the strong disorder regime, and below which thermal effects dominate. $d = 2$ appears as the *lower critical dimension* for the EW fixed point, while the existence of an *upper critical dimension* for the strong coupling regime, above which it would never appear, is still an open question. There is no known expression for $\chi$ and $z$ in $d \geq 2$. All those results were confirmed and refined in a two-loops computation performed in [25]. Most notably, the fact that $\lambda$ does not renormalize in Eq.1.17 holds at every order in $g$ because of some Ward identities extracted from the Galilean Invariance.

The case $d = 1$ stands apart, because the stationary distribution is known (for example from the Fokker-Planck equation associated to Eq.1.13):

$$P(\{h(x)\}) \sim \exp\left(-\frac{\nu}{2D}\int dx (\partial_x h)^2\right) \tag{1.19}$$

a mere Brownian, akin to the EW case [26][4]. Hence $\chi = 1/2$ and $z = 3/2$.

[3] In fact, it is the case even for the marginal dimension $d = 2$.

[4] It is a Brownian in a comoving frame, after removing the linear speed of growth of the interface.

### 1.3.2 Relation with Directed Polymer and Burgers Equation

Remarkably, there exists various mappings from Eq.1.13 to apparently unrelated problems. Applying the Cole-Hopf transform:

$$Z(x,t) = \exp\left(\lambda/2\nu h(x,t)\right)$$
$$\partial_t Z = \nu\Delta Z + \frac{\lambda}{2\nu}\eta(x,t)Z \tag{1.20}$$

Eq.1.20 is now linear, with a multiplicative noise. It sometimes bears the name of *stochastic heat equation* (SHE), or the *parabolic Anderson model* (PAM) with time-varying noise. It is one of the most studied stochastic partial differential equations, as it describes electron transport in disorder media (see Section 1.1.3) but also the evolution of a field of particles performing independent simple random walks with branching [27]. Hence it relates to population dynamics, a point of view we shortly adopt in Chapter 4. Those systems are in themselves fascinating as they exhibit *intermittency* [27], where the solution develops pronounced spatial structures on random isolated islands.

The path integral solution (or Feynman-Kac representation) of Eq.1.20 reads:

$$Z(x,t) = \int_{(0,0)}^{(x,t)} D[y(\tau)] \exp\left(-\frac{1}{2\nu}\int_0^t d\tau \left[\frac{\dot{y}(\tau)^2}{2} - \lambda\eta(y(\tau),\tau)\right]\right) \tag{1.21}$$

It is a sum over all possible paths. The initial and final conditions depend on the $t = 0$ geometry of $h(x,0)$. The most commonly used are the flat geometry $h(x,0) = cste$, corresponding to a polymer with one fixed and one free extremity (point to flat), and the droplet geometry $h(x,0) = \delta(x)$, corresponding to a polymer with two fixed extremities (point to point). Therefore $Z$ is the partition function of a directed polymer along the $t$ axis with elasticity 1, in a disordered potential $\lambda\eta(x,t)$ and at temperature $T = 2\nu$. Naturally, $Z$ is a random variable and the same scaling analysis is applicable. The most common critical exponents, concerning the spatial extension of $y(\tau)$ and the free energy $\ln Z$, are defined as:

$$\overline{\langle \ln Z(t)^2 \rangle}^c \sim t^{2\theta} \tag{1.22}$$
$$\overline{\langle x(t)^2 \rangle}^c \sim t^{2\zeta} \tag{1.23}$$

where $\overline{\cdots}^c$ is the disorder averaged cumulant, while $\langle \cdots \rangle$ defines the thermal average.

The phase of strong disorder for the DP corresponds to the strong coupling regime for the KPZ equation: both are controlled by the disorder landscape rather than thermal fluctuations. Hence the scaling exponents of both problems are related: $\theta = \chi/z$ and $\zeta = 1/z$. By equating in Eq.1.21 the elastic energy and the free energy, one obtains the scaling relation $\theta = 2\zeta - 1$ or equivalently $\chi + z = 2$.

A third interpretation of Eq.1.13 is obtained with the change of variable $v = -\lambda\nabla h$, resulting in the Burgers equation [28]:

$$\partial_t v + (v\cdot\nabla)v = \nu\Delta v + \lambda\nabla\eta \tag{1.24}$$

This equation can be seen as Navier-Stoke for the velocity field with no vorticity, no pressure term and a noisy forcing[5]. It occurs in various areas of applied mathematics,

[5]Note that, in this case, the noise is correlated as the derivative of a white noise.

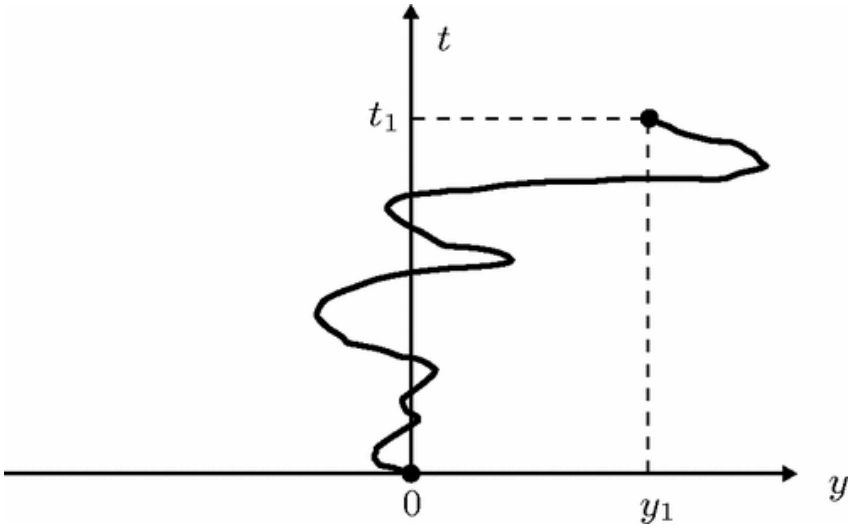


Figure 1.4: A possible configuration of a directed polymer in dimension $d = 1+1$. $t$ is the principal direction, and $y$ here, the transverse one. The polymer evolves in a disorder, modelled by a space-time random field $\eta(y, t)$Its extremities are fixed to $(0, 0)$ and $(y_1, t_1)$.

such as modelling of gas dynamics [29] and traffic flow [30], stands as a toy-model for turbulence and a prototype for equations for which the solution can develop discontinuities or shock waves. Its exact solution for any initial condition can be expressed as a path integral from Eq.1.21 (see [31] for a review).

### 1.3.3 The KPZ universality class

Eq.1.13 is believed to be the paradigmatic representative of the KPZ universality class, to which belong the growth models obeying some basic rules:

- Diffusion mechanism smoothing the interface by preferentially filling local minima. In the KPZ equation, the assumption is encoded in the Laplacian.
- Slope dependant speed. As we stated, along with the lack of preferential direction, this leads to the non linear $(\nabla h)^2$.
- A fast-decaying noise, with weak correlations, both in space and time. Departure from the KPZ class have been observed for quenched disorder[6], or long-range correlations [33].

Among the models obeying those hypothesis are the Eden growth model, the ballistic deposition model, some fracture, solid-on-solid models, invasion percolation, the polynuclear growth, fluid—fluid displacement experiments [20, 34]... A classification of the growth models falling onto the KPZ universality class is still a field of ongoing research.

As for higher dimensions, even $d = 2$ has for a long time escaped even numerical simulations, but it seems now clearly understood from that point of view. A recent study compares different lattice models, probing the universality of scalings and fluctuations

[6]The quenched disorder leads to another universality class, the Quenched KPZ (QKPZ) class [32].

distributions in $d = 2$. Various models again yield the same scaling exponents and, more strikingly, the same universal fluctuations distributions. The chase after the critical exponents in higher dimensions [35, 36, 37] seems to have crushed the hope for simple formula, and notably provides strong evidence against an upper critical dimension $d_c = 4$, in spite of its appearance in several theoretical arguments (as mode coupling [25, 38]). Elucidating the behaviour of $\chi$ in $d \geq 2$ remains one of the greatest challenges in the KPZ class.

The situation in $d = 1$ is radically different, as it lends itself to analytic approaches. One can even say, in the sense that will be detailed in Chapter 2, that the $d = 1$ is integrable. Not only $\chi$ and $z$ but the distribution of the fluctuation of $h(x, t)$ and the stochastic process $x \to h(x, t)$ are fully characterized. The origin of this solvability is not completely understood but much light can be shed by unravelling a link to systems of particles and Bethe Ansätze [39] that we extensively detail in Chapter 2.

The first exact solution of the fluctuations of the interface was obtained in [40]. The author starts from a random growth model in two dimensions with an exponentially distributed disorder, closely related to the one-dimensional totally asymmetric exclusion process (TASEP). By the mean of the RSK correspondence, the problem at $T = 0$ is linked to random matrices, although the mapping only holds for this very specific disorder. A swarm of exact results for various models followed [9, 41, 42], among them the proof that the fluctuations of solution of the KPZ equation itself obeys the same distribution [10, 43, 9, 11, 12, 44]. The identified distributions belong to a family called Tracy-Widom, and labelled by $F_\beta$. They were introduced by Tracy and Widom [45, 46] as the probability distributions of the largest eigenvalue of a random matrix in the edge scaling limit from Gaussian ensemble. Although it is possible to relate matrix models to every $\beta$ [47, 48], the most common values are $\beta = 1, 2, 4$ corresponding respectively to ensembles of Gaussian orthogonal (GOE), unitary (GUE) and symplectic (GSE) matrices [49][7].

After the fluctuations of $h(0, t)$ around its mean value were computed, the complete stochastic process $x \to h(x, t)$ for fixed and large $t$ was characterized as the Airy process $Ai_2$ [50], also known from the time evolution of the largest eigenvalue in a Dyson Brownian motion[8]. The very involved question of time correlations remains for the moment hampered by technical difficulties, although some attempts courageously head in that direction [53, 54].

## 1.4 Perspectives

The field of stochastic growth is so large today that it is impossible to list its expanding directions. Likewise for the KPZ equation alone, because of its numerous links to other fields. Therefore we postpone this daunting task and refer to excellent reviews for a larger overview [20, 34, 55, 56, 57].

[7] Note however that with a brownian initial conditions, the fluctuations follow a distribution called $F_0$ that does not possess an interpretation in terms of random matrices.

[8] This relation only holds for the droplet geometry, the flat geometry being describes by $Ai_1$ with no such analogy [51, 52].

The field of so-called integrable probabilities is living decisive advances. It represents today the best hope to reach a consistent understanding of the notion of universality in the KPZ class [58]. Much effort is done to relax the hypothesis on the microscopical details leading to universal features, but a general proof along the lines of the universality of the Ising model [59], is still lacking. It seems to us that rather brutal modifications of the microscopic details, expelling us out of the KPZ class, might be a fruitful approach to probe the boundaries of this realm. We will come back to this question in Chapter 3 with the heavy-tailed disorder. Sadly, one often sacrifices analytical tools on the way.

Another interesting direction is the fast evolving theory of stochastic partial differential equations. The attentive reader may have noticed that the KPZ equation is ill-defined, as the product $(\nabla h)^2$ can not be performed unambiguously for rough interfaces. While a small-scale cut-off is physically expected, the continuum limit remains problematic, as most tools for tackling SPDE rely on continuous equations. Luckily, recent progress has been made in giving to the KPZ equation much sense [60], through the theory of *regularity structures*. More details are given in Chapter 4. This approach enlightens the sometimes confusing analytical results extracted from the KPZ equation.

Finally, while in $d = 1$ the global picture starts to emerge, the higher dimensions retain all their mysteries, and it is fair to say that almost nothing is known on an analytical level. This probably remains one of the greatest challenges of the field of stochastic growth.

# 2 The KPZ universality class in $d = 1 + 1$

In this Chapter, we focus on the DP problem, and refer to the introduction for the detailed mapping to the KPZ interface language. We already detailed some features of the KPZ class in the introduction. Especially, in $d = 1 + 1$, the disorder is always relevant and the system converges to the strong disorder fixed point. Such a denomination tries to convey the idea that the statistical properties of the polymer are dominated by the influence of the disorder, rather than by entropy. The present study is dedicated to the existence, in $d = 1+1$, of the frozen phase and the study of its statistical properties. More specifically, we focus on the behaviour of the free energy and present some analytical tools to monitor both the flow towards the strong disorder fixed point observed on the polymer, and the non-perturbative regime itself.

## 2.1 The strong disorder fixed point of the DP

How should we quantify the fact that the disorder is relevant to the polymer behaviour, at some temperature ? Such a phase can be characterized by several properties, often bonded together.

In the mathematical community, a common definition invokes martingales (see [61] for a definition). Denoting $Z_t = \int_0^t e^{\beta H(\mathbf{x})} dP_0((x))$ - $dP_0(\mathbf{x})$ being usually the measure of random walks with either fixed or free extremities -, one can prove that $W_t = Z_t/\overline{Z}$ is a martingale [62]. By the zero-one law [61], one readily obtains that $W_\infty$ is almost surely either 0 (called the strong disorder regime) or strictly positive (for weak disorder).

Another criterion, used as well in the physics community, employs overlaps $I_t = \mu^{\otimes 2}(x_1(t) = x_2(t))$, a measure of the path shared by two different polymers subject to different thermal noises but in the same realisation of disorder. If:

$$\int \mu^{\otimes 2} \left(x_1(t) = x_2(t)\right) dt = \infty \tag{2.1}$$

the regime is said *weakly localized* [63]. It is equivalent to the *strong disorder* regime [64]. The *strong localization* amounts to requiring that there exists some (random) positions at which the polymer has a strictly positive probability of ending. It can shown that the condition of strong disorder regime implies strong localization (in any dimension) [63].

In what follows, we look at the behaviour of the polymer free energy density $-(t\beta)^{-1} \ln Z$, rather than the localization of its path. Considering the free energy density of the large size limit $f(\beta) = -\lim_{t\to\infty} \frac{1}{\beta t} \overline{\ln Z_t} = -\lim_{t\to\infty} \frac{1}{\beta t} \ln Z_t$ (a *self-averaging* quantity), one

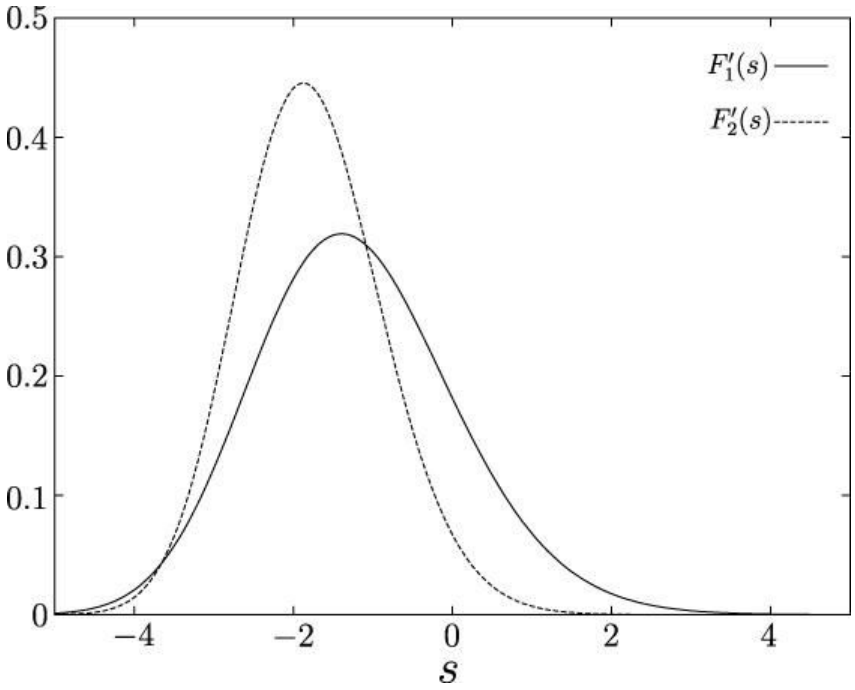


Figure 2.1: (Color online) The Tracy widom family of probability distributions. $F_1$ corresponds to shape fluctuations strating from a flat surface, while $F_2$ is observed from a curved initial conditions. Cross-overs between both distribution have been computed for certain models of polymers [65].

can easily show that this energy is bounded from above by its annealed mean $\hat{f}(\beta) = -\lim_{t\to\infty} \frac{1}{\beta t} \ln \overline{Z_t} = -\beta/2$. When the disorder is irrelevant (the polymer merely doing a random walk), both annealed and quenched free energies coincide (for the so-called *weak disorder*). When they differ, the regime is coined *very strong disorder* [63], and is believed equivalent to the strong disorder regime, at least in the cases considered here.

In the DP model, the free energy $f(\beta)$ departs from the annealed expression in its linear part, but not only. Its fluctuations $\delta f = \ln Z - tf(\beta)$ anomalously grow as $t^\theta$ with the famous KPZ exponent $\theta = 1/3$ (see the Introduction). Moreover, the left tail of the whole distribution of $\delta f$ fattens, an effect due to the effective optimisation of the polymer walk: favouring deep sites introduces a bias towards negative value of the energy sites. While the full computation of the free energy distribution is often very complicated, much can already be deduced from the moments of $Z$, by computing for example the participation ratios $\overline{Z_n^p}/\overline{Z_n}^p$: they measure the importance of the tails and can provide useful bounds on the critical temperature [66, 67].

We have in the strong disorder regime:

$$\ln Z = tf(\beta) + ct^{1/3}\chi \tag{2.2}$$

with $\chi$ the Tracy-Widom distribution decaying as $P(f < s) \sim e^{-|s|^{3/2}}$. The skewness, measuring the asymmetry of $\delta f$, is expected to be a good indicator of the establishment of the strong disorder regime because of the features detailed above. It has been previously used as a marker for the KPZ universality class [68], and most notably in recent experiments and simulations [4, 69].

## 2.2 The cross-over from EW to KPZ

Early stage behaviours are often more accessible to experiments. Anyone working with various growth models will discover that, in some cases, the early time behaviour is very different from the late stage, while in other cases, the system reaches its asymptotics in just a few layers. Hence it is important to clearly state the time scale (noted $t^*$ below) at which the transition takes place. In the present case, we start from a flat surface, where $(\nabla h)^2$ might be neglected at the very beginning.

We recall the equation of local non-linear growth given in the introduction:

$$\partial_t h(x,t) = \nu \Delta h(x,t) + \frac{\lambda_0}{2}(\nabla h(x,t))^2 + \eta(x,t) \tag{2.3}$$

with $\overline{\eta(x,t)\eta(x',t')} = R(x-x')\delta(t-t')$, $R(x)$ the spatial correlator of the noise with $\int R(u)du = D$.

The full KPZ equation presents some issues with non-universality: microscopic details about disorder distribution or dynamics might lead to variations in the macroscopic growth process, an issue we explore more in Chapter 3. A way to get rid of those dependencies is to consider the limit of high diffusivity or weak noise [70], that allows complete determination of the scale of the fluctuations as a function of only three parameters $\lambda_0$ , $\nu$, and $D$, *at all times*, by contrast to the usual identification [71] for large time. All the other microscopic details such as the disorder correlations or the lattice effects are relevant only at very short times $t < t_f$. The example with a short range correlator $R(u)$ on the continuum KPZ model is given in the related paper. This amounts to ensure that the thermal wandering averages out the microscopic details before the system flows to the strong disorder regime.

How to compare the different terms ? What are the typical scales defining the relative contributions of the diffusion and non-linear effects to the interface growth ?

### 2.2.1 The solution for EW

Let us assume first that $\lambda_0 = 0$[1], the Edwards-Wilkinson equation. Due to its linearity, it can be tackled by Fourier transform. Writing the Fourier version of the modes $h(k,t)$ of the interface:

$$\partial_t h(k,t) = -\nu k^2 h(k,t) + \eta(k,t) \tag{2.4}$$

This Langevin equation is equivalent to a Brownian motion damped by viscous effects proportional to $k^2$ and the full functional of the height fluctuations is in principle solved through its Fourier mode evolution, for example in the $1+1$ model [72]:

$$P(\{h(k,t)\}) \sim \exp\left(-\frac{\nu}{2D}\int dk \frac{k^2}{1-e^{-2\nu k^2 t}} h(k,t)\overline{h}(k,t)\right) \tag{2.5}$$

[1] We draw the attention of the reader on the fact that, only in that Chapter, we label by $\lambda_0$ the strength of the non-linearity, while $\lambda$ will serve as a rescaled time parameter.

From Eq.2.5, the correlation functions both in time and space can be computed. For example, the surface roughness $W$ (see Section 1.2 for a definition), corresponding to the spatial second moment of the rescaled free energy $f$ in the DP setup:

$$W^2(x,t) \sim \frac{D}{\nu} x^\chi f_{EW}(\nu t/x^2) \tag{2.6}$$

where the roughness exponent is $\chi = \frac{3-d}{2}$. The universal scaling function $f_{EW}$ is explicitly known as well [73]. At large time, from Eq.2.5, we recover the stationary distribution given in Eq.1.19.

We know turn on the non-linearities and monitor the departure from the EW regime through a cumulant expansion at small time.

### 2.2.2 Moments expansion at short times

Above the microscopic cutoffs $x_f$ and $t_f$, one can safely assume the underlying noise is white in space and time. New scales appear by simply balancing the diffusion and the non-linear terms in Eq.2.3:

$$t^* = \frac{2(2\nu)^5}{D^2\lambda_0^4} \tag{2.7}$$

$$x^* = \sqrt{\nu t^*} = \frac{(2\nu)^3}{D\lambda_0^2} \tag{2.8}$$

$t^*$ and $x^*$ draw the line between the EW and KPZ regimes if they are larger than the microscopic scales $(t_f, x_f)$. The strong dependence of the diffusion on those scales, explains why, at finite temperature, long times are sometimes needed to see non-linear effects setting up. We define the convenient dimensionless parameter[2] $\lambda$:

$$\lambda = (t/4t^*)^{1/3} \tag{2.9}$$

The moments of $Z(x,t) = \exp\left((\lambda_0/2\nu)h(x,t)\right)$ can be computed exactly due to some fortunate mapping to a boson problem (see Section 2.3). Because the linear shift $\overline{Z(x,t)}$ is problematic in the continuum limit, we work with the normalized variable $z = Z/\overline{Z}$. The following identity allows to extract the short time behaviour of $\ln z$ through a perturbative expansion:

$$\ln \overline{z^r} = \overline{e^{r \ln z}}^c = \sum_{n=1}^{\infty} \frac{r^n}{n!} \overline{(\ln z)^n}^c \tag{2.10}$$

At small time, $z$ is concentrated around its mean value $\overline{z} = 1$, so one can expand $\ln z$ around 1. Such an expansion is valid only when the distribution of $z$ is peaked around 1. As we mentioned, the tails of $z$ fattens at large times, hence this perturbative approach does not hold in the strong disorder regime. However, it already reveals some typical

[2] Again, we insist that this parameter $\lambda$ is a rescaled time, contrasting with $\lambda_0$, the coefficient of the non-linear term in the KPZ equation.

features of the growing non-linearities. For example, the variance of $z$ follows the formula (exact at all time):

$$\overline{z^2} = e^{2\lambda^3}\left(1 + \mathrm{erf}(\lambda^{3/2}\sqrt{2})\right) \tag{2.11}$$

More generally, the moments $\overline{z^n}$ seem to admit similar expressions made of error function, with exponentially growing in $n$ terms $e^{n(n^2-1)\lambda^3}$. While it would be interesting to fully understand the underlying structure, let us just notice that, to leading order, $\overline{z^n} \sim e^{\lambda n^3}$. Because the growth of moments with $n$ is related to the tail decay of the distribution, an estimate of the decay of $\delta f$ by a simple Laplace argument quite miraculously leads to the correct answer for the left tail of the free energy fluctuations $P(\delta f < s) \sim e^{-\alpha|s|^{3/2}}$ (see [74, 75] for more details).

Now if we reproduce for example, the variance of the (normalized) free energy:

$$\overline{(\ln z)^2}^c = -\sqrt{\frac{2}{\pi}}\lambda^{3/2} + \left(\frac{5}{3} - 6\pi\right)\lambda^3 + O(\lambda^{9/2}) \tag{2.12}$$

and revert to the language of the interface height $h(x,t)$, one finds:

$$\overline{h^2}^c = D\sqrt{\frac{t}{2\pi\nu}} + O(\lambda_0 t) \tag{2.13}$$

This dominant term is independent of the non linearity $\lambda_0$ and we retrieve the fact that, at finite temperature, there exists a characteristic time below which the height fluctuations scale with time as $\delta h \sim t^{1/4}$, in the EW regime: this result is consistent with Eq.2.5. With some more algebra, one can identify the first source of departure from the Gaussian regime in the growing of the third cumulant $\overline{(\ln z)^3}^c$, as we would expect in the introduction: the bias of the polymer towards energy-optimized paths creates an asymmetry in $\delta f$, manifest in the skewness. It is interesting to note that $\overline{(\ln z)^3}^c$ scales linearly with time, both at short and at large time, although with a different coefficient. Hence, the short time correction $\delta h \sim t^{1/3}$ is already of the form of the KPZ scaling (see Fig.2.2 and the related paper for more details).

For $\lambda > 1$ (equivalently for $t^* \lesssim t$), the crossover towards the KPZ regime is effectively observed, accompanied by a important loss in precision from the numerical simulations performed in the related paper. Indeed, such fat tails distributions are usually difficult to sample properly due to the importance of rare, but very large events.

The previous study clearly shows the limit of the perturbative expansion in exploring the strong disorder regime of the KPZ class, although it sheds light on its emergence. This expansion has to be amended to access the statistics of the large time behaviour, where the non-linearities fully control the shape of the interface.

## 2.3 Statistics of the KPZ regime

Due to the so-called moment growth problem, the probability distribution of $\ln z$ can not be uniquely determined from the knowledge of $\overline{z^n}$. However, it will be shown that

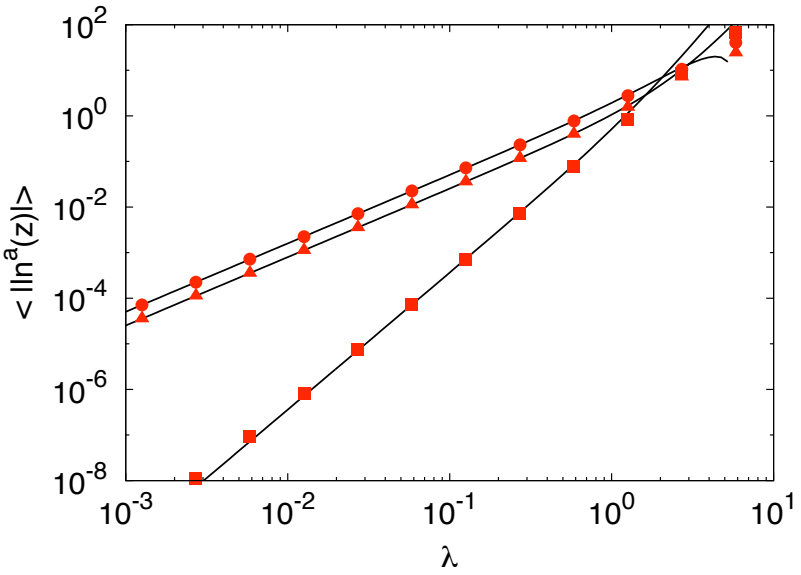


Figure 2.2: (Color online) From top to bottom, the cumulants ($15 \cdot 10^6$ samples) $\overline{\ln^2 z}^c$ (solid line, red circles), $-\overline{\ln z}^c$ (solid line, red triangles) and $\overline{\ln^3 z}^c$ (solid line, red squares) for $t = 512$. The solid lines are the analytical predictions given in the related paper, up to $O(\lambda^{9/2})$, with $\overline{c} = 1$. There are no adjustable parameters.

some analytical (albeit non rigorous) continuation of the generating function of $z$ allows to handle the infinite part of the sum and properly regularize the results.

Although this procedure appears somewhat unjustified, its main interest lays in its broad applicability. Indeed, integrable approach from Bethe Ansatz-like formula seems to represent today one of the most flexible source of exact computations in the domain of "integrable probability". A better understanding of this deep relationship would allow to enlarge the class of systems under investigation to other known integrable systems that remain to be connected with the directed polymer. Numerous works are heading in that direction, among them the Log-Gamma polymer [76], the Sine-Gordon model [77], or various boundary conditions. As a matter of fact, some works introduce a more careful regularization procedure, which gives an *a posteriori* explanation of why "the magic works": this goes through $q$-deformed models (for example the $q$-TASEP) where the parameter $q$ forces the convergence of the series involved in the computation, allowing for perfectly defined Laplace transforms [78]. The continuous limit is then retrieved by setting $q$ to specific values ($q \to 1$).

That being said, an unfortunate common feature of integrable systems is that their delicate mathematical structure immediately breaks down if the model is changed ever so slightly: no integrable approach is known for large classes of noises (and especially for moments-diverging disorders) or general noise correlations[3]. Although one may think that this limits the interest in the corresponding results, the recurring experience with integrable systems has been that the results may persist in a broader setup, alike the first approach of De Moivre to the Central Limit Theorem. Hence much insight can be gained from the white-noise case.

[3]While in some cases, spatial correlations can be handled, it seems that time correlations still escape the realm of integrability.

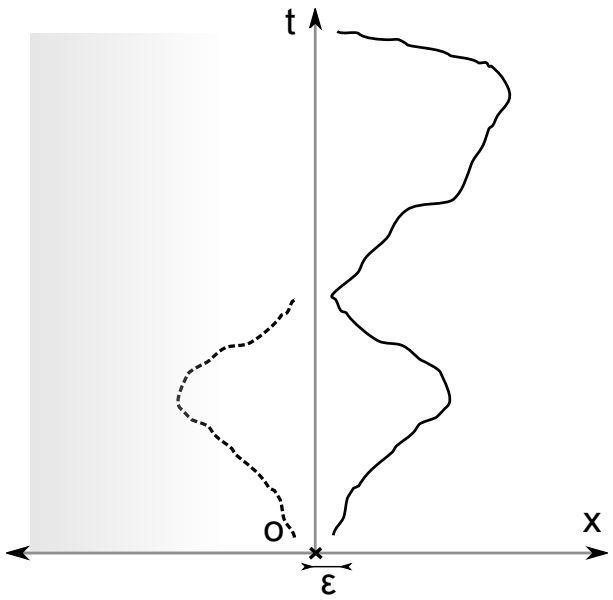


Figure 2.3: (Color online) Directed Polymer with both end points fixed at small $x = \epsilon$ and a hard wall constraint at $x = 0$. The reflected polymer, used in mirror arguments, is pictured by a dashed line.

In the following, we present the machinery of the analysis, with a small grain of salt: our polymer evolves in a half-space, restrained by a hard, non interacting wall (see Fig.2.3), rather than in the full space. This system remains integrable and allows to study more specifically the influence of confinement on the fluctuations of the free energy. This geometry is interesting as an essential ingredient to many pinned systems. This boundary condition, namely $z(0, 0, t) = 0$ for all $t$ translates as $\nabla h(x, t)|_{x=0} = +\infty$ or $h(0, t) = +\infty$. It can be schematically thought of the boundary between two domains kinetically growing at different average speeds. While we do not obtain different scaling exponents with the hard wall model, boundary conditions in generel might have a drastic effect on growth, with exponents clearly larger than in the bulk for a large range of times [79].

### 2.3.1 The Bethe Ansatz formalism

The appearance of Bethe Ansatz techniques in the KPZ field comes back to the seminal work of Kardar [39], who used it to derive the anomalous exponents. The mapping goes as follow: the central quantity is the $n$-point correlation function of the partition function:

$$\overline{Z_V(x, y, t)^n} = \overline{Z(x, t|y, 0) \cdots Z(x, t|y, 0)} \tag{2.14}$$

with the boundary conditions $Z_V(x, y, t) = 0$ for $x, y = 0$ and $x, y = L$ for all $t$. As we said, to stay in line with the work performed in that thesis, we choose a "hard wall" condition, corresponding to bosons confined in the box $[0, L]$. This constrains the polymer to optimize its path on half a space, instead of the full real space. Although leaving the anomalous exponents of the KPZ fixed point unimpaired, this choice will have an interesting effect on the fluctuations distribution.

The quantity Eq.2.14 obeys a dynamical equation equivalent to the temporal evolution

of the $n$-bosons system, ruled by the Hamiltonian $H_n$:

$$H_n = -\sum_{j=1}^{n} \frac{\partial^2}{\partial x_j^2} - 2\bar{c} \sum_{1 \leq i < j \leq n} \delta(x_i - x_j) \tag{2.15}$$

Consequently, the temporal evolution of $\overline{Z^n(x,t)}$ is simply given by:

$$\overline{Z^n(x,t)} = \sum_{\mu} |\Psi_\mu(x, \cdots, x)|^2 \frac{e^{-tE_\mu}}{\|\mu^2\|} \tag{2.16}$$

where $\Psi_\mu(x, \cdots, x)$ are the fully symmetric Bethe eigenfunctions that diagonalize $H_n$. Those are very well known from the integrability literature [80]. The bosonic (fully symmetric) eigenstates defined in the sector $x_1 < .. < x_n$ as:

$$\begin{aligned} \Psi_\mu(x_1, ..x_n) = \sum_{P \in S_n} \sum_{\epsilon_1, \cdots \epsilon_n = \pm 1} \epsilon_1 \epsilon_2 .. \epsilon_n A[\lambda_{P_1}, \epsilon_2 \lambda_{P_2}, .. \epsilon_n \lambda_{P_n}] \\ \prod_{j=1}^{n} e^{i\epsilon_1 x_1 \lambda_1 + .. + i\epsilon_n x_n \lambda_n} \\ A[\lambda_1, .., \lambda_n] = \prod_{n \geq \ell > k \geq 1} \left(1 + \frac{i\bar{c}}{\lambda_\ell - \lambda_k}\right) \left(1 + \frac{i\bar{c}}{\lambda_\ell + \lambda_k}\right) \end{aligned} \tag{2.17}$$

They satisfy the conditions:

$$\begin{aligned} \Psi_\mu(0, x_2, ..x_n) = 0 \\ \Psi_\mu(x_1, .., x_{n-1}, L) = 0 \\ (\partial_{x_{i+1}} - \partial_{x_i} + \bar{c}) \Psi_\mu(x_1, ..x_n)|_{x_{i+1} = x_i} = 0 \end{aligned} \tag{2.18}$$

When plugged into Eq.2.18, those eigenfunctions obey a quantification relation on the rapidities $\lambda_j$, called the Bethe equations:

$$e^{2i\lambda_j L} = \prod_{\ell \neq j} \frac{\lambda_j - \lambda_\ell - i\bar{c}}{\lambda_j - \lambda_\ell + i\bar{c}} \frac{\lambda_j + \lambda_\ell - i\bar{c}}{\lambda_j + \lambda_\ell + i\bar{c}} \tag{2.19}$$

This set of transcendental equations is essential, as it determines the way the bosons organize themselves under an attractive interaction of strength $\bar{c}$ in a box of size $L$. The first part is the standard set of Bethe equations for periodic boundary conditions, while the second part stems from the reflected bosonic waves on the hard wall.

Their analytic solution for finite values of $L$ is not known, although a fair amount of numerical progress can be made under certain assumptions [81]. It is quite surprising that they admit an exact solution (with exponentially small corrections) in the thermodynamic limit $L \to \infty$, where the rapidities organise as $n_s$ strings formed by $m_j$ particles [82, 83]. Within each bound state:

$$\lambda_{j,a} = k_j + \frac{i\bar{c}}{2}(m_j + 1 - 2a) \quad \text{with} \quad a = 1 \cdots m_j \tag{2.20}$$

the set $\{k_i, m_i\}$ indexing the strings. Such eigenstates have energy:

$$E_\mu = \sum_{j=1}^{n_s} (m_j k_j^2 - \frac{\bar{c}^2}{12} m_j (m_j^2 - 1)) \tag{2.21}$$

Because of the reflective bosonic waves, the states are now invariant by $\lambda_j \to -\lambda_j$.

At that point, the first approach focused on the ground state, namely the $n$ bound state, where all the particles are clustered together. This corresponds to $E_n = nk^2 - \frac{\bar{c}^2}{12} n(n^2 - 1)$, retrieving the cubic exponential growth noticed in Section.2.2.2. However, it turns out [84] that an exact summation of all excited modes are needed to access the full distribution of probability[4]. Following this program requires the knowledge of the norms of the eigenstates:

$$||\mu|| = \int_0^L dx_1 dx_2 \cdots |\Psi_{\{k_i, m_i\}}(x_1, \cdots x_n)|^2 \tag{2.22}$$

as well as the amplitude $|\Psi(x)|^2$. We can now define the generating function $g(s) = \overline{\exp(-e^{-\lambda s} Z)}$, whose power series is:

$$g(s) = 1 + \sum_{n=1}^{\infty} \frac{1}{n!} \overline{Z_V(x, x, t)^n} (-1)^n e^{-\lambda n s}$$

$g(s)$ is the Laplace transform of the random variable $Z$. Parametrizing it with $e^{-\lambda s}$ (see for example [86]) provides an immediate way to extract the cumulative of $f$:

$$\lim_{\lambda \to \infty} = \overline{\theta(f + s)} = P(f > -s) \tag{2.23}$$

Such a limit requires performing *exactly* the sum over $\mathcal{Z}_n$, as they all contribute even in the large $\lambda$ limit. It would of course be handy to access asymptopia without relying on this computation. It is a "miracle" of (at least some) integrable systems that $f$ admits an exact expression at all time, in term of functional determinants.

It is convenient to change the summation over the number of particles $n$ to a summation over the number of strings $n_s$. This allows to relax the constraint $\sum_{i=1}^{n_s} m_i = n$, a trick that will come handy later. We denote by $Z(n_s, s)$ the coefficient in the power series of $g(s)$ after such a reorganization:

$$g(s) = 1 + \sum_{n_s=1}^{\infty} \frac{Z(n_s, s)}{n_s!} \tag{2.24}$$

$g(s)$ now shall be recast in a convenient form for computing the asymptotic behaviour. Thanks to some underlying algebraic structure, one can write $g(s)$ as a Fredholm determinant. However, the necessary manipulations, initially performed in [44, 43], involve a considerable amount of subtleties and, because of their length, we postpone them for clarity, in Section 2.3.3.

We are focusing on the half space case. For that geometry, the norms of the eigenstates, and their amplitudes are written in Section 2.3.3, but additional remarks are to be made:

[4] Although nothing prevents this method to generalize to higher dimensions, analytical difficulties quickly arise. Some works have been however pursued in that direction [85].

- The norm full expression was mainly obtained by heuristics from low $n$ computations. The final formula is rather similar to the full space case, with terms obtained by transforming the rapidities $\lambda_i \to -\lambda_i$. The larger question of computing norms of eigenstates in integrable systems remains an open question. A formula coined Gaudin-Korepin [87] allows a close expression in terms of a determinant. Similar formula exist (sometimes as conjectures) for other models, f.e. the hubbard model, but no general result seems to hold. Despite that, we are confident an amended Gaudin formula should exist for an (eventually attractive) wall boundary condition, an interesting perspective to explore.

- Unfortunately, computing $\Psi(x, \cdots, x)^2$ in general seems complicated. However, the leading order in powers of x is very simple:

$$\Psi(x, \cdots, x)^2 = n! x^n \lambda_1 \cdots \lambda_n + O(x^{n+1}) \tag{2.25}$$

  This term dominates the amplitude for small $x$, a polymer whose extremities are very close to the hard wall (see Fig.2.3). It would be of course insightful to address the general case.

### 2.3.2 Fluctuations of the free energy: the result

The above expressions can be plugged into Eq.2.24, and the summation over $n_s$ rewritten in terms of Fredholm determinant, as a function of $\lambda$. At large time $\lambda \to \infty$, the main result of the present Chapter reads:

$$g(s) = F_4(2^{-2/3} s) \tag{2.26}$$

where $F_4$ is the GSE (Gaussian Symplectic Ensemble) Tracy-Widom distribution.

We recall that for the droplet (or point to point) geometry in the full space, a similar result holds with a convergence at large time to $F_2$, the GUE Tracy-Widom distribution. Comparison between the free space case and the half space is readily done by using the known characteristics of both distributions:

- The linear speed of growth of the free energy $v_\infty$ is equal in both cases (up to logarithmic corrections). Although non universal w.r.t the disorder f.e, this observable seems to show more robustness to changes in the boundary conditions. Actually, it is likely that, if the width of the space available to the polymer grows faster than $t^{2/3}$ with the polymer size, no effect on the extensive part of its energy should be observed.

- Because the confinement reduces the space available to optimization, the fluctuations between disorder realizations are slightly greater in the half space case. This effects can be seen in the variances in the half and full-space $\sigma_{HS} > \sigma_{FS}$. Nonetheless, the ratio $\sigma_{HS}/\sigma_{FS}$ decreases with time, from the value 3/2.

- Finally, the difference between the means $\mu^{F_2}$ and $\mu^{F_4}$ has an interesting interpretation in terms of extremal events. Consider a polymer in the droplet geometry in the full space. The probability that it remains on the right of the $t$-axis is given by $p = Z^{HS}/Z^{FS}$. At large $\lambda$, one has $\overline{\ln p} \sim t^{1/3}(\mu^{F_2} - \mu^{F_4})$. Hence this gap measures the exponential decay of the probability with $t$.

The $F_4$ distribution is known from the random matrix theory as the pdf of the fluctuation of the largest eigenvalue of a matrix randomly drawn from the symplectic ensemble [88]. While it is still an open question to address the striking similarity between the polymer at *finite* temperature and random matrix theory, the $T = 0$ model of polymer can be linked to probability measures over random ensembles of matrices by the mean of the so-called Robinson-Shensted-Knuth correspondence [40]. On the other hand, Pfaffian identities occur as combinatorial tools to count objects with symmetry contraints (much alike the constraint on invariance by reflection equivalent to the hard wall condition at $T = 0$) [89]. From the formula (see Section 2.3.3) appears a clear relation with the full space case, and it would certainly be enlightening to connect it with combinatorics.

## 2.3.3 The half-space case

In that subsection, we give more details about the intricate computation of the free energy in the half space, as the Letter joined to the chapter is rather concise. The avid reader can also refer to [90].

### 2.3.3.1 Strings norms and amplitudes

First we give the conjecture for the norm of an arbitrary string state in the half space:

$$\begin{aligned}
\mathcal{N} &= \int_0^L dx_1 .. \int_0^L dx_n |\tilde{\Psi}_{\{k_i,m_i\}}(x_1, ..x_n)|^2 \\
&= n! \bar{c}^{n_s - n} 2^{-n_s} \prod_{i=1}^{n_s} S_{k_i,m_i} \prod_{i<j}^{n_s} D_{k_i,m_i,k_j,m_j} L^{n_s} \qquad (2.27) \\
D_{k_1,m_1,k_2,m_2} &= \frac{(k_1 - k_2)^2 + (m_1 + m_2)^2 \bar{c}^2/4}{(k_1 - k_2)^2 + (m_1 - m_2)^2 \bar{c}^2/4} \\
&\quad \frac{(k_1 + k_2)^2 + (m_1 + m_2)^2 \bar{c}^2/4}{(k_1 + k_2)^2 + (m_1 - m_2)^2 \bar{c}^2/4} \\
S_{k,m} &= \frac{m^2}{2^{2m-2}} \prod_{p=1}^{[m/2]} \frac{k^2 + \bar{c}^2 (m + 1 - 2p)^2/4}{k^2 + \bar{c}^2 (m - 2p)^2/4}
\end{aligned}$$

with $S_{k,1} = 1$. For convenience, we absorbed a factor in $\tilde{\Psi}_\mu = \Psi_\mu/(2i)^{n-1}$. The large product splits into a intra-string term $S$ and inter-string $D$, i.e. $\prod_{i=1}^{n_s} S_i \prod_{i<j}^{n_s} D_{ij}$. This expression was obtained by computing with Mathematica the norms of the states for few particles. What prevents the Gaudin-Korepin formula to be readily used is the fact that the intra-string contributions seems to vanish, and a careful consideration of the finite size corrections has to be taken into account to properly compute the thermodynamic limit [83].

Some checks were performed on low values of $n \leq 3$. For $n = 2$:

$$\begin{aligned}\mathcal{N} &= \int_0^L dx_1 \int_0^L dx_2 [\tilde{\Psi}_{\{\lambda_1,\lambda_2\}}(x_1, x_2)]^2 \\ &= 2! \left[ \frac{\bar{c}^2}{(\lambda_1^2 - \lambda_2^2)^2} + \frac{L^2 (2\lambda_1^2 (\bar{c}^2 - \lambda_2^2) + (\bar{c}^2 + \lambda_2^2)^2 + \lambda_1^4)}{4 (\lambda_1^2 - \lambda_2^2)^2} \right. \\ &\left. - \frac{\bar{c} L (\bar{c}^2 + \lambda_1^2 + \lambda_2^2)}{(\lambda_1^2 - \lambda_2^2)^2} \right]\end{aligned} \tag{2.28}$$

Inserting a single 2-string one finds (up to subdominant terms):

$$\mathcal{N} = \frac{k^2 + \bar{c}^2/4}{\bar{c} k^2} L$$

while two 1-strings have a norm:

$$\mathcal{N} = \frac{((k_1 - k_2)^2 + \bar{c}^2)((k_1 + k_2)^2 + \bar{c}^2)}{2(k_1 - k_2)^2 (k_1 + k_2)^2} L^2$$

both in agreement with the conjecture. Similar computations on low values of $n$ confirm it as well.

For the amplitudes $|\Psi(x)|^2$, the general case for $x > 0$ does not seem easily accessible. The limit $x \to 0$ is much simpler:

$$\begin{aligned}\tilde{\Psi}_\lambda(x, ...x) &= n! x^n \lambda_1 .. \lambda_n + O(x^{n+1}) \\ &= n! x^n \prod_{j=1,n_s} A_{k_j,m_j} + O(x^{n+1}) \\ A_{k,m} &= \prod_{a=1}^{m} \left( k + i \frac{\bar{c}}{2} (m + 1 - a) \right) = (-i\bar{c})^m \frac{\Gamma(\frac{1+m}{2} + \frac{ik}{\bar{c}})}{\Gamma(\frac{1-m}{2} + \frac{ik}{\bar{c}})}\end{aligned} \tag{2.29}$$

To ensure the dominant contribution is of order $O(1)$, we rescale the moments from now on and define:

$$\tilde{Z}_V(x, x, t) = \lim_{x \to 0^+} \frac{1}{x^2} Z_V(x, x, t)$$

#### 2.3.3.2 Performing the summation of $\mathcal{Z}_n$

We have now:

$$\mathcal{Z}_n := \overline{\tilde{Z}_V(x, x, t)^n} = \sum_\mu \frac{1}{x^{2n}} \tilde{\Psi}_\mu(x, ..x) \tilde{\Psi}_\mu(x, ..x)^* \frac{1}{||\tilde{\Psi}_\mu||^2} e^{-tE_\mu}$$

Gathering the previous results Eq.2.27 and Eq.2.29 , the (rather lengthy) starting point

to the Fredholm determinant structure is:

$$\begin{aligned}
\mathcal{Z}_n &= \sum_{n_s=1}^{n} \frac{\bar{c}^n n!}{n_s!(\bar{c})^{n_s}} 2^{n_s} \times \\
\sum_{(m_1,..,m_{n_s})_n} \prod_{j=1}^{n_s} \int \frac{dk_j}{(2\pi)} \frac{B_{k_i,m_i}}{4m_i} e^{(m_j^3-m_j)\frac{\bar{c}^2 t}{12} - m_j k_j^2 t} \prod_{i<j}^{n_s} C_{k_i,m_i,k_j,m_j} & \qquad (2.30) \\
B_{k,m} &= \prod_{j=0}^{m-1} (4k^2 + j^2\bar{c}^2) \\
C_{k_1,m_1,k_2,m_2} &= \frac{(k_1-k_2)^2 + (m_1-m_2)^2\bar{c}^2/4}{(k_1-k_2)^2 + (m_1+m_2)^2\bar{c}^2/4} \times \\
&\quad \frac{(k_1+k_2)^2 + (m_1-m_2)^2\bar{c}^2/4}{(k_1+k_2)^2 + (m_1+m_2)^2\bar{c}^2/4}
\end{aligned}$$

The generating function $g(s)$ can be written as:

$$\begin{aligned}
g(s) &= 1 + \sum_{n_s=1}^{\infty} \frac{1}{n_s!} \tilde{Z}(n_s, s) \\
\tilde{Z}(n_s, s) &= \sum_{(m_1,..,m_{n_s})_n}^{\infty} (-1)^{\sum_p m_p} \prod_{p=1}^{n_s} \int_{k_p} \frac{dk_p}{2\pi} \frac{B_{m_p,k_p}}{4ik_p} \\
&\quad \prod_{i<j}^{n_s} C_{k_i,m_i,k_j,m_j} e^{\frac{t}{12} m_p^3 - m_p k_p^2 t - \lambda m_p s}
\end{aligned}$$

As forecast, resumming $g(s)$ involves exhibiting algebraic structures through formula expressing large products in terms of determinants. As an example, the initial works opening the way for a possible summation [43] used the so-called double alternant Cauchy formula:

$$\det\left[\frac{1}{x_i + y_j}\right] = \frac{\prod_{i<j}(x_i - x_j)(y_i - y_j)}{\prod_{i,j}(x_i + y_j)}$$

It does not seem to help in the present case. One has to rely on Pfaffian identities instead, following the impressive variant presented in [41, 11] for the flat geometry.

We now work in units where $\bar{c} = 1$. It is known that [11]:

$$\prod_{i<j}^{n_s} C_{k_i,m_i,k_j,m_j} = \prod_{j=1}^{n_s} \frac{m_j}{2ik_j} \operatorname{pf}\left(\frac{X_i - X_j}{X_i + X_j}\right)_{2n_s \times 2n_s} \qquad (2.31)$$

$$X_{2p-1} = m_p + 2ik_p \quad p = 1, ..n_s \qquad (2.32)$$

$$X_{2p} = m_p - 2ik_p \quad p = 1, ..n_s \qquad (2.33)$$

using Schur's identity:

$$\operatorname{pf}\left(\frac{X_i - X_j}{X_i + X_j}\right)_{2n \times 2n} = \prod_{1 \le i < j \le 2n} \frac{X_i - X_j}{X_i + X_j}$$

This identity virtually doubles the number of variables. One possible route is to duplicate the $n_s$ variables $(k_p, m_p)$, $p = 1, ..n_s$ to $2n_s$ variables with the rules $g_{2p-1} = g_{2p} = m_p$ and $Q_{2p-1} = k_p = -Q_{2p}$. This gives:

$$\begin{aligned} Z(n_s, s) = & \sum_{g_i \geq 1} (i)^{\sum_j g_j} \prod_{j=1}^{2n_s} \int_{Q_j} \prod_{q=0}^{g_j - 1} (2iQ_j + q) e^{\frac{1}{2}[\frac{\lambda^3}{3}(g_j^3 - g_j) - 4g_j Q_j^2 \lambda^3 - \lambda g_j s]} \\ & \times \prod_{p=1}^{n_s} \delta_{g_{2p}, g_{2p-1}} \frac{2\pi}{4iQ_{2p-1}} \delta(Q_{2p} + Q_{2p-1}) \\ & \times \mathrm{pf} \left( \frac{2iQ_i + g_i - 2iQ_j - g_j}{2iQ_i + g_i + 2iQ_j + g_j} \right)_{2n_s \times 2n_s} . \end{aligned} \tag{2.34}$$

The $\delta$-function in Eq.2.34 enforce the rules of duplication stated above. Their product over $p$ can be rewritten as a Pfaffian as well. The above expression is invariant by permutation of the $(g, Q)$ variables, provided that the duplication $g_{2p-1} = g_{2p}$ and $Q_{2p-1} = -Q_{2p}$ is preserved. Hence symmetrizing the product over the set of partitions of $(1, \cdots n_s)$ into pairs without regard to order (the $\frac{1}{(2n_s-1)!!}$ arising as the number of pairings of $2n_s$ objects) leads to:

$$\begin{aligned} & \prod_{p=1}^{n_s} \delta_{g_{2p}, g_{2p-1}} \frac{2\pi}{4iQ_{2p-1}} \delta(Q_{2p} + Q_{2p-1}) = \\ & \frac{1}{(2n_s - 1)!!} \mathrm{pf} \left( \frac{2\pi}{4iQ_i} \delta(Q_i + Q_j)(-1)^{g_i} \delta_{g_i, g_j} \right)_{2n_s \times 2n_s} \end{aligned}$$

We are left with:

$$\begin{aligned} Z(n_s, s) = & \frac{1}{(2n_s - 1)!!} \sum_{g_i \geq 1} (i)^{\sum_j g_j} \prod_{j=1}^{2n_s} \int_{Q_j} \prod_{q=0}^{g_j - 1} (2iQ_j + q) \times \\ & e^{\frac{1}{2}[\frac{\lambda^3}{3}(g_j^3 - g_j) - 4g_j Q_j^2 \lambda^3 - \lambda g_j s]} \\ & \times \mathrm{pf} \left( \frac{2\pi}{4iQ_i} \delta(Q_i + Q_j)(-1)^{g_i} \delta_{g_i, g_j} \right)_{2n_s \times 2n_s} \\ & \times \mathrm{pf} \left( \frac{2iQ_i + g_i - 2iQ_j - g_j}{2iQ_i + g_i + 2iQ_j + g_j} \right)_{2n_s \times 2n_s} \end{aligned} \tag{2.35}$$

Using the representation:

$$\frac{X_i - X_j}{X_i + X_j} = 2 \int_{v_i > 0, v_j > 0} \delta'(v_i - v_j) e^{-v_i X_i - v_j X_j}$$

one can take the integration out of the second Pfaffian thanks to the identity [11]:

$$\begin{aligned} & \mathrm{pf} \left( \int dv_i dv_j a_i(v_i) a_j(v_j) \, B_{ij}(v_i, v_j) \right) \\ & \qquad = \left[ \prod_i^{n_s} \int dv_i a_i(v_i) \right] \mathrm{pf} \left( B_{ij}(v_i, v_j) \right) \end{aligned}$$

an extended version of $\mathrm{pf}(BAB^T) = \det(B)\,\mathrm{pf}(A)$. Using again Eq.2.36, but this time to force the summation and integration over $v_i$ and $k_p$ inside the first Pfaffian, and reverting to the old variables $(k_j, m_j)$, one finds:

$$Z(n_s,s) = \frac{1}{(2n_s-1)!!}\prod_{j=1}^{2n_s}\int_{v_j>0}\mathrm{pf}(f(v_i,v_j))_{2n_s\times 2n_s} \times \mathrm{pf}(\delta'(v_i-v_j))_{2n_s\times 2n_s} \tag{2.36}$$

with the kernel:

$$f(v_1,v_2) = \sum_{m=1}^{\infty}\int\frac{dk}{2\pi}\frac{(-1)^m B_{k,m}}{2ik}e^{m^3\frac{\lambda^3}{3}-4mk^2\lambda^3-\lambda ms} \times e^{-m(v_1+v_2)-2ik(v_1-v_2)} \tag{2.37}$$

The product of the two Pfaffians can be rewritten in one, by using a block diagonal matrice of size $4n_s$ to obtain an explicit Fredholm pfaffian[5]:

$$Z(n_s,s) = \prod_{j=1}^{2n_s}\int_{v_j>0}\mathrm{pf}\begin{pmatrix} K_{11}(v_i;v_j) & 0 \\ 0 & K_{22}(v_i;v_j)\end{pmatrix}_{4n_s\times 4n_s}$$

with

$$K_{11} = \sum_{m=1}^{\infty}\int\frac{dk}{2\pi}\frac{(-1)^m B_{k,m}}{2ik}e^{m^3\frac{\lambda^3}{3}-4mk^2\lambda^3-\lambda ms}$$
$$K_{22} = 2\delta'(v_i-v_j). \tag{2.38}$$

We now need to take care of the sum of exponentials appearing in the kernel $f(v_1,v_2)$, and especially cancel the divergent part. The so-called Airy trick tames the divergence by removing the cubic dependence of $m$:

$$\int dy 2^{1/3}Ai(2^{1/3}y)e^{ym} = e^{m^3/6}$$

Rescaling $v_j \to \lambda v_j$ and $k_j \to k_j/\lambda$ with a shift $y \to y+s+v_1+v_2$ gives the new "regularized" kernel:

$$f(v_1,v_2) = \int\frac{dk}{2\pi}\int_y Ai(y+s+v_1+v_2+4k^2) \times f_{k/\lambda}(e^{\lambda y})\frac{e^{-2ik(v_1-v_2)}}{2ik} \tag{2.39}$$

$$f_k(z) = \sum_{m=1}^{\infty} b_{k,m}(-z)^m \tag{2.40}$$

[5]Note that our definition of the Pfaffian of a matrix Kernel $K_{ab}(v_1,v_2) = K(a,v_1;b,v_2)$ assumes the order $1,v_1;1,v_2;..1,v_{2n_s};2,v_1;2,v_2;..2;v_{2n_s}$.

The weight function is central in computing the long-time limit:

$$f_k[z] = \sum_{m=1}^{\infty} \prod_{q=0}^{m-1} (4k^2 + q^2)(-z)^m \tag{2.41}$$

more specifically, the limit $\lim_{\lambda\to\infty} f_{k/\lambda}[e^{\lambda y}]$. Unfortunately, this alternating serie grows too fast to uniquely define a function. However that, after analytical continuation, $f_k$ can be seen as the asymptotic expansion of a well-defined function.

First, assume $y > 0$, and write Eq.2.41 in a more compact form using:

$$\begin{aligned} \Gamma[t+n] &= t(t+1)\cdots(t+n-1)\Gamma[t] \\ \Gamma[t]\Gamma[1-t] &= \frac{\pi}{\sin \pi t} \end{aligned}$$

leading to:

$$f_k[z] = \frac{2k \sinh(2k\pi)}{\pi} \sum_{m=1}^{\infty} \Gamma(m+2ik)\Gamma(m-2ik)(-z)^m \tag{2.42}$$

One can convert the alternating series into a integral on the complex plane by a Mellin-Barnes representation:

$$\sum_{m=1}^{\infty} (-1)^m f(m) = -\frac{1}{2i} \int_C ds \frac{f(s)}{\sin(\pi s)} ds$$

where $C$ is a contour around the positive x-axis, hence picking all the strictly positive pole of the sinus but avoiding 0. Here $f(s) = \Gamma(s+2ik)\Gamma(s-2ik)z^s$. Because this integrand has no pole in the half-plane $Re(s) > 0$, we can deformed $C$ into a contour along the imaginary axis $\epsilon + i\mathbb{R}$[6]. This procedure transforms Eq.2.42 into:

$$f_k[z] = \frac{-k \sinh(2k\pi)}{\pi i} \int_{\epsilon-i\infty}^{\epsilon+i\infty} \frac{\Gamma(t+2ik)\Gamma(t-2ik)z^t}{\sin(\pi t)} dt \tag{2.43}$$

In the long-time limit $\lambda \to \infty$, Eq.2.43 can be computed by a limit inversion and the application of Cauchy formula. Closing the contour on the negative real half-plane, the poles of the integrands are $t = \pm 2k\, i/\lambda$ and $t = 0$. It leads to:

$$\lim_{\lambda\to\infty} f_{k/\lambda}[e^{\lambda y}] = -1 + \cos(2ky) \tag{2.44}$$

For $y < 0$, both $k$ and $z$ vanish and the above continuation converges to 0. Note that a closed form of Eq.2.42 exists and could formally be used to calculate the distribution $f$ at all times:

$$\begin{aligned} f_k[z] &= \frac{2k \sinh(2k\pi)}{\pi} \sum_{m=1}^{\infty} \Gamma(m+2ik)\Gamma(m-2ik)(-z)^m \\ &= \frac{2\pi k}{\sinh(4\pi k)} \left( J_{-4ik}(\frac{2}{\sqrt{z}}) + J_{4ik}(\frac{2}{\sqrt{z}}) \right) \\ &- {}_1F_2\left(1; 1-2ik, 1+2ik; -1/z\right) \end{aligned} \tag{2.45}$$

[6]More details can be found in [90].

Nonetheless, it is not clear if this summation procedure leads to a proper asymptotic expansion for $\lambda$ finite. It would certainly be an important point to check it numerically, but it is hindered by the difficulty of evaluating numerically the multiple integrals of the kernel Eq.2.39.

The generating function $g(s)$ simply takes the form:

$$g(s) = \mathrm{pf}[J+K] \quad J = \begin{pmatrix} 0 & I \\ -I & 0 \end{pmatrix} \quad K = \begin{pmatrix} K_{11} & 0 \\ 0 & -K_{22} \end{pmatrix} \tag{2.46}$$

Following the procedure, and after several manipulations detailed in [11], computing the square $g(s)^2$ leads to:

$$g(s)^2 = \det[I - JK] = \det[I + K] \tag{2.47}$$

with $K(v_1, v_2) = -2\partial_{v_1} f(v_1, v_2)\theta(v_1)\theta(v_2)$. Hence we obtain:

$$g(s) = \sqrt{\det[I+K]} \tag{2.48}$$

In principle, Eq.2.48 gives access to the probability distribution of $\ln Z$ *for all time*. We refer to the related paper for the complete expression and pursue the study of the asymptotic behaviour for $\lambda \to \infty$. Using Eq.2.44, the large time kernel turns into:

$$\begin{aligned} K(v_1, v_2) &= -2\partial_{v_1} f_\infty(v_1, v_2) \\ &= -\int \frac{2k}{2\pi} \int_{y>0} Ai(y + s + v_i + v_j + k^2) e^{-i(v_i - v_j)k} (1 - e^{iky}) \end{aligned} \tag{2.49}$$

Integrating the first term in the above equation gives the more familiar expression:

$$\begin{aligned} g(s)^2 &= \det[I - P_u K P_u] \ , \quad u = 2^{-2/3} s \\ K(v_1, v_2) &= K_{Ai}(v_1, v_2) - \frac{Ai(v_1)}{2} \int_{y>0} Ai(y + v_2) \end{aligned} \tag{2.50}$$

where $K_{Ai}(v_1, v_2)$ is the Airy Kernel:

$$K_{Ai}(v_1, v_2) = \int_{y>0} Ai(v_1 + y) Ai(v_2 + y) \tag{2.51}$$

Eq.2.50 is the generating function of a well-known distribution, in disguise. It can be rewritten as:

$$g(s)^2 = \frac{1}{4} \left( \det[I - B_s] + \det[I + B_s] \right)^2 \tag{2.52}$$

with $B_s(x, y) = Ai(x + y + s)\theta(x)\theta(y)$. Finally, in [91], it was shown that Eq.2.52 corresponds to the Tracy-Widom distribution $F_4$ describing the fluctuations of the largest eigenvalue of the Gaussian Symplectic Ensemble (GSE) ! Note that a similar result for the Polynuclear Growth Model with specific nucleation rates has been obtained in [92] in the half-space geometry. This allows us to assert that the half-space case presents universal features, amongst them the height fluctuations distribution $F_4$.

## 2.4 Conclusion

In this Chapter, we provided some insight into the KPZ universality class through the study of its continuum representative, the KPZ equation. An expansion from the linear EW regime allows to scrutinize the rise of the non-linearities as the essential mechanism for the notably anomalous values of the scaling exponents. Tools for tackling the non perturbative strong disorder regime in $d = 1 + 1$ were introduced and much detailed.

We stress that those tools should be amenable to the whole cosmos of integrable models and their scope exceeds beyond the standard polymers geometries, droplet [43] or flat [11]. Integrability can be retained with other disorder distributions, and other initial or boundary conditions. An illustration of that fact is given in Section 2.3.3, where the boundary conditions are changed to half space. This modification, one of the few available exact results in confined geometry [92], leads to a new distribution for the fluctuations, $F_4$. Yet again, some mysterious connections with random matrices seem to be at play. This results gives a better understanding of the scope of the universality of the fluctuations: more specifically, while details of the disorder or of the evolution rules have little influence on those distributions, both initial and boundary conditions do play an essential role.

Those systems possess hidden structures that somehow lend themselves to analytical approaches. Much could be said about the more general conceptual framework in which integrable probabilities are embedded. Unfortunately, a detailed account of those works would take us too far and we refer to [93, 78, 57]. While recent years have unearthed a tremendous amount of connections with apparently unrelated objects (symmetric polynomials, random matrices, quantum field theories), the emergence of a coherent picture is still inchoate, but exciting to witness.

# Short-time growth of a Kardar-Parisi-Zhang interface with flat initial conditions

Thomas Gueudré,[1] Pierre Le Doussal,[1] Alberto Rosso,[2] Adrien Henry,[2] and Pasquale Calabrese[3]
[1]*CNRS–Laboratoire de Physique Théorique de l'Ecole Normale Supérieure, 24 rue Lhomond, 75231 Paris Cedex, France*
[2]*CNRS–Université Paris-Sud, LPTMS, UMR 8626, Bâtiment 100, 91405 Orsay Cedex, France*
[3]*Dipartimento di Fisica dell'Università di Pisa and INFN, 56127 Pisa, Italy*
(Received 6 August 2012; published 31 October 2012)

The short-time behavior of the $(1+1)$-dimensional Kardar-Parisi-Zhang (KPZ) growth equation with a flat initial condition is obtained from the exact expressions for the moments of the partition function of a directed polymer with one end point free and the other fixed. From these expressions, the short-time expansions of the lowest cumulants of the KPZ height field are exactly derived. The results for these two classes of cumulants are checked in high-precision lattice numerical simulations. The short-time limit considered here is relevant for the study of the interface growth in the large-diffusivity or weak-noise limit and describes the *universal* crossover between the Edwards-Wilkinson and the KPZ universality classes for an initially flat interface.

DOI: 10.1103/PhysRevE.86.041151 PACS number(s): 05.40.−a, 05.20.−y, 05.70.Np

## I. INTRODUCTION

The growth of interfaces in the presence of noise can be classified into several universality classes. When the growth rate does not depend on the slope of the interface, the growth process falls in the simplest Edwards-Wilkinson (EW) class. When instead the growth rate is slope dependent (e.g., in the so-called lateral growth), the process falls into the class defined by the nonlinear continuum Kardar-Parisi-Zhang (KPZ) equation [1,2]

$$\partial_t h = \nu\nabla^2 h + \frac{1}{2}\lambda_0(\nabla h)^2 + \xi(x,t), \tag{1}$$

where $h(x,t)$ is the interface height, $\nu$ the diffusivity, and $\lambda_0$ the strength of the slope-dependent growth (with $\lambda_0 = 0$ giving the EW model). $\xi(x,t)$ is the stochastic noise, chosen as a centered Gaussian with short-range correlations:

$$\overline{\xi(x,t)\xi(x',t')} = R_\xi(x-x')\delta(t-t'), \tag{2}$$

where $\int_x R_\xi(x)dx = D$. Concerning the space dependence, the most usual choice is to take uncorrelated random disorder, i.e., $R_\xi(x-x') = D\delta(x-x')$.

In one spatial dimension, the KPZ universality class shows a fairly robust anomalous scaling exponent [3] for the fluctuations of the height of the interface $h(x,t) \sim t^{1/3}$ and indeed such anomalous behavior at large time has been proved for several discrete solvable models [4–7] which are believed to belong to the KPZ class. However, this exponent is only one of the facets of the universality of the KPZ equation: further universal information is encoded in the full probability distribution function (PDF) of these fluctuations, but their exact calculation is an extremely difficult task which is complicated by the fact that, even after a long time, the system keeps some memory of the initial conditions. Remarkably, these initial conditions can be classified in a few subclasses, each leading to a distinct universal result for the statistics of the height field at large time [8,9]. Impressive theoretical progress has been recently achieved and has led to exact solutions directly of the continuum KPZ equation for a wedge (or droplet) [10–13] and flat [14,15] and stationary [16] initial conditions. In the first two cases the PDF of the height $h(x,t)$ at a given point converges at large time to the so-called Tracy-Widom Gaussian unitary ensemble (GUE) and Gaussian orthogonal ensemble (GOE) universal distributions [17], for droplet and flat initial conditions, respectively. Further impetus to the field has been given by recent experiments on turbulent liquid crystals [18,19] in which these two long-time predictions have been confirmed with high accuracy.

In the literature, much emphasis has been given to the long-time limit, mainly because of the connection with random matrix theory valid for all models belonging to the KPZ class. However, in the general case the scale of the fluctuations heavily depends on the microscopic details of the model: for instance, the exact values of the mean and the variance of the height fluctuations are known only for a few solvable discrete models. On the contrary, the limit of high diffusivity or weak noise allows complete determination of the scale of the fluctuations as a function of only three parameters $\lambda_0$, $\nu$, and $D$. All the other microscopic details such as the disorder correlations or the lattice effects are relevant only at very short times, $t < t_f$. In particular the above mentioned exact solutions for the KPZ height distributions are valid for arbitrary times $t > t_f$ in the limit of high diffusivity.

Indeed, these solutions can be expressed in terms of Fredholm determinants with rather complicated kernels, from which it is not always easy to extract the limiting behavior for long and short times. It is then interesting to obtain, by simpler means, the small-time behavior in an explicit form, and to confirm it in numerical simulations. This has been achieved in the case of the droplet initial conditions [11,20], and the aim of this paper is to present a similar result in the case of the flat initial condition. As discussed in more detail below, there are generically three time regimes:

(i) a nonuniversal very-short-time regime $t \sim t_f$ where the growth depends on the short-scale details of the system [e.g., small deviations from the flat initial condition, the precise form of $R_\xi(x)$, etc., . . .];

(ii) a short-time regime $t_f \ll t \ll t^*$ where the crossover from the EW to the KPZ regime takes place;

(iii) a large-time regime $t \gg t^*$ where KPZ scaling holds.

In the high-diffusivity limit, since $t^*$ is fixed to be very large, the height distribution can be exactly computed for all times $t \gg t_f$. Conversely, in the low-diffusivity limit, the height

 

distribution depends on the microscopic details of the system for all times and, when $t \to \infty$, these nonuniversal details affect only the typical scale of the height fluctuations, which are Tracy-Widom distributed.

The paper is organized as follows. In the next section we discuss the mapping of the KPZ equation to the directed polymer. In Sec. III, we report the small-time expansion of the moments of the partition function of the directed polymer (DP) obtained in Ref. [15] and we check them in numerical simulations. In Sec. IV we calculate analytically the small-time expansion of the connected moments of the height field and in Sec. V we check them by numerical simulations. Three Appendices contain some more technical calculations.

## II. MAPPING TO THE DIRECTED POLYMER

Via the Cole-Hopf transformation, the KPZ equation (1) can be mapped onto the directed polymer in a random environment which is an equilibrium statistical physics problem [1,21,22]. A growth starting from a droplet initial condition is mapped onto a fixed-end-point polymer, while a flat initial surface translates to a directed polymer with one end point fixed and the other free [15]. Indeed, the canonical partition function of a directed polymer $x(\tau)$ at temperature $T$ in a random environment is defined in the continuum by the path integral

$$Z(x,t|y,0) = \int_{x(0)=y}^{x(t)=x} Dx e^{-(1/T)\int_0^t d\tau[(1/2)(dx/d\tau)^2 + V(x(\tau),\tau)]}, \tag{3}$$

and maps to the KPZ equation after the identifications

$$\frac{\lambda_0}{2\nu} h = \ln Z, \quad 2\nu = T, \quad \lambda_0 \xi(x,t) = -V(x,t). \tag{4}$$

A Gaussian noise $\xi(x,t)$ corresponds to a random potential $V(x,t)$ which is a centered Gaussian with correlator $\overline{V(x,t)V(x',t)} = R_V(x-x')\delta(t-t')$ with $R_V(x) = \lambda_0^2 R_\xi(x)$. The white noise in the KPZ equation corresponds in polymer language to disorder with $\delta$ correlations,

$$\overline{V(x,t)V(x',t)} = \bar{c}\delta(t-t')\delta(x-x'), \quad \bar{c} = D\lambda_0^2. \tag{5}$$

This mapping is valid in the bulk and does not depend on the KPZ initial condition which translates into conditions for the end points of the polymer. For the KPZ equation with flat initial condition, one should consider the partition sum with one fixed end point (at $x$) and another free (at $y$) [14,15], resulting in the partition function

$$Z(x,t) = \int_{-\infty}^{\infty} dy Z(x,t|y,0). \tag{6}$$

The recent analytical progress has been made possible by the calculation of the moments $\overline{Z(x,t)^n}$ of the DP partition sum. By replicating the partition function $Z(x,t)$, the DP is mapped [23] onto the quantum mechanics of a bosonic system of $n$ particles interacting with an attractive $\delta$-function potential, i.e., the celebrated Lieb-Liniger model [24]. This model is integrable via the Bethe ansatz and the eigenstates are known for both repulsive [24] and attractive interactions [25], which is the case of our interest. The moments can be expressed as a sum over these eigenstates [14,15] (generically labeled by $\mu$ in the following),

$$\overline{Z(x,t)^n} = \sum_\mu \frac{\Psi_\mu^*(x,\ldots,x)}{\|\mu\|^2} e^{-tE_\mu} \times \int_{-\infty}^{\infty} \prod_{j=1}^{n} dy_j \Psi_\mu(y_1,\ldots,y_n), \tag{7}$$

in terms of the many-body wave function $\Psi_\mu(y_1,\ldots,y_n)$ and of the eigenenergies $E_\mu$ of the state $\mu$. In the infinite system the eigenstates are easily enumerated, being organized in clusters of bound particles, called strings. The norms of the states $\|\mu\|$ and the equal-point wave functions have simple expressions [26] and lead to a time-dependent PDF starting from a droplet initial condition [11,12]. The integral over the $y_i$ in Eq. (7), necessary to treat the flat initial condition, is more delicate but was handled in Refs. [14,15], leading to the moments $\overline{Z(x,t)^n}$ for arbitrary $n$. From these the moment's generating function at all times has been written in terms of a Fredholm Pfaffian [14,15] (the square root of a Fredholm determinant). This allowed a proof that the PDF of $\ln Z(x,t)$, i.e., of the height field $h(x,t)$, converges at large times to the GOE Tracy-Widom distribution.

Here we follow a different route. We recall in the next section the exact expressions for the lowest moments $n = 2,3,4$ and from them we extract the small-time cumulants of $\ln Z$, i.e., of the KPZ height field.

## III. Moments $\overline{Z^n}$ AND THEIR SMALL-TIME BEHAVIOR

For a flat initial condition, the one-point distribution of $Z(x,t)$ does not depend on $x$ because of translational invariance. Thus in the following, we simply denote

$$Z \equiv Z(x,t). \tag{8}$$

Since we are dealing with an initially flat interface we must have $\overline{Z^n} = 1$ at $t = 0$ (which is a nontrivial condition in terms of the Bethe ansatz). Taking the average of Eq. (3) over the Gaussian disorder gives the mean partition function

$$\overline{Z(x,t|y,0)} = \frac{1}{\sqrt{2\pi T t}} e^{-(x-y)^2/2Tt} e^{[R_V(0)/2T^2]t}, \tag{9}$$

and so from the integral in Eq. (6) we have

$$\overline{Z} = e^{v_0 t} \quad \text{with} \quad v_0 = \frac{R_V(0)}{2T^2}. \tag{10}$$

To eliminate this nonuniversal (self-energy) contribution, it is convenient to define

$$z = Z/\overline{Z}, \tag{11}$$

which by construction satisfies $\overline{z} = 1$ at all times. (Note that in Ref. [15] the self-energy contribution was omitted, but we indicate it here explicitly for later purposes. What is called $Z$ in Ref. [15] is thus $z$ here.) This will be useful later for comparison with the numerical simulation of lattice models.

All results for the continuum DP and KPZ models are expressed in terms of a dimensionless parameter

$$\lambda = \left(\frac{t}{4t^*}\right)^{1/3} \quad \text{with} \quad t^* = \frac{2T^5}{\bar{c}^2} = \frac{2(2\nu)^5}{D^2\lambda_0^4}, \tag{12}$$

where, in the language of the DP, $t^*$ is the crossover time scale between the Brownian diffusion at small time (i.e., $\lambda < 1$) and the glassy large-time behavior (i.e., $\lambda > 1$). Within the context of the growth model, $t^*$ is the crossover scale between Edwards-Wilkinson and KPZ regimes. Note that a spatial crossover scale can also be defined as $x^* = \sqrt{\nu t^*} = T^3/\bar{c} = (2\nu)^3/D^2\lambda_0^2$. Both scales become very large in the large-diffusivity limit or, equivalently, in the weak-noise limit.

It is important to recall that for any given microscopical model with a cutoff (e.g., a lattice model) there are additional time and space scales. The easiest example is the same continuum KPZ equation (or DP model) with disorder correlated over a nonzero correlation length $r_f$, i.e., $R_\xi(x)$ is a function decaying on a scale $r_f$. Then, it is easily shown [11] that if $x^* \gg r_f$ one can replace $R_\xi(x) \to D\delta(x)$ in which $D = \int dx R_\xi(x)$. More generally, the condition for the existence of the universal short-time regime studied here is that $t^*$ and $x^*$ must be much larger than any characteristic microscopic scale—generically called $r_f$ and $t_f$ here—such as the lattice spacing for a lattice model. Note also that if the initial condition is not perfectly flat on scales of the order of $r_f$, this will also not affect any result as long as $x^* \gg r_f$. Of course, the very short time and space regime with $t \leqslant t_f$ and $x \leqslant r_f$ is nonuniversal.

We now recall the results of Ref. [15] for the four lowest moments, together with their small-time (i.e., small-$\lambda$) behavior:

$$\overline{z^2} = e^{2\lambda^3}[1 + \mathrm{erf}(\lambda^{3/2}\sqrt{2})] = 1 + 2\sqrt{\frac{2}{\pi}}\lambda^{3/2} + 2\lambda^3 + \frac{8}{3}\sqrt{\frac{2}{\pi}}\lambda^{9/2} + O(\lambda^6), \quad (13)$$

with (note the misprint in Ref. [15] for the definition of the error function) $\mathrm{erf}(z) = \frac{2}{\sqrt{\pi}}\int_0^z dt e^{-t^2}$,

$$\overline{z^3} = 4e^{8\lambda^3} - 2e^{2\lambda^3} - 2e^{8\lambda^3}\mathrm{erfc}(\lambda^{3/2}2\sqrt{2}) + e^{2\lambda^3}\mathrm{erfc}(\lambda^{3/2}\sqrt{2}) = 1 + 6\sqrt{\frac{2}{\pi}}\lambda^{3/2} + 14\lambda^3 + 40\sqrt{\frac{2}{\pi}}\lambda^{9/2} + O(\lambda^{11/2}), \quad (14)$$

with $\mathrm{erfc}(x) = 1 - \mathrm{erf}(x)$, and finally

$$\overline{z^4} = 8e^{20\lambda^3} - 8e^{8\lambda^3} - 4e^{20\lambda^3}\mathrm{erfc}(3\sqrt{2}\lambda^{3/2}) - 4e^{8\lambda^3}[-2\mathrm{erfc}(2\lambda^{3/2}) + e^{12\lambda^3}\mathrm{erfc}(4\lambda^{3/2})] + 48\int_0^\infty dx \frac{\left(\frac{2x+1}{\sqrt{4x+1}} - \frac{\sqrt{2x+1}}{x+1}\right)e^{-8\lambda^3 x}}{4\pi[4x(x+3)+5]} \quad (15)$$

$$= 1 + 12\sqrt{\frac{2}{\pi}}\lambda^{3/2} + \left(44 + \frac{24}{\pi}\right)\lambda^3 + 8(21 + 8\sqrt{2})\sqrt{\frac{2}{\pi}}\lambda^{9/2} + O(\lambda^6), \quad (16)$$

where the series expansion of the integral is performed in Appendix A.

Before embarking on the calculation of the cumulants of $\ln Z$, we now report the results of numerical simulations for the determination of $\overline{z^n}$ for $n = 2,3$. As explained in more detail in Sec. V, the simulations are performed for a directed polymer on a square lattice. We also consider the high-temperature limit, which ensures that all details of the lattice become irrelevant and the results can be expressed as functions of the single parameter $\lambda$. The procedure and the identification of $\lambda$ on the lattice have been introduced already in Refs. [11,27] and are described again in Sec. V. We report the numerical data for $\overline{z^n}$ in Fig. 1 which are found to be in excellent agreement with our analytic predictions up to $\lambda \approx 0.6$, while some deviations at larger $\lambda$ are evident. These deviations are caused by the undersampling due to the growing importance of the tails in the distribution of $z$, and will be properly explained in Sec. V.

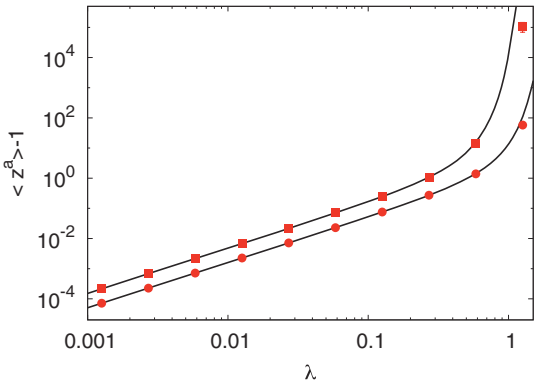


FIG. 1. (Color online) From top to bottom the moments $\overline{z^3} - 1$ (solid line, red squares) and $\overline{z^2} - 1$ (solid line, red circles) for different values of $\lambda$. Solid lines correspond to the analytical predictions in Eqs. (13) and (14). Averages are performed over $15 \times 10^6$ samples of size $t = 512$ and $\bar{c} = 1$. There are no adjustable parameters.

## IV. CUMULANTS OF ln $Z$ AT SMALL TIME

From the above formulas for $\overline{z^n}$ and following the procedure described in Appendix B, we obtain the small-$\lambda$ (i.e., small-time) expansion of the first four cumulants of the free energy:

$$\overline{\ln z} = -\sqrt{\frac{2}{\pi}}\lambda^{3/2} + \left(\frac{5}{3} - \frac{6}{\pi}\right)\lambda^3 + \left(\frac{106}{3} - 16\sqrt{2} - \frac{40}{\pi}\right)\sqrt{\frac{2}{\pi}}\lambda^{9/2} + O(\lambda^6), \quad (17)$$

$$\overline{(\ln z)^2}^c = 2\sqrt{\frac{2}{\pi}}\lambda^{3/2} + \left(\frac{20}{\pi} - 6\right)\lambda^3 + \left(\frac{176\sqrt{2}}{3} + \frac{512}{3\pi} - \frac{412}{3}\right)\sqrt{\frac{2}{\pi}}\lambda^{9/2} + O(\lambda^6), \quad (18)$$

$$\overline{(\ln z)^3}^c = \frac{8(\pi - 3)\lambda^3}{\pi} + \left(248 - 96\sqrt{2} - \frac{352}{\pi}\right)\sqrt{\frac{2}{\pi}}\lambda^{9/2} + O(\lambda^6), \quad (19)$$

$$\overline{(\ln z)^4}^c = \left[64\sqrt{2} + \frac{320}{\pi} - 192\right]\sqrt{\frac{2}{\pi}}\lambda^{9/2} + O(\lambda^6), \quad (20)$$

and of course $\overline{(\ln Z)^p}^c = \overline{(\ln z)^p}^c$ for $p \geqslant 2$. As explained in Appendix B, in order to compute the next term $O(\lambda^6)$ in the small-time expansion, or the fifth and higher cumulants, we would need the fifth moment $\overline{z^5}$ that we did not analyze here, but which is in principle known [15]. A simple check can be performed on these formulas, namely, one can compute the

series expansion in $\lambda^{3/2}$ of $\exp[\sum_{p=1}^{4} \frac{n^p}{p!}\overline{(\ln z)^p}^c]$ and check that the expansion of all $\overline{z^n}$ for $n = 1,2,3,4$ given above is reproduced up to order $o(\lambda^{9/2})$. Although this procedure also allows the derivation of Eqs. (17)–(20) by adjusting the coefficients of the series expansion in $\lambda^{3/2}$, the method described in Appendix B is more systematic.

For short times, the dominant term in the PDF is the variance $\overline{(\ln z)^2}^c$ which increases as $t^{1/2}$. Using $\ln Z = \lambda_0 h/(2\nu)$, one finds

$$\overline{h^2}^c = D\sqrt{\frac{t}{2\pi\nu}} + O(\lambda_0^2 t). \tag{21}$$

Hence the first term of the expansion of $\overline{h^2}^c$ is independent of $\lambda_0$, the coefficient of the nonlinear growth in the KPZ equation. It corresponds to the Edwards-Wilkinson Gaussian scaling regime $\delta h \sim t^{1/4}$, also found in Appendix C; cf. Eq. (C3), where we derive the leading short-time behavior for the average height and variance using perturbation theory directly on the KPZ equation.

The third and fourth cumulants behave as $t$ and $t^{3/2}$, respectively, suggesting that the fourth cumulant is subdominant and that the first corrections to the EW Gaussian scaling are given by the third cumulant as $\delta h \sim t^{1/3}$, which is the form of the KPZ scaling. Indeed, it is interesting that the third cumulant is linear in $t$ *at both short and long times* (but with an amplitude going from $\frac{8(\pi-3)}{\pi} = 0.360\,563$ to $\mu_3^{\rm GOE} = 0.598\,268$; see below).

From the above we can compute the skewness

$$\begin{aligned}\gamma_1 &= \frac{\overline{(\ln Z)^3}^c}{[\overline{(\ln Z)^2}^c]^{3/2}} = \frac{2^{3/4}(\pi-3)}{\sqrt[4]{\pi}}\lambda^{3/4} \\ &\quad + \frac{\pi(67-48\sqrt{2}+9\pi)-86}{(2\pi)^{3/4}}\lambda^{9/4} + O(\lambda^{15/4}) \\ &= 0.178\,865\cdots\lambda^{3/4} + 0.0138\cdots\lambda^{9/4} + O(\lambda^{15/4}),\end{aligned} \tag{22}$$

which at short times scales as $\gamma_1 \sim t^{1/4}$, and the kurtosis

$$\begin{aligned}\gamma_2 &= \frac{\overline{(\ln Z)^4}^c}{[\overline{(\ln Z)^2}^c]^2} = (40-24\pi+8\sqrt{2}\pi)\sqrt{\frac{2}{\pi}}\lambda^{3/2} + O(\lambda^3) \\ &= 0.115\,565\cdots\lambda^{3/2} + O(\lambda^3),\end{aligned} \tag{23}$$

which scales as $t^{1/2}$.

Now we recall that at large time one can write [14,15]

$$\frac{\lambda_0 h}{2\nu} = \ln Z = v_\infty t + \lambda\eta_t, \tag{24}$$

such that $\eta_t$ converges to the GOE Tracy-Widom (TW) distribution $\lim_{t\to\infty} \mathrm{Prob}(\eta_t < s) = F_1(s)$. The skewness and kurtosis thus converge for large times to their GOE values

$$\gamma_1 \to \gamma_1^{\rm GOE} = 0.293\,464\,524\,08\ldots, \tag{25}$$

$$\gamma_2 \to \gamma_2^{\rm GOE} = 0.165\,242\,938\,4\ldots, \tag{26}$$

consistent with a crossover for $\lambda \approx 1.6 \pm 0.3$. The amplitude of the (nonfluctuating) linear term is nonuniversal, $v_\infty = v_0 - \bar{c}^2/12 = v_0 - D^2\lambda_0^4/12$, where $v_0 = \frac{R_V(0)}{2T^2} = \frac{\lambda_0^2 R_\xi(0)}{8\nu^2}$ is the amplitude at short time (after the very-short-time regime $t \gg t_f$). Note that the difference $v_\infty - v_0$ is universal. At large time one also has that $\overline{\ln z} = \overline{\ln Z} - \ln\overline{Z} = \lambda\mu_1 - D^2\lambda_0^4 t/12$ is universal, where $\mu_1^{\rm GOE} = -1.206\,533\,574\,582\,0\ldots$ is the mean of the TW distribution, while $\overline{(\ln Z)}^c \to \lambda^2\mu_2$ where $\mu_2^{\rm GOE} = 1.607\,781\,034\,581\ldots$ is the variance of the TW distribution.

## V. NUMERICAL RESULTS

Numerical simulations are performed for the square lattice model depicted in Fig. 2. Directed paths grow along the diagonals of the lattice with only (0,1) or (1,0) moves (hard constraint condition), starting at (0,0) and with the second end left free. With each site of the lattice is associated an independent and identically distributed random number $V(x,t)$ (here we use a Gaussian distribution with variance equal to 1). The time coordinate is given by $t = i + j$ and the space coordinate by $x = (i - j)/2$ (see Fig. 2). The partition sum over all paths $\gamma_t$ growing from (0,0) up to time $t$ is defined as

$$Z(t) = \sum_{\gamma_t} \exp\left[-\beta \sum_{(x,\tau)\in\gamma_t} V(x,\tau)\right]. \tag{27}$$

The partition function satisfies the following transfer matrix recurrence relation implemented in our simulation:

$$Z_{x,t+1} = (Z_{x-1/2,t} + Z_{x+1/2,t})e^{-\beta V_{x,t+1}}, \tag{28}$$

with $Z_{x,0} = \delta_{x,0}$. The free end partition function is computed by summing over all end points $Z(t) = \sum_x Z(x,t)$. To avoid numerical instabilities we divide all partition functions at fixed $\tau$ by the biggest one and record its logarithmic value. As in the model in the continuum, on the lattice also $Z(x,t)$ grows exponentially in time, as can be seen by averaging the sum over all possible paths:

$$\overline{Z(t)} = \sum_{\gamma_t}\prod_{x\in\gamma_t}\overline{e^{-\beta V(x)}} = 2^t e^{\beta^2 t/2}. \tag{29}$$

For this reason we work numerically with the ratio $\ln(z) = \ln(Z/\overline{Z})$, which remains small, but exhibits strong fluctuations.

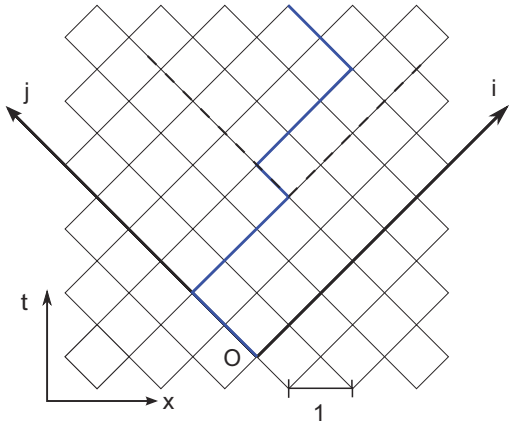


FIG. 2. (Color online) Sketch of the directed polymer model analyzed in numerical simulations. The blue solid line corresponds to a polymer growing over the square lattice under the hard constraint condition.

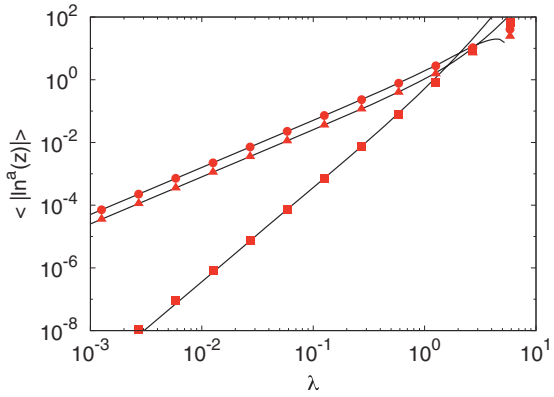


FIG. 3. (Color online) From top to bottom, the cumulants ($15 \times 10^6$ samples) $\overline{\ln^2 z}^c$ (solid line, red circles), $-\overline{\ln z}^c$ (solid line, red triangles), and $\overline{\ln^3 z}^c$ (solid line, red squares) for $t = 512$. The solid lines are the analytical predictions in Eqs. (17)–(19) up to $O(\lambda^{9/2})$, with $\overline{c} = 1$. There are no adjustable parameters.

In the limit of high $T$, the statistical fluctuations of $z$ depend only on the unique dimensionless variable

$$\lambda = \left(\frac{\overline{c}^2 \kappa t}{8T^5}\right)^{1/3}, \tag{30}$$

which is the lattice version of Eq. (12). Note that the scaling $T \to T/\kappa, \overline{c} \to \overline{c}/\kappa^2$ allows one to go from the discrete model variables Eq. (30) to the continuous model variables Eq. (12).

In the high-temperature regime, the parameters $\kappa$ and $\overline{c}$ can be computed explicitly [27]. Indeed $\overline{c}^2$ is just the variance of the uncorrelated random numbers. Instead $\kappa$ can be extracted from the model without disorder, for which the polymer behaves like a particle diffusing on a one-dimensional lattice ($x$ being the particle position at time $t$). The mean square displacement of the particle is given by $\langle x^2(t)\rangle_T = Tt/\kappa$. Within the normalization used in this paper, we have $\kappa = 4T$.

Using this algorithm, we have numerically computed the cumulants on the square lattice at high temperature and compared them with the analytic predictions in Eqs. (17)–(19). The data for $\overline{\ln^n z}^c$ for $n = 1,2,3$ are reported in Fig. 3. The

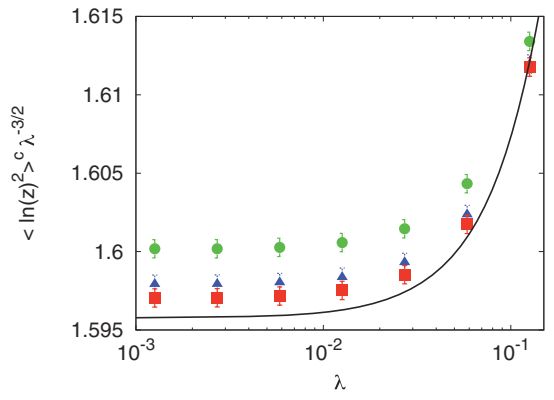


FIG. 4. (Color online) Finite-size effects for $\overline{\ln^2 z}^c$. Solid line, analytical prediction Eq. (18). Numerical data, from top to bottom, $t = 128$ (green circles), $t = 256$ (blue triangles), $t = 512$ (red squares). Averages are performed over $15 \times 10^6$ samples with $\overline{c} = 1$.

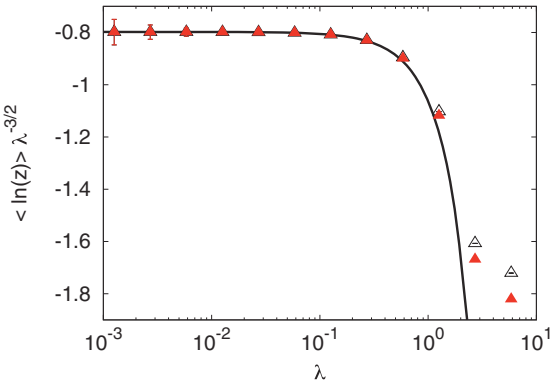


FIG. 5. (Color online) Finite-size effects for $\overline{\ln z}^c$. Solid line, analytical prediction Eq. (17). Numerical data, from top to bottom, $t = 256$ (empty triangles), $t = 512$ (full triangles). Averages are performed over $15 \times 10^6$ samples with $\overline{c} = 1$. The large error bars when $\lambda < 10^{-2}$ are due to the vanishing value of $\overline{\ln z}^c$ as $\lambda \to 0$.

agreement with the analytical predictions is excellent, which is even more impressive when we consider that these figures are produced *without any fit parameter*. In Figs. 4 and 5 we show in more detail the convergence to the theoretical value for a fixed value of $\lambda$ as a function of polymer length. The increase of the polymer length $t$ is equivalent to heating up the system, hence approaching the universal prediction of the high-temperature regime.

The analytical predictions for the moments of $z$ are exact for all $\lambda$. However, we can see in Fig. 1 that precision is quickly lost above the threshold $\lambda \sim 1$. This is due to the fact that, for large $\lambda$, typical values of $z$ strongly differ from the average value $\overline{z} = 1$. The moments of $z$ are then dominated by rare occurrences of very large $z$ induced by the presence of heavy tails. This is shown in Fig. 6 where we see that, as $\lambda$ grows, the mode of the distribution quickly goes to 0 while the tail becomes fatter. A simple example of this peculiar behavior lies in the log-normal probability distribution which is characterized by an exponentially small typical value and a

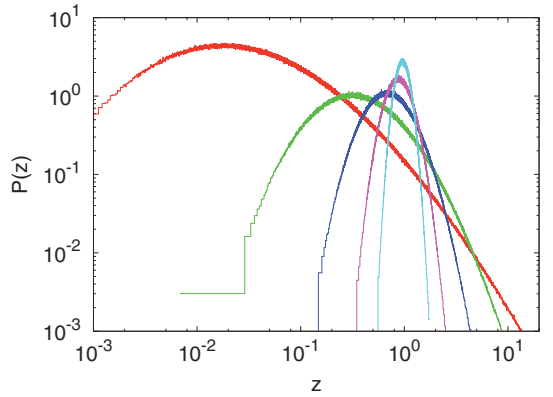


FIG. 6. (Color online) $P(z)$ with $z = Z/\overline{Z}$ for $\lambda = 1.26, 0.58, 0.27, 0.126$, and $0.058$, from left to right. Histograms are obtained from numerical simulations with $t = 512$, $\overline{c} = 1$, and $15 \times 10^6$ samples. When $\lambda$ is very small, $P(z)$ is self-averaging. When $\lambda$ grows, a heavy tail is developed and $z_{\text{typ}} \ll \langle z \rangle = 1$.

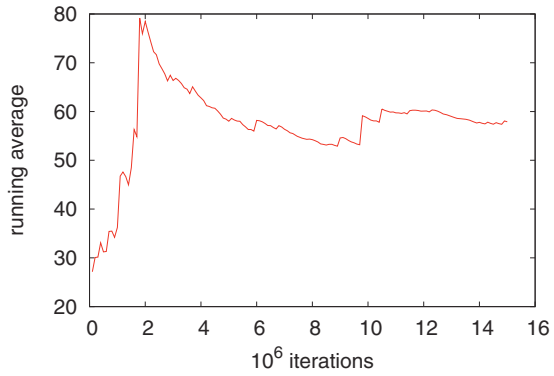


FIG. 7. (Color online) Estimator of $\overline{z^2}-1$ given by $M_N = (1/N)\sum_{i=1}^{N} z_i^2 - 1$, where $z_i$ is the rescaled partition function of a single disorder realization and $N$ is the number of realizations (iterations), for $\lambda = 1.26$. The sudden variations around $10 \times 10^6$ samples shows that one *single* event contributes to a finite fraction (around 10%) of the whole sum.

heavy tail $\sim e^{-\ln^2 z}$. Here, for large $\lambda$, the heavy tail behaves as $e^{-\ln^{3/2} z}$ with the exponent $3/2$ corresponding to the Tracy-Widom asymptotic behavior. In practice, because of this tail, the moment estimators converge extremely slowly, even for important sampling. An example is shown in Fig. 7, where we estimate $\overline{z^2}-1$ for $\lambda = 1.26$ with $N = 15 \times 10^6$ samples. While the prediction from Eq. (18) is $\overline{z^2}-1 = 109.023$, we found a value around 60 from numerical simulations. This discrepancy is explained by the central limit theorem which predicts fluctuations of order $\sim(\overline{z^4}/N)^{1/2}$. Using Eq. (20), we see that $\overline{z^4}$ grows very fast in $\lambda$ and would require $N = 10^{14}$ samples for us to have a good estimation of $\overline{z^2}$ for $\lambda = 1.26$.

## VI. CONCLUSION

In this paper we have studied the stochastic KPZ equation with flat initial conditions and extracted from the results of Ref. [15] the short-time behavior of the connected moments of the distribution of the height field at a given point. In this way, we have been able to probe universality specifically with respect to the introduction of a short scale in the noise correlations, or a discretization in the DP model. A wider domain of investigation, ranging from step bunching instabilities in crystal growth to ballistic deposition (see, e.g., Ref. [5]) and going beyond the goals of this work, is to prove the universality in a broader sense (including, e.g., change in the nonlinear KPZ term, as in Ref. [28], or biased diffusion current, as in Ref. [29]).

The importance of the results presented here stems from the proof of the existence of a short-time *universal* regime which describes the crossover from the Edwards-Wilkinson to the KPZ growth and which can be observed when the diffusivity is large or the noise is weak. We have compared our analytical predictions to high-precision numerical simulations of a discrete model, which shows how this universality arises. Apart from the theoretical interest *per se*, these predictions, valid for all times, should be useful also in future experiments in which the parameters of the growth could be varied and controlled in a more refined way so as to easily access this universal crossover.

## APPENDIX A: EXPANSION OF AN INTEGRAL

We need to compute the small-$\lambda$ expansion of the integral

$$I = \int_0^\infty dx f(x) e^{-8\lambda^3 x}, \tag{A1}$$

where $f(x)$ and its large-$x$ expansion are

$$f(x) = 48\frac{\left(\frac{2x+1}{\sqrt{4x+1}} - \frac{\sqrt{2x+1}}{x+1}\right)}{4\pi(4x(x+3)+5)} = \frac{3}{\pi}x^{-3/2} - \frac{3(21+8\sqrt{2})}{8\pi}x^{-5/2} + O(x^{-7/2}). \tag{A2}$$

It is convenient to write

$$I = \int_0^\infty dx f(x) + \int_0^\infty dx \frac{3}{\pi x^{3/2}}(e^{-8\lambda^3 x} - 1) + \int_0^\infty dx f_1(x)(e^{-8\lambda^3 x} - 1), \tag{A3}$$

with $f_1(x) = f(x) - 3x^{-3/2}/\pi$. Two integrals are easily done, giving

$$I = 1 - 12\sqrt{\frac{2}{\pi}}\lambda^{3/2} + \int_0^\infty dx f_1(x)(e^{-8\lambda^3 x} - 1), \tag{A4}$$

and the remaining integral is $O(\lambda^3)$. This can again be written as

$$\begin{aligned}\int_0^\infty dx f_1(x)(e^{-8\lambda^3 x} - 1) &= (-8\lambda^3)\int_0^\infty dx x f_1(x) + \int_0^\infty dx f_1(x)(e^{-8\lambda^3 x} - 1 + 8\lambda^3 x) \\ &= \left(44 + \frac{24}{\pi}\right)\lambda^3 + \int_0^\infty dx f_1(x)(e^{-8\lambda^3 x} - 1 + 8\lambda^3 x),\end{aligned} \tag{A5}$$

where the remaining integral is now $O(\lambda^{9/2})$ and can be split again as

$$\begin{aligned}\int_0^\infty dx f_1(x)(e^{-8\lambda^3 x} - 1 + 8\lambda^3 x) &= \int_0^\infty dx\left[-\frac{3(21+8\sqrt{2})}{8\pi}x^{-5/2}\right](e^{-8\lambda^3 x} - 1 + 8\lambda^3 x) \\ &+ \int_0^\infty dx f_2(x)(e^{-8\lambda^3 x} - 1 + 8\lambda^3 x),\end{aligned} \tag{A6}$$

with

$$f_2(x) = f_1(x) + \frac{3(21+8\sqrt{2})}{8\pi}x^{-5/2}. \tag{A7}$$

Thus, putting together the three pieces, we have

$$I = 1 - 12\sqrt{\frac{2}{\pi}}\lambda^{3/2} + \left(44 + \frac{24}{\pi}\right)\lambda^3 - 8(21+8\sqrt{2})\sqrt{\frac{2}{\pi}}\lambda^{9/2} + O(\lambda^6). \tag{A8}$$

## APPENDIX B: FROM THE MOMENTS OF $Z$ TO THE MOMENTS OF $\ln Z$

In general the knowledge of the moments $\overline{z^n}$ for some low integer $n$ does not allow one to extract much information about the cumulants $\overline{(\ln z)^n}^c$. In the present case, however, for small time (small $\lambda$), $z$ is concentrated around its mean value $\overline{z}=1$ and this allows one to obtain the behavior of the cumulants at small times.

Let us write $z=1+u$ with $\overline{u}=0$ and compute its connected moments. In order to lighten the notation we introduce the notation $\mu_p \equiv \overline{z^p}^c$. Using the expressions for $\overline{z^n}^c$ in the main text, $\overline{u^n}^c$ are given by

$$\mu_2 = \overline{u^2} = \overline{z^2} - 1 = 2\sqrt{\frac{2}{\pi}}\lambda^{3/2} + 2\lambda^3 + \frac{8}{3}\sqrt{\frac{2}{\pi}}\lambda^{9/2} + O(\lambda^6), \quad \text{(B1)}$$

$$\mu_3 = \overline{u^3} = (\overline{z^3}-1) - 3(\overline{z^2}-1) = 8\lambda^3 + 32\sqrt{\frac{2}{\pi}}\lambda^{9/2} + O(\lambda^6), \quad \text{(B2)}$$

$$\mu_4 = \overline{u^4}^c = \overline{z^4} - 1 - 4(\overline{z^3}-1) + 6(\overline{z^2}-1) - 3(\overline{z^2}-1)^2 = 64\sqrt{2}\sqrt{\frac{2}{\pi}}\lambda^{9/2} + O(\lambda^6). \quad \text{(B3)}$$

Given the above trend it is reasonable to assume that $\overline{z^p}^c = \overline{u^p}^c = O((\lambda^{3/2})^{p-1})$. Based on this assumption, we want to construct a systematic series expansion of $\overline{(\ln z)^n}^c$ in powers of the cumulants of $z$. The reasoning is the following. First we write

$$\sum_{n=1}^{\infty}\frac{r^n}{n!}\overline{(\ln z)^n}^c = \ln\overline{z^r} = \ln\overline{(1+u)^r} = \ln\left(1+\sum_{k=1}^{\infty}\frac{r(r-1)\cdots(r-k+1)}{k!}\overline{u^k}\right). \quad \text{(B4)}$$

Expanding the right-hand side in powers of $r$, we obtain formally each $\overline{(\ln z)^n}^c$ as an (infinite) series of the moments $\overline{u^k}$. The moments $\overline{u^k}$ can themselves be expressed as functions of the cumulants $\mu_p$ by writing

$$\overline{e^{wu}} = 1 + \sum_{k=2}^{\infty}\frac{w^m}{m!}\overline{u^m} = \exp\left(\sum_{p=2}^{\infty}\frac{w^p}{p!}\mu_p\right), \quad \text{(B5)}$$

and identifying them order by order in $w$. We can now replace $\mu_p \to a^{p-1}\mu_p$ where $a$ is to be set to unity at the end. This replacement allows us to keep track of the order in $\lambda^{3/2}$ of each cumulant. Using MATHEMATICA, it is now simple to first generate the expansion (B5), truncate it to a given order in $a$, and then insert it in Eq. (B4). During this process, we see that, e.g., $\overline{u^4} = O(a^2) = \overline{u^3}$, i.e., in Eq. (B4) one must keep a few more orders compared to Eq. (B5). Since we have not computed $\overline{z^5} = O(a^4)$, we can get our cumulants only up to order $a^3$. Doing so we obtain

$$\overline{\ln(z)} = -\frac{a\mu_2}{2} + a^2\left(\frac{\mu_3}{3} - \frac{3\mu_2^2}{4}\right) + a^3\left(-\frac{5\mu_2^3}{2} + 2\mu_3\mu_2 - \frac{\mu_4}{4}\right) + O(a^4), \quad \text{(B6)}$$

$$\overline{\ln(z)^2}^c = a\mu_2 + a^2\left(\frac{5\mu_2^2}{2} - \mu_3\right) + a^3\left(\frac{32\mu_2^3}{3} - 8\mu_3\mu_2 + \frac{11\mu_4}{12}\right) + O(a^4), \quad \text{(B7)}$$

$$\overline{\ln(z)^3}^c = a^2\left(\mu_3 - 3\mu_2^2\right) + a^3\left(-22\mu_2^3 + 15\mu_3\mu_2 - \frac{3\mu_4}{2}\right) + O(a^4), \quad \text{(B8)}$$

$$\overline{\ln(z)^4}^c = a^3\left(20\mu_2^3 - 12\mu_3\mu_2 + \mu_4\right) + O(a^4). \quad \text{(B9)}$$

Setting $a=1$ and replacing the $\mu_p$ by their actual values above, we find the result given in the text.

## APPENDIX C: SHORT-TIME PERTURBATION THEORY FOR THE KPZ EQUATION

As a further final check, we recover here the leading short-time behavior for the first and second cumulants of the height directly from the perturbative expansion of the KPZ equation. We start from the second cumulant, which is easier. The KPZ equation can be studied in perturbation in $\lambda_0$, which is equivalent to short time. This is clear from the definition of $\lambda$ in Eq. (12) which gives the perturbative parameter $\lambda^{3/2} \propto \sqrt{t/t^*} \propto \sqrt{t}\lambda_0^2$. We can write $h = h^{(0)} + h^{(1)} + \cdots$ where $h^{(n)} = O(\lambda_0^n)$. With the flat initial condition, the lowest order is just the Edwards-Wilkinson result, which in Fourier space is

$$h^{(0)}_{q,t} = \int_0^t dt_1 e^{-\nu q^2(t-t_1)}\xi_{q,t_1}; \quad \text{(C1)}$$

this leads to the variance

$$\overline{h^{(0)}_{q,t}h^{(0)}_{q',t}} = 2\pi\delta(q+q')\int_0^t dt_1 e^{-2\nu q^2 t_1}\tilde{R}_\xi(q), \quad \text{(C2)}$$

where $\tilde{R}_\xi(q)$ is the Fourier transform of the noise correlator $R(x)$, assumed to be of range $r_f$ in space. Then simple algebra gives

$$\overline{h^{(0)}(x,t)^2} = \int\frac{dq}{2\pi}\int_0^t dt_1 e^{-2\nu q^2 t_1}\tilde{R}_\xi(q) = \int\frac{dq}{2\pi}\tilde{R}_\xi(q)\frac{1-e^{-2\nu q^2 t}}{2\nu q^2} = \frac{D}{\sqrt{\nu}}\sqrt{\frac{t}{2\pi}}, \quad \text{(C3)}$$

where the last equation is valid for $t \gg r_f^2/\nu$, i.e., away from the (nonuniversal) very-short-time regime. Here $D = \tilde{R}_\xi(q=0) = \int dx\, R(x)$ is the only memory of the short-scale details and thus for $t \gg t_f$ one can set $\tilde{R}_\xi(q=0) = D$, i.e., we have a $\delta$ correlator in space. Using the correspondence $\ln Z = \lambda_0 h/(2\nu)$ and $\lambda^{3/2} = D\lambda_0^2(t/8)^{1/2}/(2\nu)^{5/2}$ one recovers exactly the leading term in Eq. (21).

The discussion of the average height $\overline{h}$ is more subtle because we need to retain $R_\xi(x)$ in an essential way, as there are nonuniversal contributions. For a flat initial condition, $\overline{h(x,t)}$

is $x$ independent; hence the following equation is exact at all times:

$$\partial_t \overline{h} = \frac{\lambda_0}{2}\overline{(\nabla h)^2}. \tag{C4}$$

At small time we can use

$$\partial_t \overline{h} = \frac{\lambda_0}{2}\overline{(\nabla h^{(0)})^2} = \frac{\lambda_0}{4\nu}\int_q \tilde{R}_\xi(q)(1-e^{-2\nu q^2 t}). \tag{C5}$$

Splitting this term in two pieces and integrating each of them separately over time, we obtain

$$\overline{h} = \frac{\lambda_0 R(0)}{4\nu}t - \frac{\lambda_0}{4\nu}\int \frac{dq}{2\pi}\tilde{R}_\xi(q)\frac{1-e^{-2\nu q^2 t}}{2\nu q^2}. \tag{C6}$$

One recognizes the same integral entering the second moment, and so for $t \ll t^*$ we have

$$\overline{h} = v_0 t - \frac{\lambda_0}{4\nu}\overline{h^2}, \tag{C7}$$

which indeed reproduces exactly, for $t \gg t_f$, the leading *negative* correction in Eq. (17). The first term linear in time is, however, always present, and nonuniversal. The same exact term arises in the DP, and corresponds to the multiplicative contribution to the moments $\overline{Z^n} = e^{tn(1/2T^2)R_V(0)} \equiv e^{tn(\lambda_0^2/8\nu^2)R_\xi(0)}$ arising from the equal replica (self-energy) terms after averaging the replicated partition sum. Although usually dropped, these terms are present and correspond to an additive (nonuniversal) nonrandom correction $\frac{\lambda_0^2}{8\nu^2}R_\xi(0)t$ to $\ln Z$.


[1] M. Kardar, G. Parisi, and Y. C. Zhang, Phys. Rev. Lett. **56**, 889 (1986).

[2] A.-L. Barabasi and H. E. Stanley, *Fractal Concepts in Surface Growth* (Cambridge University Press, Cambridge, 1995); J. Krug, Adv. Phys. **46**, 139 (1997).

[3] D. A. Huse, C. L. Henley, and D. S. Fisher, Phys. Rev. Lett. **55**, 2924 (1985).

[4] K. Johansson, Commun. Math. Phys. **209**, 437 (2000).

[5] M. Prahofer and H. Spohn, Phys. Rev. Lett. **84**, 4882 (2000); J. Stat. Phys. **108**, 1071 (2002); **115**, 255 (2004).

[6] J. Baik and E. M. Rains, J. Stat. Phys. **100**, 523 (2000).

[7] P. L. Ferrari, Commun. Math. Phys. **252**, 77 (2004).

[8] I. Corwin, arXiv:1106.1596.

[9] P. L. Ferrari and H. Spohn, arXiv:1003.0881

[10] T. Sasamoto and H. Spohn, Phys. Rev. Lett. **104**, 230602 (2010); Nucl. Phys. B **834**, 523 (2010); J. Stat. Phys. **140**, 209 (2010).

[11] P. Calabrese, P. Le Doussal, and A. Rosso, Europhys. Lett. **90**, 20002 (2010).

[12] V. Dotsenko, Europhys. Lett. **90**, 20003 (2010); J. Stat. Mech. (2010) P07010; V. Dotsenko and B. Klumov, *ibid.* (2010) P03022.

[13] G. Amir, I. Corwin, and J. Quastel, Commun. Pure Appl. Math **64**, 466 (2011).

[14] P. Calabrese and P. Le Doussal, Phys. Rev. Lett. **106**, 250603 (2011).

[15] P. Le Doussal and P. Calabrese, J. Stat. Mech. (2012) P06001.

[16] T. Imamura and T. Sasamoto, Phys. Rev. Lett. **108**, 190603 (2012); J. Phys. A **44**, 385001 (2011).

[17] C. A. Tracy and H. Widom, Commun. Math. Phys. **159**, 151 (1994).

[18] K. A. Takeuchi and M. Sano, Phys. Rev. Lett. **104**, 230601 (2010); K. A. Takeuchi, M. Sano, T. Sasamoto, and H. Spohn, Sci. Rep. (Nature) **1**, 34 (2011).

[19] L. Miettinen, M. Myllys, J. Merikosks, and J. Timonen, Eur. Phys. J. B **46**, 55 (2005).

[20] S. Prolhac and H. Spohn, Phys. Rev. E **84**, 011119 (2011).

[21] M. Kardar and Y-C. Zhang, Phys. Rev. Lett. **58**, 2087 (1987); T. Halpin-Healy and Y-C. Zhang, Phys. Rep. **254**, 215 (1995).

[22] J. M. Burgers, *The Non-Linear Diffusion Equation* (Reidel, Dordrecht, 1974); J. Bec and K. Khanin, Phys. Rep. **447**, 1 (2007).

[23] M. Kardar, Nucl. Phys. B **290**, 582 (1987).

[24] E. H. Lieb and W. Liniger, Phys. Rev. **130**, 1605 (1963).

[25] J. B. McGuire, J. Math. Phys. **5**, 622 (1964).

[26] P. Calabrese and J.-S. Caux, Phys. Rev. Lett. **98**, 150403 (2007); J. Stat. Mech. (2007) P08032.

[27] S. Bustingorry, P. Le Doussal, and A. Rosso, Phys. Rev. B **82**, 140201 (2010).

[28] J. Krug and H. Spohn, Phys. Rev. A **38**, 4271 (1988).

[29] A. Pimpinelli, V. Tonchev, A. Videcoq, and M. Vladimirova, Phys. Rev. Lett. **88**, 206103 (2002).

epl A Letters Journal Exploring the Frontiers of Physics

October 2012

EPL, **100** (2012) 26006
doi: 10.1209/0295-5075/100/26006

www.epljournal.org

# Directed polymer near a hard wall and KPZ equation in the half-space

Thomas Gueudré and Pierre Le Doussal

*CNRS-Laboratoire de Physique Théorique de l'Ecole Normale Supérieure - 24 rue Lhomond, 75231 Cedex 05, Paris, France, EU*

received 10 September 2012; accepted 5 October 2012
published online 31 October 2012

PACS 68.35.Rh – Phase transitions and critical phenomena

**Abstract** – We study the directed polymer with fixed endpoints near an absorbing wall, in the continuum and in the presence of disorder, equivalent to the KPZ equation on the half-space with droplet initial conditions. From a Bethe Ansatz solution of the equivalent attractive boson model we obtain the exact expression for the free-energy distribution at all times. It converges at large time to the Tracy-Widom distribution $F_4$ of the Gaussian symplectic ensemble (GSE). We compare our results with numerical simulations of the lattice directed polymer, both at zero and high temperature.



Progress was achieved recently in finding exact solutions in one dimension for noisy growth models in the Kardar-Parisi-Zhang (KPZ) universality class [1,2], and for the closely related equilibrium statistical-mechanics problem of the directed polymer (DP) with quenched disorder [3]. The KPZ class was explored in several recent experiments [4,5], and applications to the DP range from biophysics [6] to describe the glass phase of pinned vortex lines [7] and magnetic walls [8]. The height of the growing interface, $h(x,t)$, corresponds to the free energy of a DP of length $t$ starting at $x$, under a mapping which is exact in the continuum (Cole-Hopf), and for some discrete realizations. Not only the scaling exponents $h \sim t^{1/3}$, $x \sim t^{2/3}$ are known [9,10], but also the one-point (and in some cases the many-point) probability distribution (PDF) of the height [11,12]. Their dependence on the initial condition exhibits remarkable universality at large time, with only a few subclasses, most being related to Tracy-Widom (TW) distributions [13] of the largest eigenvalues of random matrices. Most of these subclasses were initially discovered in a discrete growth model (the PNG model) [14–16] which can be mapped onto the statistics of random permutations [17], and a zero-temperature lattice DP model [10]. Recently, exact solutions were obtained directly in the continuum at arbitrary time $t$, for the droplet [18–21], flat [22,23] and stationary [24] initial conditions. The PDF of the height $h(x,t)$ converges at large time to $F_2$, the Gaussian unitary ensemble (GUE), and to $F_1$, the Gaussian orthogonal ensemble (GOE) universal TW distributions, for droplet and flat initial conditions, respectively. One useful method which led to these solutions introduces $n$ replicas and maps the DP problem to the Lieb Liniger model, *i.e.*, the quantum mechanics of $n$ bosons with delta-function attraction, a model solved using the Bethe Ansatz.

The KPZ equation on the half-line $x > 0$, equivalently a DP in the presence of a wall, is also of great interest. In the statistical-mechanics context, constrained fluctuations are important for the study of fluctuation-induced (Casimir) forces [25,26] and for extreme value statistics. In the surface growth context one can study an interface pinned at a point, or an average growth rate which jumps across a boundary. The half-space problem was previously studied in a discrete version, for the (symmetrized) random permutations/PNG model [27,28] and found to involve also TW distributions in the limit of large system size. In order to exhibit full KPZ universality, it is important to solve the problem directly in the continuum, *i.e.*, for the KPZ equation itself. Previous approaches did not address the finite time behavior which is also universal[1].

The aim of this letter is to present a solution of the directed polymer problem in the continuum in the presence of a hard wall (absorbing wall) using the Bethe Ansatz (BA). Equivalently, we obtain the one-point height probability distribution for the KPZ equation on the

[1]In the large diffusivity, weak noise regime, equivalently high temperature regime for the DP, see below.

half-line $x>0$ with fixed large negative value of $h$ or of $-\nabla h$ (*i.e.*, a small contact angle) at $x=0$. For simplicity we study a DP with both endpoints fixed —which corresponds to the droplet initial condition in KPZ— near the wall. We do not consider the case of the attractive wall (we briefly mention it at the end). We obtain an exact expression for the generating function of the moments of the DP partition sum as a Fredholm Pfaffian, from which we extract the PDF of the free energy of the DP (height of KPZ) at all times. We then show that this PDF converges to $F_4$, the Tracy-Widom distribution of the largest eigenvalue of the Gaussian symplectic ensemble (GSE). Calculations are performed for the DP, consequences for the KPZ equation are detailed at the end. Our results are checked against numerics on a discrete DP model, both at high and zero temperature, confirming universality. Consequences for extreme value statistics are discussed. This is the first occurrence of the $F_4$ distribution and of the GSE within a continuum BA calculation. It is consistent with the results of [27,28] for the discrete model and confirms that these belong to the same universality class as the continuum KPZ equation on the half-space, solved here for all times.

*Directed polymer: analytical solution.* We consider the partition function of a DP at temperature $T$ in the continuum, *i.e.*, the sum over positive paths $x(\tau)\in R^+$ starting at $x(0)=y$ and ending at $x(t)=x$,

$$Z(x,y,t)=\int_{x(0)=y}^{x(t)=x} Dx(\tau)e^{-\frac{1}{T}\int_0^t \mathrm{d}\tau[\frac{1}{2}(\frac{\mathrm{d}x}{\mathrm{d}\tau})^2+V(x(\tau),\tau)]}, \tag{1}$$

with initial condition $Z(x,y,0)=\delta(x-y)$. The hard wall requires $Z(0,y,t)=Z(x,0,t)=0$. The random potential $V(x,t)$ is a centered Gaussian with correlator $\overline{V(x,t)V(x',t)}=\bar{c}\delta(t-t')\delta(x-x')$. The natural units for the continuum model are $t^*=2T^5/\bar{c}^2$ and $x^*=T^3/\bar{c}$ which allow to remove $T$ and set $\bar{c}=1$ (see footnote [2]). The time (*i.e.*, polymer length) dependence is embedded in a single dimensionless parameter:

$$\lambda=(t/4t^*)^{1/3} \tag{2}$$

as defined in our previous works [19,22,23] and in [20].

Replicating (1) and averaging over disorder, the $n$-th integer moment of the DP partition sum can be expressed [29] as a quantum-mechanical expectation for $n$ particles described by the attractive Lieb-Liniger Hamiltonian [30]

$$H_n=-\sum_{j=1}^n \frac{\partial^2}{\partial x_j^2}-2\bar{c}\sum_{1\leqslant i<j\leqslant n}\delta(x_i-x_j). \tag{3}$$

in natural units (for the moment not rescaling by $\bar{c}$, as in [19]). The moments of the partition sum with both endpoints fixed at $x$ can be written as

$$\overline{Z(x,x,t)^n}=\sum_\mu |\Psi_\mu(x,\dots,x)|^2\frac{e^{-tE_\mu}}{\|\,\mu\,\|^2}, \tag{4}$$

[2] In the final result performing $x\to x/x^*$, $t\to t/t^*$ and in the free energy $F=-T\ln Z$, restores the $T$-dependence.

*i.e.*, a sum over the un-normalized eigenfunctions $\Psi_\mu$ (of norm denoted $\|\,\mu\,\|$) of $H_n$ with energies $E_\mu$. Here we used the fact that only symmetric (*i.e.*, bosonic) eigenstates contribute. In the presence of a hard wall at $x=0$, $\Psi_\mu(x_1,\dots,x_n)$ vanishes when any of the $x_j$ vanishes. It is solved by a generalization of the standard BA [31,32]. The Bethe states $\Psi_\mu$ are superpositions of plane waves [30] over permutations $P$ of the rapidities $\lambda_j$ $(j=1,\dots,n)$, with here an additional summation over $\pm\lambda_j$. The eigenfunctions read

$$\Psi_\mu(x_1,\dots,x_n)=\frac{1}{(2i)^{n-1}}\sum_{P\in S_n}\sum_{\epsilon_2,\dots,\epsilon_n=\pm1}\epsilon_2\dots\epsilon_n$$
$$\times A_{\lambda_{P_1},\epsilon_2\lambda_{P_2},\dots,\epsilon_n\lambda_{P_n}}\sin(x_1\lambda_1)\prod_{j=2}^n e^{i\epsilon_j x_j\lambda_{P_j}}, \tag{5}$$

$$A_{\lambda_1,\dots,\lambda_n}=\prod_{n\geqslant\ell>k\geqslant1}\left(1+\frac{i\bar{c}}{\lambda_\ell-\lambda_k}\right)\left(1+\frac{i\bar{c}}{\lambda_\ell+\lambda_k}\right) \tag{6}$$

for $x_1<\ldots<x_n$, recalling that $\Psi_\mu(x_1,\dots,x_n)$ is symmetric in its arguments. Imposing a second boundary condition at $x=L$, *e.g.*, also a hard wall, one gets Bethe equations [31] which determine the possible sets of $\lambda_j$. The large-$L$ limit was studied in [32] and we do not reproduce the analysis here. The structure of the states is very similar to the standard case, *i.e.*, the general eigenstates are built by partitioning the $n$ particles into a set of $n_s$ bound states formed by $m_j\geqslant1$ particles with $n=\sum_{j=1}^{n_s}m_j$. Each bound state is a perfect string [33], *i.e.*, a set of rapidities $\lambda^{j,a}=k_j+\frac{i\bar{c}}{2}(m_j+1-2a)$, where $a=1,\dots,m_j$ labels the rapidities within the string. Such eigenstates have energy $E_\mu=\sum_{j=1}^{n_s}(m_jk_j^2-\frac{\bar{c}^2}{12}m_j(m_j^2-1))$. The difference with the standard case is that the states are now invariant by flipping any of the momenta $\lambda_j\to-\lambda_j$, *i.e.*, $k_j\to-k_j$.

To simplify the problem, we restrict here to a DP with endpoints near the wall, *i.e.*, we define the partition sum for $x=\epsilon=0^+$, $Z=\lim_{x\to0^+}Z_V(x,x,t)/x^2$. Then, one factor in (4) drastically simplifies as $\lim_{x\to0^+}|\Psi_\mu(x,\dots,x)|^2/x^{2n}=n!^2\lambda_1^2\dots,\lambda_n^2$. The last needed factor in (4) is the norm, usually not trivial to obtain [34]. With some amount of heuristics we arrive at the following formula [35] (we now fully use the natural units, hence setting $\bar{c}=1$):

$$\|\,\mu\,\|^2=n!2^{-n_s}\prod_{i=1}^{n_s}S_{k_i,m_i}\prod_{1\leqslant i<j\leqslant n_s}D_{k_i,m_i,k_j,m_j}L^{n_s},$$
$$S_{k,m}=\frac{m^2}{2^{2m-2}}\prod_{p=1}^{[m/2]}\frac{k^2+(m+1-2p)^2/4}{k^2+(m-2p)^2/4}, \tag{7}$$

$$D_{k_1,m_1,k_2,m_2}=\frac{4(k_1-k_2)^2+(m_1+m_2)^2}{4(k_1-k_2)^2+(m_1-m_2)^2}$$
$$\times\frac{4(k_1+k_2)^2+(m_1+m_2)^2}{4(k_1+k_2)^2+(m_1-m_2)^2}. \tag{8}$$

We now have a starting formula for the integer moments

$$\overline{Z^n} = \sum_{n_s=1}^{n} \frac{n! 2^{n_s}}{n_s!} \times \sum_{(m_1,\ldots,m_{n_s})_n} \prod_{j=1}^{n_s} \int \frac{\mathrm{d}k_j}{2\pi} \frac{b_{k_j,m_j}}{4m_j} e^{(m_j^3-m_j)\frac{t}{12}-m_j k_j^2 t} \times \prod_{1\leqslant i<j\leqslant n_s} D_{k_i,m_i,k_j,m_j} \quad (9)$$

with $b_{k,m} = \prod_{j=0}^{m-1}(4k^2+j^2)$. Here $(m_1,\ldots,m_{n_s})_n$ stands for all the partitioning of $n$ such that $\sum_{j=1}^{n_s} m_j = n$ with $m_j \geqslant 1$ and we used $\sum_{k_j} \to m_j L \int \frac{\mathrm{d}k}{2\pi}$ which holds also here in the large $L$ limit.

This formula allows for predictions at small time. Defining[3] $z = Z/\overline{Z}$ we obtain $\overline{z^2}^c = \overline{z^2} - 1$ as

$$\overline{z^2}^c = \sqrt{\frac{\pi}{2}} e^{2\lambda^3} \left(4\lambda^3+3\right) \lambda^{3/2} (\mathrm{erf}(\sqrt{2}\lambda^{3/2})+1) + 2\lambda^3 = \frac{3}{2}\sqrt{2\pi}\lambda^{3/2} + 8\lambda^3 + O(\lambda^{9/2}) \quad (10)$$

and the short time (*i.e.*, small $\lambda$) expansion of $\overline{z^3}^c = 42.99376\lambda^3$, and

$$\overline{\ln z} = -\frac{3}{2}\sqrt{\frac{\pi}{2}}\lambda^{3/2} - 0.27162097\ \lambda^3, \quad (11)$$

$$\overline{(\ln z)^2}^c = \frac{3}{2}\sqrt{2\pi}\lambda^{3/2} + 0.349154645\ \lambda^3,$$

$$\overline{(\ln z)^3}^c = 0.58226188\ \lambda^3, \quad (12)$$

up to $O(\lambda^{9/2})$ terms. The skewness of the PDF of $\ln z$ behaves at short time as

$$\gamma_1 = \frac{\overline{(\ln z)^3}^c}{(\overline{(\ln z)^2}^c)^{3/2}} \simeq 0.079863175\ \lambda^{3/4}. \quad (13)$$

It is interesting to compare with the same results in ref. [19] in the absence of the hard wall (full space) and we find the universal ratio of the variances at small time:

$$\rho = \frac{\overline{(\ln z)^2}^{c,HS}}{\overline{(\ln z)^2}^{c,FS}} = \frac{3}{2} - 0.076597089\ \lambda^{3/2} + O(\lambda^3) \quad (14)$$

and of the skewness $\gamma_1^{HS}/\gamma_1^{FS} = 0.63689604 + O(\lambda^{3/2})$.

We now study arbitrary time, *i.e.*, any $\lambda$, and to this aim we define the generating function of the distribution $P(f)$ of the scaled free energy $\ln Z = -\lambda f$:

$$g(s) = \overline{\exp(-e^{-\lambda s} Z)} = 1 + \sum_{n=1}^{\infty} \frac{(-e^{-\lambda s})^n}{n!} \overline{Z^n} \quad (15)$$

from which $P(f)$ is immediately extracted at $\lambda \to \infty$:

$$\lim_{\lambda\to\infty} g(s) = \overline{\theta(f+s)} = \mathrm{Prob}\,(f > -s) \quad (16)$$

[3] $\overline{Z} = 1/\sqrt{4\pi t}$ for full space and $\overline{Z} = 1/\sqrt{4\pi}t^{3/2}$ with a hard wall. The non-universal global multiplicative factor [36] $e^{R_V(0)t/(2T^2)}$ does not affect $z$ and was dropped.

and below we recall how it is extracted at finite $\lambda$. The constraint $\sum_{i=1}^{n_s} m_i = n$ in (9) can then be relaxed by reorganizing the series according to the number of strings:

$$g(s) = 1 + \sum_{n_s=1}^{\infty} \frac{1}{n_s!} Z(n_s, s). \quad (17)$$

Solvability arises from the Pfaffian identity:

$$\prod_{1\leqslant i<j\leqslant n_s} D_{k_i,m_i,k_j,m_j} = \prod_{j=1}^{n_s} \frac{m_j}{2ik_j} \mathrm{pf}\left(\frac{X_i - X_j}{X_i + X_j}\right)_{2n_s\times 2n_s}, \quad (18)$$

where $X_{2p-1} = m_p + 2ik_p$, $X_{2p} = m_p - 2ik_p$, $p = 1,\ldots,n_s$, a consequence of Schur's identity as used in refs. [22,23] to which we refer for details. We recall that the pfaffian of an antisymmetric matrix $A$ is defined as $\mathrm{pf}\,A = \sqrt{\det A}$. Equation (18) allows to write the $n_s$ string partition sum as[4]

$$Z(n_s,s) = \sum_{m_1,\ldots,m_{n_s}=1}^{\infty} (-1)^{\sum_p m_p} \prod_{p=1}^{n_s} \int \frac{\mathrm{d}k_p}{2\pi} \frac{b_{m_p,k_p}}{4ik_p} \times e^{m_p^3 \frac{t}{12} - m_p k_p^2 t - \lambda m_p s} \mathrm{pf}\left(\frac{X_i - X_j}{X_i + X_j}\right)_{2n_s\times 2n_s} \quad (19)$$

Now, as in refs. [22,23] we use the representation $\int_{v_i,v_j>0} 2\delta'(v_i - v_j) e^{-v_i X_i - v_j X_j} = \frac{X_i - X_j}{X_i + X_j}$ and standard properties of the Pfaffian allow to take the integral over the $2n_s$ variables outside the Pfaffian. After manipulations very similar to refs. [22,23] the integration and summation over $k_j, m_j$ can be performed, leading to

$$Z(n_s,s) = \frac{1}{(2n_s-1)!!} \prod_{j=1}^{2n_s} \int_{v_j>0} \mathrm{pf}(f(v_i,v_j))_{2n_s\times 2n_s} \cdot \times \mathrm{pf}(\delta'(v_i - v_j))_{2n_s\times 2n_s}, \quad (20)$$

where $(2n_s-1)!! = (2n_s)!/(n_s! 2^{n_s})$ is the number of pairings of $2n_s$ objects, with the kernel:

$$f(v_1,v_2) = \sum_{m=1}^{\infty} \int \frac{\mathrm{d}k}{2\pi} \frac{(-1)^m b_{k,m}}{2ik} e^{m^3\frac{\lambda^3}{3} - 4mk^2\lambda^3 - \lambda m s} \times e^{-m(v_1+v_2) - 2ik(v_1-v_2)}. \quad (21)$$

We used that in the natural units $t(\equiv \frac{t}{t^*}) = 4\lambda^3$. $g(s)$ has now the form of a Fredholm Pfaffian. One shows [35]

$$g(s) = \sqrt{\mathrm{Det}[I + \mathcal{K}]}, \quad (22)$$
$$\mathcal{K}(v_1,v_2) = -2\theta(v_1)\theta(v_2)\partial_{v_1} f(v_1,v_2).$$

It is interesting that $g(s)^2$ is precisely the generating function for the two independent half-spaces (on each side of the hard wall) and that it is itself a Fredholm determinant (FD). Performing the rescaling $v_j \to \lambda v_j$ and $k_j \to k_j/\lambda$ leaves the result (22) unchanged with the scaled

[4] We have performed the usual shift $Z = e^{-c^2 t/12}\hat{Z}$ (we drop the hat below) which does not affect $z = Z/\overline{Z}$.

kernel:

$$f(v_1,v_2) = \int \frac{\mathrm{d}k}{2\pi}\int_y Ai(y+s+v_1+v_2+4k^2) \times f_{k/\lambda}(e^{\lambda y})\frac{e^{-2ik(v_1-v_2)}}{2ik}, \quad (23)$$

where we have used the now standard Airy trick $\int_y Ai(y)e^{wy} = e^{w^3/3}$ to transform the cubic exponential in an exponential, together with the shift $y \to y+s+v_1+v_2$. The weight function $f_k(z) := \sum_{m=1}^{\infty} b_{k,m}(-z)^m$ can be calculated explicitly and we find

$$f_k[z] = \frac{2\pi k}{\sinh(4\pi k)}\left(J_{-4ik}\left(\frac{2}{\sqrt{z}}\right)+J_{4ik}\left(\frac{2}{\sqrt{z}}\right)\right) - {}_1F_2\left(1;1-2ik,1+2ik;-1/z\right). \quad (24)$$

Equations (22), (23) (24) are our result at finite time for $g(s)$.

We now obtain the PDF of the free energy (*i.e.*, of the KPZ height), first at large time, *i.e.*, for $\lambda \to \infty$. Examination of (24) leads to [35]

$$\lim_{\lambda\to\infty} f_{k/\lambda}[e^{\lambda y}] = -\theta(y)(1-\cos(2ky)). \quad (25)$$

Rescaling $k \to k/2$ and taking the derivative in (22) one finds after integrations by part with respect to $y$:

$$g(s)^2 = \mathrm{Det}[I+P_0K_sP_0] = \mathrm{Det}[I+P_{s/2}K_0P_{s/2}],$$
$$K_s(v_i,v_j) = -\int \frac{\mathrm{d}k}{2\pi}\int_{y>0} Ai(y+s+v_i+v_j+k^2) \times e^{-i(v_i-v_j)k}(1-e^{iky}), \quad (26)$$

where $P_x \equiv \theta(v-x)$ projects all $v_j$ integrations on $[x,+\infty[$. Using an Airy function identity [19] we find $K_0(v_i,v_j) = -2^{1/3}\tilde{K}(2^{1/3}v_i, 2^{1/3}v_j)$ and upon rescaling of the $v_i$:

$$g(s)^2 = \mathrm{Det}[I-P_{\mathsf{s}}\tilde{K}P_{\mathsf{s}}], \qquad \mathsf{s} = 2^{-2/3}s, \quad (27)$$
$$\tilde{K}(v_i,v_j) = K_{Ai}(v_i,v_j) - \frac{1}{2}Ai(v_i)\int_{y>0} Ai(y+v_j),$$

where $K_{Ai}$ is the Airy Kernel $K_{Ai}(v_i,v_j) = \int_{y>0} Ai(v_1+y)Ai(v_2+y)$. Our result (27) for the half-space at large time can be compared with the full-space result [18–21] $g_{FS}(s) = \mathrm{Det}[I-P_{\mathsf{s}}K_{Ai}P_{\mathsf{s}}] = F_2(\mathsf{s})$, *i.e.*, the GUE distribution. Hence, the second term (projector) in (27) encodes for the effect of the DP configurations which in full space cross $x=0$ at least once. Interestingly, since i) the set of paths in the full space includes right and left half-space paths, $Z_{FS} > Z_{HS}^{\mathrm{right}} + Z_{HS}^{left}$ and ii) the two half-spaces are statistically independent, this implies, using the definition (16), that

$$g_{FS}(s) < g_{HS}(s)^2, \quad (28)$$

a bound valid at all times (not just for infinite $\lambda$).

We can now transform our result (27). Noting that $\theta(v_1)\theta(v_2)\tilde{K}(v_1+\mathsf{s},v_2+\mathsf{s}) = \mathcal{B}_{\mathsf{s}}^2 - \frac{1}{2}|\mathcal{B}_{\mathsf{s}}\delta\rangle\langle 1\mathcal{B}_{\mathsf{s}}|$, where $\mathcal{B}_{\mathsf{s}}(x,y) := \theta(x)Ai(x+y+\mathsf{s})\theta(y)$ one obtains, via manipulations as in refs. [23,37] using $\langle 1|\frac{1}{1\pm\mathcal{B}_{\mathsf{s}}}|\delta\rangle = \mathrm{Det}(I\mp\mathcal{B}_{\mathsf{s}})/\mathrm{Det}(I\pm\mathcal{B}_{\mathsf{s}})$ and $F_1(\mathsf{s}) = \mathrm{Det}(I-\mathcal{B}_{\mathsf{s}})$, $F_2(\mathsf{s}) = \mathrm{Det}(I-\mathcal{B}_{\mathsf{s}}^2)$:

$$g(s) = \frac{1}{2}\left(F_1(\mathsf{s}) + \frac{F_2(\mathsf{s})}{F_1(\mathsf{s})}\right) = F_4(\mathsf{s}=2^{-2/3}s) \quad (29)$$

in the conventions[5] of ref. [38]. To summarize, for the continuum DP model with fixed endpoints near the hard wall we find

$$\ln z = 2^{2/3}\lambda\ \xi_t, \quad (30)$$

where $z = Z/\overline{Z}$ and $\xi_t$ converges at large time in distribution to the GSE Tracy-Widom distribution $F_4$. The same formula holds for the full space but with $\xi_t$ converging at large time to the GUE distribution $F_2$.

We now obtain the PDF of the free energy at finite time. We follow the method in [19]. It is written as a convolution, *i.e.*, $\ln Z = \ln Z_0 + \lambda u_0$ is the sum of two independent random variables, where $\ln Z_0$ has a unit Gumbel distribution (*i.e.*, $P(Z_0) = e^{-Z_0}$). Then the PDF of $u$ is obtained by analytical continuation $p(u) = \frac{\lambda}{\pi}\mathrm{Im}g(s)|_{e^{\lambda s}\to -e^{\lambda u}+i0^+}$. Using (22), (23) and (24) and some complex analysis we find the free-energy distribution as the difference of two (complex) Fredholm Pfaffians (FP):

$$p(u) = \frac{\lambda}{2i\pi}\left(\sqrt{\mathrm{Det}[I+P_0K_uP_0]} - \sqrt{\mathrm{Det}[I+P_0K_u^*P_0]}\right) \quad (31)$$

with the kernel

$$K_u(v_i,v_j) = \frac{\mathrm{d}}{\mathrm{d}v_i}\int\frac{\mathrm{d}k}{2\pi}\int_y Ai(y+u+v_i+v_j+4k^2) \times \frac{\sin(2(v_i-v_j)k)}{k}[f_{k/\lambda}^r(e^{\lambda y}) + if_{k/\lambda}^i(e^{\lambda y})], \quad (32)$$

$$f_k^r(z) = \frac{\pi k}{\sinh(2\pi k)}\left(I_{-4ik}\left(2\sqrt{\frac{1}{z}}\right)+I_{4ik}\left(2\sqrt{\frac{1}{z}}\right)\right) - {}_1F_2\left(1;1-2ik,1+2ik;\frac{1}{z}\right),$$
$$f_k^i(z) = 4k\sinh(2k\pi)K_{4ik}\left(2\sqrt{\frac{1}{z}}\right). \quad (33)$$

Note that the same formula (31) with each FP replaced by its square, *i.e.*, the FD, holds for the free energy associated to the union of the two independent half-spaces.

*Numerical simulations:* Here we call $\hat{t}$ the (integer) polymer length. At high temperature, we follow [19,36,39] and define the partition sum (PS) $Z(\hat{t}) = \sum_{\gamma_{\hat{t}}} e^{-\frac{1}{T}\sum_{(x,\tau)\in\gamma_{\hat{t}}}V(x,\tau)}$ of paths $\gamma_{\hat{t}}$ directed along the diagonal of a square lattice from $(0,0)$ to $(\hat{t}/2,\hat{t}/2)$ with only $(1,0)$ or $(0,1)$ moves. We denote space $x=(i-j)/2$ and time $\tau = i+j$. An i.i.d. random number $V(x,\tau)$ is defined at each site of the lattice (we use a unit centered Gaussian). The disorder averaged full space PS is $\overline{Z} = N_{\hat{t}}e^{\beta^2\hat{t}/2}$ where $N_{\hat{t}}^{FS} \simeq 2^{\hat{t}}\sqrt{2/(\pi\hat{t})}$ is the number of paths of length $\hat{t}$. The half-space PS is obtained

[5] Other conventions for $F_4$ (*e.g.*, wikipedia) differ by a factor $\sqrt{2}$.

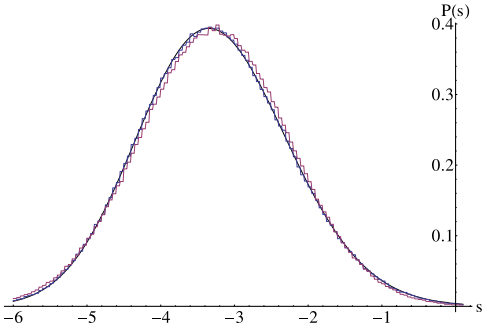


Fig. 1: (Colour on-line) Rescaled PDF of (minus) the free energy at large time. i) Solid line: analytical prediction $\frac{\mathrm{d}}{\mathrm{ds}}F_4(\mathsf{s})$. Histograms: ii) *in blue*, ground-state energy PDF ($T=0$) for a polymer $\hat{t}=2^{10}$ with $N=10^6$ samples; iii) *in red*, PDF of $\mathsf{s}=-2^{-2/3}f$ for a polymer $\hat{t}=2^{10}$ at $\lambda=6.3$, with $N=10^6$ samples. The numerical PDFs are rescaled to adjust the mean and the variance of $F_4$. The variable $s$ in all figures is called $\mathsf{s}$ in the text.

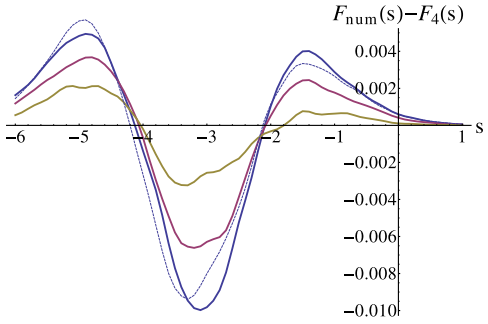


Fig. 2: (Colour on-line) Convergence as a function of $\lambda$: the difference between the numerical CDFs, $F_{num}(s)$, and the prediction for infinite $\lambda$, $F_4(s)$, is plotted for $\lambda=0.2$ (in blue), 1 (in red), 3 (in yellow) with $N=2.10^5$ samples. $\hat{t}=2^{11}$ is hold fixed. For $\lambda=0.2$ the data for $\hat{t}=2^9$ (dashed line) illustrates finite-size effects. The statistical fluctuations due to finite sample $N$ are visible.

by summing only on paths with $x\geqslant 0$, equivalent to an absorbing wall (hard wall), with $N_{\hat{t}}^{HS}\simeq 2^{\hat{t}}(2/\hat{t})^{3/2}/\sqrt{\pi}$. We compute $\ln z$ with $z=Z/\overline{Z}$ with the transfer matrix algorithm. As established in [19,36,39] in the high-$T$ limit at fixed $\lambda$, where $\lambda=(\hat{t}/(2T^4))^{1/3}$ for the lattice model, $\ln z$ can be directly compared —*with no free parameter*— with the analytical predictions of the continuum model with the same value of $\lambda$, defined there by (2). In addition we also compute the optimal path energy ($T=0$).

In fig. 1 we show the convergence to the GSE TW distribution both for i) $T=0$ and large polymer length $\hat{t}$ and ii) at $T>0$ and large $\lambda$. The agreement is very good. The variation for $T>0$ as a function of $\lambda$ is shown in more detail in fig. 2 where the (small) differences in the cumulative distributions (CDF) are shown on a larger scale. As in fig. 1 the mean and variance of the numerical PDFs are adjusted to those of $F_4$. In fig. 3 we show the ratio of half-space (HS) to full-space (FS) variances as a function of $\lambda$. Since the two TW distributions have variances $\sigma^{F_2}=0.8131947928$ and $\sigma^{F_4}=1.03544744$, the ratio $\rho$ should converge to the value 1.273308 at large time, which is apparent in fig. 3, up to finite $\hat{t}$ effects discussed there. Similarly the two TW distributions have skewness $\gamma_1^{F_2}=0.2240842$ and $\gamma_1^{F_4}=0.16550949$ hence the skewness ratio is predicted to increase from 0.636896 at small time (see above) to 0.738604 at large time.

Interestingly, the difference of the means $\mu$ of the GSE and GUE TW distributions gives information about extreme value properties of the DP. $p=Z^{HS}/Z^{FS}$ is the probability that, in the full space and for endpoints fixed at position $x>0$ the DP does not cross $x=0$. $p$ is defined for each disorder realization, with $p\simeq x^2\tilde{p}/t$ for small $x$. Then at large time (*i.e.*, large $\lambda$) one has $\overline{\ln\tilde{p}}=2^{2/3}\lambda(\mu^{F_4}-\mu^{F_2})$, where $\mu^{F_4}=-3.2624279$ while $\mu^{F_2}=-1.7710868$. At small time (*i.e.*, small $\lambda$) one finds from above (and [19]) $\overline{\ln\tilde{p}}=-\frac{1}{2}\sqrt{\frac{\pi}{2}}\lambda^{3/2}-0.0082964\lambda^3+\ldots$ hence $-\overline{\ln\tilde{p}}$ crosses over from $\sim t^{1/2}$ to $\sim t^{1/3}$. Note that $p$ is highly non–self-averaging at low temperature: at $T=0$ it is either 0 or 1, and a numerical study [35] indicates that $\overline{p}=\mathrm{Prob}(p=1)$ decays algebraically with time. Computing the PDF of $p$ seems a hard, although interesting, task.

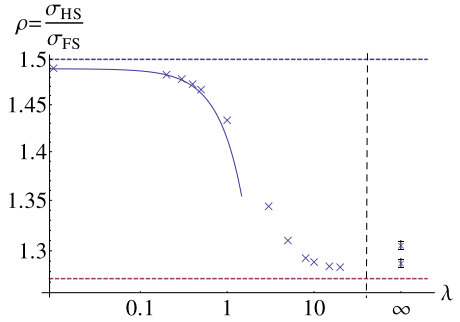


Fig. 3: (Colour on-line) Ratio of variances $\rho=\frac{\sigma_{HS}}{\sigma_{FS}}$, for $\lambda$ from 0.2 to 20. Crosses: numerical data ($N=2\cdot 10^5$ samples, $\hat{t}=2^{11}$, error estimation $\epsilon=3\cdot 10^{-3}$). Dashed horizontal lines: analytical predictions in both limits, $\frac{3}{2}$ for $\lambda\to 0$ and $\frac{\sigma^{F_4}}{\sigma^{F_2}}=1.2733$ for $\lambda\to\infty$. A finite $\hat{t}$ causes a small gap between these limits and the data, which decreases as $\hat{t}$ increases. Solid line: Taylor expansion (14) globally rescaled to account for finite $\hat{t}$. The right part of the graph shows the convergence of $\rho$ at $T=0$ as a function of $\hat{t}$: the upper point is $\hat{t}=2^8$, the lowest $\hat{t}=2^{10}$.

*KPZ equation*: let us now detail how our results translate in terms of the KPZ equation,

$$\partial_t h=\nu\nabla^2 h+\frac{\lambda_0}{2}(\nabla h)^2+\eta(x,t), \tag{34}$$

where $\overline{\eta(x,t)\eta(x',t')}=R_\eta(x-x')\delta(t-t')$, with Gaussian noise correlator $R_\eta(x)=D\delta(x)$. The Cole-Hopf mapping generally implies $\frac{\lambda_0}{2\nu}h=\ln Z$ and $\bar{c}=D\lambda_0^2$. To be more specific, the initial condition (1) corresponds to a wedge $h(x,0)=-w|x-y|$ in the limit $w\to\infty$, before $y\to 0$. Because of the hard wall one has $\frac{\lambda_0}{2\nu}h(x,t)=\ln(xy)+\frac{\lambda_0}{2\nu}\tilde{h}(x,t)$, where $\tilde{h}$ is not singular when both $x$ and $y$

approach zero, and the correspondence is really $\frac{\lambda_0}{2\nu}\tilde{h}(0,t) = \ln Z$. Schematically the boundary conditions (BC) can be stated as $h(0,t) = -\infty$ or $\nabla h(0,t) = +\infty$ (see more general ones below). Hence from (30):

$$\frac{\lambda_0}{2\nu}\tilde{h}(0,t) = \ln \overline{Z} + 2^{2/3}\lambda\ \xi_t \tag{35}$$

with, at large $t$, $\ln \overline{Z} \simeq v_\infty t$. From footnotes [3] and [4], $v_\infty = \frac{\lambda_0^2 R_\eta(0)}{8\nu^2} - \frac{D^2\lambda_0^4}{12}$ is the same non-universal constant (see discussion in [36]) in both HS and FS cases, the difference in $\ln \overline{Z}$ being only sublinear in time, as $\sim \ln t$.

Finally, we discuss the universality of our results. Another standard BC is the reflecting wall (RW) $\nabla Z = 0$, *i.e.*, $\nabla h = 0$ (contact angle $\pi/2$) which may be of experimental interest. For the DP it is achieved considering two symmetric half-spaces, *i.e.*, $V(-x,t) = V(x,t)$ (see footnote [6]). At $T = 0$ there is no difference in the optimal path energy between the hard and reflecting wall. At $T > 0$ they become different, since there is more entropy in the RW. However, the longer the polymer, the closer it becomes, effectively, to $T = 0$. Hence we expect different $g(s)$, which become equal at large time. In fact all BC such that $\nabla h \geqslant 0$ should converge to $F_4$. This is consistent with the results of [28] translated into the $T = 0$ lattice DP model (although the equivalent of the hard wall was not explicitly considered there). In the PNG model it corresponds to an absent or weak enough boundary source [27]. We will not discuss here the case of BC $\nabla h < 0$ which leads to an unbinding transition. A similar transition was studied in the random permutation model [28] and in the PNG model [14,27], but not using the BA (see, however, [40]). Work on that case is in progress.

Our results apply to the conductance $g$ of disordered 2D conductors deep in the localized regime. Extending ref. [41] we predict that $L^{-1/3}\ln g$ should be distributed as $F_4$ if the leads are small, separated by $L$, and placed near the frontier of the sample (which occupy, say, a half-space).

* * *

We thank P. Calabrese and A. Rosso for helpful remarks, and N. Crampe, A. Dobrinevski and M. Kardar for interesting discussions. This work was supported by ANR grant 09-BLAN-0097-01/2.

REFERENCES

[1] Kardar M., Parisi G. and Zhang Y. C., *Phys. Rev. Lett.*, **56** (1986) 889.
[2] Barabasi A.-L. and Stanley H. E., *Fractal Concepts in Surface Growth* (Cambridge University Press) 1995; Krug J., *Adv. Phys.*, **46** (1997) 139.
[3] Kardar M. and Zhang Y.-C., *Phys. Rev. Lett.*, **58** (1987) 2087; Halpin-Healy T. and Zhang Y.-C., *Phys. Rep.*, **254** (1995) 215.
[4] Takeuchi K. A. and Sano M., *Phys. Rev. Lett.*, **104** (2010) 230601; Takeuchi K. A., Sano M., Sasamoto T. and Spohn H., *Sci. Rep.*, **1** (2011) 34.
[5] Miettinen L. *et al.*, *Eur. Phys. J. B*, **46** (2005) 55.
[6] Hwa T. and Lassig M., *Phys. Rev. Lett.*, **76** (1996) 2591.
[7] Blatter G. *et al.*, *Rev. Mod. Phys.*, **66** (1994) 1125; Le Doussal P., *Int. J. Mod. Phys. B*, **24** (2010) 3855.
[8] Lemerle S. *et al.*, *Phys. Rev. Lett.*, **80** (1998) 849.
[9] Huse D. A., Henley C. L. and Fisher D. S., *Phys. Rev. Lett.*, **55** (1985) 2924.
[10] Johansson K., *Commun. Math. Phys.*, **209** (2000) 437; arXiv:math/9910146.
[11] Corwin I., arXiv:1106.1596.
[12] Ferrari P. L. and Spohn H., arXiv:1003.0881.
[13] Tracy C. A. and Widom H., *Commun. Math. Phys.*, **159** (1994) 151; **161** (1994) 289.
[14] Prahofer M. and Spohn H., *Phys. Rev. Lett.*, **84** (2000) 4882; *J. Stat. Phys.*, **108** (2002) 1071.
[15] Baik J. and Rains E. M., *J. Stat. Phys.*, **100** (2000) 523.
[16] Ferrari P. L., *Commun. Math. Phys.*, **252** (2004) 77.
[17] Baik J., Deift P. and Johansson K., *J. Am. Math. Soc.*, **12** (1999) 1119.
[18] Sasamoto T. and Spohn H., *Phys. Rev. Lett.*, **104** (2010) 230602; *Nucl. Phys. B*, **834** (2010) 523; *J. Stat. Phys.*, **140** (2010) 209.
[19] Calabrese P., Le Doussal P. and Rosso A., *EPL*, **90** (2010) 20002.
[20] Dotsenko V., *EPL*, **90** (2010) 20003; *J. Stat. Mech.* (2010) P07010; Dotsenko V. and Klumov B., *J. Stat. Mech.* (2010) P03022.
[21] Amir G., Corwin I. and Quastel J., *Commun. Pure Appl. Math.*, **64** (2011) 466.
[22] Calabrese P. and Le Doussal P., *Phys. Rev. Lett.*, **106** (2011) 250603.
[23] Le Doussal P. and Calabrese P., *J. Stat. Mech.* (2012) P06001.
[24] Imamura T. and Sasamoto T., *Phys. Rev. Lett.*, **108** (2012) 190603; *J. Phys. A*, **44** (2011) 385001.
[25] Emig T., *Int. J. Mod. Phys. A*, **25** (2010) 2177.
[26] Le Doussal P. and Wiese K. J., *EPL*, **86** (2009) 22001.
[27] Sasamoto T. and Imamura T., *J. Stat. Phys.*, **115** (2004) 749, arXiv:cond-mat/0307011.
[28] Baik Jinho and Rains Eric M., arXiv:math/9910019.
[29] Kardar M., *Nucl. Phys. B*, **290** (1987) 582.
[30] Lieb E. H. and Liniger W., *Phys. Rev.*, **130** (1963) 1605.
[31] Oelkers N., Batchelor M. T., Bortz M. and Guan X. W., *J. Phys. A*, **39** (2006) 1073.
[32] Hao Y. *et al.*, *Phys. Rev. A*, **73** (2006) 063617.
[33] McGuire J. B., *J. Math. Phys.*, **5** (1964) 622.
[34] Calabrese P. and Caux J.-S., *Phys. Rev. Lett.*, **98** (2007) 150403; *J. Stat. Mech.* (2007) P08032.
[35] Le Doussal P. and Gueudre T., in preparation.
[36] Gueudre T., Le Doussal P., Rosso A., Henry A. and Calabrese P., arXiv:1207.7305.
[37] Ferrari P. L. and Spohn H., *J. Phys. A*, **38** (2005) L557.
[38] Baik J., Buckingham R. and DiFranco J., *Commun. Math. Phys.*, **280** (2008) 463.
[39] Bustingorry S., Le Doussal P. and Rosso A., *Phys. Rev. B*, **82** (2010) 140201.
[40] Kardar M., *Phys. Rev. Lett.*, **55** (1985) 2235.
[41] Somoza A. M., Ortuno M. and Prior J., *Phys. Rev. Lett.*, **99** (2007) 116602.

[6] Note that if one chooses $V(-x,t) = V(x,t)$ the usual image method works, *i.e.*, $Z(x,y,t) \pm Z(x,-y,t)$ is the PS in the half-space with reflecting (respectively, absorbing) BC.

# 3 Large tails and anomalous fluctuations

In the previous Chapter, we gave a detailed analysis of the statistical properties of the free energy that relies on the continuum model of stochastic growth, the KPZ equation. This analysis was performed in the weak noise/high diffusivity limit, a necessary requirement for a complete determination of the scale of the fluctuations as a function of the three parameters $\lambda$, $\nu$ and $D$. All the other microscopic details such as the disorder correlations or the lattice effects are then relevant only at very short times $t < t_f$.

At finite temperature however, the existence of a continuum model is more doubtful. This can be easily seen by a coarse-graining type of argument. If we try to replace every step of the polymer by a larger step, and substitute the disorder by its mean over the sites encountered, we might destroy the original optimal path because some particularly advantageous sites are deleted in the averaging process. As the statistical properties of the DP are controlled by the ground state in a essential way at large time, the continuum limit of the discrete model is rather ambiguous.

Motivated by experiments exhibiting different roughness exponents (see Fig.3.1), it was soon noticed that the KPZ universality is surprisingly fragile to modifications of the disorder. The heavy-tail noise is a typical example [94, 95, 96, 97][1]. It possesses an algebraic decay:

$$P(V) \sim \frac{A}{V^{1+\mu}}$$

with $\mu$ the decay exponent. We refer here to distributions that do not have all their moments finite. Their popularity is currently growing fast, as they are believed to well describe strongly fluctuating systems.

For the DP, the ill-defined continuum limit leads to a surprising feature: even for $\mu > 2$, with a well defined variance, the macroscopic properties of the interface are much influenced by large events: the Central Limit Theorem (CLT) does not readily apply in that context. Nonetheless, it is commonly believed that new scaling exponents $(\theta_\mu, \zeta_\mu)$ can still be defined, simply controlled by $\mu$, as the static properties of the polymer are determined by the rare events in the tail. Those new exponents could potentially explain the deviations observed in experiments (as in [99], Fig.3.1). In that case, the bulk of the disorder distribution becomes totally irrelevant. One could regard the KPZ class as a marriage between the CLT and the Extreme Value theorem (EVT). The CLT defines

[1] Long-range correlations, with a algebraic decay notably, is another possible avenue to follow, but it will not be mentioned in the following. Extensive studies (with quite some unresolved issues) have been conducted numerically [98] or analytically [33].

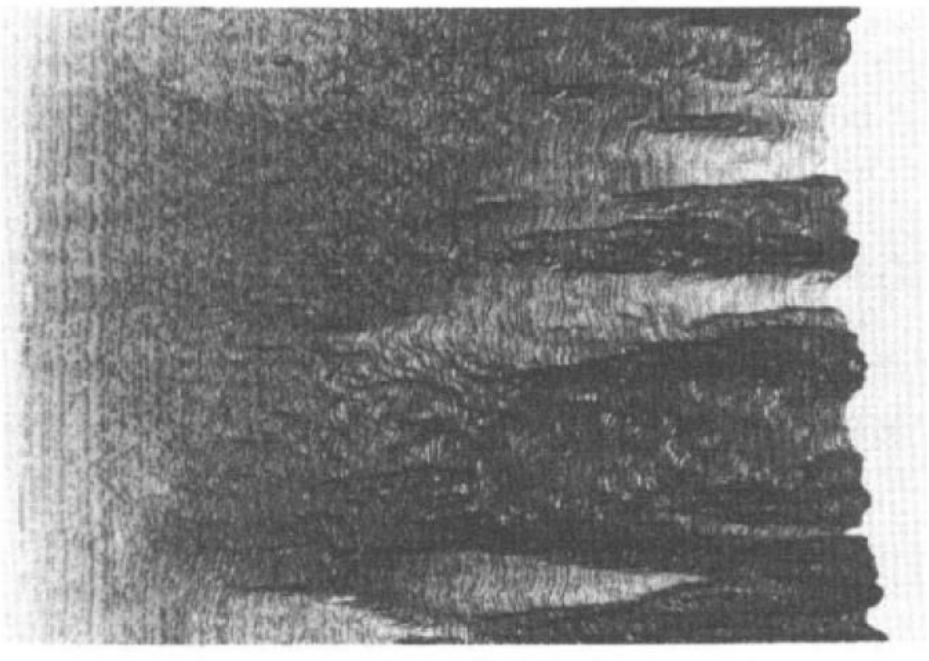

Figure 3.1: A front of glycerol invading a 2-dimensional Hele-Shaw cell filled with randomly spread beads. The roughness of the front was evaluated at $\chi \simeq 0.81$ and surprisingly deviates from the standard result 1/2. From [99].

two main classes of distributions, depending on their tail behaviour with a critical value $\mu_c = 2$, while the EVT gives us three classes depending on the fact that the distribution is compactly supported, or exhibits an algebraic decay (but with no critical value for $\mu$). The KPZ class is somewhat in between: the optimization mixes both sums and minimums of random variables.

Although we already presented numerous ways to derive the anomalous exponents $\theta = 1/3$ and $\zeta = 2/3$, a simple argument that would unveil the deep physical origin of these results and extend these results to similar problems, such as the DP in $d+1$ dimensions, is still lacking. Emphasizing the importance of large events compared to the more global optimisation of Gaussian disorder could potentially investigate the range of validity of techniques exploited in the context of Gaussian disorder (such as replica method or the functional RG). Moreover, it would be much enlightening to derive a Flory-type argument for the Gaussian regime.

Therefore we revisit the 1+1 DP problem with heavy-tailed disorder. We first recall the Flory argument, as well as a scaling theory developed in [100, 101] and tailored for heavy-tailed distributions. To gain some analytical insight of the fluctuations distributions, we consider a toy-model in $d = 0$, where most of the observables can be exactly computed, before embarking on the $d = 1$ case. We establish numerically, as convincingly as possible, the violation of the standard DP/KPZ 2/3 scaling and the corresponding Tracy-Widom statistics. Our results are in good agreement with the naive Flory predictions for the diffusion exponent $\zeta$ and the energy exponent $\theta$, which confirms that the value $\zeta = 2/3$ only holds if the distribution of the pinning energy $V$ decays faster that $1/V^6$. We then focus more on the optimization strategy in presence of extreme events and study various statistical properties of the DP in the anomalous regime, as an attempt to directly validate

the main assumption of the Flory argument, namely that the accessible extreme values of the pinning potential dominate the scaling behaviour.

## 3.1 Flory argument and scaling theory

Analytical methods to tackle noises with diverging moments are still inchoate. Most of the formalism used in disordered systems, from Langevin equations to FRG techniques, tends to break down when strongly fluctuating noises are present. Nevertheless, because of the importance of extremal events, these systems lend themselves very well to Flory-type arguments.

In the DP language, the exponents can be estimated by balancing the energy of the deepest sites with the deformation energy it would cost to reach them [94, 102, 103]. Noting $t$ the length and $x$ the size of a typical excursion of the polymer, a result from extreme statistics of heavy-tailed distributions gives, for the available volume $xt$, an estimation of the energy of the minimum: $E_{min} \sim (xt)^{1/\mu}$. On the other hand, the deformation cost behaves as $S \sim -x^2/t$. Balancing both estimations, $E_{min} \sim S$, leads to the estimates:

$$\begin{aligned} \zeta_\mu &= \frac{1+\mu}{2\mu-1} \\ \theta_\mu &= \frac{3}{2\mu-1} \end{aligned} \tag{3.1}$$

Those formula are valid for $1/2 \leq \mu \leq 5$. The hypothesis that elastic and total energies are of same order of magnitude is closely linked to the scaling (STS) relation $\theta = 2\zeta - 1$. The generalization to $d$ dimensions is performed in the related paper.

Above the critical value $\mu_c = 5$, we find $\theta_\mu < 1/3$ and, instead of a strategy focusing on deep sites of the disorder, the behaviour of the polymer is dominated by a *collective* strategy similar to the Gaussian case. It is interesting to note that there is no simple scaling argument to recover the Gaussian exponents: it hints the fact that the subtle optimisation in Gaussian-like disorder is global and introduces large correlations between sites energies along the polymer.

The assumption that the interface remains self-affine in an heavy-tail disorder allows to develop a new scaling theory that recovers Eq.3.1 with additional information. This scaling theory was elaborated in [100, 101]. We reproduce their instructive analysis here. To fix the ideas, we choose the disorder to follow a Pareto distribution:

$$P(\eta) = \begin{cases} A\mu/\eta^{1+\mu} & \text{if} \quad \eta > \eta_m \\ 0 \quad \text{if} \quad \eta < \eta_m \end{cases} \tag{3.2}$$

The scale invariance $P(b\eta) = b^{-\mu-1}P(\eta)$ is usually true only in the tails, due to the existence of a constant cut-off $\eta_m$

Consider a simplified KPZ Equation, involving only the non-linear term:

$$\partial_t h = \frac{\lambda}{2}(\nabla h)^2 + \eta(x,t) \tag{3.3}$$

First, we investigate the scaling invariance of Eq.3.3. The noise (and the cutoff $\eta_m$) will be scaled along with the interface. Therefore, the following results are exact: they merely correspond to an affine change of units.

The noise, uncorrelated in space and time, follows a Pareto distribution with a density:

$$\overline{n}(x,t,V)\,dx\,dt\,dV = \frac{A\mu}{\eta^{1+\mu}}\,dx\,dt\,dV \quad \text{for} \quad \eta > \eta_m \tag{3.4}$$

We call $A$ the intensity of the noise, $\eta_m$ the lower cut-off. With the change of units:

$$\begin{aligned} x &= bx' \\ t &= b^z t' \\ h(x,t) &= b^\chi h(x',t') \\ \eta &= b^\chi \eta' \\ \eta(x,t) &= b^{\chi-z}\eta'(x',t') \end{aligned}$$

and requiring the invariance of the density $\overline{n}(x,t,\eta)\,dx\,dt\,d\eta^2$, it gives back Eq.3.1 in the interface language, as well as $\chi_\mu = 3/(\mu+1)$. At the present stage, where the cutoff and the noise are scaled, the scaling properties are not approximations or asymptotic results but exact for all $L$ and $A$ and for all $\mu \geq d+1$, even beyond $\mu_c$.

Now we consider the following KPZ equation with both Gaussian and Pareto noises $\eta_G$ and $\eta_P$, with $\mu < \mu_c$:

$$\partial_t h = \nu\Delta h + \frac{\lambda}{2}(\nabla h)^2 + \eta_G(x,t) + \eta_P(x,t) \tag{3.5}$$

If again a change of scale is performed on Eq.3.5 with this time the gaussian exponents $\chi = 1/2$ and $z = 3/2$, one can readily check that the intensity $A$ grows, stretching the interface more and more. The effective roughness exponent $\chi(L)$ for system size $L$ thus crosses over from $\chi_G$ to $\chi_P$ as $L$ increases. Conversely , if $\mu > \mu_c$, the intensity $A$ will vanish under rescaling, recovering $\chi_G$.

In the usual model introduced by Zhang [96], the bare cutoff $\eta_m$, representing the typical size above which the distribution of noise events algebraically decays, is not rescaled. Therefore, upon rescaling, the effective cutoff $\tilde{\eta}_m \sim \eta_m/b^{\chi_P}$ goes to 0 and the bulk of the disorder distribution is irrelevant. [100] argue that the presence of this fixed cutoff is nonetheless responsible for the very long cross-over towards $\chi_P$ observed in many numerical simulations. Inspired by the exactly solvable EW case, they postulate some logarithmic corrections at the critical transition $\mu = \mu_c$ .

All the above relations heavily rely on some self-affinity assumptions, and the shared belief that large noise events are the most relevant mechanism in power-law disorder. In the DP picture, such a strong disorder is expected to greatly stretch the polymer, its statistical properties being mainly controlled by a population of very deep sites. As we stated above, it seems very delicate to back up those hypothesis with analytical calculations, even in the $d = 1$ case.

[2] As we mentioned in the introduction, the Galilean invariance protects $\lambda$ from renormalization.

Nonetheless, if we can single out a site responsible for the extra wandering of the polymer, most of the competing effects of a large elastic energy and a very negative potential will sit precisely here. Therefore some insight might be gained by ignoring the remaining path followed by the polymer. This amounts to study a particle in a random landscape, attached to the origin by a spring. Although this rather drastic simplification can not reproduce the statistics of the polymer, both models share some characteristic features.

## 3.2 Preliminary: the model in $d = 0$

Although the exponents change in heavy-tail disorder, it is likely that all the universality is not lost, but the continuum limit has to be taken with care in order to ensure that the tails are not erased. In that respect, the toy-model in $d = 0$ is interesting because it is possible to monitor the transition from the discrete to the continuum model, and to scrutinize how the disorder is renormalized in this limit. Moreover, it gives the decay exponents of numerous quantities like the total energy of the particle, or its position.

### 3.2.1 From the discrete model...

We consider the minimization problem:

$$H(r) = \min_u H(r,u) = H(r,u(r))$$
$$H(r,u) = \frac{m^2}{2}(u-r)^2 + V(u)$$

where $V(u)$ is a random potential (a random function of $u$) and we define $u(r) = \operatorname{argmin} H(r,u)$ the position of the minimum. The quadratic term confines the position $u$ of the particle and mimics the elastic term for interfaces (see Fig.3.2). This toy-model has been frequently considered before [104, 105, 106, 107, 108, 28, 109]... Here we focus on the case of an uncorrelated (or short range correlated) disorder:

$$P(V) \sim \frac{\mu}{|V|^{1+\mu}} \tag{3.6}$$

for large negative $V$.

In this model, $m$ sets an internal length $L_m = 1/m$ [110]. This parameter will effectively control the continuum limit, as $m$ goes to 0 or equivalently $L$ to $\infty$. As we said, the particle mimics the extremal position of a polymer. By analogy, one can again define the exponents:

$$u(r) - r \sim m^{-\zeta} \quad , \quad H(r) - \overline{H(r)} \sim m^{-\theta}$$

The probability that the minimum total energy $H$ is attained in position $u$ with a value of the disorder $V$ is simply equal to the infinite product:

$$p(u,V) = P(V) \prod_{u' \neq u} P_> \left( H - \frac{m^2 u'^2}{2} \right) \tag{3.7}$$

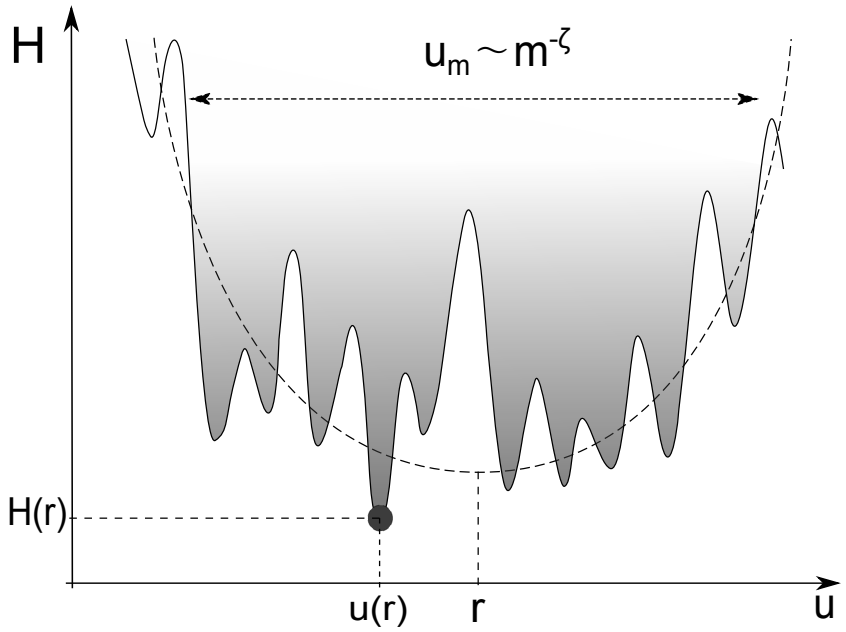


Figure 3.2: A particle in a random potential landscape confined by an elastic force (i.e. a quadratic potential centered at $r$). $u(r)$ is the position with minimal total energy $H(r)$. Its fluctuations from sample to sample scale as $u_m \sim m^{-\zeta}$.

To study the limit of small $m$, it is convenient in the following to absorb the dependence with $m$ in the units $(u_m, H_m, V_m)$ defined for the variables $(u, H, V)$ respectively:

$$u \to u/u_m = m^{\zeta} u$$
$$V \to V/V_m = m^{\theta} V$$
$$H \to H/H_m = m^{\theta} H$$

Except if stated, in the whole Section, we work now in the dimensionless system of units defined above.

The computation of the joint distribution $P(u, V)$ in the small $m$ limit can be written (as detailed in the related paper):

$$p(u,V) \approx \frac{\mu}{|V|^{1+\mu}} \exp\left(-F_\mu |V + \frac{u^2}{2}|^{\frac{1}{2}-\mu}\right) \theta_{V+\frac{u^2}{2}<0} \tag{3.8}$$

with $F_\mu = \sqrt{2\pi}\Gamma[\mu - 1/2]/\Gamma[\mu]$. Eq.3.8 is obtained after taking the limit of the quantity:

$$\exp\left(-\int du' m^{-\zeta} P_<(m^{-\theta}(H - \frac{u'^2}{2}))\right) \theta_{H<0} \tag{3.9}$$

Before that step, the exponents $\theta$ and $\zeta$ were not specified. But the requirement of a non-trivial continuum limit in Eq.3.8, very reminiscent of the scaling invariance hypothesis detailed in the previous section, imposes both:

$$\theta = 2\zeta - 2 \tag{3.10}$$
$$\zeta = \theta\mu \tag{3.11}$$

This choice indeed leads to the subsistence of the disorder tails in the continuum, contrary to what one would obtain after a coarse-graining scheme. With the use of Tauberian theorems [111], one can show the quantity Eq.3.9 converges to Eq.3.8 for any disorder distribution with algebraic decay of index $\mu$. In particular, the bulk of the distribution is irrelevant.

Unlike the directed polymer in $d = 1$, there is no critical $\mu_c$ where the Gaussian regime is recovered: in $d = 0$, $\mu_c = \infty$. The reason is transparent: the Gaussian regime is a global optimisation that cannot be captured by our extremal toy-model.

From Eq.3.8, much of the statistics of the particle can be computed. We refer to the related paper for detailed results. Let us just emphasize some interesting facts. After rescaling, the total energy follows a universal fluctuation distribution that decays as a power-law of index $\mu - 1/2$. This surprising shift can be recovered by invoking results from record statistics theory. Consider a realisation of the disorder with a particularly deep minimum, where the particle sits. From record statistics, it is known that the tail of the minimum of $N$ heavy-tailed random variables decays as $\sim \frac{N}{V^{1+\mu}}$. Balancing elastic energy and potential leads to $E \sim u^2 \sim V$, and then to $N \sim u \sim V^{1/2}$. Hence the dependence of $N$ with $V$, inherent to the fact that large deviations in the disorder allows the particle to explore a larger space, leads to a modified exponent $\mu - 1/2$ of the tail of $H$ and $V$.

In a similar flavour, the distribution of the position of the particle around the center of the parabolic potential decays with an index $2\mu$, a fact that can be quickly recovered from the balance between elastic and total energy.

### 3.2.2 ...to the continuum limit

The continuum limit is described by some random Poisson process on the plane $(u, \phi)$ - the spatial and potential variables - with the intensity $f(u, \phi)$ controlling the distribution of the disorder in the cell of size $du\, d\phi$ centred in $(u, \phi)$. In the present case of a translation invariant noise, $f$ only depends on $\phi$. For a continuum model model to be a "fixed point" of a more general class of models (e.g., the discrete model above) one should require scale invariance, as was discussed in Section 3.1. Within our choice of self-affine scaling, this imposes:

$$f(m^\theta V) = m^{-\zeta-\theta} f(V + C_m) \tag{3.12}$$

There are three types of solutions of Eq.3.12, some of them already detailed in [112]. Each of them corresponds to a possible continuum limit, representative of a "toy" universality class. A clear analogy with the well-known universality classes of extremal statistics very naturally appears, considering that the optimization problem involves finding a minimum amongst random variables:

- $f(\phi) = e^\phi$. This leads to the analogous of the *Gumbel* class, for fast-decaying disorder distributions (in particular the Gaussian disorder). Much of the statistics of this toy model has been studied by Kida in his seminal paper [104].
- $f(\phi) = \phi^{-1-\mu}\theta_{\phi>0}$. This corresponds to disorders bounded from below, and therefore coined the *Weibull* class. It was studied in [112].

- Finally, $f(\phi) = |\phi|^{-1-\mu}\theta_{\phi<0}$. As forecast from Eq.3.8, this represents the continuum limit of the discrete model above, and we shall refer to it as the *Frechet* class.

Of course, all the results about the decay of the distributions given previously can be readily recovered from the continuum. This toy model possesses another interpretation in terms of decaying Burger turbulence, mentioned in the Introduction. In particular, one can compute in general the distribution of the shocks as a functional of the velocity initial condition. As we did not adopt much of the language of Burger turbulence in this Thesis, we will not elaborate on those questions and refer to the related paper for more details.

## 3.3 The Directed Polymer in $d = 1 + 1$

In the following, we investigate the properties of the DP in $d = 1 + 1$. Because we are mainly interested in asymptotics, we consider the slightly simpler case $T = 0$. Hence the free energy is replaced by the total energy $E(t)$. For this discrete model, directed paths grow along the diagonals of the lattice with only $(0, 1)$ or $(1, 0)$ moves (hard constraint condition), starting in $(0, 0)$ and with the second end left either free or fixed. To each site of the lattice is associated a i.i.d. random number $V(x, t)$. The time coordinate is given by $t = i + j$ and the space coordinate by $x = (i - j)/2$. The total energy of the polymer is the minimum over all paths $\gamma_t$ growing from $(0, 0)$ up to time $t$ is defined as

$$E(t) = \min_{\gamma_t} \sum_{(x,\tau)\in\gamma_t} V(x, \tau)$$

with $2x \in [-t, t]$ and $\tau \in [0, t]$. The energy can be computed with the fast transfer matrix method, relying on the recursion:

$$E_{x,t+1} = \min\left(E_{x-\frac{1}{2},t}, E_{x+\frac{1}{2},t}\right) + V(x, t + 1)$$

with $E_{x,0} = \delta_{x,0}$.

This discrete model can be seen as a natural regularization of the continuum elastic DP model, with arbitrary disorder distribution. A subtlety arises for very low $\mu < 2$, as $\zeta$ in the discrete model saturates to 1 due to the hard constraint. Hence both models are not equivalent anymore below $\mu < 2$. For consistency, we only consider the discrete model in the following, even in the limit $\mu \to 0^+$.

### 3.3.1 Scaling exponents

Measuring the scaling exponents in presence of heayv-tailed disorder requires a bit of care. The statistical estimator for $\overline{E^2}^c$ never averages when $\mu < 4$ and shows large jumps even for a very important sampling. This is related to the convergence of its statistical error $(\overline{E^4}^c/N)^{1/2}$. Due to the presence of heavy tails in the disorder, high enough moments of the distribution of energy $P(E)$ could diverge.

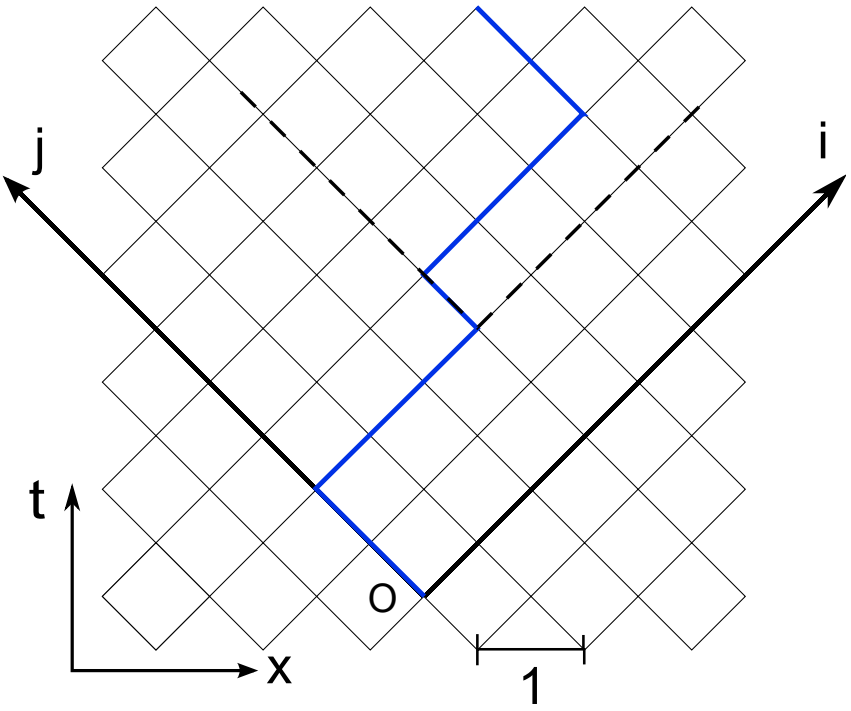


Figure 3.3: Sketch of the directed polymer model. The blue solid line corresponds to a polymer growing over the square lattice under the hard constraint condition. This model is equivalent to the elastic polymer model for disorder with decay exponents down to $\mu = 2$.

Another estimator of the spread of the distribution is the mean absolute deviation (MAD) $\Delta E$:

$$\Delta E = \frac{1}{N} \sum_i |E_i - \overline{E}| \tag{3.13}$$

This estimator is more resilient to extreme events and works better with heavy-tailed distributions. Contrary to the standard deviation, which squares the distance from the average, MAD is well controlled as soon as the second moment of the pdf exists. When needed, we use this more robust estimator.

The check of the prediction, for different values of $\mu$ compared to the theoretical result, is summarized in a table in the related paper. The numerical estimations have been made with the maximum likelihood method. We present the estimations of $\zeta$ in Fig.3.4. It shows a good agreement between numerics and theory, but one clearly notes, in the inset, that the quantities $\overline{x(t)^2}/t^{\zeta_\mu}$ saturates at larger and larger times as $\mu \to 5$. This is caused by a growing cross-over to the heavy-tail regime around $\mu = 5^-$ we obtained in Section 3.1. For $\mu > 5$, the standard values $\zeta = 1/3$ and $\theta$ are recovered, after a similarly behaving cross-over. The marginal case $\mu = 5$ presents an sub-growing behaviour, akin to a logarithmic correction (see also [101]), although we did not simulate large enough polymers to back up that prediction with satisfying precision.

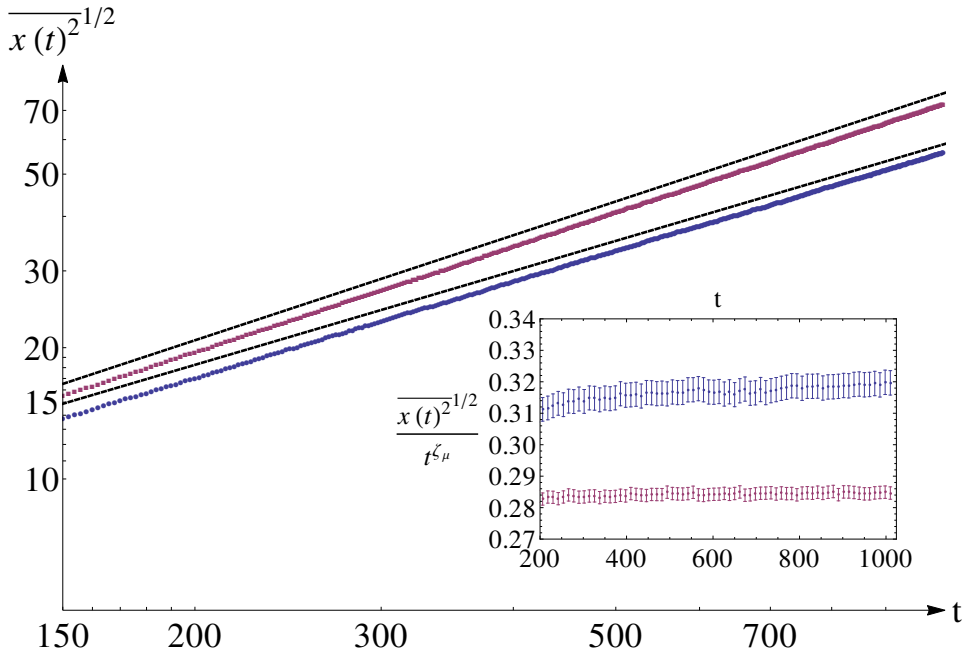


Figure 3.4: Mean square displacement of the end position of the optimal path for $\mu = 3$ (in red) and $\mu = 4$ (in blue). Dashed lines correspond to the Flory estimation. Inset : $\overline{x(t)^2}/t^{\zeta_{th}}$ showing saturation at large $t$ in both cases.

### 3.3.2 Fluctuations of the free energy and end position

While the scaling exponents have been well investigated before, we could not find any study about the universal limit distributions of the fluctuations for the free energy and the extremity. The heavy tail of the disorder is expected to pervade in their own tails. As they correspond to rare and large fluctuations, they likely relate to the presence of rare and deep sites in the disorder. In what follows, we define the rescaled variable:

$$s(t) = (E(t) - \overline{E}(t))/(\overline{E^2}^c(t))^{1/2} \tag{3.14}$$

with the rescaled energy distribution $\phi(s)$.

It is worthwhile to note that not only the Gaussian scaling exponents, but also the TW universality class, extend for $\mu > 5$. The shadowed presence of heavy tails can only be perceived for very negative $s$, where $\phi(s)$ remains algebraic below some threshold $s < s_t^*$. However, when $t \to \infty$, the crossover towards the algebraic behaviour $s_t^*$ moves to $-\infty$.

For $2 < \mu < 5$, the limiting distribution is very different. In particular, $\phi(s)$ exhibits an algebraic decay $1/s^{1+\mu}$. Relying on the above analysis for $d = 0$, we expect the tail to actually decay with an exponent $\mu - 1/2$ rather than $\mu$ because of the presence of the elastic energy. Unfortunately, the simulations are quite inconclusive. Even by using a rather high sampling (about $N = 5 \cdot 10^6$ polymers of size $L = 512$) and logarithmically binning the histogram, we were not able to clearly determine a value between $\mu$ and $\mu - 1/2$, as the decay seems to sit in between (see Fig.3.5). A more careful study of the finite size effects is in progress to unambiguously answer that question. It is however complicated by the concern of different tails, universal and non-universal, appearing at very large values of $\phi(s)$. Although it turns out that they share the same exponential

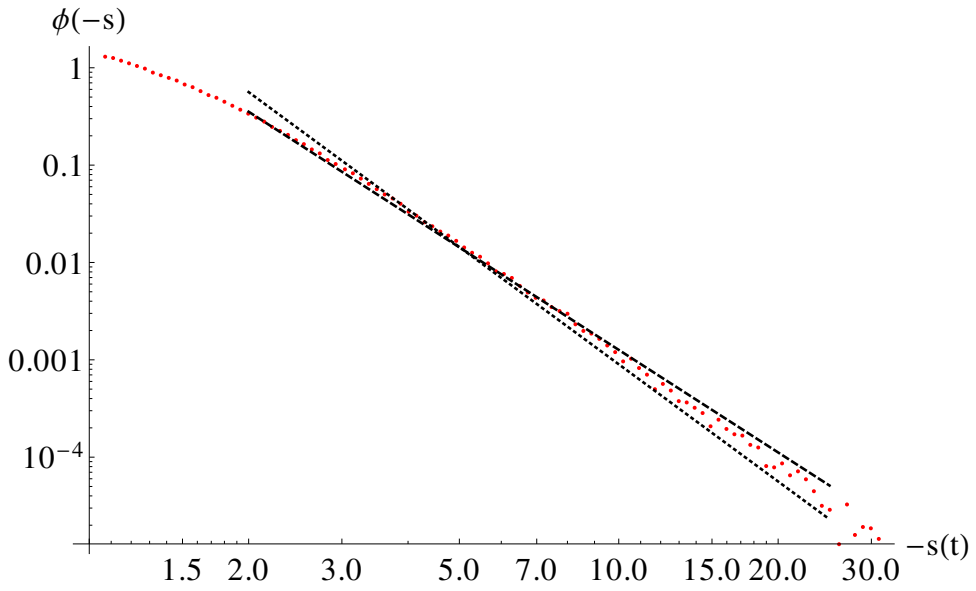


Figure 3.5: The left tail of the energy distribution $\phi(-s)$ for a polymer of size $L = 512$ ($N = 5 \cdot 10^6$) with $\mu = 3$. While it shows a clear algebraic decay, the decay exponent can not be determined without ambiguity.

decay in the Gaussian regime [113], it is not obvious that this coincidence holds in the heavy-tails case.

More generally, the family of limiting distributions $F_\mu$ only depends on $\mu$ and on the boundary conditions. Its analytical expression is still unknown. Inspired by results from extreme statistics, a natural guess would be the Frechet distribution $\mathbb{P}(X < x) = \exp(-\alpha|x|^{-\mu})$ or some convolutions thereof [103]. However, this distribution is supported on the half real line, while our numerical results indicate that the support of the limiting distributions $F_\mu$ is the whole real line. An interesting feature of $F_\mu$ is the fact that its right tail, corresponding to unfavourable configurations of the disorder, seems to decay as $e^{-\alpha s^3}$, similarly to TW. This fact would support a mixture of some Frechet and TW distribution as a possible guess. An interesting avenue to explore concerns the optimal fluctuation theory developed in [114, 113, 115] for the directed polymer. It could relate large positive fluctuations of the free energy to the disorder landscape for heavy-tailed disorder, and explain the robustness of the right tail decay.

One expects the rescaled position $z = x(t)/t^\zeta$ to converge in law towards a limiting distribution $Q_\zeta(z)$. The marginal $Q_{2/3}(z)$ can not be computed explicitly, but it has been shown that it has an infinite support with a rather small departure from the Gaussian distribution [116, 117]. The heavy-tailed disorder exhibits a radically different behaviour, as $Q_\zeta(z)$ is strongly influenced by the large excursions of the optimal path to reach pinning sites. The result from the $d = 0$ case hints at an algebraic decay of exponent $2\mu$.

Note that, for $\mu < 2$, $\zeta$ saturates to 1 due to the hard constraint and the support of $Q_\mu(z)$ reduces to the interval $(-1, 1)$: the extremity has a finite probability to reach any point of the available space, even at large $t$. Remarkably the distribution $Q_\mu(z)$ can be explicitly computed in the limit $\mu \to 0^+$, where the optimization becomes a hierarchical

recursive process[3]:

$$Q_{\text{greedy}}(z) = \frac{3}{4}\left(1 - z^2\right) \tag{3.15}$$

Actually, Eq.3.15 asymptotically holds for the range $0 < \mu < 1$ because, when the mean does not exist, the sum of energy is totally dominated by one single term: the polymer obeys a *greedy* strategy, only picking the deepest site available.

Because the regimes considered in that section can be described in terms of various optimization strategies, we study them in more details in the following.

### 3.3.3 Optimization strategies

As we said, the difference of extremal statistics for different disorders reflects in the optimization strategies adopted by the polymer:

- For a Gaussian disorder, the optimisation strategy is *collective*: the total energy of the polymer is equally shared between all the sites.
- For an heavy-tailed pdf with $1 < \mu < 5$, the optimisation strategy is *elitist*: an important fraction of the total energy is hold by a small fraction of the sites belonging to the path.
- For an heavy-tailed pdf with $\mu < 1$, the optimisation strategy is *individual*: most of the total energy of the polymer is localized on one particularly deep site.

The Flory argument precisely relies on the assumption that the fluctuations of $E$ are controlled by the fluctuations of the deepest sites, specifically reached by the polymer.

For example, one could check the validity of the *elitist* optimisation strategy through the following procedure: consider an envelope of length $t$ and width $1/2t^{\alpha}$, its volume scales as $t^{1+\alpha}$. We estimate the probability $P_c(\alpha)$ that the minimum on the polymer is one of the $\log(t)$ deepest sites inside of the envelope. If $\alpha$ is chosen too small compared to $\zeta$, then the minimum on the polymer should be smaller than the minimum in the envelop. On the contrary, if $\alpha \gg \zeta$, the minimum on the polymer should be higher, as the elastic energy prevents it from reaching this favourable site. One expect that when $t \to \infty$, $P_c(\alpha)$ will become more and more peaked around $\alpha = \zeta$ for the *elitist* strategy, while in the *collective* regime, $P_c(\alpha)$ should vanish for all $\alpha$. Fig.3.6 indeeds suggests a different qualitative behaviour for $\mu = 3$ and $\mu = 7$, in agreement with our prediction. Note that the maxima of the curves in Fig.3.6 corresponding to an estimation of the rugosity according to the scaling argument are moving to the left, from 1 to 0.90 up to $t = 2^{12}$. They are expected to converge to $\zeta_\mu = 4/5$ for $\mu = 3$ although the convergence is very slow.

Another interesting observable to quantify the departure from the global strategy is the position of the minimum energy site *along the polymer*. Because with fast-decaying disorder, the value of a single site does not matter to the polymer, its position $t_{\min}$

[3]Details of the computation can be found in the related paper.

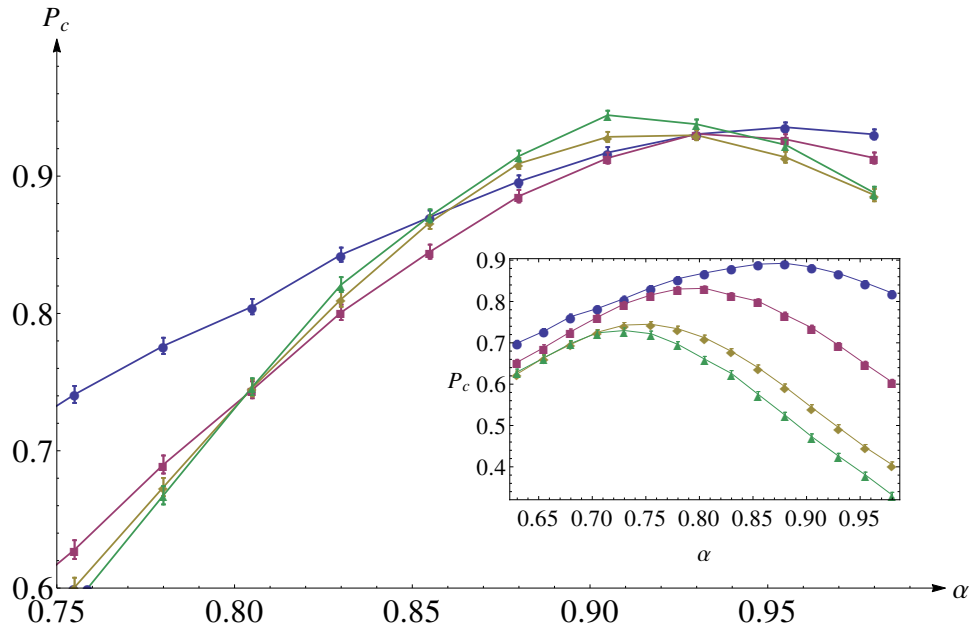


Figure 3.6: Probability $P_c(\alpha)$ as defined in the text for a heavy tailed disorder with $\mu = 3$. Symbols correspond to different lenghts: $L = 2^6$ (circles), $2^9$ (squares), $2^{11}$ (losanges), $2^{12}$ (triangles). The averages are performed over $N = 2 \times 10^5$ samples. Inset: the same analysis is performed for $\mu = 8$.

should be uniformly distributed over the whole length. On the contrary, in heavy-tailed disorder, it is more likely to find such a minimum where the entropy is the largest, in the middle for the droplet geometry. This phenomenon is clearly seen Fig.3.7. For $\mu < 1$, the histogram adopts, at large $L$, a triangle shape that can be readily explained by the greedy model.

The limiting case of a greedy strategy in the limit $\mu \to 0^+$ is easier to handle analytically, because it reduces to a hierarchical process, where recursive equations can be written down. Hence, we gave in Eq.3.15 the probability distribution of the extremity, reduced to a simple parabola. In [118], the multi-fractal spectrum of the polymer path was computed as well. In [119], a family of limiting curves is obtained for the paths of the polymer when the temperature is scaled with the length $L$ as $\beta \sim L^{1-2/\mu}$. Works are in progress to obtain the general phase diagram for any $\mu$ and scaling of $\beta$ [120]. Finally, the use of hierarchical processes have been used before to provide upper bounds on the free energy for Gaussian disorder [121]. Because the above numerical study gives the intuition that, for $\mu < 5$, the optimization strategy becomes more local, focusing on specific deep sites, it would be enlightening to adapt the multi-fractal formalism developed in these works to any exponent $\mu$, as a sort of multiplicative cascade seems at play. Note however that the interplay between elastic energy and potential greatly complicates this task, compared to the greedy model where the elastic energy is neglected.

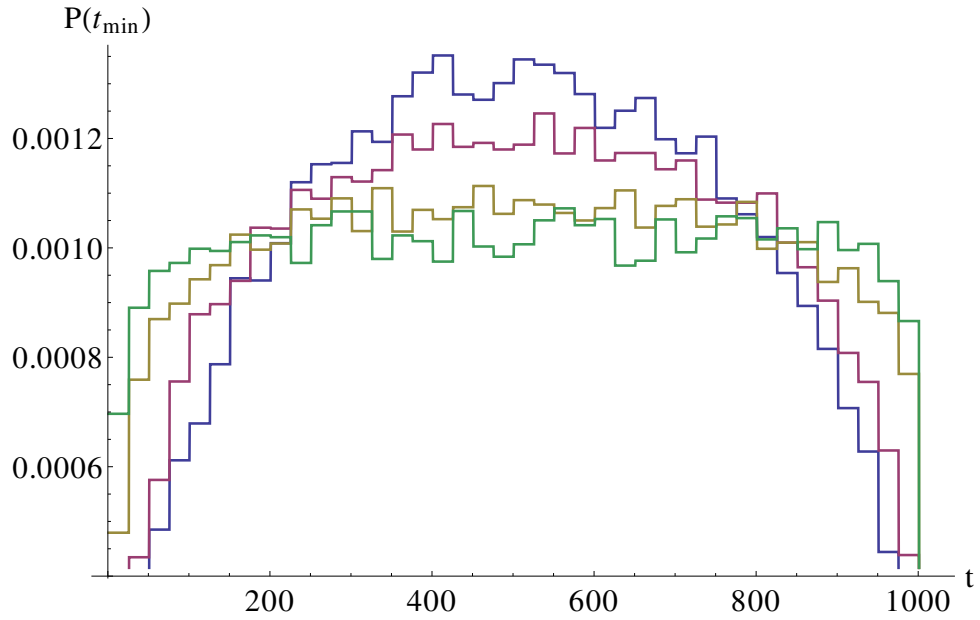


Figure 3.7: Probability $P(t_{\min})$ to find the minimum energy site at position $t_{\min}$ along the polymer, with a droplet geometry. From the flattest histogram to the least one: Gaussian disorder (green), $\mu = 7$ (yellow), $\mu = 3$ (red), $\mu = 2.2$ (blue).

## 3.4 Conclusion

We presented a study of the modification of the KPZ universality class under heavy-tailed disorder. Those modifications are deep, and the presence of rare and large events pervade from the scaling exponents to the fluctuations distributions. Nonetheless, this simply leads to new universality classes, as both the exponents and the fluctuations distributions seem uniquely controlled by $\mu$, the bulk of disorder being irrelevant. Aside this new dependence, many features are shared in common in those universality classes, like the dependence with initial conditions, or the far right-tail, corresponding to anomalously high energies. This supports our hope to get a better grasp on the KPZ class itself by studying its surrounding.

However, because of the lack of theoretical tools robust to heavy-tailed noise, exact results are rather scarce and numerics have been extensively used to enlighten the situation. They indicate a sharp transition between the scaling exponents $(\theta_\mu, \zeta_\mu)$ and the Gaussian values $(1/3, 2/3)$ at $\mu_c = 5$. This is at odd with the result about random matrices with heavy-tailed distributed entries, where a similar transition takes place at $\mu_c = 4$, questioning the existence of an exact mapping between the DP problem and random matrices ensemble.

Because the optimization strategy apparently decomposes into recursive processes, where a single advantageous sites is picked, the exactly solvable case in $d = 0$ gives rather good estimates of several quantities involved in the $d = 1$ case. However, they fail to reproduce the most subtle features. Nonetheless the detailed numerical study of the polymer statistics reveals that the new statistics possess an underlying recursive structure akin to multiplicative cascades, or multifractal processes. This hypothesis is backed by the solvable greedy limit $\mu \to 0^+$, where the recursion equations are explicit. Hopefully, this formalism, that already provides upper bounds on Gaussian disorder, could be adapted

to tackled the whole range $0 < \mu < 5$.

Finally, the possibility of a Flory-type argument for Gaussian disorder remains open. From the above study, both collective and elitist strategies apparently coexist. We observed that a specific rescaling of the disorder with the length can suppress the critical threshold $\mu_c = 5$. A possibility would be to study the dependence of the free energy with a finite lower cut-off on the disorder. This should allow to tune more precisely the transition from the collective to the elitist strategy, and give a better understanding of the small population of sites responsible for the departure from the standard KPZ class.

PHYSICAL REVIEW E **89**, 042111 (2014)

# Statistics of shocks in a toy model with heavy tails

Thomas Gueudré and Pierre Le Doussal
*CNRS-Laboratoire de Physique Théorique de l'Ecole Normale Supérieure 24 rue Lhomond, 75005 Paris, France*
(Received 16 January 2014; published 4 April 2014)

We study the energy minimization for a particle in a quadratic well in the presence of short-ranged heavy-tailed disorder, as a toy model for an elastic manifold. The discrete model is shown to be described in the scaling limit by a continuum Poisson process model which captures the three universality classes. This model is solved in general, and we give, in the present case (Frechet class), detailed results for the distribution of the minimum energy and position, and the distribution of the sizes of the shocks (i.e., switches in the ground state) which arise as the position of the well is varied. All these distributions are found to exhibit heavy tails with modified exponents. These results lead to an "exotic regime" in Burgers turbulence decaying from a heavy-tailed initial condition.

DOI: 10.1103/PhysRevE.89.042111 PACS number(s): 05.40.−a, 02.50.−r, 46.65.+g, 68.35.Rh

## I. INTRODUCTION AND MODEL

Strongly pinned elastic objects, such as interfaces, occur in nature in the presence of substrate impurity disorder which exhibits large fluctuations. The ground-state configuration is determined by a competition between the energy cost of deforming the interface and the energy gain in exploring larger regions of disorder. In the well-studied case of Gaussian disorder, no impurity site particularly stands out and the optimum arises from a global optimization. The typical interfaces are rough, with nontrivial roughness exponents $u \sim L^{\zeta}$, where $u$ is the deformation field and $L$ an internal coordinate scale. The total optimal energy $H$ fluctuates from sample to sample with another exponent $H \sim L^{\theta}$. For directed lines (i.e., internal dimension $d = 1$) wandering in one dimension, $\zeta = 2/3$ and $\theta = 1/3$, which in turn are related to the exponents of the standard universality class for the Kardar-Parisi-Zhang growth equation [1].

In some physical systems however, the picture is completely different: a small fraction of the impurity sites produce a finite contribution to the total pinning energy, and the interface is deformed over large macroscopic scales, pinned specifically on those particular regions. One can see realizations of that situation in various areas such as transition in chemical reaction of BZ type, or in granular flows [2]. One expects that the usual critical exponents are modified, but much less is known in this case, both about equilibrium (e.g., ground states) and about nonequilibrium dynamics (e.g., depinning).

The present paper focuses on heavy-tailed disorder, which is paradigmatic of that situation, and whose probability distribution function[1] (PDF), $P(V)$, shows an algebraic tail. In terms of the cumulative distribution function (CDF), denoted $P_<(V) = \int_{-\infty}^{V} P(V')dV'$, we have

$$P_<(V) \simeq \frac{A}{(-V)^{\mu}} \quad \text{for } V \to -\infty. \tag{1}$$

As was found in numerous works, such a scale-free distribution often leads to behaviors dominated by rare events. They have been much studied in the context of diffusion in random media, where they generate anomalous diffusion [3]. More recently, heavy-tailed randomness was studied in the context of spin glasses and random matrices [4,5]. For instance, in [6] it was found that the PDF of the maximal eigenvalue of a large random matrix with i.i.d. entries distributed as changes from the standard Tracy-Widom distribution (the Gaussian universality class) to a Frechet distribution as $\mu$ is decreased below $\mu = 4$.

Only a few works address the pinning problem in the presence of heavy tails. In [6] it was argued, based on a Flory argument, that for a directed polymer in the so-called $(1 + 1)$-dimensional geometry (meaning internal dimension $d = 1$ and displacement $u \in R^D$ with $D = 1$), for $\mu < 5$ the roughness and energy exponents at $T = 0$ change to $\zeta = (1 + \mu)/(2\mu - 1)$ and $\theta = 3/(2\mu - 1)$. For $\mu \geqslant 5$ one recovers the above-mentioned values for Gaussian disorder, i.e., the tails have subdominant effect. While some mathematical results are available for $\mu < 2$ [7], little is presently known rigorously for general $\mu$ or on the effect of a nonzero temperature on the problem [8].

In this paper we solve the much simpler case of a particle, which can be seen as the limit $d = 0$ of the elastic interface problem. We consider the minimization problem:

$$H(r) = \min_{u} H(r,u) = H(r,u(r)), \tag{2}$$

$$H(r,u) = \frac{m^2}{2}(u - r)^2 + V(u), \tag{3}$$

where $V(u)$ is a random potential (a random function of $u$) and we define $u(r) = \mathrm{argmin} H(r,u)$ the position of the minimum. The quadratic term confines the position $u$ of the particle and mimics the elastic term for interfaces (see Fig. 1). More precisely, this model can be extended to an interface in a quadratic well and there $m$ sets an internal length $L_m = 1/m$ [9]. The PDF of $u(r) - r$ and $H(r) - \overline{H(r)}$ (where we denote by $\overline{\cdots}$ the average over the disorder) are independent of $r$ if $V(u)$ is statistically invariant by translation. Hence one can again define the exponents, as $m \to 0$ (see Sec. II A for more details):

$$u(r) - r \sim m^{-\zeta}, \quad H(r) - \overline{H(r)} \sim m^{-\theta}. \tag{4}$$

This "toy model" has been much studied in the context of disordered systems for Gaussian disorder. It also appears in the context of the decaying Burgers equation with random initial

[1] Also called probability density function below.

 

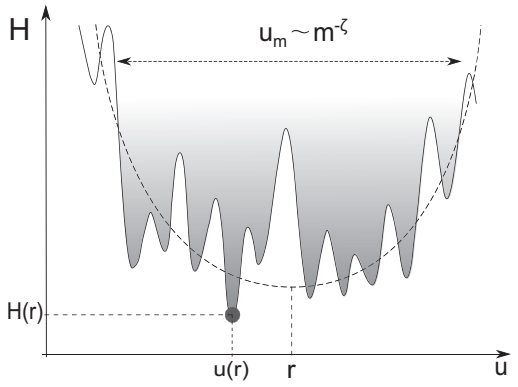


FIG. 1. Particle in a random potential landscape confined by an elastic force (i.e., a quadratic potential centered at $r$). $u(r)$ is the position with minimal total energy $H(r)$. Its fluctuations from sample to sample scale as $u_m \sim m^{-\zeta}$.

conditions, in the limit of vanishing viscosity (see Appendix A for details of the mapping). The case of short-range correlations corresponding to a short-range potential $V(u)$ was solved in the seminal paper of Kida [10]. An elegant derivation using replica was also given in [11]. Other derivations are given in [12] (Appendix J) and [13] (Appendix A). The case of Brownian correlations for $V(u)$ is related to the Sinai model studied in [12,14–18]. Other type of correlations have been studied in [19–23].

Here we consider the case where (i) correlations of $V(u)$ are short range and (ii) the PDF of $V(u)$ contains heavy tails. We then ask how the exponents and the PDF of $u(r)$ and $H(r)$ depend on the heavy-tail exponent $\mu$. Another interesting observable are the jumps of the process $u(r)$. Indeed in the limit of small $m$ the process $u(r)$ consists mostly of jumps called "static avalanches" or shocks (see below), and one defines the shock sizes $s = u(r^+) - u(r^-)$.

To be specific we solve here two variants of the model as follows.

(i) The discrete model: one starts with $u$ on a discrete lattice and i.i.d. random variables $V(u)$. In the limit $m \to 0$ by rescaling the position $u$ the process converges to a continuum limit.

(ii) The second is defined directly in the continuum for $u$: there $V(u)$ is defined as a Poisson point process.

Both models enjoy the same universal scaling limit.

In the absence of the quadratic well, $H = \min_u V(u)$ and the discrete problem reduces to the standard extreme value statistics problem. It must then be defined for a fixed system size $u = 1, \ldots, N$. For i.i.d. random variable (or weakly correlated ones) $H$ then grows to infinity with the system size $N$ and, after a proper rescaling, the PDF of $a_N H + b_N$ converges to one of the famous three universality classes [24]: (i) Gumbel when $P(V)$ decays faster than a power law; (ii) Frechet of index $\mu$ when $P(V)$ decays as a power law (1), and Weibull when $P(V)$ vanishes below some threshold (e.g., for $V < 0$). In the presence of the confining quadratic well, the same three classes survive: the Kida case belongs to the Gumbel class, while the heavy tail case belongs to the Frechet class. There are, however, some different universal features, such as the exponents and the distributions of shock sizes and minimum position.

In this paper we derive a general formula for the PDF of the position of the minimum $u(r)$, and for the distribution of the shock sizes $s$. Although our formula is valid for the three universality classes, we give a detailed calculation in the case of the Frechet class with power-law exponent $\mu$. We find that both distributions exhibit algebraic tails with modified exponents. These results are extended to space dimension $D > 1$.

Note that some of our results were anticipated in the context of the decaying Burgers equation. In [25] Bernard and Gawedzki looked for universality classes distinct from Kida for statistically scale-invariant velocity fields: they focused on the Weibul class and called it an "exotic regime" for Burgers turbulence. In [26], a more general study was presented, encompassing the three regimes. However, in none of these works the distribution of the shock sizes was obtained. The present work thus gives results on another exotic regime for decaying Burgers turbulence.

Note that the nonequilibrium version of this toy model, where one studies the dynamics of a particle pulled quasistatically by the harmonic well in the random potential $V(u)$ was studied in [27]. The three universality classes were also found to appear, and the distribution of the avalanche sizes were obtained for the three classes.

In Sec. II, we solved the discrete toy model and obtain the joint PDF of the energy and the position in the small $m$ limit. In Sec. III we consider the Poisson process model, and derive the shock size distribution. In Sec. IV, we consider the discrete toy model in higher dimension. Finally, in Sec. V, we discuss the case of a more general elastic manifold of internal dimension $d$ using Flory arguments. The Appendixes contains the mapping to Burgers, and mode details.

## II. FROM THE DISCRETE MODEL TO THE CONTINUUM: ONE-POINT DISTRIBUTIONS

### A. Scaling exponents and dimensionless units

We now start from the discrete model where $u \in Z$ and $V(u)$ are i.i.d. random variables drawn from the distribution $P(V)$. We show that one obtains a nontrivial continuum limit in the limit $m \to 0$ upon rescaling of $u$ (in what we call dimensionless units below). This procedure makes the universality appear clearly.

Let us study first the one-point distributions. For that purpose we can set $r = 0$ and consider $H = H(r = 0)$. The probability that the minimum total energy $H$ is attained in position $u$ with a value of the disorder $V$ is equal to the product of (i) the probability $P(V)$ of having $V$ in $u$ and (ii) the probability to have higher total energies on all the other sites $u' \neq u$. It is thus given by the infinite product:

$$p(u,V) = P(V) \prod_{u' \neq u} P_>\left(H - \frac{m^2 u'^2}{2}\right). \tag{5}$$

To study the limit of small $m$, it is convenient in the following to absorb the dependence with $m$ in the units $(u_m, H_m, V_m)$ defined for the variables $(u, H, V)$, respectively. One can then recover the dimensionful results by the substitution in all

dimensionless results:

$$u \to u/u_m = m^{\zeta} u,$$
$$V \to V/V_m = m^{\theta} V,$$
$$H \to H/H_m = m^{\theta} H.$$

Except if stated, we work now in the dimensionless system of units defined above. Without loss of generality, $A$ in Eq. (1) has been set to 1 by a rescaling of $V$.

At this stage the exponents $\theta$ and $\zeta$ are not specified. To obtain a nontrivial limit one needs to scale $V$ as $m^2u^2$ which imposes the exponent relation:

$$\theta = 2\zeta - 2, \tag{6}$$

which is known in the directed polymer context as the STS relation [28].

The joint PDF Eq. (5) for the optimal position $u$ and the value of the random potential $V$ on the optimal site then becomes, in the small $m$ limit,

$$\begin{aligned} p(u,V) &= m^{-\zeta-\theta} P(m^{-\theta}V) \prod_{u' \neq u} P_{>}\left[m^{-\theta}\left(H - \frac{u'^2}{2}\right)\right] \\ &\approx \frac{\mu}{|V|^{1+\mu}} \exp\left\{-\int du' m^{-\zeta} P_{<}\left[m^{-\theta}\left(H-\frac{u'^2}{2}\right)\right]\right\} \\ &\quad \times \theta_{H<0} \\ &\approx \frac{\mu}{|V|^{1+\mu}} \exp\left(-F_{\mu}\left|V + \frac{u^2}{2}\right|^{\frac{1}{2}-\mu}\right)\theta_{V+\frac{u^2}{2}<0}, \end{aligned} \tag{7}$$

where $H = V + \frac{u^2}{2}$ and we denote everywhere $\theta_{x<0}$ the characteristic function of the interval (Heaviside function). Here and below we denote

$$F_{\mu} = \frac{\sqrt{2\pi}\,\Gamma[\mu - 1/2]}{\Gamma[\mu]}. \tag{8}$$

The joint PDF of $u$ and $H$ is simply $p(u, V = H - \frac{u^2}{2})$. Going from the infinite product to the exponential in the second line of Eq. (7) requires that $P_{>}(\cdot) \sim 1$ at all sites, or equivalently $H < 0$, which is verified for $m$ small enough. The final expression for the joint PDF Eq. (7) is normalized to unity $\int dV\, du\, p(u,V) = 1$, which shows that we have correctly taken the small mass limit (no regions have been overlooked). More precisely, and as is further explained in Appendix B, as $m \to 0$ (the continuum limit), the rescaled cumulative (CDF) $m^{-\zeta} P_{<}(m^{-\theta} y)$ converges to $\frac{\theta_{-y}}{(-y)^{1+\mu}}$ [under the condition that the right tail is in $o(V^{-(1+\mu)})$; cf. Appendix B]. Hence only the contribution of the left tail of $P_{<}(\cdot)$ contributes to the integral in Eq. (7), a typical behavior in power-law statistics, and one can readily replace $P_{<}(\cdot)$ by its asymptotic expression (such estimates can be established rigorously by the use of Tauberian theorems [29]). This implies the second relation:

$$\zeta = \mu\theta, \tag{9}$$

which leads to

$$\zeta = \frac{2\mu}{2\mu - 1}, \tag{10}$$

$$\theta = \frac{2}{2\mu - 1}. \tag{11}$$

One could wonder about the existence of a threshold value $\mu_c$ above which the algebraic decay of the tails is fast enough to recover the behavior in the Gaussian disorder $\zeta = \zeta_{SR}$ and $\theta = \theta_{SR}$ (where $SR$ stands for *short-range Gaussian disorder*). One notes that, unlike the directed polymer (see Sec. V), such a finite critical value $\mu_c$ for the disorder tail doesn't exist. In other words, any power-law tail matters. More precisely, one can say that $\mu_c = +\infty$. In that limit, indeed, $\zeta \to 1$ which is the value for the Gumbel class [12]. There is an interesting crossover in that limit where the leading contribution goes from the bulk of $P(V)$ (as is the case for the Gumbel class) to the tail (for the present power-law case).

### B. Results for the one-point distributions

From Eq. (7), one can obtain the joint distribution of $(H,V)$. Taking into account the Jacobian $\frac{\partial(u,V)}{\partial(H,V)} = [\sqrt{2}(H-V)]^{-1/2}$ and a factor of 2 from integration over positive and negative $u$ yields

$$p(H,V) = \frac{\mu\sqrt{2}}{|V|^{1+\mu}\sqrt{H-V}} e^{-F_{\mu}|H|^{\frac{1}{2}-\mu}} \theta_{H<0, V<H}. \tag{12}$$

After integration, one obtains the various marginal distributions of $H$, $V$, and $u$. First we obtain

$$p(H) = \frac{\left(\mu - \frac{1}{2}\right)F_{\mu}}{|H|^{\mu+\frac{1}{2}}} e^{-F_{\mu}|H|^{\frac{1}{2}-\mu}} \theta_{H<0}. \tag{13}$$

Hence the PDF of the total energy $H$ is a Frechet distribution. On one hand, this appears as natural since we are dealing with extreme value statistics of heavy-tailed distributions. However, the index of the Frechet distribution is not $\mu$ (as would be naively expected) but $\mu - 1/2$, which is thus a correction coming from the competition with the elastic energy. As the particle chooses amongst the deepest sites, the distribution of its energy acquires a power-law tail which is even broader than the initial disorder. It is easy to extend the above calculation to a generalized elastic energy growing as $u^{\alpha}$, the modified index being then $\mu - 1/\alpha$.

Next we also obtain the PDF of the potential $V$ at the position of the minimum as

$$p(V) = \frac{\mu}{|V|^{\mu+1}} \phi_{\mu}(|V|)\theta_{V<0}, \tag{14}$$

where we have defined the auxiliary function:

$$\phi_{\mu}(x) = \sqrt{2}\int_0^x \frac{dy}{\sqrt{x-y}} e^{-F_{\mu} y^{\frac{1}{2}-\mu}}. \tag{15}$$

Note that the factor $\phi_{\mu}(|V|)$ gives the relative change of the tail of the PDF of the potential at the optimal site with respect to the tail of the original PDF of the disorder. For $|V|$ of order one it is of order one; hence the original tail exponent is not

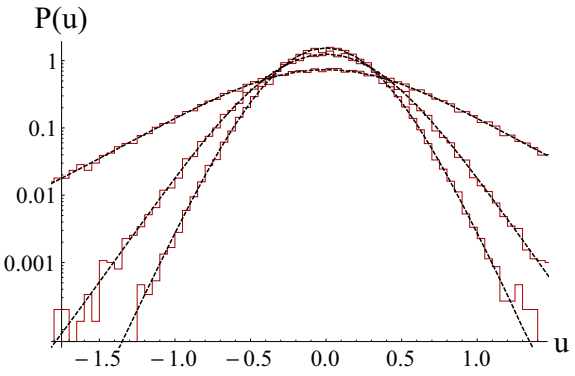


FIG. 2. (Color online) Comparison of the PDF for the position $u$ as given in Eq. (17) (black dashed lines) with numerical simulations (red solid lines). The algebraic tails are clearly distinguishable as straight lines on the semilogarithmic plot. From the narrowest shape to the broadest (corresponding to the fatter tails), $\mu = 15$, 10, and 4. The sample size is $N = 5 \times 10^5$.

changed, but the amplitude is changed.[2] For large negative $V$, it diverges; hence we find

$$p(V) \simeq \frac{2\sqrt{2}\mu}{|V|^{\mu+\frac{1}{2}}}, \quad V \to -\infty, \tag{16}$$

which is again the original tail but with the same shift in the exponent $\mu \to \mu - \frac{1}{2}$ as noticed above, and a different amplitude. This surprising shift can be recovered by invoking results from record statistics theory. Consider a realization of the disorder with a particularly deep minimum, where the particle sits. From record statistics, it is known that the tail of the minimum of $N$ heavy-tailed random variables decays as $\sim \frac{N}{V^{1+\mu}}$. Balancing elastic energy and potential leads to $E \sim u^\alpha \sim V$, and then to $N \sim u \sim V^{1/\alpha}$. Hence the dependence of $N$ with $V$, inherent to the fact that large deviations in the disorder allows the particle to explore a larger space, leads to a modified exponent $\mu - 1/\alpha$ of the tail of $H$ and $V$.[3]

Finally we obtain the PDF of the optimal position $u$ of the particle as

$$p(u) = \mu\, \psi_\mu\left(\frac{u^2}{2}\right) \tag{17}$$

in terms of the auxiliary distribution:

$$\psi_\mu(x) = \int_0^\infty \frac{dy}{(x+y)^{\mu+1}} e^{-F_\mu y^{\frac{1}{2}-\mu}}. \tag{18}$$

The PDF of $u$ decreases from a constant at $u = 0$ to a power law at large $u$. The position of the particle is thus heavy tailed as well as its PDF decays as

$$p(u) \simeq \frac{2^\mu}{u^{2\mu}}, \quad |u| \to +\infty. \tag{19}$$

[2]One should keep in mind that here $V$ denotes the dimensionless potential; hence it is deep in the tail, since we use units of $V_m \sim m^{-\theta}$.

[3]We thank Jean-Philippe Bouchaud for helping to set up this argument.

The moments $\overline{u^{2n}}$ thus exist only for $2n < 2\mu - 1$ and are given in Appendix C. The comparison with numerics is made in Fig. 2. Finally, note that for $\mu < \frac{1}{2}$ the particle explores the whole space $u \sim W$, as the energy of the optimal site $\sim u^{1/\mu}$ grows faster than the elastic energy $\sim u^2$.

We note that the PDF of the "elastic energy" $E = u^2/2$ has also a tail:

$$p(E) \simeq \frac{1}{\sqrt{2}} \frac{1}{E^{\frac{1}{2}+\mu}}, \tag{20}$$

with exponent $\mu - \frac{1}{2}$ analogous to Eq. (16) for large values.

To conclude, the typical $H, V$ of order one are already drawn in the original tail of $P(V)$ with exponent $\mu$ (since we work in the units $m^{-\theta}$) and the rare events acquire a tail with exponent $\mu - \frac{1}{2}$.

## III. STATISTICS OF THE SHOCKS

As the center of the harmonic potential $r$ is shifted, the optimal position $u(r)$ of the particle is changed as shown in Fig. 3. This corresponds to a jumpy motion of the particle; each jump is called a shock because corresponding to traveling shocks in the Burgers velocity field (see Appendix A). We now introduce the Poisson process model.

### A. General case

#### 1. Poisson process model and one-point distribution

The computation on the discrete model being rather cumbersome, we follow [25] and start directly in the continuum by distributing the random energies over the line as a Poisson process over the plane $(V,u)$ of density $f(V)dV\,du$. Each cell of size $dV\,du$ is then either occupied or not, depending on the value of the random potential $V_i$ at site $u_i$. This means that the potential is defined only at the $u_i$ with values $V(u_i) = V_i$ and that

$$H(r) = \min_j H_j(r) = \min_j \left(V_j + \frac{(u_j - r)^2}{2}\right), \tag{21}$$

$$u(r) = \operatorname{argmin} H_j(r). \tag{22}$$

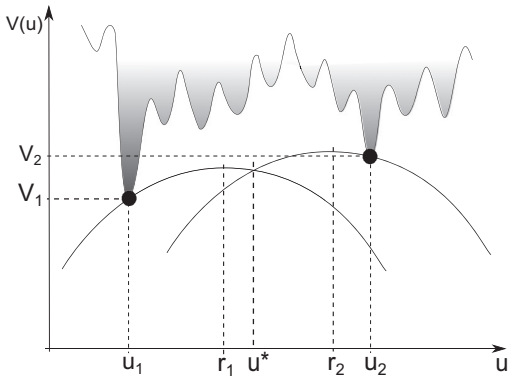


FIG. 3. Parabola construction for the minimization problem: when the center $r$ of the parabola is shifted from $r_1$ to $r_2$, the position of the particle moves from $u_1$ to $u_2$. For given $r_1$ and $r_2$, the intersection of both the parabola is called $u^*$. More details are displayed in Appendix E.

We denote the primitive $F(x) = \int_{-\infty}^{x} f(t)dt$ and assume that $F(+\infty) = +\infty$. We now calculate, using methods similar to the one of [25], the one- and two-point characteristic function of the field $u(r)$.

For the one-point function we can choose $r = 0$, and define $u = u(0)$. Using formulas similar to Eq. (5) we find for the joint distribution of position and potential at the minimum

$$p(u,V)dV\,du = f(V)dV\,du \prod_{dV'du'} \left(1 - \theta_{V'+\frac{u'^2}{2}<V+\frac{u^2}{2}} f(V')dV'du'\right). \tag{23}$$

From the infinitesimal version of Eq. (5), and after the change of variables $z = u'$, $\phi = V + \frac{u^2}{2}$, the one-point distribution of the position of the minimum can be expressed as

$$p(u) = \int d\phi\, f\left(\phi - \frac{u^2}{2}\right) \exp\left[ - \int dz\, F\left(\phi - \frac{z^2}{2}\right)\right]. \tag{24}$$

It is easy to check the normalization $\int du\, p(u) = 1$ by noting that the integral is a total derivative. This result is valid for arbitrary Poisson measure $f(V)$. As we discuss below one can recover the results of the previous section in a particular case.

### 2. *Shock and droplet size distributions*

To describe the statistical properties of the jumps of the optimal position $u(r)$ of the particle as $r$ is varied one defines the shock density as

$$\rho(s) = \lim_{\delta r \to 0^+} \frac{1}{\delta r} \overline{\delta[u(r+\delta r) - u(r) - s]}. \tag{25}$$

Another definition, equivalent in the present case, uses the decomposition

$$u(r) = \sum_i s_i \theta_{r>r_i} + \tilde{u}(r), \tag{26}$$

where $\tilde{u}(r)$ is the smooth part of the field $u(r)$, which, for the Poisson process model can be set to zero. For other models in the same universality class this part is subdominant. The shock density is then defined as [9]

$$\rho(s) = \overline{\delta(r - r_i)\delta(s - s_i)}, \tag{27}$$

where the $(r_i, s_i)$ are the positions and sizes of the shocks. Note that all the $s_i > 0$.

The shock density is intimately related to another quantity, the droplet density $D(s)$, namely the probability density for the total energy $H_j(r)$ in (21) for a given $r$, to exhibit two degenerate minima at positions $u_1$ and $u_2$, separated in space by $s = u_2 - u_1$ (see Fig. 4). By construction $D(s)$ is a symmetric function $D(s) = D(-s)$ and has dimension $1/(sE)$, where $E$ is an energy. More precisely, it is defined as $D(s) = \int du_1 du_2 \delta(s - u_2 + u_1) p(u_1, u_2, 0)$, where $p(u_1, u_2, E)$ is the probability density for the absolute minimum in $u_1$ and the secondary minimum in $u_2$ separated by $E > 0$ in energy. Note that the knowledge of this function allows one to study more generally the statistics of several interesting observables (e.g., the position $u$) at low (but nonzero) temperature (for more details of the procedure, see, e.g. [12,30]).

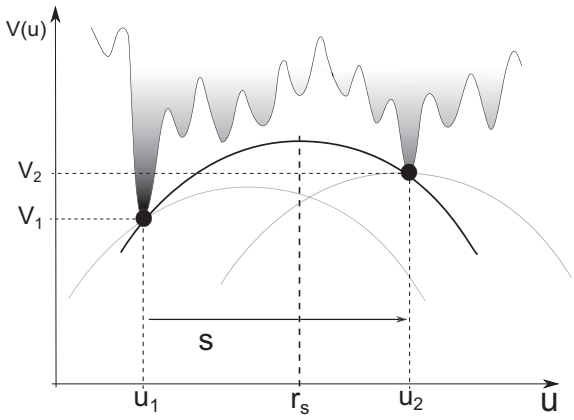


FIG. 4. Discontinuous motion of the particle can be decomposed in shocks. Those shocks occur (here in $r_s$) while the parabola is shifted and touches the potential at two positions $u_1$ and $u_2$, as depicted. The size of the shock is denoted $s = u_2 - u_1$.

As before, we denote the minimal total energy $\phi = H(u_1) = H(u_2)$. Requiring all the other sites to have higher total energy induces a factor $\exp[-\int F(\phi - z^2/2)dz]$ similar to Eq. (24). Then the integrated probability over the value $\phi$ of the minimum and the positions $u_1$ and $u_2$ at fixed $s = u_2 - u_1$ lead to

$$D(s) = \int d\phi\, du_1 du_2 f\left(\phi - \frac{u_1^2}{2}\right) f\left(\phi - \frac{u_2^2}{2}\right) \times \exp\left[ - \int F\left(\phi - \frac{z^2}{2}\right) dz\right] \delta(s - u_2 + u_1). \tag{28}$$

The relation between the shock and the droplet density can be written (see Ref. [12], Secs. IV B 5 and E 4) for $s > 0$:

$$\rho(s) = s D(s) \theta_{s>0}. \tag{29}$$

The factor $s$ originates from the change of variable from energy to position as $\frac{\partial H}{\partial r}$ noting that a small change in the position of the parabola around the point of degeneracy amounts to shift the relative energies of the two states by

$$\delta H = \delta r \times (u_1 - u_2). \tag{30}$$

Using this relation, from Eq. (29) we now obtain the shock density, which can be rewritten as, for $s > 0$,

$$\rho(s) = \frac{s}{2} \int d\phi\, dz\, f\left(\phi - \frac{(z-s)^2}{8}\right) \times f\left(\phi - \frac{(z+s)^2}{8}\right) e^{-\int dz' F(\phi - \frac{z'^2}{2})}, \tag{31}$$

where we denoted $z = u_1 + u_2$.

From the shock density one can define a normalized size probability distribution as

$$\rho(s) = \rho_0 p(s), \tag{32}$$

where $\int_0^\infty ds\, p(s) = 1$ and $\rho_0$ is the total shock density. The density $\rho(s)$ satisfies the following "normalization" identity:

$$\int_0^\infty ds\, s\, \rho(s) = 1, \tag{33}$$

which expresses that all the motion occurs in the shocks. Similarly $D(s)$ satisfies $\int_{-\infty}^{+\infty} ds\, s^2 D(s) = 2$. This identity, proved in Appendix D, is a signature of the STS relations which originate from the statistical translational invariance of the problem.

As a consistency check, $\rho(s)$ can also be extracted from the small separation behavior of the two-point characteristic function of the position field $u(r)$, for $r > 0$:

$$\overline{e^{\lambda[u(r)-u(0)]}} = 1 + r \int_0^\infty ds\, \rho(s)(e^{\lambda s} - 1) + O(r^2). \quad (34)$$

The calculation of this function is more cumbersome and displayed in Appendix E. As shown there, by identification in the above formula one recovers Eq. (31).

### B. Scale invariance and universality classes

From Eq. (31), one can read the distribution of the shock sizes for any disorder in the continuum Poisson process model. For this model to be a "fixed point" (i.e., continuum limit) of a more general class of models (e.g., the discrete model studied in Sec. II as $m \to 0$) one should in addition require scale invariance. Then, similar to the usual problem of extremal statistics [31], and to the problem of the driven particle [27], three different classes of universality emerge. The nice feature of the Poisson process model is that it contains the three scale-invariant models.

#### 1. Three universality classes

Let us consider again the minimization problem (22) in a dimensionful form:

$$H_m(r) = \min_j \left( V_j + m^2 \frac{(u_j - r)^2}{2} \right). \quad (35)$$

Let us require that $H_m(r)$ is scale invariant *in law*, i.e., that $H_m(m^{-\zeta} r)$ has the same distribution as $m^{-\theta} H_{m=1}(r)$, possibly up to an additive constant in $H$. One easily sees that it implies that $f(m^\theta V) = m^{-(\theta+\zeta)} f(V + C_m)$ and the STS exponent relation (6). There are three type of solutions.

(i) The "Gumbel" class, where the disorder left tail is exponentially fast decaying. This case corresponds to the well-known Kida statistics of the Burgers equation [10], and is obtained for a Poisson density $f(\phi) = e^\phi$ with the density of shocks:

$$\rho(s) = \frac{1}{2\sqrt{\pi}} s\, e^{-s^2/4}. \quad (36)$$

(ii) The "Weibull" class, where the disorder is bounded from below. It corresponds to the Poisson process model with $f(\phi) = \frac{1}{\phi^{1+\mu}} \theta_{\phi>0}$ with $-\infty < \mu < -1$. This model was studied in [25].

(iii) The "Frechet" class, the focus of the present paper, where the disorder presents an algebraic left tail, accounting for rare but large events. It corresponds to the choice $f(\phi) = \frac{1}{|\phi|^{1+\mu}} \theta_{\phi<0}$. As discussed above, this choice represents the continuous limit of the system defined in Sec. II.

Note that in all three classes the exponents are given by (10), the Gumbel class corresponding to $\mu = +\infty$ (with additional logarithmic corrections in that case).

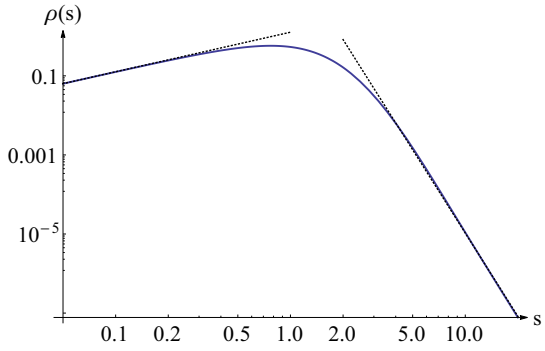


FIG. 5. (Color online) PDF $\rho(s)$ of the shock size, plotted from Eq. (37) for $\mu = 3/2$. In black dotted lines are the asymptotics for small and large $s$ as given by Eqs. (38) and (39).

We now study in more detail the distribution of shock sizes in the Frechet class, and compare to the classical Kida statistics.

#### 2. Shock size distribution in the Frechet universality class

Let us consider the Poisson process model with the choice

$$f(\phi) = \frac{\mu}{(-\phi)^{1+\mu}} \theta_{\phi<0},$$
$$F(\phi) = \frac{1}{(-\phi)^\mu} \theta_{\phi<0} + \infty \times \theta_{\phi>0}.$$

With this choice one sees that Eq. (24) for $p(u)$ for the Poisson model becomes identical (identifying $y = -\phi$) to Eq. (17) for the discrete model with the same constant $F_\mu$ given by (8). Note that the exponential factor in Eq. (24) vanishes if $\phi > 0$; hence the $\phi$ integration is in effect restricted to $\phi < 0$.

We now consider the shock size distribution from Eq. (31):

$$\rho(s) = \mu^2 s \int_0^\infty dz \int_{-\infty}^0 d\phi\, \exp(-F_\mu |\phi|^{\frac{1}{2}-\mu}) \times \left[ \left( \frac{(z+s)^2}{8} - \phi \right) \left( \frac{(z-s)^2}{8} - \phi \right) \right]^{-(1+\mu)} \quad (37)$$

and we assume here $\mu > 1/2$. This distribution is plotted Fig. 5.

This function does not exhibit any divergence for small shock sizes, rather it behaves similarly to the Kida distribution at small $s$ with

$$\rho(s) \simeq C_\mu s \quad (38)$$

and the constant $C_\mu$ is displayed in Appendix F. The main difference arises in the behavior of the large shocks. Instead of the exponential tail $e^{-s^2/2}$ in the Kida case, it shows algebraic tails of the form (see Fig. 5)

$$\rho(s) \simeq \frac{2^{2+\mu}\mu}{s^{\tau'}} \text{ for large } s, \quad (39)$$

with the decay exponent $\tau'$ for the right tail:[4]

$$\tau' = 1 + 2\mu. \tag{40}$$

To obtain this result from Eq. (37) one notes that it is the region for $z$ near $s$ which contributes most; hence one shifts $z \to z + s$ in Eq. (37) and replaces $\frac{1}{8}(z+2s)^2 - \phi \to s^2/2$ in the first factor. The remaining integral can be extended from $z \in [-\infty, \infty]$ and can then be performed exactly, being related to the normalization of the distribution $p(u)$ of a single minimum (17): one uses $\int dz\, \psi_\mu(z^2/8) = 2/\mu$. Note that since we assumed $\mu > 1/2$ it implies that $\tau' > 2$; hence the integral (33) exists, as required. However, the second moment of the shock size, $\int_0^{+\infty} ds\, s^2 \rho(s)$, is finite only for $\mu > 1$.[5]

Finally, it is useful to recall for comparison the avalanche size distribution for the nonequilibrium version of this model, i.e., the quasistatic depinning. There the jumps occur between the metastable states actually encountered in the driven dynamics as $r$ increases, which are different from the absolute energy minima. The result of [27] for the Frechet class for the normalized distribution is

$$p(s) = \frac{(\alpha+1)(\alpha+2)}{\Gamma\left(2+\frac{1}{\alpha}\right)} \int_0^{+\infty} \frac{dy}{(y+s)^{3+\alpha}} e^{-y^{-\alpha}}, \tag{41}$$

where the local disorder *force* is short-range distributed with a heavy-tail index $\mu = 1 + \alpha$. The large $s$ behavior is also a power law $p(s) \sim s^{-(2+\alpha)} \sim s^{-(1+\mu)}$.

## IV. MODEL IN DIMENSION $D > 1$

The methods of solution presented in the previous sections can be extended to the toy model of the particle (i.e., $d = 0$) in general (external) space dimension $\mathbf{u} \in R^D$. The position of the minimum when the quadratic well is centered in $\mathbf{r} \in R^D$ is now denoted as $\mathbf{u}(\mathbf{r})$, a vector process which exhibits jumps; in fact it is constant on cells in $R^D$, separated by shock walls with discontinuities where it jumps by $\mathbf{s}$. To generalize most of the calculations one must simply replace the integrals over the spatial variable $u$ by integrals over vectors $\mathbf{u}$. The new scaling exponents necessary to retain invariance of the tail of the potential are

$$\zeta = \frac{2\mu}{2\mu - D}, \tag{42}$$

$$\theta = \frac{2D}{2\mu - D}, \tag{43}$$

which reduce to Eq. (10) for $D = 1$ and still satisfy the relation (6). Let us first discuss one-point probabilities, hence setting $\mathbf{r} = 0$.

[4]We use the notation $\tau'$ to distinguish from the exponent for the divergence of *small* shocks usually called $\tau$.

[5]In the functional RG this quantity equals $-\Delta'(0^+)/m^4$, while the second moment of $p(u)$ in Eq. (17) is $m^2\overline{u^2} = \Delta(0)$ (which exists only for $\mu > 3/2$), where $\Delta(u)$ is the correlator of the renormalized disorder (see [9,12] for definitions).

### A. One-point distribution

Due to the rotational invariance of the elastic energy, one readily obtains the joint distribution:

$$p(\mathbf{u}, V) = \frac{\mu}{|V|^{1+\mu}} e^{-F_{\mu,D}|H|^{\frac{D}{2}-\mu}} \theta_{H<0}, \tag{44}$$

where $H = V + \frac{u^2}{2}$. It is normalized to unity $\int d^D\mathbf{u}\, dV\, p(\mathbf{u}, V) = 1$ and we have defined

$$F_{\mu,D} = S_D 2^{D/2-1} \frac{\Gamma[D/2]\Gamma[\mu - D/2]}{\Gamma[\mu]}, \tag{45}$$

where $S_D$ is the surface of the unit sphere in dimension $D$ ($S^1 = 2$). From this we extract the joint distribution of $V$ and $H$ as

$$p(V,H) = S_D 2^{\frac{D}{2}-1} (H - V)^{\frac{D}{2}-1} \frac{\mu}{|V|^{1+\mu}} \tag{46}$$

$$\times \exp\left(-F_{\mu,D}|H|^{\frac{D}{2}-\mu}\right) \theta_{H<0, V<H}, \tag{47}$$

which exhibit a "level repulsion" between $H$ and $V$ for $D > 2$.

The marginal distribution for $H$ is again a Frechet with index now $\mu - \frac{D}{2}$:

$$p(H) = \frac{\left(\mu - \frac{D}{2}\right) F_{\mu,D}}{|H|^{\mu - \frac{D}{2} + 1}} e^{-F_{\mu,D}|H|^{\frac{D}{2}-\mu}} \theta_{H<0}, \tag{48}$$

while the PDF of $V$ takes the form

$$p(V) = \frac{\mu S_D}{2^{1-D/2}|V|^{\mu+1}} \phi_\mu^D(|V|)\theta_{V<0}, \tag{49}$$

where we have defined

$$\phi_\mu^D(x) = \int_0^x \frac{dy}{(x-y)^{1-D/2}} e^{-F_{\mu,D} y^{\frac{D}{2}-\mu}}. \tag{50}$$

Finally, the distribution of the optimal position is

$$p(\mathbf{u}) = \mu\, \psi_\mu^D\left(\frac{u^2}{2}\right), \tag{51}$$

where

$$\psi_\mu^D(x) = \int_0^\infty \frac{e^{-F_{\mu,D} y^{\frac{D}{2}-\mu}}}{(x+y)^{\mu+1}} \tag{52}$$

and, interestingly, the tail exponent of $P(\mathbf{u})$ is independent of $D$:

$$p(\mathbf{u}) \simeq \frac{2^\mu}{u^{2\mu}}, \quad |u| \to +\infty, \tag{53}$$

while the PDF for the radius $|u|$ decays as $\simeq 2^\mu S_D/|u|^{2\mu+1-D}$.

Note that the condition for the thermodynamic limit to be defined is now $\mu > \frac{D}{2}$, as the typical minimum site energy at a distance $u$ of the center grows as $u^{D/\mu}$.

### B. Droplet and shock densities

Note that the formula for the droplet density also generalizes easily in $D$ dimension as

$$D(\mathbf{s}) = \int d\phi\, d^D\mathbf{u}_1 d^D\mathbf{u}_2 f\left(\phi - \frac{u_1^2}{2}\right) f\left(\phi - \frac{u_2^2}{2}\right)$$

$$\times \exp\left[-\int F\left(\phi - \frac{z^2}{2}\right) d\mathbf{z}\right] \delta^D(\mathbf{s} - \mathbf{u}_2 + \mathbf{u}_1), \tag{54}$$

where $\vec{s}$ is the vector joining the two degenerate minima. It is now normalized as

$$\int d^D\mathbf{s}\, s^2 D(\mathbf{s}) = 2D \tag{55}$$

as shown in Appendix D. The shock density is now defined by reference to a direction of unit vector $\mathbf{e}_x$ as

$$\rho(\mathbf{s}) = \lim_{\delta r\to 0^+} \frac{1}{\delta r}\overline{\delta^D[\mathbf{u}(\mathbf{r}+\delta r\mathbf{e}_\mathbf{x}) - \mathbf{u}(\mathbf{r}) - \mathbf{s}]}. \tag{56}$$

Since Eq. (30) generalizes to $\delta H = \delta r\mathbf{e}_\mathbf{x}\cdot(\mathbf{u}_1 - \mathbf{u}_2)$, one sees that the relation between the shock and droplet densities is now

$$\rho(\mathbf{s}) = s_x D(\mathbf{s})\theta_{s_x>0}, \tag{57}$$

where $s_x = \mathbf{s}\cdot\mathbf{e}_x$ denotes the component of the jump along the direction $x$.

Using isotropy it now enjoys the normalization

$$\int_{s_x>0} d^D\mathbf{s}\, s_x\rho(\mathbf{s}) = 1, \tag{58}$$

which, again, expresses that all motion when $\mathbf{r}$ varies along a line occurs in shocks. Note that the relation Eq. (57), combined with the isotropy of $D(\mathbf{s})$ implies a number of relations[6] between moments, for instance,

$$\langle s_x^2\rangle = 2\langle s_y^2\rangle, \tag{59}$$

as well as $\langle s_x^4\rangle = \frac{8}{3}\langle s_y^4\rangle = 4\langle s_x^2 s_y^2\rangle$ and so on *provided these moments exist*, i.e., that the tail of $D(\mathbf{s})$ decays fast enough.[7]

It is interesting to note that Eqs. (54) and (57) factorize in the Kida (i.e., Gumbel) universality class [i.e., with the choice $f(\phi) = e^\phi$] leading to the simple result, after some Gaussian integrations:

$$\rho(\mathbf{s}) = \frac{s_x}{(4\pi)^{\frac{D}{2}}} e^{-s_x^2/4} e^{-\mathbf{s}_\perp^2/4}, \tag{60}$$

where we denote $\mathbf{s} = (s_x, \mathbf{s}_\perp)$ and $s_\perp$ represents the "wandering" part of the shock motion, transverse to the shift direction of the parabola. For instance, in two dimension $\mathbf{s} = (s_x, s_y)$, Eq. (60) reads $\rho(\mathbf{s}) = \rho_{D=1}(s_x)D_{D=1}(s_y)$. Hence, in the Kida case, higher dimension statistics of the shocks are completely solved from the $D = 1$ case.

The Frechet case, however, does not simplify as nicely. One now obtains

$$\rho(s) = \mu^2 \frac{s_x}{2^D}\int_0^\infty d^D\mathbf{z}\int_{-\infty}^0 d\phi\, \exp\left(-F_{\mu,D}|\phi|^{\frac{D}{2}-\mu}\right) \times\left[\left(\frac{(\mathbf{z}+\mathbf{s})^2}{8}-\phi\right)\left(\frac{(\mathbf{z}-\mathbf{s})^2}{8}-\phi\right)\right]^{-(1+\mu)} \tag{61}$$

and we assume here $\mu > D/2$. The tail for large $s = |\mathbf{s}|$ is obtained, by manipulations similar to the case $D = 1$ as

$$\rho(s) \simeq \frac{2^{2+\mu}\mu s_x}{s^{2+2\mu}} \text{ for large } s. \tag{62}$$

Interestingly, going to higher dimensions allows the fluctuations of the particle motion to spread even more. To illustrate that fact one can compute the marginal shock density along $\mathbf{e}_x$ defined as

$$\rho(s_x) = \int_{s_\perp}\rho(\mathbf{s}) = s_x\theta_{s_x>0}\int_{s_\perp} D(\mathbf{s}). \tag{63}$$

After some integrations from Eq. (61) one finds

$$\rho(s_x) = \mu^2 F_{\mu+1,D-1}^2 s_x\int_0^\infty dz\int_{-\infty}^0 d\phi\, e^{-F_{\mu,D}|\phi|^{\frac{D}{2}-\mu}} \times\left[\left(\frac{(z+s_x)^2}{8}-\phi\right)\left(\frac{(z-s_x)^2}{8}-\phi\right)\right]^{-(\frac{3-D}{2}+\mu)}. \tag{64}$$

Hence a formula very similar to Eq. (37), but with a modified exponent $\tilde{\mu} = \mu - (D-1)/2$, leading to an asymptotic algebraic decay of the shock size along $x$ with exponent $\tau' = 2 - D + 2\mu$. The thermodynamic condition $\mu > D/2$ again ensures that the normalization integral (58) exists.

## V. ELASTIC MANIFOLDS: RECALLING THE GENERAL FLORY ARGUMENT

We now check that the obtained values for the exponents agree with the general argument. For this we now recall the Flory argument given in [6] for the directed polymer, which we straightforwardly generalize to a manifold of internal dimension $d$ (internal coordinate $x \in R^d$) with $D$ displacement components $u \in R^D$. We consider that the random potential $V(x,u)$ lives in a total embedding space dimension $d + D$ and has short-range correlations with a heavy-tailed PDF (1) indexed by $\mu$. Assume that a piece of size $L$ (in $x$) explores typically $W \sim L^\zeta$ in dimension $D$. The volume explored by the manifold is $L^d W^D$; hence the minimal value of $V$ on this volume behaves as $\sim(L^d W^D)^{1/\mu}$. This leads to $\mu\theta = d + D\zeta$. Imposing again that elasticity and disorder scale the same way (this is guaranteed by the general STS symmetry, i.e., statistical invariance under tilt) leads to $\theta = 2\zeta + d - 2$. Hence we obtain

$$\zeta = \frac{d+\mu(2-d)}{2\mu - D}, \tag{65}$$

$$\theta = \frac{2d + D(2-d)}{2\mu - D}, \tag{66}$$

with the (naive) threshold value beyond which one (presumably) recovers Gaussian disorder universality class:

$$\mu_c = \frac{d + D\zeta_{SR}}{d - 2 + 2\zeta_{SR}}, \tag{67}$$

where $\zeta_{SR}$ is the roughness exponent for short-range Gaussian disorder. For $d = 0$ one recovers the above values Eq. (42) and Eq. (43) for the toy model in general dimension $D$. For $d = 1$, $\zeta_{SR} = 2/3$ and $\theta_{SR} = 1/3$, which gives the value $\mu_c = 5$ given in [6] and recalled in the Introduction. It is interesting

[6] These are easily shown, e.g., by integrating with respect to $D(\mathbf{s}) \to e^{-\mu s^2}$, since any isotropic distribution can be represented as a superposition of such weights.

[7] The relation (59) is believed to be more general (i.e., to extend to interfaces) and was anticipated in [32], where it was related via the functional RG to the existence of a cusp in the effective action of the theory (see also [33]).

to note that at the upper-critical dimension $d_{uc} = 4$, $\zeta_{SR} = 0$; hence the critical value is $\mu_c = 2$.

## VI. CONCLUSION

In the present paper we have studied the toy model for the interface, i.e., a point in a random potential, in presence of heavy-tailed disorder with exponent $\mu$. In the scaling regime it leads to a universality class analogous to the Frechet class for extreme value statistics. It was found that all the relevant distributions (minimum energy, position, and sizes of shocks) exhibit also power-law tails with modified exponents continuously dependent on $\mu$. Hence the presence of heavy tails in the underlying disorder pervades through all observables and modifies the behavior for every value of $\mu$. That has to be compared with the directed polymer problem, where the effect of heavy tails disappears in favor of a "Gaussian" behavior for $\mu > 5$.

In addition, we have obtained here the shock size distribution for an "exotic" example of decaying Burgers turbulence, close from the Kida class because of the short-range correlations in the initial potential, but markedly different because of the heavy tails.

Finally, because of these heavy tails the functional RG method which, in its present form, is based [12,27] on the existence of the moments of the position of the minimum $u(r)$ cannot be applied in a standard way (at least in $d = 0$). We hope our study will inspire progress on the more general problem of the elastic manifold in the heavy-tailed disorder.

## ACKNOWLEDGMENT

We thank J. P. Bouchaud for useful discussions.

## APPENDIX A: EXOTIC REGIME IN DECAYING BURGERS TURBULENCE

The above particle model is directly related to the Burgers equation for a velocity field $\mathsf{v}(r,t)$, a simplified version of Navier-Stokes used to model compressible fluids:

$$\partial_t \mathsf{v} = \nu \partial_r^2 \mathsf{v} - \tfrac{1}{2}\partial_r \mathsf{v}^2. \tag{A1}$$

This equation can be integrated using the Cole-Hopf transformation. Here we study only the inviscid limit (of zero viscosity $\nu = 0^+$). In that case the solution is given by

$$\mathsf{v}(r,t) = \partial_r H(r) = \frac{r - u(r)}{t}. \tag{A2}$$

In terms of (3) one defines the "time" $t$ as

$$t = m^{-2} \tag{A3}$$

and the initial condition

$$\mathsf{v}(r, t = 0) = \partial_r H(r)|_{t=0} = \partial_r V(r), \tag{A4}$$

where $V(u)$ is the bare disorder of the toy model. In this paper we focused on the case when $V(u)$ is short-range correlated with a heavy tail. This corresponds to a well defined but peculiar type of distribution for the initial velocity field: it also has a tail exponent $\mu$, but exhibits local anticorrelations so that $V(u)$ remains short-range correlated [if $\mathsf{v}(r,t = 0)$ was short-range correlated with a heavy-tail distribution, that would correspond to $V(u)$ following a Levy process, either a Brownian motion for $\mu > 2$ or a Levy flight for $\mu < 2$].

As is well known evolution from a smooth initial condition presents shocks in finite time, i.e., the velocity field $\mathsf{v}(r,t)$ does not remain continuous but presents (negative) jumps in a discrete set of locations $r_\alpha$, where $\mathsf{v}(r_\alpha^+,t) - \mathsf{v}(r_\alpha^-,t) = \Delta\mathsf{v} < 0$. These correspond to the (positive) jumps in $u(r)$, more precisely one has $\Delta\mathsf{v} = -S/t$, where $S$ is the dimensionful shock size $S = u_m s = m^{-\zeta} s$ with the dimensionless size $s$ studied in the present paper. To translate our results in terms of velocity jumps in Burgers, one thus just identifies $\Delta\mathsf{v} = -t^{\frac{\zeta}{2}-1} s$ (indeed the length scale is $m^{-\zeta} = t^{\zeta/2}$), where $\zeta$ is given by Eq. (42).

Finally, the time dependence of the mean energy density $E$ is given by $E = \frac{1}{2}\mathsf{v}^2 \sim t^{-(2-\zeta)} = t^{-2(\mu-D)/(2\mu-D)}$, which recovers the result of [26]. Note that the regime $D/2 < \mu < D$ is very peculiar since it predicts an energy density growing instead of decaying, as discussed there.

## APPENDIX B: FROM INFINITE PRODUCT TO INTEGRAL

To understand better the convergence to the continuum limit let us first choose a Pareto distribution, i.e., with a hard cutoff,

$$P_>(V) = \left(1 - \frac{1}{(-V)^\mu}\right)\theta_{V<V_0}, \tag{B1}$$

and consider again the infinite product Eq. (5). It can be rewritten, in the rescaled units, i.e., $u \to m^{-\zeta} u$, $V \to m^{-\theta} V$ as (taking into account the Jacobian involved in the rescaling)

$$p(u,V) = m^{-(\zeta+\theta)} \frac{\mu}{(m^{-\theta}|V|)^{1+\mu}} \theta_{V<V_0 m^\theta} \times \prod_{u' \neq u} \theta\left(H - \frac{u'^2}{2} < V_0 m^\theta\right) e^{\ln[1 - m^{\mu\theta}(-H + \frac{u'^2}{2})^{-\mu}]}. \tag{B2}$$

We see here that for $m \to 0$ it vanishes unless $H - \frac{u'^2}{2} < 0$ for all $u' \neq u$, but since in that limit the lattice grid tends to continuum, this condition becomes equivalent to $H < 0$. Since $V < H$ we do not need to retain the constraint $V < 0$. The infinite product becomes an integral, and the logarithm can be expanded, leading to

$$p(u,V) = \frac{\mu}{|V|^{1+\mu}} \theta_{H<0} e^{-\int du' (-H + \frac{u'^2}{2})^{-\mu}},$$

which leads to the result given in the text.

The mechanism holds for more general distributions with the same tail. As discussed in the text the rescaled $P_>(m^{-\theta} y)$ converges to unity for $y < 0$ and to zero for $y > 0$ so the precise shape of the distribution does not matter. More precisely, the weight of the events with $H > 0$ vanishes. To illustrate the point consider the worst case, i.e., when $P_>(V)$ is slowly decaying on the positive $V$ side, e.g., as $V^{-\alpha}$. Then, for $H > 0$ (and $m \to 0$), there is an additional factor:

$$\approx \prod_{u' \neq u} \frac{\theta_{H - \frac{u'^2}{2} > 0}}{m^{-\alpha\theta}\left(H - \frac{u'^2}{2}\right)^\alpha} \simeq m^{\alpha\theta} e^{-\int_{-\sqrt{2H}}^{\sqrt{2H}} du' \ln(H - \frac{u'^2}{2})} = O(m^{\alpha\theta}),$$

since the integral is convergent, and this factor kills the contribution of the events with $H > 0$ (more precisely all the events with $H > -m^{-\gamma}$ with any $0 < \gamma < \theta$, in the original units).

## APPENDIX C: MOMENTS OF $u$

From Eq. (17) and Eq. (18), we find the moments, for any real $n > 0$ such that $2n < 2\mu - 1$:

$$\overline{u^{2n}} = F_\mu^{\frac{2n}{2\mu-1}} \frac{2^n \Gamma\left(n+\frac{1}{2}\right)\Gamma\left(\frac{\mu-\frac{1}{2}-n}{\mu-\frac{1}{2}}\right)\Gamma\left(\mu+\frac{1}{2}-n\right)}{\sqrt{\pi}\,\Gamma\left(\mu+\frac{1}{2}\right)}.$$

The $2n$th moment thus diverges as $n \to \mu - \frac{1}{2}|^-$ as

$$\overline{u^{2n}} \simeq \frac{2^\mu}{\mu - \frac{1}{2} - n}. \tag{C1}$$

## APPENDIX D: NORMALIZATION OF THE SHOCK DENSITY

A consistency check for the shock density is to check the normalization given in Eq. (33), i.e., $\int ds\, s\, \rho(s) = 1$. We recall that

$$I = \int_{s>0} ds\, s\, \rho(s) = \frac{1}{2}\int_s s^2 D(s) = \frac{1}{2}\int du_1 du_2 d\phi (u_1-u_2)^2 \times f\left(\phi - \frac{u_1^2}{2}\right) \times f\left(\phi - \frac{u_2^2}{2}\right) e^{-\int dz' F(\phi - \frac{(z')^2}{2})}. \tag{D1}$$

Due to the symmetry in the variables $(u_1,u_2)$, one can only consider, for example,

$$\begin{aligned} I_{u_1} &= \int du_1 du_2 d\phi u_1^2 f\left(\phi - \frac{u_1^2}{2}\right) \times f\left(\phi - \frac{u_2^2}{2}\right) e^{-\int dz' F(\phi - \frac{(z')^2}{2})} \\ &= -\int du_1 d\phi\, u_1^2 f\left(\phi - \frac{u_1^2}{2}\right) \partial_\phi e^{-\int dz' F(\phi - \frac{(z')^2}{2})} \\ &= \int du_1 d\phi\, u_1^2 \partial_\phi f\left(\phi - \frac{u_1^2}{2}\right) e^{-\int dz' F(\phi - \frac{(z')^2}{2})}, \end{aligned} \tag{D2}$$

where we used the fact that, because of the limits $f(\phi) \to 0$ at $\phi \to -\infty$ and $F(\phi) \to \infty$ at $+\infty$, the boundary terms vanish. Considering the argument $\phi - u_1^2/2$ in $f(\cdot)$, one has the equivalence of the operators $\partial_\phi \leftrightarrow -u_1^{-1}\partial_{u_1}$ acting on $f(\cdot)$. Switching to $\partial_{u_1}$ derivatives in Eq. (D2), and integrating by parts once again,

$$\begin{aligned} I_{u_1} &= -\int du_1 d\phi\, u_1 \partial_{u_1} f\left(\phi - \frac{u_1^2}{2}\right) e^{-\int dz' F(\phi - \frac{(z')^2}{2})} \\ &= \int du_1 d\phi\, f\left(\phi - \frac{u_1^2}{2}\right) e^{-\int dz' F(\phi - \frac{(z')^2}{2})} = 1, \end{aligned}$$

where again the boundary terms vanish due to $f(\phi - u^2/2) \to 0$ for $u \to \pm\infty$. Hence $I = \frac{1}{2}(I_{u_1} + I_{u_2}) = 1$ and the normalization is properly recovered. The deeper reason behind these identities arises from the STS symmetry, i.e., the fact that the disorder is statistically translationally invariant (see, e.g. [12,30]).

Note that all the steps of this calculation easily generalize to higher $D$, the only change being that now $u_1^2\partial_\phi \equiv -\mathbf{u}_1 \cdot \nabla_{\mathbf{u}_1}$ acting on $f(\phi - u_1^2/2)$. The final result is then $I = D$ as discussed in the text.

## APPENDIX E: TWO-POINTS FUNCTION

Let us consider the joint probability that $(V_1,u_1)$ and $(V_2,u_2)$ realize the minimum total energy respectively when the quadratic well is centered in $r_1$ and when it is centered in $r_2$, in the same realization of the disorder. The minimal energies are denoted by

$$H_j = V_j + \frac{(u_j - r_j)^2}{2}, \quad j = 1,2. \tag{E1}$$

This probability reads

$$\begin{aligned} &p(V_1,u_1,V_2,u_2)dV_1 du_1 dV_2 du_2 \\ &\quad = f(V_1)f(V_2)dV_1 du_1 dV_2 du_2 \\ &\qquad \times \prod_{\substack{dV_j', du_j' \\ u_1' < u^* \\ u_2' > u^*}} \left(1 - \theta_{V_1' + \frac{(u_1'-r_1)^2}{2} < V_1 + \frac{(u_1-r_1)^2}{2}} f(V_1')dV_1' du_1'\right) \\ &\qquad \times \left(1 - \theta_{V_2' + \frac{(u_2'-r_2)^2}{2} < V_2 + \frac{(u_2-r_2)^2}{2}} f(V_2')dV_2' du_2'\right), \end{aligned} \tag{E2}$$

where $u^*$ is the intersection abscissa of the two parabola, as represented in Fig. 3 given by

$$H_1 - \frac{(u^* - r_1)^2}{2} = H_2 - \frac{(u^* - r_2)^2}{2}, \tag{E3}$$

whose common value is denoted $\phi$ below. The additional Heaviside functions ensure that the random potential lies above these two parabola and touches those parabola on the two points $u_1$ and $u_2$.

The characteristic function can then be written

$$\begin{aligned} \langle e^{\lambda[u(r_2)-u(r_1)]}\rangle = \int dV_1 dV_2 du_1 du_2 e^{\lambda(u_2-u_1)} \big[ & f(V_1)\delta_{V_2=V_1,u_2=u_1} \\ & + f(V_1)f(V_2)\theta_{u_1<u^*<u_2}\big] \\ & \times e^{-\int_{u<u^*} F(H_1 - \frac{(u-r_1)^2}{2}) - \int_{u>u^*} F(H_2 - \frac{(u-r_2)^2}{2})}, \end{aligned} \tag{E4}$$

where the first term accounts for the contribution when there is no shock between $r_1$ and $r_2$ and the second when there is at least one. Let us now perform the change of variables:

$$\begin{aligned} x &= \frac{r_2 - r_1}{2} \quad \text{and} \quad y = u^* - \frac{r_1 + r_2}{2}, \\ z &= u - r_1 \quad \text{and} \quad z' = r_2 - u, \\ z_1 &= u_1 - r_1 \quad \text{and} \quad z_2 = r_2 - u_2, \\ \phi &= H_1 - \frac{(x+y)^2}{2} = H_2 - \frac{(x-y)^2}{2}. \end{aligned} \tag{E5}$$

Hence $x + y = u^* - r_1$ and $x - y = r_2 - u^*$. In terms of the auxiliary functions,

$$\begin{aligned} J_+(\phi,y,x) &= \int_{z_1 \leqslant x+y} dz_1 f\left(\phi + \frac{(x+y)^2 - z_1^2}{2}\right) e^{-\lambda z_1}, \\ J_-(\phi,y,x) &= \int_{z_2 \leqslant x-y} dz_2 f\left(\phi + \frac{(x-y)^2 - z_2^2}{2}\right) e^{-\lambda z_2}, \\ I_+(\phi,y,x) &= \int_{z \leqslant x+y} dz\, F\left(\phi + \frac{(x+y)^2 - z^2}{2}\right), \\ I_-(\phi,y,x) &= \int_{z' \leqslant x-y} dz' F\left(\phi + \frac{(x-y)^2 - z'^2}{2}\right), \end{aligned}$$

the characteristic function of the difference $u(r_2) - u(r_1)$ takes the form

$$\langle e^{\lambda[u(x)-u(-x)]}\rangle = \int d\phi\, dy [f(\phi) + 2x\, e^{2\lambda x} J_+(\phi,y,x) J_-(\phi,y,x)] \times \exp[-I_+(\phi,y,x) - I_-(\phi,y,x)], \quad \text{(E6)}$$

where the $2x = r_2 - r_1$ factor comes from the Jacobian $dV_1 dV_2 du_1 du_2 = 2x\, d\phi\, du^* dz_1 dz_2$.

This formula generalizes to arbitrary $f(\phi)$ the one given in [25] for a particular function $f(\phi)$. There it is given in terms of the (scaled) Burgers velocity field $v(r) = r - u(r)$. One easily checks the normalization, i.e., that for $\lambda = 0$ Eq. (E6) is a total derivative and integrates to unity.

It is now rather straightforward to expand this formula to $O(x)$ and to recover the expression for the shock density $\rho(s)$ given in the text using the identification (34).

## APPENDIX F: ASYMPTOTICS OF THE SHOCK DENSITY

The constant $C_\mu$ in the text can be obtained as

$$C_\mu = \frac{\mu(2\mu-1)(2\pi)^{\frac{\mu+1}{1-2\mu}}}{3(4\mu+1)} \times \frac{\left(\frac{\Gamma(\mu-\frac{1}{2})}{\Gamma(\mu)}\right)^{\frac{4\mu+1}{1-2\mu}} \Gamma\left(2\mu+\frac{3}{2}\right)\Gamma\left(4+\frac{3}{2\mu-1}\right)}{\Gamma(2\mu+2)}, \quad \text{(F1)}$$

where $C_\mu$ is an increasing function which vanishes at $\mu = 1/2^+$ with an essential singularity $C_\mu \simeq \exp(-\frac{3}{4}\frac{2-\ln(9/8)}{\mu-\frac{1}{2}})$ and grows as $C_\mu \simeq \frac{\mu^{3/2}}{2\sqrt{\pi}}$ at large $\mu$.


[1] M. Kardar, G. Parisi, and Y.-C. Zhang, Phys. Rev. Lett. **56**, 889 (1986).
[2] S. Atis, S. Saha, H. Auradou, D. Salin, and L. Talon, Phys. Rev. Lett. **110**, 148301 (2013).
[3] J.-P. Bouchaud and A. Georges, Phys. Rep. **195**, 127 (1990).
[4] Z. Burda, J. Jurkiewicz, M. A. Nowak, G. Papp, and I. Zahed, Phys. Rev. E **75**, 051126 (2007).
[5] K. Janzen, A. Engel, and M. Mézard, Eur. Phys. Lett. **89**, 67002 (2010).
[6] G. Biroli, J.-P. Bouchaud, and M. Potters, Eur. Phys. Lett. **78**, 10001 (2007).
[7] B. Hambly and J. Martin, Probab. Theory Relat. Fields **137**, 227 (2007).
[8] A. Auffinger and O. Louidor, Commun. Pure Appl. Math. **64**, 183 (2010).
[9] P. Le Doussal and K. J. Wiese, Phys. Rev. E **79**, 051106 (2009).
[10] S. Kida, J. Fluid Mech. **93**, 337 (1979).
[11] J.-P. Bouchaud and M. Mézard, J. Phys. A: Math. Gen. **30**, 7997 (1997).
[12] P. Le Doussal, Ann. Phys. (N.Y.) **325**, 49 (2009).
[13] M. Bauer and D. Bernard, J. Phys. A: Math. Gen. **32**, 5179 (1999).
[14] Y. G. Sinai, Theory Probab. Appl. **27**, 256 (1983).
[15] P. Le Doussal and C. Monthus, Physica A **317**, 140 (2003).
[16] J. Burgers, *The Non-Linear Diffusion Equation: Asymptotic Solutions and Statistical Problems* (Springer, New York, 1974).
[17] L. Frachebourg and P. Martin, J. Fluid Mech. **417**, 323 (2000).
[18] P. Valageas, J. Stat. Phys. **137**, 729 (2009).
[19] P. Valageas, Phys. Rev. E **80**, 016305 (2009).
[20] Y. Fyodorov, P. Le Doussal, and A. Rosso, Europhys. Lett. **90**, 60004 (2010).
[21] Y. Sinai, Commun. Math. Phys. **148**, 601 (1992).
[22] Z. She, E. Aurell, and U. Frisch, Commun. Math. Phys. **148**, 623 (1992).
[23] P. Valageas, J. Stat. Phys. **134**, 589 (2009).
[24] L. De Haan and A. Ferreira, *Extreme Value Theory: An Introduction* (Springer, New York, 2007).
[25] D. Bernard and K. Gawedzki, J. Phys. A **31**, 8735 (1998).
[26] S. N. Gurbatov, Phys. Rev. E **61**, 2595 (2000).
[27] P. Le Doussal and K. J. Wiese, Phys. Rev. E **79**, 051105 (2009).
[28] T. Hwa and D. S. Fisher, Phys. Rev. B **49**, 3136 (1994).
[29] D. J. Daley and P. Hall, Ann. Probab. **12**, 571 (1984).
[30] C. Monthus and P. Le Doussal, Eur. Phys. J. B **41**, 535 (2004).
[31] G. Schehr and S. N. Majumdar, arXiv:1305.0639.
[32] P. Le Doussal and K. Wiese (unpublished).
[33] P. Le Doussal, A. Rosso, and K. Wiese, Eur. Phys. Lett. **96**, 14005 (2011).

# Directed polymer in hilly landscape

Thomas Gueudre, Alberto Rosso, Pierre Le Doussal, Jean-Philippe Bouchaud
*CNRS-Laboratoire de Physique Théorique de l'Ecole Normale Supérieure, 24 rue Lhomond,75231 Cedex 05, Paris, France + CFM + LPTMS Orsay*
(Dated: May 19, 2014 – "heavy tails v2")

We study the behaviour of a polymer at zero temperature, evolving in a hilly landscape. Undergoing a Gaussian disorder, the polymer minimizes its total energy by a global optimization, where all the sites stay rather small and weakly contributes to the sum. Unlike this situation, a hilly landscape (typically described by underlying heavy tailed disorder distribution) forces the polymer to distort and explore further to reach some particularly deep sites. This local strategy modifies the scaling exponents depending on the control parameter of the heavy tails. The present article describes the main features of this local behaviour and focuses on the transition to the classical Gaussian exponents.

PACS numbers: 68.35.Rh

## I. INTRODUCTION

The so-called "Directed Polymer" (DP) problem has attracted an enormous amount of interest in the last thirty years. It is stylized model for the pinning of directed one-dimensional elastic objects (polymers, vortex lines, dislocations,...) by random impurities. It is perhaps the simplest model that captures the notion of "frustration" that is so crucial in many more complex disordered materials, such as spin-glasses: the elasticity of the polymer competes with the energy of very favorable, but distant pinning sites that would lead to a costly distortion of the polymer. The huge amount of work on this problem is justified not only because of its intrinsic interest, but also because it can be mapped to a host of other problems: the Stochastic Heat Equation, itself mapped onto the Kardar-Parisi-Zhang equation and the stochastic Burgers' equation, population dynamics, problems of jammed transport (TASEP), crystal growth, random matrices, etc. etc.

In 1+1 dimensions (one transverse, one longitudinal, often taken as the "time" dimension), the problem is considered to be exactly solved, at least in some special limits and for some particular observables. It is now well established that in the limit of "long" polymers of length $t \to \infty$, the transverse excursions $x$ are of order $t^{2/3}$, i.e. much larger than $\sqrt{t}$ that would correspond to the excursion of the polymer in the absence of disorder. The total free-energy of the polymer is furthermore known to be $-ct + \xi t^{1/3}$, where $c$ is a non universal constant and $\xi$ is a random variable with a Tracy-Widom distribution, identical to the one governing the statistics of the largest eigenvalue of random matrices (GOE or GUE, depending on the boundary conditions). Although these scalings have been known at the level of physical rigour since the 80's (using either replica theory, the exact stationary state of the corresponding KPZ equation, RG techniques or Mode-Coupling theory), it is fair to say that there is up to now no simple, heuristic derivation of the diffusion exponent $\zeta = 2/3$ and the energy exponent $\theta = 1/3$ that would a) unveil the deep physical origin of these results and b) allow one to extend these results to other, similar problems, such as the Directed Polymer problem in $d + 1$ dimensions, for which the situation is still quite unclear. For example, the existence of an upper critical dimension $d_c$ beyond which $\zeta = 1/2$ even in the low temperature, pinned phase, is still highly debated.

We would in fact go as far as to say that in spite of the amazing flurry of exact results, the 1+1 directed polymer problem is far from understood. Consider for example the role of the distribution of the pinning energy on the large scale properties of the polymer. One would naively expect that, as with many other problems, the existence and finiteness of the second moment of the distribution is enough to ensure that the above scaling results (valid for Gaussian or exponential disorder) hold asymptotically. Surprisingly, though, this does not seem to be the case. A heuristic, Flory-type argument that dates back from the early 90's suggest that as soon as the fifth moment of the distribution diverges, one should leave the realm of the standard DP/KPZ 2/3 scaling, and enter a new regime, where the extreme values taken by the pinning potential matter and change the scaling results. In fact, the same Flory argument suggests that the situation becomes worse and worse as the dimension increases. In fact, any sub-exponential tail of the potential should play a crucial role at and above $d_c$. [The Derrida-Spohn solution of the DP on a tree indeed breaks down as soon as the potential has sub-exponential tails.].

The sensitive dependence of large scale properties on the far-tails of the disorder is certainly unsual and highlights our poor grasp of the standard case. It also raises many technical questions, for example on the validity of techniques that have been exploited in the context of Gaussian disorder, such as replica method or the functional RG. It is clear that if confirmed, these far-tailed induced effects would require new, specific theoretical methods that could, indirectly, shed new light on the DP problem altogether. Before embarking on such a program, we wanted to revisit the 1+1 DP problem with heavy-tailed disorder, and establish numerically, as convincingly as possible, the violation of the stan-

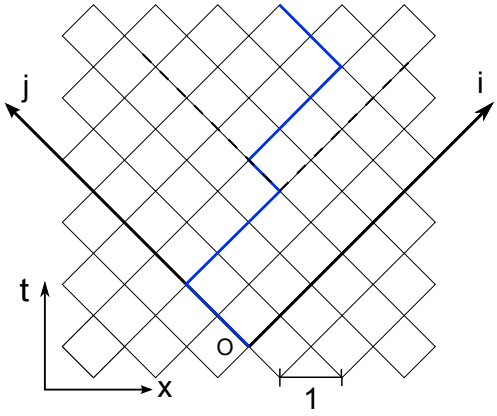


FIG. 1: Sketch of the directed polymer model. The blue solid line corresponds to a polymer growing over the square lattice under the hard constraint condition.

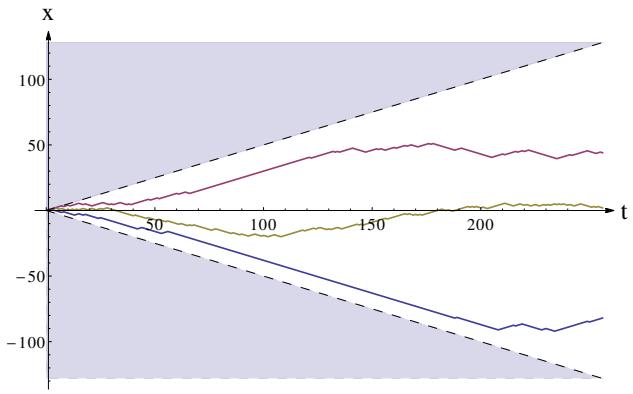


FIG. 2: Optimal path ($t = 512$) for three different random environments: the Gaussian disorder (in yellow), the heavy-tailed disorder with $\mu = 0.1$ (in blue) and with $\mu = 2.5$ (in red). The shape of the path is strongly affected by the underlying disorder. Because of the hard constrain, the path can only evolve inside the cone delimited by the dashed lines.

dard DP/KPZ 2/3 scaling and the corresponding Tracy-Widom statistics. Our results are, quite remarkably, in perfect agreement with the naive Flory predictions for the diffusion exponent $\zeta$ and the energy exponent $\theta$, which confirms that the value $\zeta = 2/3$ only holds if the distribution of the pinning energy $V$ decays faster that $1/V^6$. We study various statistical properties of the DP in the anomalous regime, and attempt to define and measure certain quantities that directly validates the main assumption of the Flory argument, namely that the accesible extreme values of the pinning potential dominate the scaling behaviour. We conclude with several open problems.

## II. THE MODEL

Here we consider a one dimensional directed polymer growing on the two dimensional square lattice depicted in Fig.1.

Directed paths grow along the diagonals of the lattice with only $(0, 1)$ or $(1, 0)$ moves (hard constraint condition), starting in $(0, 0)$ and with the second end left free. To each site of the lattice is associated a i.i.d. random number $V(x, t)$. The time coordinate is given by $t = i+j$ and the space coordinate by $x = (i - j)/2$. The total energy of the polymer is the minimum over all paths $\gamma_t$ growing from $(0, 0)$ up to time $t$ is defined as

$$E(t) = \min_{\gamma_t} \sum_{(x,\tau)\in\gamma_t} V(x, \tau) \qquad (1)$$

with $2x \in [\![-t, t]\!]$ and $\tau \in\in [\![0, t]\!]$. The energy of the polymer satisfies the following transfer matrix recurrence relation:

$$E_{x,t+1} = \min(E_{x-\frac{1}{2},t}, E_{x+\frac{1}{2},t}) + V(x, t + 1) \qquad (2)$$

with $E_{x,0} = \delta_{x,0}$. The free end ground state is computed by taking the minimum of the energies over all endpoints

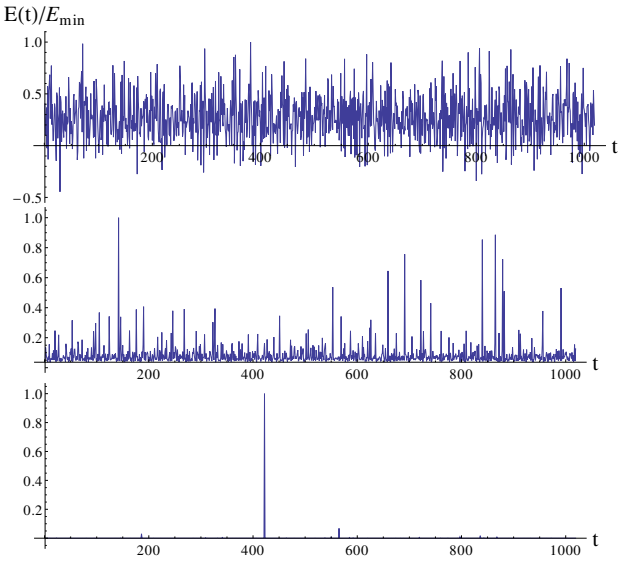


FIG. 3: Rescaled energies $V(\tau) = V(x_{opt}(\tau), \tau)/\min_{\tau<t} V(x_{opt}(\tau), \tau)$ of the sites along the optimal paths ($t = 1024$) for different random environments: the Gaussian disorder (upper plot), the heavy-tailed disorder with $\mu = 3.0$ (middle plot) and with $\mu = 0.5$ (lower plot).

$E(t) = \min_x E(x, t)$. In this paper, we study the properties of the DP for different disorder distributions $P(V)$, in particular we focus on heavy-tailed pdf decaying as:

$$P(V) \sim \frac{1}{V^{1+\mu}} \qquad (3)$$

It is known that, in one dimension, the search for an optimal path in a disorder landscape leads to excursions larger than the thermal ones, which are of order $\sqrt{L}$. The shape of the optimal path strongly depends on the underlying disorder landscape, as shown in Fig.2. In particular, the excursions are more important for a heavy-tailed

disorder than for a Gaussian disorder. Those differences correspond to different optimisation strategies, as shown in Fig.3:

- For a Gaussian disorder, the optimisation strategy is *collective*: the total energy of the polymer is equally shared between all the sites. (Fig.2 top)
- For an heavy-tailed pdf with $1 < \mu < 5$, the optimisation strategy is *elitist*: an important fraction of the total energy is hold by a small fraction of the sites belonging to the path. (Fig.2 middle)
- For an heavy-tailed pdf with $\mu < 1$, the optimisation strategy is *individual*: most of the total energy of the polymer is localized on one particularly deep site. (Fig.2 bottom)

Such differences in optimisation have marked effects on the fluctuations properties at large $t$, in particular on the observables:

$$\overline{x(t)^2} \sim t^{2\zeta} \tag{4}$$

$$\overline{E(t)^2}^c = \overline{E^2(t)} - \overline{E(t)}^2 \sim t^{2\theta} . \tag{5}$$

Here $\theta$ and $\zeta$ are respectively the energy and the roughness exponents and show some universal features: they only depend on the behaviour of the disorder tails, namely the index $\mu$. Note that other important quantities, as the average energy $\overline{E(t)}$, strongly depend on all the microscopic details of the chosen model.

For a fast decaying disorder, the value of the exponents is known to be $\zeta = 2/3$ and $\theta = 1/3$ ([1, 2]) and has been recently proved, via mathematical ([3, 4]) and physical ([5, 6]) approaches, for specific fast decaying distributions such as the Gaussian, the exponential or the Log Gamma distribution. For heavy-tailed disorder, where extremes play a major role in the choice of the optimal path, the values of the exponents rely on a scaling argument that balances the energy of the deep sites with the deformation energy it would cost to reach them ([7–9]). Noting $t$ the length and $x$ the size of a typical excursion of the polymer, a result from extreme statistics of heavy-tailed distributions gives, for the volume $xt$ available to the polymer, an estimation of the energy of the deepest sites: $E_{min} \sim (xt)^{1/\mu}$. On the other hand, for the model with hard constraint the deformation cost is entropic and, provided that $x \ll t$, follows a scaling similar an elastic energy as $S \sim -x^2/t$. Balancing both estimations, $E_{min} \sim S$, leads to the estimates;

$$\zeta_\mu = \frac{1+\mu}{2\mu - 1} \tag{6}$$

$$\theta_\mu = \frac{3}{2\mu - 1} \tag{7}$$

We can guess that those formula are valid for $2 \leq \mu \leq 5$. Note that the values of the exponents are compatible with the scaling relation $\theta = 2\zeta - 1$. This relation comes from the statistical tilt symmetry (STS), originating in the invariance of the problem upon tilting transformation $x(\tau) \to x(\tau) + \epsilon\tau$ in the large scale limit ***ref schulz villain brezin orland**** .

| | $\mu > 5$ | $5 > \mu > 2$ | $2 > \mu > 0$ |
|---|---|---|---|
| $\theta_\mu$ | $1/3$ | $3/(2\mu - 1)$ | $2/\mu$ |
| $\zeta_\mu$ | $2/3$ | $(1+\mu)/(2\mu - 1)$ | $1$ |

TABLE I: $\theta_\mu$ and $\zeta_\mu$ as a function of $\mu$. For $0 < \mu < 5$ the values of the exponents are estimated by scaling arguments. On the contrary in the *collective* optimization regime ($\mu > 5$) no simple scaling argument is known.

Above $\mu = 5$, we find $\theta_\mu < 1/3$ and, instead of a strategy focusing on deep sites of the disorder, the behaviour of the polymer is dominated by a *collective* strategy similar to the Gaussian case. On the other hand for $\mu = 2$ we have $\zeta_\mu = 1$ so that $x \sim t$ and the entropy can't be approximated by an elastic energy. Due to the hard constraint, the excursions of the polymer are confined in a cone. This observation leads to a new estimation of the exponents $\zeta_\mu = 1$ and $\theta_\mu = 2/\mu$ for $0 < \mu < 2$. All those estimates are summarized in Table I.

When $\mu < 1$, the first moment of the disorder distribution diverges. That leads to a huge separation of energy scale in the disorder, where all the sites can be neglected compared to the value of the most profound site through which the optimal path has to go. Hence the optimization becomes *individual* and it allows to construct recursively the optimal path by picking the deepest site that pins the polymer, and applying the same strategy amongst the sites inside the area delimited by the hard constraint. Such a hierarchical optimization strategy was coined *greedy* in [10], where some of its properties were studied for the limit $\mu \to 0^+$. Here we will show that this approximation seemingly becomes asymptotically exact as $t \to \infty$ for all $\mu \leq 1$. In particular the end point distribution of the polymer is computed analytically for the *greedy* strategy and very well reproduces the numerical behavior for all $\mu < 1$. *****dessin???*****

## III. NUMERICAL SIMULATIONS

In this section, we present numerical simulations done with the matrix transfer method, which allows to keep track of both the energy and the position of the optimal path at every time $t$.

We verify the estimates of $\theta$ and $\zeta$ from the scaling arguments given in the the previous section, and add additional informations about the whole pdf of the fluctuations of the energy, which shares with the disorder distribution the same power decay $P(E) \sim |E|^{-(1+\mu)}$. Due to important finite size effects, those estimates have been conjectured (see [8]) to be a good approximation only in the limit $\mu \to 2^+$. However a careful analysis of those effects leads to the conclusion that they are in

fact asymptotically exact. Finally, we give strong numerical evidence of the existence of different optimization strategies as $\mu$ varies. This supports the correctness of the scaling argument in the regime of strong disorder for $\mu < 5$.

### A. The scaling exponents

To measure the exponents $\theta$ and $\zeta$, we can use the definitions given in Eq.5. However, in Fig.4, we observe that the statistical estimator for $\overline{E^2}^c$ never averages when $\mu < 4$ and shows large jumps even for a very important sampling. Note that the statistical estimator of $\overline{E^2}^c$ converges only if both $\overline{E^2}^c$ and its statistical error $(\overline{E^4}^c/N)^{1/2}$ are finite. But, due to the presence of heavy tails in the disorder, high enough moments of the distribution of energy $P(E)$ could diverge. We will see in Sec.III B that for $2 < \mu < 4$, $\overline{E^2}^c$ is finite while $\overline{E^4}^c$ diverges.

Another estimator of the spread of the distribution is the mean absolute deviation (MAD) $\Delta E$:

$$\Delta E = \frac{1}{N}\sum_i |E_i - \overline{E}| \tag{8}$$

This estimator is more resilient to extreme events and works better with heavy-tailed distributions. Contrary to the standard deviation, which squares the distance from the average, MAD is well controlled as soon as the second moment of the pdf exists, in our case for $\mu > 2$, and allows to properly extract $\theta_{num}$ (see Fig.4). Note that $\overline{x^2(t)}$ does not present this kind of problem, because it is compactly supported due to the hard constraint(see Fig.4).

The check of the prediction, for different values of $\mu$ compared to the theoretical result, is summarized in Table II. The numerical estimations have been made with the maximum likelihood method. Fig.5 and Fig.6 show a good agreement between numerics and theory. One can note in the inset of the figures that the quantities $\overline{x(t)^2}/t^{\zeta_\mu}$ and $\overline{|E-\overline{E}|}(t)/t^{\theta_\mu}$ saturate, as expected if the scaling argument is correct, but at larger and larger times as $\mu \to 5$. Indeed, close to $\mu = 5^-$, the strategy remains *elitist*, but the effect of deep sites is not as strong and needs a large value of $t$ to be clearly distinguished from the crowd. For $\mu > 5$, the strategy becomes *collective*, and the exponents $\theta = 1/3$ and $\zeta = 2/3$ are recovered.

### B. The probability distribution of the fluctuations of $E$

It has been shown, for some fast decaying disorder distributions (see [4, 6, 11]) that, after the proper rescaling the probability distribution converges to a family of distributions, called Tracy-Widom (TW) distributions. It is

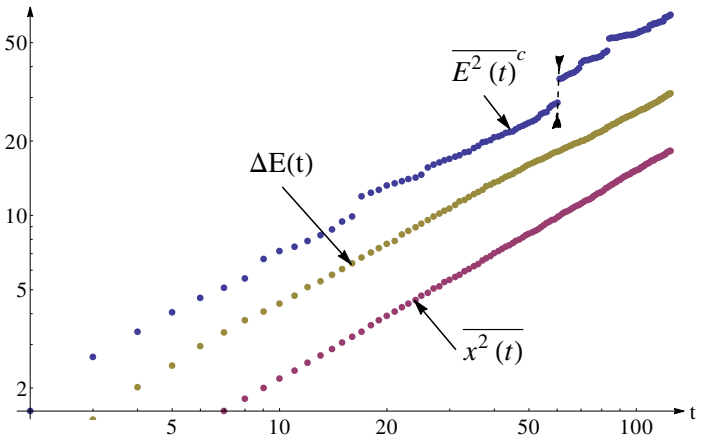


FIG. 4: Stability analysis of our numerical results. The averages are performed over $N = 10^5$ samples. The mean squared displacement $\overline{x^2(t)}$ shows a well-defined smooth behaviour, while the variance of the energy $\overline{E^2(t)}^c$ displays a jump around $t = 70$, which stems from a very deep single pin. This makes $\overline{E^2(t)}^c$ numerically unstable. On the contrary, for $\mu > 2$, the quantity $\Delta E(t)$ displays a well-defined behaviour allowing correct estimations of the exponent $\theta_{num}$.

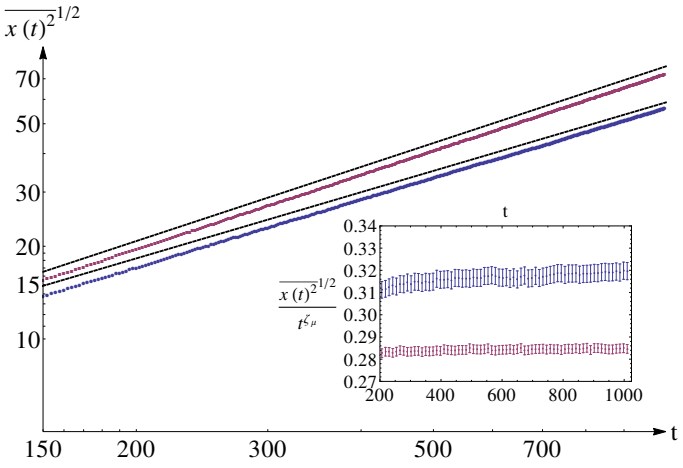


FIG. 5: Mean square displacement of the end position of the optimal path for $\mu = 3$ (in red) and $\mu = 4$ (in blue). Dashed lines correspond to the Flory estimation given in Table.I. Inset : $\overline{x(t)^2}/t^{\zeta_{th}}$ showing saturation at large $t$ in both cases.

| $\mu$ | $\theta_{th}$ | $\theta_{num}$ | $\zeta_{th}$ | $\zeta_{num}$ |
|---|---|---|---|---|
| 3 | $3/5 = 0.60$ | $0.605 \pm 0.006$ | $4/5 = 0.80$ | $0.802 \pm 0.004$ |
| 4 | $3/7 \simeq 0.43$ | $0.44 \pm 0.02$ | $5/7 \simeq 0.714$ | $0.715 \pm 0.005$ |
| 5 | $1/3$ | $0.36 \pm 0.03$ | $2/3$ | $0.69 \pm 0.04$ |
| 7 | $1/3$ | $0.338 \pm 0.008$ | $2/3$ | $0.669 \pm 0.004$ |

TABLE II: Flory prediction compared to numerical estimations for several values of $\mu$. Note that, close to the transition value $\mu = 5$, the numerical estimation is less precise due to important size effects.

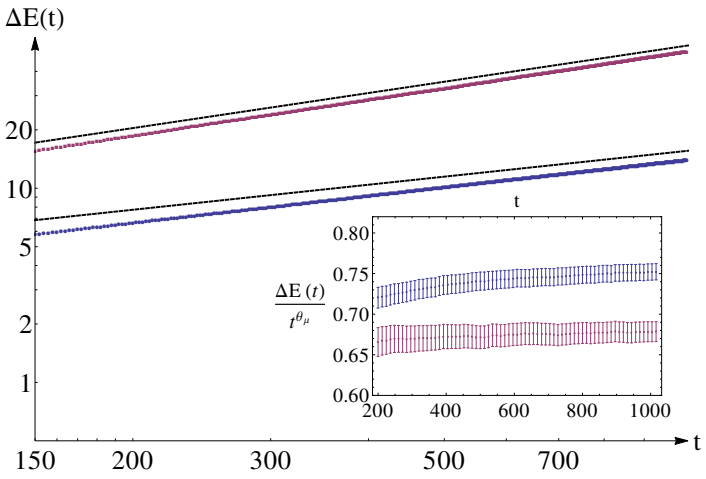


FIG. 6: Mean absolute deviation $\Delta E$ of the optimal energy for $\mu = 3$ (in red) and $\mu = 4$ (in blue). Dashed lines correspond to the Flory estimation given in Table.I. Inset : $\Delta E(t)/t^{\theta_{th}}$ showing saturation at large $t$ in both cases.

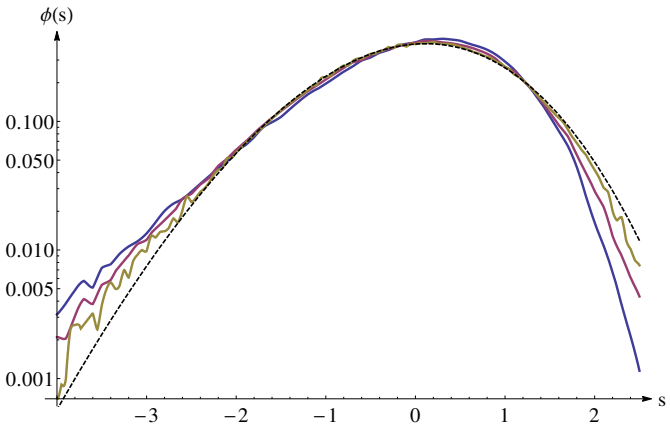


FIG. 7: FIGURE TO BE REDONE FOR THE NOTATION $\phi(s)$. Collapse of the pdf $\phi(s)$, for several lengths $L = 2^4$ (blue), $2^7$ (red), $2^8$ (yellow) for an disorder pdf with $\mu = 8$. Comparison is made with the Tracy Widom distribution $F_2$ after centring and rescaling (in dotted black). Average over $N = 2 \times 10^5$ samples.

believed that this universality extends to all fast decaying distributions. We define the rescaled variable:

$$s(t) = (E(t) - \overline{E}(t))/(\overline{E^2}^c(t))^{1/2} \tag{9}$$

and compute n Fig.7 the rescaled energy distribution $\phi(s)$. It seems clear that the TW universality class extends for $\mu = 5$ and more generally for any disorder with $\mu > 5$. Note that, for very negative $s$, $\phi(s)$ remains algebraic below some threshold $s < s_t^*$. However, when $t \to \infty$, the crossover towards the algebraic behaviour $s_t^*$ moves to $-\infty$.

On the contrary, for $0 < \mu < 5$, the limiting distribution is very different. In particular, $\phi(s)$ shares the same algebraic decay $1/s^{1+\mu}$ as the disorder pdf (see Fig.8), with however a different tail prefactor (see Fig.?? for the case $mu = 3$). The family of limiting distributions $F_\mu$ depends only on $\mu$ and on the boundary conditions. Its analytical expression is still unknown; inspired by results from extreme statistics, a natural guess would be the Frechet distribution $\mathbb{P}(X < x) = \exp(-\alpha|x|^{-\mu})$ or some convolutions thereof (see [9]). However, this distribution is supported on the half real line, while our numerical results indicate that the support of the limiting distributions $F_\mu$ is the whole real line. An interesting feature of $F_\mu$ is the fact that its right tail, corresponding to unfavourable configurations of the disorder, seems to decay as $e^{-\alpha s^3}$, similarly to TW. This fact would support a mixture of some Frechet and TW distribution as a possible guess.

For future reference, the tails analysis of $F_3(s)$ leads to the following numerical estimation: the left tail decays as $\int^s dx F_3(x) \sim 0.75|s|^{-3}$ for $s \to -\infty$ while for the right tail $F_3(s) \sim 0.57e^{-1.5s^3}$ for $s \to \infty$ (see Fig. ???).

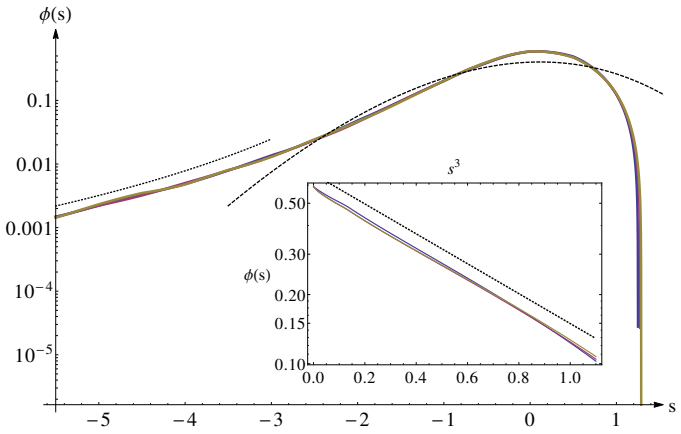


FIG. 8: FIGURE TO BE REDONE FOR THE NOTATION $\phi(s)$. Collapse of $\phi(s)$, for several lengths $L = 2^4$ (blue), $2^7$ (red), $2^{10}$ (yellow) and for an disorder pdf with $\mu = 3$. Comparison is made with the Tracy Widom distribution $F_2$ after centring and rescaling (in dotted black). Inset: far right tail of $\phi(|s|)$ compared to a power law of index 3 (in dotted black). Average over $N = 2 \times 10^5$ samples.

### C. The optimisation strategies

Although the scaling argument gives the correct estimates, it relies on the assumption that the fluctuations of $E$ are controlled by the fluctuations of the deepest sites in the disorder. This stems from the fact that the optimal path does large excursions specifically to reach some pinning sites. Note that, at variance with $\mu < 1$ where one site is much more negative than the others, for $1 < \mu < 5$, there is still a large population of sites being of order $V_{min}$. Hence to check the validity of the *elitist* optimisation strategy, one has to test the fact that the optimal path picks some sites amongst the deepest, for example

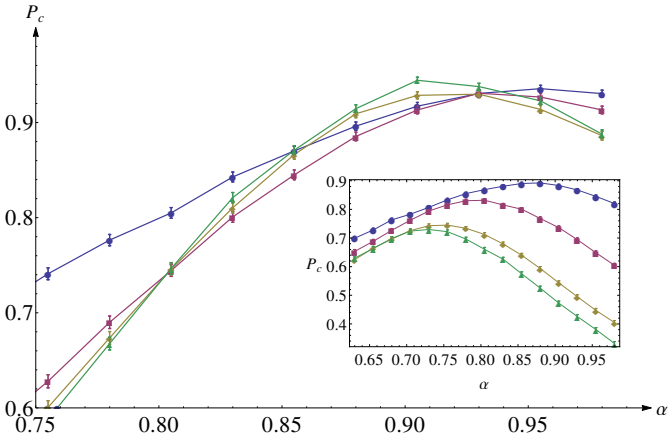


FIG. 9: Probability $P_c(\alpha)$ as defined in the text for a heavy tailed disorder with $\mu = 3$. Symbols correspond to different lenghts: $L = 2^6$ (circles), $2^9$ (squares), $2^{11}$ (losanges), $2^{12}$ (triangles). The averages are performed over $N = 2 \times 10^5$ samples. Inset: the same analysis is performed for $\mu = 8$.

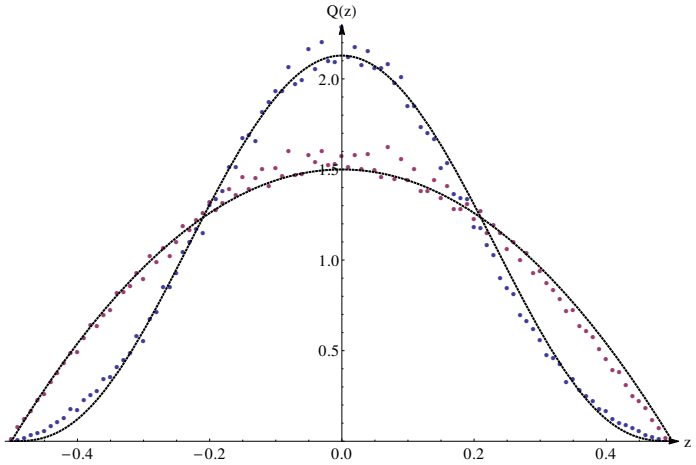


FIG. 10: *REDO: the range of x doesn't have the same convention than the text.* The pdf $Q(z)$ of the position of the free end as a function of $z = t/L$. In blue for a disorder pdf of $\mu = 1.5$, in red $\mu = 0.5$. In dotted black, the theoretical estimation for the parabola (and the guess with a Beta distribution with $\alpha = \beta = 3.8$). $L = 2^{11}$ and $N = 2 \times 10^5$.

through the following procedure: Consider an envelop of length $t$ and width $1/2t^\alpha$, its volume scales as $t^{1+\alpha}$. We estimate the probability $P_c(\alpha)$ that the minimum on the polymer is one of the $\log(t)$ deepest sites inside of the envelope. If $\alpha$ is chosen too small compared to $\zeta$, then the minimum on the polymer should be smaller than the minimum in the envelop. On the contrary, if $\alpha \gg \zeta$, the minimum on the polymer should be higher, as the elastic energy prevents it from reaching this favourable site. One expect that when $t \to \infty$, $P_c(\alpha)$ will become more and more peaked around $\alpha = \zeta$ for the *elitist* strategy, while in the *collective* regime, $P_c(\alpha)$ should vanish for all $\alpha$. Fig.9 highlights a different qualitative behaviour for $\mu = 3$ and $\mu = 7$, in agreement with our prediction. Note that the maxima of the curves in Fig.?? corresponding to an estimation of the rugosity according to the scaling argument are moving to the left, from 1 to 0.90 up to $t = 2^{12}$. They are expected to converge to $\zeta_\mu = 4/5$ for $\mu = 3$ although the convergence is very slow.

## IV. DISTRIBUTION OF THE END POINT

Another observable of interest is the end point of the optimal path. Compared to the fluctuations of the energy $E(t)$, we know much less about the statistics of $x(t)$. Accordingly to the scaling exponent $\zeta$ of the lateral excursions, one expects the rescaled position $z = x(t)/t^\zeta$ to converge in law towards a limiting distribution $Q_\zeta(z)$

For an exponential distribution of the disorder, the whole process $E(t, x)$ is characterized as the so-called Airy process [12], which allows to extract the joint distribution of the position and total energy of the optimal path $\mathbb{P}(E(t), x(t))$. Although the marginal $Q_{2/3}(z)$ can't be computed explicitly, it has been shown that it has an infinite support with a rather weak departure from the Gaussian distribution [13, 14]. The heavy-tailed disorder exhibits a radically different behaviour, as $Q_\zeta(z)$ is strongly influenced by the large excursions of the optimal path to reach pinning sites. For $\mu < 2$, $\zeta$ saturates to 1 due to the hard constraint and the support of $Q_\mu(z)$ reduce to the interval $(-1, 1)$: the extremity has a finite probability to reach any point of the available space, even at large $t$.

Denoting $z = x(t)/t \in [-1/2, 1/2]$, remarkably the distribution $Q_\mu(z)$ can be explicitly computed for the *greedy* strategy, where the optimization becomes a hierarchical recursive process. In Appendix A we give the details of the computation and the final results reads:

$$Q_{\text{greedy}}(z) = 6(\frac{1}{4} - z^2) \tag{10}$$

This results becomes exact for very small $\mu$, but, in Sec.II it was argued that the greedy strategy should asymptotically hold for every $\mu < 1$. This assumption is further confirmed by numerics for $Q_\mu(z)$ (see Fig.9), retaining its parabola shape until $\mu = 1$. For $\mu > 1$, the support still remains the interval $(-1, 1)$, but $Q_\mu(z)$ is modified. The numerics are relatively well fitted by the Beta distributions family $\mathbb{B}(\alpha, \alpha) = c_\alpha(1/2 - x)^\alpha(1/2 + x)^\alpha$, where $\alpha$ is a fitting parameter depending on $\mu$ (see Fig.9).

## V. CONCLUSION

Blablabliblabla

### Appendix A: Appendix: Derivation of $Q_\mu(x)$ in $\mu \to 0$

The derivation is eased by taking the continuum limit, where for convenience we rescale the position of the end point to $z \in [-1, 1]$. We introduce the sequence of variables $\xi_i = \frac{x_i+y_i}{2}$ and $2r_i = y_i - x_i$, $(x_i, y_i)$ being the coordinates of the pinning site chosen at step $i$ (see Fig.?? for the conventions). The measure being uniform over the space of intervals, it stays uniform if we fix the barycentre, under the constrain that the end points can't leave $[-1/2, 1/2]$. The joint probability distribution is, constrained on $[-1, 1] \times [0, 1]$:

$$P_0(\xi, r)d\xi dr = \Theta(r \leq 1 - |\xi|)d\xi dr \tag{A1}$$

Due to self similarity of the process, there are recursive relations between the end point after $i$ steps and $i + 1$ steps. we are eventually interested in the limit of the foolowing process, describing the position of the end point at $n \to \infty$:

$$z_i = \xi_1 + r_1\xi_2 + r_1r_2\xi_3 + \cdots \tag{A2}$$

All couples $(\xi_i, r_i)$ having the same joint distribution $P_0$ and being independent for $i \neq j$. this bears some similarities with Kesten variables (see Ref???) but note that $\xi_i$ and $r_i$ are not independent themselves. The variable $z_\infty$ obeys the following equation:

$$z_\infty =_{inlaw} \xi + rz_\infty \tag{A3}$$

This leads to an integral equation for $P(z_\infty$ the PDF of the end point, for example if we choose to condition over the value of $z$ in the above equation:

$$P(u) = \int_{r,z} P_0(u_r z, r)P(z)dz \tag{A4}$$

$$= \int_{r,z} \Theta(r < 1 - |u - rz|)P(z)dz \tag{A5}$$

Although there is no generic way to solve such integral equations, we can recursively compute the moments or use the above equation to write down a differential equation for $\phi(\lambda) = E(e^{i\lambda z_\infty})$. Or on can simply check that a parabola is the proper solution $P(z) = \frac{3}{4}(1 - x^2)$. $\Theta(r < 1 - |u - rz|)$ is non zero for $r < \frac{1+u}{1+x}$ if $u < x$ and $r < \frac{1-u}{1-x}$ if $x < u$. Hence, the right side of Eq.?? is equal to:

$$\frac{3}{4}\left(\int_{-1<x<u} \frac{1+u}{1+x}(1 - x^2)dx \right. \tag{A6}$$

$$\left. + \int_{u<x<1} \frac{1-u}{1-x}(1 - x^2)dx\right) \tag{A7}$$

$$= \frac{3}{4}(1 - u^2) \tag{A8}$$

And the result follows as given Eq. after the rescaling $z \to z/2$.


[1] David A. Huse, Christopher L. Henley, and Daniel S. Fisher. Huse, henley, and fisher respond. *Phys. Rev. Lett.*, 55(26):2924–2924, December 1985.

[2] Mehran Kardar and Yi-Cheng Zhang. Scaling of directed polymers in random media. *Phys. Rev. Lett.*, 58(20):2087–2090, May 1987.

[3] Kurt Johansson. Shape fluctuations and random matrices. *Comm Math Phys*, 209(2):437–476, February 2000.

[4] Michael Prhofer and Herbert Spohn. Universal distributions for growth processes in 1+1 dimensions and random matrices. *Phys. Rev. Lett.*, 84(21):4882–4885, May 2000.

[5] Tomohiro Sasamoto and Herbert Spohn. One-dimensional kardar-parisi-zhang equation: An exact solution and its universality. *Phys. Rev. Lett.*, 104(23):230602, June 2010.

[6] P. Calabrese, P. Le Doussal, and A. Rosso. Free-energy distribution of the directed polymer at high temperature. 90(2):20002, April 2010.

[7] Yi-Cheng Zhang. Growth anomaly and its implications. *Physica A: Statistical Mechanics and its Applications*, 170(1):1–13, December 1990.

[8] Joachim Krug. Kinetic roughening by exceptional fluctuations. 1(1):9–12, January 1991.

[9] G. Biroli, J.-P. Bouchaud, and M. Potters. On the top eigenvalue of heavy-tailed random matrices. *EPL*, 78(1):10001, April 2007.

[10] Ben Hambly and James B. Martin. Heavy tails in last-passage percolation. *Probab. Theory Relat. Fields*, 137(1-2):227–275, January 2007.

[11] Kurt Johansson. *Shape fluctuations and random matrices*. 1999.

[12] Kurt Johansson. Discrete polynuclear growth and determinantal processes. *Commun. Math. Phys.*, 242(1-2):277–329, November 2003.

[13] Gregory Schehr. Extremes of n vicious walkers for large n: Application to the directed polymer and kpz interfaces. *Journal of Statistical Physics*, 149(3):385–410, 2012.

[14] Gregorio Moreno Flores, Jeremy Quastel, and Daniel Remenik. Endpoint distribution of directed polymers in 1 + 1 dimensions. *Commun. Math. Phys.*, 317(2):363–380, January 2013.

# 4 Effects of correlations and optimal diffusion

We saw how some modifications of the disorder lead to exceptional fluctuations in the free energy, to the point the universality breaks down and the formalism has to be re-built. While long range interactions are always thought of as potential mechanisms to depart from the gaussian noise case [33, 122, 98], short range correlations are generally harmless, or irrelevant in the RG lingua.

Up to now, we have not really brought much attention to the actual dominant part of the free energy, its extensive part. It is usually removed by a simple shift, to focus on fluctuations. The reason for this lack of attention is mainly based on non-universality concerns: different microscopic models, although in the KPZ class, or even in the KPZ equation class, will not exhibit the same free energy density. Hence, only after this trimming will the model in consideration reveal its universality [123, 68].

Nonetheless, being the dominant part, one would expect this quantity to retain much of the information about the strategy the polymers uses to optimize its energy. For example, the finite size correction to the average growth exhibits some universality [124]. In what follows, we scrutinize the particular case of time correlations in disorder, where we emphasize the interplay between correlations and free energy growth through optimisation, and how very general features survive in that case.

## 4.1 Correlations in space and time

Short range correlations (noted $r_f$ for spatial and $\tau$ for temporal correlations) are often assumed to play little role in critical systems, as emphasized by a coarse graining argument. It amounts to replace every step by a larger patch, and to substitute the disorder by its average over a patch of size $(r_f, \tau)$; the disorder is then considered independent from patch to patch. As we detailed in Chapter 3, in the Directed Polymer setup, this replacement is not innocuous, but the universality of the anomalous exponents supersedes those effects: they remain unchanged.

In what follows, we consider the behaviour of the free energy density $\lim_{t\to\infty} f(t)/t$, or equivalently the average speed of growth of an interface $v_\infty = \overline{\partial_t h(x,t)}$.

For a growth dominated by diffusion, it is equal to the energy collected by a pure random walk in the directed polymer setup. We stated in Chapter 2 for a Gaussian noise $V(x,t)$ with:

$$\overline{V(x,t)V(x',t')} = R(x-x')\delta(t-t') \tag{4.1}$$

white in time, not necessarily in space, that $v_0 = \frac{R(0)^2}{2T^2}$. More generally, for an Ornstein-Uhlenbeck process $\eta(\cdot, t)$ (see later for definition), the variance of its integral grows as well like $t$, irrespectively of $\tau$ (see Appendix A.1). In purely thermal regimes, short-range correlations do not matter much. On the other hand, the problem is more subtle when non linearities are involved.

### 4.1.1 The delicate problem of the free energy density

A rigorous definition of the white noise KPZ equation is problematic. Indeed, the term $(\nabla h)^2$ pathologically diverges and escapes the formalism that was developed for stochastic calculus. The easiest way to approach the KPZ equation is through the Cole-Hopf transform $Z(x,t) = e^{\lambda h(x,t)}$. $Z(x,t)$ obeys the SHE $dZ = \Delta Z dt + \lambda Z dW(x,t)$, where the ill-defined non linearities are removed. However some subtleties remain in the prescription (Ito versus Stratonovitch).

To illustrate that, let us introduce the space mollified noise $W_\epsilon(x,t)$: if $\partial_t W(x,t)$ is a white noise in $(x,t)$, whose Fourier transform is itself a white noise, multiplying the spatial Fourier coefficients by $\phi(\epsilon q)$ mollifies the spatial direction, a process we note $\partial_t W_\epsilon(x,t)$. Writing $h(x,t) = \lambda^{-1} \log Z(x,t)$ and applying Ito's formula for the time variable [125, 126]:

$$\begin{aligned} dh(x,t) &= \lambda^{-1}\frac{dZ}{Z} - \lambda^{-1}\frac{d[Z]}{Z^2} \\ &= \Delta h(x,t) + \lambda(\nabla h)^2 + dW_\epsilon - \lambda^{-1}\frac{d[Z]}{Z^2} \end{aligned} \tag{4.2}$$

where $[\cdot]$ denotes the quadratic variation. Using:

$$\overline{\partial_t W_\epsilon(x,t)\partial_t W_\epsilon(x',t')} = \delta(t-t')C_\epsilon(x-x') \tag{4.3}$$

with $C_\epsilon(x) = \int_q dq e^{iqx}\phi(\epsilon q)\phi(-\epsilon q)$, the Itô term in Eq.4.2 gives a constant:

$$\partial_t h(x,t) = \Delta h(x,t) + (\lambda \nabla h(x,t))^2 + \xi_\epsilon - \lambda C_\epsilon(0) \tag{4.4}$$

with $C_\epsilon(0) \simeq \epsilon^{-1}\int_q \phi^2(q)dq$. The speed of growth goes to infinity in the limit of white noise in space $\epsilon \to 0$ ! One has to renormalise the diverging $(\nabla h)^2$ by a infinite constant [126, 127].

Although such an approach was considered as the proper way to tackle the KPZ equation, it is not obvious how to derive a general and satisfactory approximation scheme to the continuum white noise limit, except for the space mollification. Much progress in that direction has been recently made by the theory of *regularity structures* [128, 60, 129, 130].

A detailed account of this theory is way out of the scope of this Chapter, but roughly speaking, it lifts the solution in a abstract space, with an algebraic structure mimicking the standard Taylor expansion. This opens a way for a clean definition of the pointwise multiplication of two distribution through their Taylor expansion. It is suited for a very broad class of stochastic partial differential equations. An additional -but common in ill-defined PDE- peculiarity of the KPZ equation is the fact that even the abstract model

diverges in the white-noise limit. Fortunately, those admissible models can be cast into perfectly convergent models by introducing careful counter-terms. Specifically for the KPZ equation, the counter-term $C_\epsilon$ is written:

$$C_\epsilon = \frac{c_1}{\epsilon} + c_2 \log \epsilon + c_3 \tag{4.5}$$

with $c_2 = c_3 = 0$ due to additional symmetries, and $c_1 = \int \phi^2(x)dx$ with $\phi$ the mollifier. Time and space in the regularity structure theory somehow play a similar role, after a scaling where, for parabolic equations, the time direction "counts as" two space directions. For the space mollification, it recovers $C_{r_f} \sim 1/r_f$, while for an time mollification, $C_\tau \sim 1/\sqrt{\tau}$: the space singularity of Eq.4.4, involving two spatial derivatives, is naturally worst than the time singularity.

To summarize, there exists universal limits in the continuum of the KPZ equation: although the constants in the counter-terms depend on the regularization procedure, the rate of divergence (of the free energy, in the DP language) is universal. While this digression seems a bit esoteric, this insight will come handful in the later sections.

### 4.1.2 Explore or exploit ?

In the following, we suggest the existence of another universal mechanism, namely the existence of an optimal diffusion maximizing the free energy density, when time correlations are present.

First come back to the SHE, ruling the evolution of $Z(x,t)$:

$$\partial_t Z(x,t) = J\Delta Z(x,t) + \eta(x,t)Z(x,t) \tag{4.6}$$

It can be seen as the continuum, homogeneous limit of a more general model $Z_i(t)$ on the nodes $i$ of a graph (f.e. a population of bacteria living on site $i$ or wealth invested in stock $i$). The population grows multiplicatively with the (random) resources $\eta_i(t)$ it collects on site $i$. With migration rates $J_{ij}$ from site $i$ to site $j$, we obtain a sketchy but fairly general model of population migration on graphs, ruled by the master equation:

$$\partial_t Z_i(t) = \sum_j J_{ij}(Z_j - Z_i) + \eta_i(t)Z_i(t) \tag{4.7}$$

This model is referred in Econophysics as the Bouchaud-Mézard model [131] (see Fig.4.1), and remarkable in the fact that the stationary distribution exhibits algebraic tails, seemingly reproducing some features of the Zipf Law. A host of studies has already been conducted on the equilibrium state of such a system for various noises and migration rates [132, 133, 134, 135].

In the following, we will investigate a different aspect by introducing a finite time correlation $\tau$ in the random resources. How does it influence the growth of the population ? The model somehow contains two ingredients: the collection of $J_{ij}$ enforcing the migration strategy of the bacteria, and the time scale given by $\tau$. One could wonder how to adapt

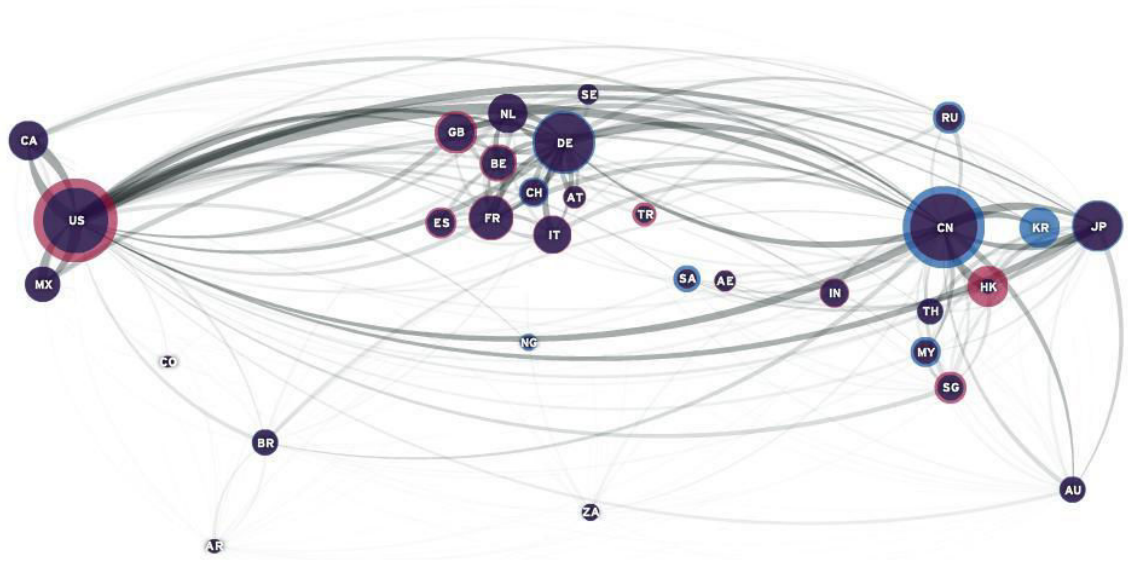


Figure 4.1: (Color online)A flow map of the international trade in the last decades, with imports and exports balance as coloured rings. Although the dynamics of the trading volume is certainly complicated, the model given in Eq.4.7 already reproduces interesting features of economical markets, as intermittency or heavy-tailed distributions.

the strategy of migration to make the best out of the environment, knowing its typical variability measured by $\tau$.

Those preoccupations fall into a broader category of problems, coined as "Explore or Exploit" type of problems, where two mechanisms, the exploration and the exploitation of resources, compete for growth. It is often illustrated by the *secretary problem* [136]: you need to hire a secretary, but with no clue of the skills of the average secretary. Hence you need to sample the available population, and so explore your environment, with a limited amount of time. What is the best stopping rule, maximizing the probability to select the best secretary out of the sample ? In that simple case, for $n$ available secretaries, one should interview (and reject) $n/e$ first applicants and then stop at the first applicant who is better than every applicant interviewed so far, a strategy leading to a probability $1/e$ of selecting the best in the whole population.

Here, in a similar flavour, the population needs agents on a site to collect the resources (due to the multiplicative nature of the growth) but has to explore new sites as well. Local conservation of population leads to competing effects both in exploration and exploitation. The importance of $\tau$ lays in the fact that a site may remain fruitful for some time $\tau$, encouraging the bacteria to stay on that particular site instead of exploring further. Exploring too fast does not make profit out of that correlation, while exploring too slowly prevents you from finding good spots. Thus an optimal migration strategy is expected, maximizing the overall "growth" (to be defined later), for a given $\tau$. On the other hand, pure white noise does not give any reward for exploitation and one would then expect the fastest exploration to be the best strategy.

## 4.2 A model of migration on graphs

The rather general model given Eq.4.7 is likely hard to solve. Hence we adopt the drastic simplification $J_{ij} = J$, an homogeneous migration over the whole system.

The geometry of the graph has notable effects as well. The most usual choices are:

- the Euclidian geometry in dimension $d$, where every node has $2^d$ neighbours. We will be mainly concerned with the case of a line $d = 1$.
- the tree geometry, where any two vertices are connected by only one simple path. This geometry allows to write recursive equations that lend themselves to analytical treatment, as will be shown later. The tree is sometimes thought as similar to high dimensional Euclidian space.
- The fully connected graph, where every node is connected to all the other nodes. This is assumed to be equivalent to Euclidian geometry in high dimensions.

Arguably the simplest coloured stochastic process is the Ornstein-Ulhenbeck (OU) process, as it is stationary, Gaussian and enjoys the Markov property (for more details, see Appendix A.1). It can be simulated through its Ito evolution equation:

$$d\eta(t) = -\frac{1}{\tau}\eta + \frac{\sigma}{\tau}dW \tag{4.8}$$

with $W(t)$ a Wiener process. The unusual scaling of $\sigma$ with $\tau$ used here ensures a proper white-noise limit as $\tau \to 0$. Due to the Gaussian propagator of the OU process, the various correlations can be exactly computed and some of them are displayed in Appendix A.1. Most importantly, the perturbation theory is very amenable with respect to such noise. Actually, the knowledge of the propagator at all time allows to exactly simulate realizations of the noise, without issues about discrete time step, or approximation schemes. The method used in this thesis, obtained from [137], is detailed in Appendix A.1. This is extremely useful, as stochastic PDE approximation schemes can be highly unstable. To circumvent some limitations, a two-step simulation, by first analytically computing the noise, and then plugging it in the approximate PDE, drastically improves the accuracy of the simulations [138].

Finally, we need to define a proper observable to quantify the growth of the population. While $c_a = \ln \overline{Z}$ would seem a natural choice, the systems under study exhibit intermittency: a large part of the population might be concentrated in very few sites. Hence the typical growth speed $c = \overline{\ln Z}$ (that by analogy we call the *quenched growth*), observed on most of the sites, differs from $c_a$ (the *annealed* speed) due to localized activity.

### 4.2.1 Scaling and perturbation approach

We first address the Euclidian geometry, mostly on a line $d = 1$ but the methods in this chapter should extend to higher dimensions. To exhibit a maximum, one can try to infer the behaviour of $c(J)$ at small $J$ and large $J$, hoping for a non monotonic behaviour.

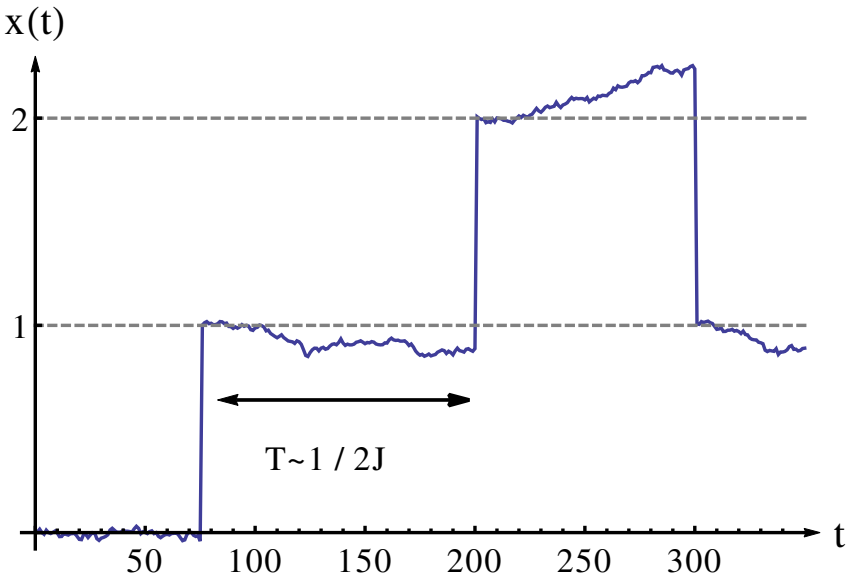


Figure 4.2: (Color online) A random walk on spatial sites $x = 0, 1, 2$. The walker rests an time $T$ distributed as an exponential distribution of mean $2J$ (in one dimension), collecting an energy proportional to $W(T)$.

Let us consider the case $J = 0$. It reduces Eq.4.7 to:

$$\partial_t Z_i = \eta(t) Z_i(t) \tag{4.9}$$

$Z_i(t)$ is simply the exponential of an integral OU process (in the Stratonovitch sense):

$$Z(t) = \exp\left(\int_0^t \eta(u)du\right) \tag{4.10}$$

The integral of an OU is not Markovian anymore but it remains Gaussian as a sum of (correlated) normal increments, with mean:

$$\overline{\int_0^t \eta(u)du} = \eta(0)\tau(1 - e^{-t/\tau}) \tag{4.11}$$

If we assume a flat initial condition, $c(0) = 0$: no exploration leads to sub-exponential growth. On the other hand, we obtain $c_a(0) = \tau\sigma^2/2(e^{-t/\tau} - 1 + t/\tau)$ from the generating functional of the OU.

Small $J$ corresponds to the low temperature regime. In that regime, the population very slowly diffuses, and $\tau$ is mostly irrelevant: small $J$ limits for coloured and white noises are essentially equivalent. So in what follows, we come back to white noise, in unit $\sigma = 1$. We expect the exact value of $c(J)$ to be dependent of the disorder, but the dependence in $J$ can be inferred from the Feynman-Kac representation of the solution of Eq.4.6:

$$Z(x,t) = \mathrm{E}_\pi\left[Z(X(t),0)\exp\left(\int_0^t \eta_{X(s)}(t-s)\right)\right] \tag{4.12}$$

where $X(t)$ is a random walk of diffusion $J$ starting at $X(0) = x$, and $\mathrm{E}_\pi$ the expectation over its probability space. The quantity $\int_0^t \eta_{X(s)}(t-s)$ amounts to sum independent

increments along a random walk on a sequence of positions held by $X(s)$ from $s = 0$ to $s = t$ (see Fig.4.2). It is certainly possible to provide very sharp bonds on this quantity, but assuming the random walk jumps $N$ times between 0 and $t$, $\int_0^t \eta_{X(s)}(t-s) \sim \sqrt{tN}$: the more jumps, the better. This has to be balanced with the probability of performing $N$ jumps in $[0, t]$, which follows a Poisson distribution of intensity $dJ$, with $d$ the space dimension:

$$P(N) = e^{-2dJt} \frac{(2dJt)^N}{N!} \tag{4.13}$$

Looking for a maximum of $P(N) \exp(\sqrt{tN})$ leads to the estimated optimal number of jumps $N^*$, at small $J$:

$$N^* = \frac{\alpha^2 t}{4 \log(1/dJ)^2} \tag{4.14}$$

$\alpha$ being a factor dependent of the noise through its extremal statistics (for example, influenced by the eventual correlations of the disorder). Thus we expect:

$$c(J) = \frac{\alpha^2}{4 \log(1/dJ)} \tag{4.15}$$

So $c(J) \to 0 = c(0)$ for $J$ going to 0, but $c(J)$ is not differentiable: switching on a small amount of diffusion tremendously improves the typical growth of the population, as one could expect from the advantages of the exploration. Of course, this estimation is restrained at least to $J < 1$. From the very same Feynman-Kac representation, we can compute the annealed speed $c_a(J)$. Inverting the expectations, we are led to calculate the quantity:

$$\overline{\exp\left(\int_0^t \eta_{X(s)}(t-s)\right)} \tag{4.16}$$

It is not hard to see that it is independent of the jumps of the process $X(t)$ ! Hence $c_a(J) = 1/2$, and $c(J) \to 1/2$ at large $J$[1].

In the large diffusion limit, because of the important wandering, the details of the disorder are averaged out. The high $J$ behaviour can be understood heuristically as follows. Because coarse graining is now possible, the problem for $\tau > 0$ must be equivalent, for large times, to the standard uncorrelated case $\tau = 0$, but with a renormalized disorder amplitude. For large $J$ and finite $\tau$, the disorder cannot change the random walk nature of the exploration up to time $\tau$. The walk therefore freely visits $N = O(\sqrt{\tau J})$ in $d = 1$ different sites during this time[2], leading to a pre-averaging of the random disorder that reduces the variance $\sigma^2$ by a factor $N$. Since for $\tau = 0$, $c(0) \sim \sigma^2$, the above renormalization immediately leads to $c(J) \sim \sigma^2/\sqrt{J\tau}$ at large $J$.

This behaviour can be recovered by a perturbation theory around the linear Edwards-Wilkinson equation (done in Appendix A.2), with the non-linear interactions as small parameter. We obtain:

$$c(J) = \frac{\sigma^2}{4\sqrt{\tau J}} \tag{4.17}$$

[1]Unlike the tree, and consistently with the strong disorder regime, there is no critical value of $J$ for which both $c(J)$ and $c_a(J)$ coincide, for $d < 3$.

[2]More generally, in $d$ dimensions, $N = O((\tau J)^{d/2})$.

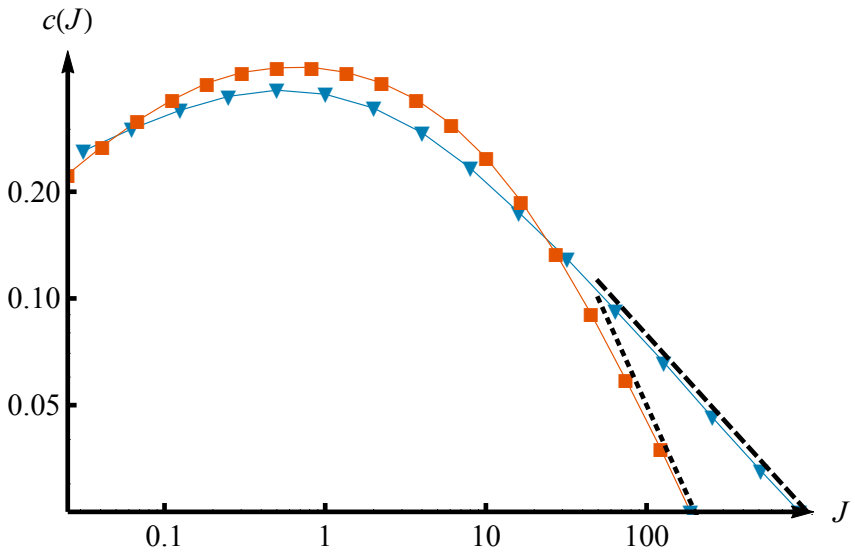


Figure 4.3: (Color online) Comparison of simulations of a discretization of Eq.4.6 (blue triangles) and of Eq.4.27 (red squares) for $N = 512$ and $\tau = 0.1$, as functions of the branching (diffusion) rate $J$. We fix $\sigma = 1$. The dashed black line is the large $J$ asymptotics Eq.4.17. The dotted line reveals the $J^{-1}$ behaviour of $c(J)$ for large $J$, predicted by the tree-approximation.

with an excellent agreement with numerical simulations (see Fig.4.3). It is interesting to note that the next order in $J$ is the white-noise term. Although we carefully chose the scaling of $\tau$ and $\sigma$ so that the OU process converges in probability to white noise, the limit $\tau \to 0$ seems rather problematic. To better understand this, we refer again to Section 4.1.1, and we recall that the procedure of sending $\tau$ to 0 selects the Stratonovitch prescription, while the rigorous definition of SHE requires Ito. Both differ by a diverging part, and the speed of divergence is universal. With the regularity structures, it is understood as the dominant counter-term, diverging as $\frac{1}{\sqrt{\tau}}$ and, in fact, independent of the coloured noise chosen.

So they are strong hints of the existence of an optimum in a fairly general way, as $c(J)$ exhibits non monotonic behaviour with respect to $J$. Unfortunately, those rough estimates do not give much information about the optimum itself. Therefore, it would be enlightening to obtain an exact solution for every $J$, even in a particular case. This is the goal of the next section, in the rather peculiar tree geometry.

### 4.2.2 Exact results on trees

The tree geometry allows numerous computations, because of the ease to write down recursive equations. Those simplifications can be traced to the *ultrametric* structure: when two paths starting at the root part, they become independent. A very clever trick, first performed in [139], maps the problem to a travelling wave problem, that can be tackled analytically. This approach is very fruitful, especially in the field of evolution and genetics [140, 141].

First, we illustrate the method with a white noise. We mainly follow [139], asides small variations: additional factors 1/2 ensure conservation of the total population at each

branching. We remove the $\beta$ variable, the control parameter being the branching rate. Then we extend this approach to OU processes. In the following, we restrain ourself to 2-branchings, the general case is treated in the related paper.

#### 4.2.2.1 The white-noise case

The population $Z_t$ in continuous time, evolves coupled to a branching process of intensity $J$. We denote $J$ this intensity because the branching rate is encoding the strength of exploration, much alike the diffusion constant in the previous section. Along the branches of the tree, $Z_t$ multiplicatively collects the resources $Z_{t+dt} = e^{-\xi_t dt} Z_t$ and new branches appear at each time step with probability $Jdt$. When it happens, $Z_t$ is equally split between the two branches:

$$Z_{t+dt} = \begin{cases} e^{-\xi_t dt} Z_t & \text{with prob. } (1 - J\,dt) \\ \frac{1}{2}\left(Z_t^{(1)} + Z_t^{(2)}\right) & \text{with prob. } J\,dt \end{cases} \tag{4.18}$$

We define the generating function:

$$g_t(x) := \overline{\exp\left[-e^{-x} Z_t\right]}.$$

$g_t(-\infty) = 0$ and $g_t(+\infty) = 1$, a behaviour typical of the travelling waves functions, describing the propagation of a front (see Fig.4.4). Invoking the integral representation of the logarithm:

$$\log z = \int_{-\infty}^{\infty} dx \exp(-e^{-x}) - \exp(-e^{-x} z)$$

$c(J)$ relates to the evolution of $g_t$ through:

$$c(J) = \frac{1}{t} \int_{-\infty}^{\infty} dx \left[g_0(x) - g_t(x)\right] \tag{4.19}$$

If $g_t$ is a travelling wave of speed $c$, $\int_{-\infty}^{\infty} dx \left[g_0(x) - g_t(x)\right] \sim ct$ so the typical growth $c(J)$ coincides with the front speed of $g_t$ !

From Eq.4.18, $g_t(x)$ satisfies:

$$g_{t+dt} = \begin{cases} \overline{g_t(x + \xi_t dt)} & \text{with prob. } (1 - J\,dt) \\ g_t(x + \log 2)^2 & \text{with prob. } J\,dt \end{cases} \tag{4.20}$$

$$= \int \mathrm{d}\xi_y \, P(\xi_y) g_t(x + \xi_y dt) + J\,dt \left[g_t(x + \log 2)^2 - g_t(x)\right]. \tag{4.21}$$

In the last line, we used that $\xi_t$ is independently distributed according to $P(\xi)$, with $dt$ small (dropping all terms of order $dt^2$). $\xi_t dt$ is a Gaussian white noise and scales as $\sigma\sqrt{dt}$:

$$\int \mathrm{d}\xi_t \, P(\xi_t) g_t(x + \xi_t dt) =$$

$$\int_{-\infty}^{\infty} \mathrm{d}\xi \, \frac{1}{\sqrt{2\pi\sigma^2\,dt}} e^{-\xi^2/(2\sigma^2 dt)} g_t(x + \xi) = g_t(x) + \frac{\sigma^2}{2} dt\, \partial_x^2 g_t(x) \tag{4.22}$$

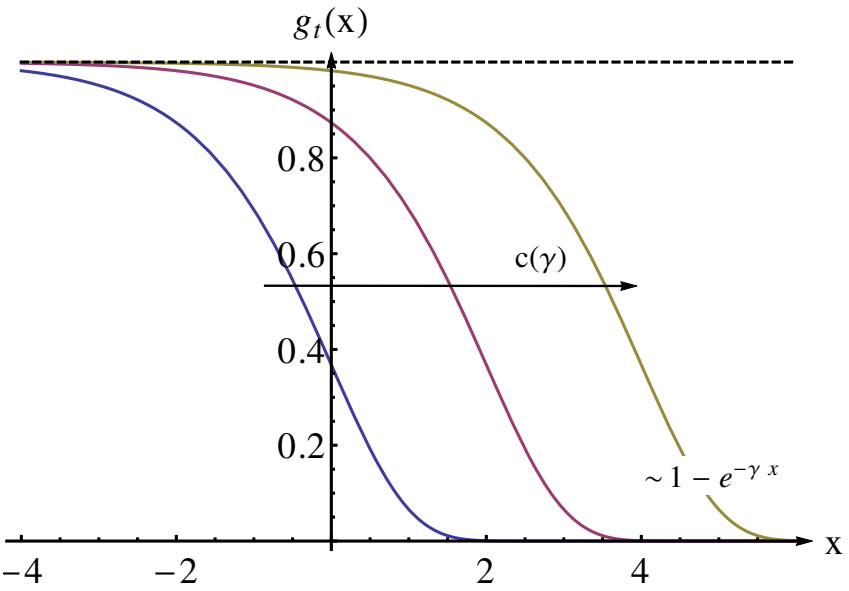


Figure 4.4: (Color online) A travelling wave at different times. The speed of the front is denoted $c(\gamma)$ and a function of the exponential decay of the precursor of the front $g_t(x) \sim 1 - e^{-\gamma x}$.

Gathering Eq.4.20 and Eq.4.22:

$$\partial_t g_t(x) = \frac{\sigma^2}{2}\partial_x^2 g_t(x) + J\left[g_t(x+\log 2)^2 - g_t(x)\right] \tag{4.23}$$

Although not the classical form of a KPP equation, as obtained in [139], its solution is again a travelling wave, whose front speed can be extracted by postulating $g_t(x) = w(u = x - ct)$:

$$-cw'(u) = \frac{\sigma^2}{2}w''(u) + J\left[w\left(u+\log 2\right)^2 - w(u)\right]. \tag{4.24}$$

The velocity $c$ is fixed by the decay of $w(u)$ at $u \to \infty$. With the Ansatz $w(u) \sim 1 - e^{-\gamma u}$ (see Fig.4.4):

$$\begin{aligned} -c\gamma e^{-\gamma u} &= -\frac{\sigma^2}{2}\gamma^2 e^{-\gamma u} + J\left[-2e^{-\gamma(u+\log 2)} + e^{-\gamma u}\right] \\ -c\gamma &= -\frac{\sigma^2}{2}\gamma^2 + J\left[1 - 2^{1-\gamma}\right] \\ c &= \frac{\sigma^2}{2}\gamma + \frac{J(2^{1-\gamma}-1)}{\gamma}. \end{aligned} \tag{4.25}$$

The interpretation of Eq.4.25 is that the speed of the front depends on the asymptotic decay of $g_t(x)$. With the flat initial condition $Z_0(x) = 1$, $g_0(x) \sim 1 - e^{-x}$, so $\gamma_{t=0} = 1$. But $c(\gamma)$ exhibits a minimum for some value $\gamma_{min}$. This peculiar feature is well known in the KPP theory: a front prepared with a decay sharper than $\gamma_{min}$ will slow down to a speed $c = c(\gamma_{min})$, while for an initial $\gamma_{t=0} < \gamma_{min}$, it will maintain the corresponding speed $c(\gamma_{t=0})$. As here $\gamma_{t=0}$ is fixed to 1, the criterion $\gamma_{min} = 1$ (corresponding to $J_c = 1$) separates the two regimes.

- For $J > J_c$, $\gamma_{min} > 1$, hence the front propagates at a steady speed $c(1) = \sigma^2/2$. We recover a result of the flavour of Eq.4.16: $c(J)$ becomes independent of $J$ above a threshold $J_c$, where it coincides with the annealed speed $c_a(J)$.

- For $J < J_c$, $\gamma_{min} < 1$. As the only range $0 < \gamma < \gamma_{min}$ is allowed, the front initially prepared with $\gamma_{t=0} = 1$ slows down to $\gamma_{min}$, and $c(\gamma_{min}) = \sqrt{2\sigma^2 J} + O(J)$.

With white noise, there is no inherent advantage to exploit the same site over a period of time. Hence a higher diffusion $J$ is always desirable, a principle true in all geometries. To observe no optimum does not come as a surprise (see Fig.4.5). We now turn to coloured noises.

#### 4.2.2.2 The Ornstein-Ulhenbeck noise case

Replacing the noise by an Ornstein Ulhenbeck (OU) process $\eta_t$ in the $t$ direction:

$$\partial_t \eta_t = -\frac{\eta_t}{\tau} + \frac{\sigma}{\tau}\xi_t, \tag{4.26}$$

where $\xi_t$ still plays the role of the white noise. Because of the correlations, the future of the OU at each branching has to be carefully considered. Logically, one of the branches has to retain the old OU process, while a natural choice for the initial condition of the new OU process on the other branch is a completely independent value $\eta_2$ taken from the stationary distribution. The new generating function now keeps track of the OU realization as well:

$$\begin{aligned} g_t(x,\eta) :=& \overline{\exp\left[-e^{-x} Z_i(t)\right] \delta\left[\eta_i(t) - \eta\right]} \\ \hat{g}_t(x) :=& \int_{-\infty}^{\infty} \mathrm{d}\eta \, g_t(x,\eta) = \overline{\exp\left[-e^{-x} Z_i(t)\right]} \end{aligned}$$

The variables $Z_i$ obey a similar set of equations[3]:

$$Z_{t+dt} = \begin{cases} e^{\eta_t dt} Z_t & \text{with prob. } (1 - J\,dt) \\ \frac{1}{2}\left(Z_t^{(1)} + Z_t^{(2)}\right) & \text{with prob. } J\,dt \end{cases} \tag{4.27}$$

leading to the evolution of $g_t(x,\eta)$:

$$\begin{aligned} g_{t+dt}(x,\eta) = (1 - Jdt)\, & \overline{\exp\left[-e^{-x+\eta_1(t)dt} Z_1(t)\right] \delta(\eta_i(t+dt) - \eta)} \\ & + Jdt\, \overline{\exp\left[-e^{-x-\ln 2} Z_1(t) \delta(\eta_1(t) - \eta)\right]} \\ & \times \overline{\exp\left[-e^{-x-\ln 2} Z_2(t)\right]} \end{aligned} \tag{4.28}$$

As we said above, $\eta_2$ is an independent value taken from the stationary distribution:

$$P_{OU}(\eta) = \sqrt{\frac{\tau}{\pi\sigma^2}} \exp\left[-\frac{\tau\eta^2}{\sigma^2}\right] = \int \mathrm{d}x \, g_t(x,\eta) \tag{4.29}$$

[3]Correcting a small typo in the related paper.

Expanding in $dt$ in the same way than Eq.4.22, we get the PDE:

$$\partial_t g_t(x,\eta) = \frac{\sigma^2}{2\tau^2}\partial_\eta^2 g_t + \frac{1}{\tau}\partial_\eta(\eta g_t) - \eta\partial_x g_t + J\left[g_t(x+\ln 2,\eta)\hat{g}_t(x+\ln 2) - g_t(x,\eta)\right]. \tag{4.30}$$

We obtain another Fisher-KPP type equation for $g_t$, where the diffusion operator is replaced by the Ornstein-Uhlenbeck operator, involving the additional state variable $\eta$.

Again, we want to determine the dispersion relation between $c(J)$ and the initial decay of the front. However, the PDE now involves the additional state variable $\eta$. For $x \to \infty$, $g_t(\infty,t) = \langle\delta(\eta(t)-\eta)\rangle$. Moreover, we expect $c$ to be asymptotically independent of $\eta$. Therefore, we make the following ansatz for the tail of $g_t$:

$$g_t(x,\eta) = Q(\eta) - R(\eta)e^{-\gamma(x-ct)} + ...$$

with $\int \mathrm{d}\eta\, Q(\eta) = 1$, with $Q$ expected to be the stationary distribution of the OU process Eq.4.29. Inserting this Ansatz into Eq.4.30, one finds, by identification that $Q(\eta)$ indeed obeys Eq.4.29 while $R(\eta)$ satisfies:

$$Rc\gamma = \frac{\sigma^2}{2\tau^2}\partial_\eta^2 R + \frac{1}{\tau}\partial_\eta(\eta R) + \eta R + J2^{-\gamma}Q\int \mathrm{d}\eta R(\eta) + R(\eta)J(2^{-\gamma}-1). \tag{4.31}$$

Because Eq.4.31 is linear in $R$, this can be simplified by imposing $\int \mathrm{d}\eta\, R(\eta) = 1$. Absorbing $\partial_\eta$ by setting $R = \phi e^{-\eta^2\tau/2\sigma^2}$, $\sigma^2\hat{c} = \gamma c - J(2^{-\gamma}-1) - \sigma^2\gamma^2/2$ and $y = \eta/\sigma^2 - \gamma$:

$$-\frac{1}{2\sigma^4\tau^2}\phi'' + \frac{1}{2}y^2\phi + (\hat{c} - \frac{1}{2\sigma^2\tau})\phi = \frac{Je^{-\gamma q_2}}{\sigma^2}\frac{e^{-\frac{(y+1)^2\sigma^2\tau}{2}}}{\sqrt{\pi\sigma^2/\tau}}.$$

On the left part, one can recognize the Hamiltonian of an harmonic oscillator, with a Gaussian source term. Introducing the harmonic oscillator eigenfunctions $\phi_n(y) = e^{-y^2\sigma^2\tau/2}H_n(y\sigma\sqrt{\tau})$, the solution of the above equation can be decomposed as $\phi(y) = \sum_{n=0}^{\infty} A_n\phi_n(y)$ where the coefficients $A_n$ are given by:

$$A_n\left[\frac{n}{\sigma^2\tau} + \hat{c}\right] = \frac{J2^{-\gamma}}{\sigma^2}\frac{e^{-\gamma^2\sigma^2\tau/4}\frac{(-1)^n}{n!}\left(\frac{\sigma\sqrt{\tau}}{2}\right)^n}{\sqrt{\pi\sigma^2/\tau}}.$$

Finally, the condition $\int \mathrm{d}\eta\, R(\eta) = 1$ yields an implicit equation for $c$, valid for arbitrary $\tau$:

$$1 = Je^{-\gamma\log 2 - \gamma^2\sigma^2\tau/2}\sum_{n=0}^{\infty}\frac{(\gamma^2\sigma^2\tau/2)^n}{n!\left[\frac{n}{\tau} + \gamma c - J(e^{-\gamma\log 2}-1) - \frac{\sigma^2}{2}\gamma^2\right]} \tag{4.32}$$

Again $c(\gamma)$ is found to reach a minimal value in $\gamma_{min}$ and we can perform a similar analysis to the white-noise case. Although it lends itself to expansion, Eq.4.32 is not particularly friendly and will be dissected in the following section. More importantly, it unravels some connections between freezing transition and optimal growth.

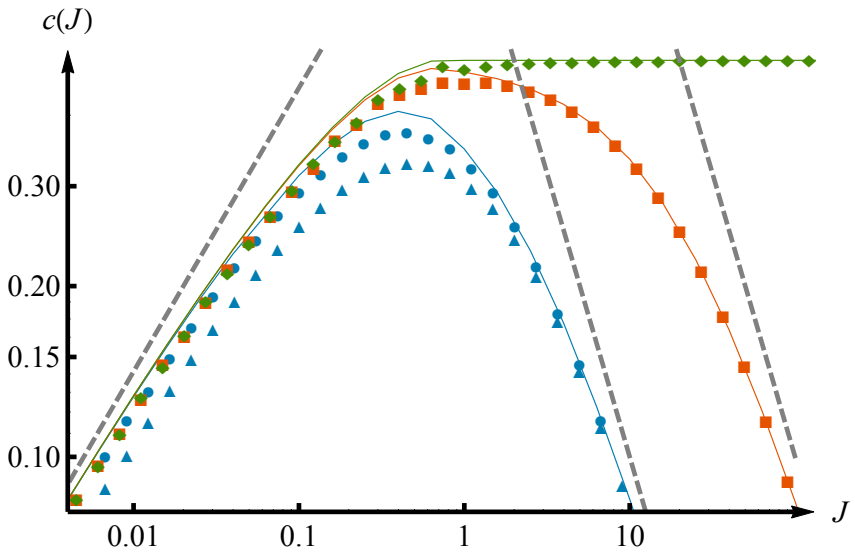


Figure 4.5: (Color online) Comparison of simulations of Eq.4.27 for various $N$ and $\tau$, as a function of the branching rate $J$. Green diamonds, orange squares and blue circles were obtained for $\tau = 0, 0.1$ and 1 with $N = 2^{20}$. Blue triangles correspond to $\tau = 1$ and $N = 2^8$. $\sigma = 1$. The solid curves were obtained from Eq.4.32, with asymptotics as dashed grey lines.

### 4.2.3 Freezing transition and optimal growth

The infinite sum over $n$ can be rewritten in a integral form:

$$1 = Je^{-\gamma \ln 2 - \gamma^2\sigma^2\tau/2} \int_0^\infty \mathrm{d}t \, \exp\left( -\left[\gamma c - J\left(2^{-\gamma} - 1\right) - \frac{\sigma^2\gamma^2}{2}\right] t + \frac{\gamma^2\sigma^2\tau}{2} e^{-t/\tau} \right) \tag{4.33}$$

Let us first consider the large $J$ regime, where we can set $\gamma = 1$ from the analysis above. It simplifies Eq.4.33 to:

$$1 = Je^{-\sigma^2\tau/2} \int_0^\infty dt \exp\left[ -\left(c - J - \frac{\sigma^2}{2}\right) t + \frac{\sigma^2\tau}{2} e^{-t/\tau} \right] \tag{4.34}$$

The dominant part of this integral corresponds to small $t$, of order $1/J$. Rescaling $u = Jt$:

$$0 = \int_0^\infty du e^{-u} \left[ \exp\left( -c\frac{u}{J} + \frac{\sigma^2\tau}{2}(e^{-u/J\tau} - 1 + \frac{u}{J\tau}) \right) - 1 \right] \tag{4.35}$$

Expanding $c(J)$ in powers of $1/J$ leads to:

$$c = \frac{\sigma^2}{2\tau J} - \frac{\sigma^2}{2\tau^2 J^2} + O(J^{-3}) \tag{4.36}$$

The low $J$ limit is a bit more involved, as $c = c(\gamma_{min})$. Observing that $\gamma_{min} \to 0$ in that limit, and that the dominant contribution now comes from $t \sim 1/J$ large, we set:

$$\gamma = \sqrt{J}\gamma' \quad \text{and} \quad c = \sqrt{J}c_1 + O(J)$$

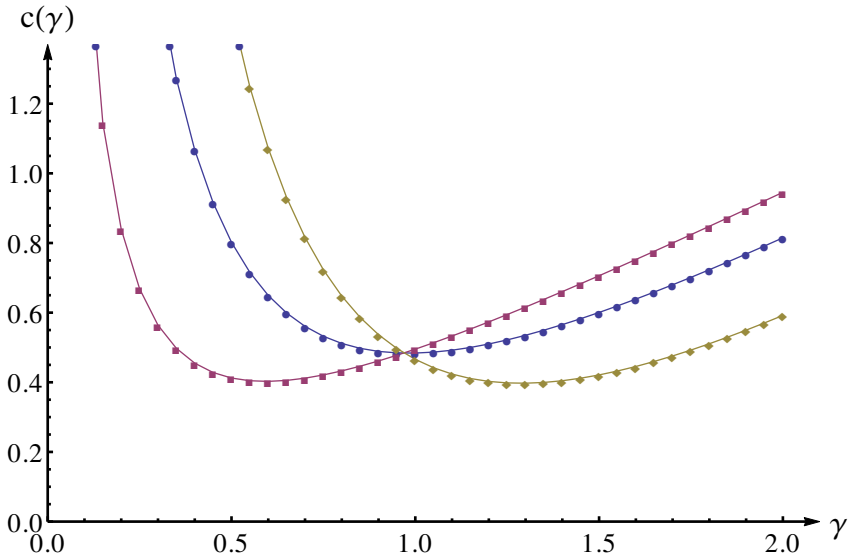


Figure 4.6: (Color online) Various $c(\gamma)$ for $\tau = 0.1$ and several values of $J$ (red squares $J = 1.5$, blue circles $J = 0.68$ and yellow diamonds $J = 0.2$). $\gamma_{min}$ goes above 1 at low $J$, corresponding to the frozen regime. $J_c = 0.68$ is the critical transition.

Dropping the term in $\exp(-t/\tau)$ in Eq.4.35 leads to:

$$\gamma c - J(e^{-\gamma \ln 2} - 1) - \frac{\sigma^2\gamma^2}{2} = Je^{-\gamma \ln 2 - \gamma^2\sigma^2\tau/2} \tag{4.37}$$

Inserting the expansions in $J$, we obtain the relation:

$$c_1 = \frac{1 + \sigma^2/2\gamma'^2}{\gamma'} \tag{4.38}$$

$$\gamma'_{min} = \sqrt{\frac{2}{\sigma^2}} \tag{4.39}$$

The final result is exactly similar to the white noise case:

$$c = \sqrt{2J\sigma^2} + O(J) \tag{4.40}$$

Satisfyingly, we retrieve the existence for $c(J)$ of an optimum value of $J$. While the large $J$ decay was expected from the scaling argument given in Section 4.2.1, the algebraic decay for small $J$ is more surprising. It does not reproduce the supposedly logarithmic behaviour obtained from a Feynman-Kac representation. On the other hand, a similar computation over fully connected graphs recovers the logarithm. Although both models can be seen as high dimensional limits, the Cayley tree exhibits unusual features because of its geometrical rigid structure [142]. The peculiar square root dependence of Eq.4.40 probably belongs to those.

The advantage of the analytical solution over simple scaling arguments comes when studying the behaviour of the optimum. Unfortunately, the cumbersome Eq.4.32 does not allow exact formula for its position. Nonetheless, $c(1)$ decreases with $J$ and, by definition, $c(\gamma_{min}) < c(1)$. From those observation, it can be concluded that $c(J)$ attains its maximum precisely when $c(\gamma_{min}) = c(1)$, hence at the point $J = J_c$.

Remember that the frozen phase is characterized by the condensation of the measure of the polymer on one particular path. It can be interpreted as a weak explorative regime. On the other hand, for large $J$, the system is annealed and the population diffuses too much. It is not so suprising that the precise point where optimality is attained realises the best compromise between the advantages and the drawbacks of both strategies. Hence, a population grows the fastest while being almost frozen, or alternatively, almost annealed.

It would be rather instructive to explore this fact in more general contexts. The participation ratio introduced earlier wears many habits in different fields. In ecology, the Simpson index is used as a measure of species diversity. In economy, it is coined the Herfindahl–Hirschman index, a measure of the size of firms in relation to the industry and an indicator of the amount of competition among them. It is widely applied in competition law, antitrust and also technology management. The above computation gives the idea that an "optimal" tuning (in a very specific way) is obtained when two antagonist mechanisms simultaneously encourage or prevent the system from condensing. One can for example think of the tendency of companies to merge being counterbalanced by antitrust state action.

## 4.3 Conclusion

In this Chapter, we explored the influence of time correlations of the linear speed of growth of an interface. Although this point of view is rather peculiar in the field of stochastic growth field, it makes more sense to describe population dynamics. While the exact value of this growth speed depends on the chosen model, the existence of an optimum value with respect to diffusion seems very robust. We did not try to identify the dynamics of the population in the localized phase, or address the question of intermittency. We expect however that the white noise results, known in the field of population dynamics [143] (sometimes still as conjectures) persist with coloured noises. Note that several other questions could be tentatively extend the analysis. The limit $\tau \to \infty$ corresponds to the so-called columnar disorder, much studied and interpreted as steps of Punctuated Evolution [144, 145, 146]. It would correspond to the rescaling $\sigma \to \sigma\sqrt{\tau}$. However, the FKPP approach uses the assumption of stationary $t \to \infty$, a limit that does not commute with $\tau \to \infty$. A more worrisome concern is the fact that $c(J)$ in the quenched case strongly depends on the extremal statistics of the underlying disorder. For a Gaussian disorder, we would expect $c(J)$ growing to $\infty$ with $t$ (albeit slowly) rather than reaching a asymptotic limit. Hence, the present framework does not adapt nicely to that case.

Presence of heterogeneities in the ressources or other geometries are other interesting routes to follow, as they relate to various experimental interests, from vortices in superconductors to rebalancing in portfolio management. The above analysis could be enlarged to economy or ecology, for example by studying how economic growth is impacted by the ability of societies to find a tradeoff between tradition and innovation, or else collapse. It enlightens some aspects of the *Rich gets richer* strategies commonly observed in those contexts, where localization of resources is encouraged, up to a certain point. But those extensions require a detailed study of the robustness of the optimum to various perturbations. The apparent close relationship of the optimal growth with localization transition,

if it survives in other contexts, should be a possible route for broadening the scope of the present work.

# Explore or Exploit? A Generic Model and an Exactly Solvable Case

Thomas Gueudré,[1,*] Alexander Dobrinevski,[1] and Jean-Philippe Bouchaud[2]
[1]CNRS-Laboratoire de Physique Théorique de l'Ecole Normale Supérieure, 24 rue Lhomond, 75231 Cedex 05, Paris, France
[2]Capital Fund Management, 21 rue de l'université, 75007 Paris, France
(Received 20 October 2013; published 5 February 2014)

Finding a good compromise between the exploitation of known resources and the exploration of unknown, but potentially more profitable choices, is a general problem, which arises in many different scientific disciplines. We propose a stylized model for these exploration-exploitation situations, including population or economic growth, portfolio optimization, evolutionary dynamics, or the problem of optimal pinning of vortices or dislocations in disordered materials. We find the exact growth rate of this model for treelike geometries and prove the existence of an optimal migration rate in this case. Numerical simulations in the one-dimensional case confirm the generic existence of an optimum.

DOI: 10.1103/PhysRevLett.112.050602 PACS numbers: 05.10.Gg, 68.35.Rh

The exploration-exploitation tradeoff problem pervades a large number of different fields (see [1] and the many references therein). Two early examples concern the management of firms [2] (should one exploit an already known technology or explore other avenues, potentially more profitable, but risky?) and the so-called multiarm bandit problem [3] (sticking with the seemingly most profitable arm to date, or switching in search of potentially more profitable ones?). Clearly, this is a universal paradigm that ranges from population growth and animal foraging to economic growth, investment strategies, or optimal research policies. As we will show below, the same issues also arise, in a slightly disguised form, in the context of vortex or dislocation pinning by impurities, and are relevant for material design. Intuitively, neither staying at the same place (and missing interesting opportunities) nor changing places too rapidly (and failing to exploit favorable circumstances) are optimal strategies. An optimal, nonzero search rate should thus exist in general. However, there are no exactly solvable cases where the exploration-exploitation tradeoff can be investigated in details. The aim of this Letter is to propose a general, stylized model for these exploration-exploitation situations, which encompasses all the examples given above. We obtain exact solutions of this model in two cases (a fully connected and a tree geometry), for which we explicitly prove the existence of a nontrivial optimal search rate. Euclidean geometries are also considered, as these correspond to physical situations, like the pinning problem alluded to above. In this case, perturbation theory and numerical simulations confirm the existence of an optimum as well.

Our model describes the dynamics of a quantity we generically call $Z_i$, defined on the nodes $i$ of an arbitrary graph, that evolves according to the following equation [4]:

$$\frac{\partial Z_i(t)}{\partial t} = \sum_{j\neq i} J_{ij} Z_j(t) - \sum_{j\neq i} J_{ji} Z_i(t) + \eta_i(t) Z_i(t). \quad (1)$$

The first two terms encode "migration" effects, with $J_{ij}$ the migration rate from $j$ to $i$. The last term describes the growth (or decay) of the quantity $Z_i$ with a random growth rate $\eta_i(t)$. We will choose $\eta_i$ to be Gaussian, centered, and uncorrelated from site to site, with a exponential time correlator:

$$\langle \eta_i(t_1)\eta_j(t_2)\rangle = \delta_{ij}\frac{\sigma^2}{2\tau} e^{-(|t_1-t_2|/\tau)}. \quad (2)$$

Our qualitative conclusions are, however, independent of the precise form Eq. (2), provided correlations decay on a finite scale $\tau$, which will play an important role in the following.

Many different problems are described by Eq. (1). Population dynamics (bacteria, humans, animals) is one example with $Z_i$ the number of individuals around site (or habitat) $i$. In this setting, $\eta_i(t)$ encodes the local balance between beneficial and detrimental effects on population growth [5] (i.e., quality and quantity of resources or nutrients, climate, illnesses, etc.). A slightly different interpretation can be given in the context of evolutionary dynamics, where the sites $i$ correspond to different alleles and the $J_{ij}$ are mutation rates. In the context of pinning problems, $Z_i$ corresponds to the partition function of a linear object of length $t$ (polymers, vortices, dislocations), ending on site $i$, that can hop between sites and interact with a local random pinning potential $\eta_i(t)$ [6]. In an economics setting, Eq. (1) can be interpreted as describing the dynamics of the wealth of individuals that exchange and invest in risky projects, or of the total activity in a sector of the economy $i$, that may shift from one sector to another, and grow or decay depending on innovations, raw material

 

prices, etc. Another interesting application is that of portfolio theory, where $Z_i$ is the amount of money invested in asset $i$ [7]. Then $\eta_i(t)$ is the return streams of this assets and the $J_{ij}$ describe the reallocation of the gains made on some assets towards the rest of the portfolio. Without this rebalancing, the portfolio would end up being concentrated in one (or a few) assets only (see, e.g., [8], p. 37), and hence, be exceedingly risky.

In the case where $J_{ij} \equiv J$ and the nodes $i$ are on a regular lattice in $d$ dimensions, Eq. (1) is a discretized version of the "stochastic heat equation,"

$$\frac{\partial Z(\vec{x},t)}{\partial t} = J\nabla^2 Z(\vec{x},t) + \eta(\vec{x},t)Z(\vec{x},t). \tag{3}$$

Upon a Cole-Hopf transformation $Z = e^h$, this equation maps into the celebrated KPZ equation $\partial_t h = J\nabla^2 h + J(\nabla h)^2 + \eta$ that appears in a wide variety of domains: cosmology and turbulence [9,10], surface growth [11,12], directed polymers [13], or Hamilton-Jacobi-Bellmann optimization problems [14].

A host of exact results have recently been obtained for the one dimensional ($d = 1$) case, in particular, concerning the scaling properties of the fluctuations of the $h$ field (for a review, see [15]). Here, however, we will not be concerned with these fluctuations but interested in the long-time average "velocity" $c$ of the $h$ field, defined in the discrete case as

$$c := \lim_{t\to\infty} \frac{1}{Nt} \sum_{i=1}^{N} \ln Z_i(t), \tag{4}$$

where $N$ is the total number of sites. This velocity $c$ has a clear interpretation in all of the examples mentioned above: it represents the average asymptotic growth rate of the population, or of the economic wealth in models of growth, the free energy of the polymer, vortex, etc., in the context of pinning. It is therefore very natural to look for the maximum of this quantity as a function of the parameters of the model, since these will correspond to the optimal situation—either in terms of population, economic or portfolio growth, or in terms of pinning efficiency, which is relevant for material design, for example, superconductors with high critical currents [16]. In this case, so-called "columnar disorder" [17] (corresponding to a time correlated random noise $\eta$ in the present language) is known to be highly effective at pinning vortices [18,19]. Our central result is that for the nonzero correlation time of the random noise or potential $\eta_i(t)$, there exists an optimal migration rate $J$ such that $c$ reaches a maximum. This optimal rate realizes the "exploration-exploitation" compromise: moving too slowly ($J$ small) does not allow the system to probe the environment efficiently, and some favorable opportunities are missed. Moving too fast ($J$ large), on the other hand, does not allow the system to fully benefit from favorable spots that last for a time $\sim\tau$, as it leaves these spots too early.

Let us first present numerical simulations of the $1+1$ directed polymer problem with time-correlated disorder. The equation we simulated is

$$Z_i(t+dt) = (1-2Jdt)Z_i(t) + Jdt[Z_{i+1}(t) + Z_{i-1}(t)] + \eta_i(t)dtZ_i(t), \tag{5}$$

with $i = 1, \ldots, N$ and $\eta_i(t)$ an exponentially correlated Gaussian noise, as in Eq. (2). We considered a system with $N = 512$ sites and periodic boundary conditions. We determined $c(J)$ after a time $t = 40$ long enough to reach a stationary state, and much greater than the correlation time fixed here to $\tau = 0.1$. The dependence of $c$ on $J$ for $\sigma = 1$ and $\tau = 0.1$ is shown in Fig. 1, together with (a) the result of direct perturbation theory of the KPZ equation, *a priori* valid for large $J$, and (b) the prediction of the "tree approximation" with $a = 1/2$ and $m = 1$ that we detail below. The former predicts $c(J) \approx \sigma^2/4\sqrt{J\tau} + O(\sigma^4/J)$ for $J \to \infty$, which indeed fits the data quite well in the large $J$ region, without any adjustable parameter. The tree approximation, on the other hand, is quantitatively incorrect as expected for a one-dimensional system. For example, it predicts a $J^{-1}$ decay of $c$ (see below) but still manages to capture approximately the overall behavior of $c(J)$, in particular, the existence of a maximum.

Let us now turn to a simplified model, where the interplay between exploration and exploitation, and the optimal migration rate, can be fully understood analytically. We first note that our general model Eq. (1) for a regular lattice with $J_{ij} = J$ for neighboring sites, can be slightly altered as the following evolution rule:

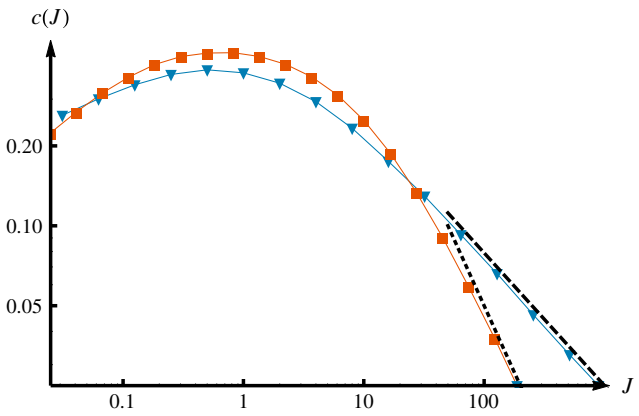


FIG. 1 (color online). Comparison of simulations of Eq. (5) (blue triangles) and of Eq. (6) (red squares) for $N = 512$ and $\tau = 0.1$, as functions of the branching (diffusion) rate $J$. We fix $\sigma = 1$. The dashed black line is the large $J$ asymptotics obtained from perturbation theory, $c(J) \approx \sigma^2/4\sqrt{J\tau}$. The dotted line reveals the $J^{-1}$ behavior of $c(J)$ for large $J$, predicted by the tree approximation (with $a = 1/2$ and $m = 1$).

$$Z_i(t+dt) = \begin{cases} Z_i(t+dt)\exp[\eta_i(t)dt] & \text{prob. } 1-Jdt, \\ (1-a)Z_i(t) + \frac{a}{m}\sum_{j\wedge i} Z_j(t) & \text{prob. } Jdt, \end{cases} \tag{6}$$

where $m$ is the number of neighbors of $i$, $j \wedge i$ means that $i$, $j$ are neighbors, and "prob." represents "with probability." To obtain a solvable model, we neglect all spatial correlations between the $Z_i$'s, which amounts to the tree approximation introduced by Derrida and Spohn for the directed polymer problem in 1988 [20]. Following these authors, we define the generating functions

$$G_t(x,\eta) := \langle \exp[-e^{-x}Z_i(t)]\delta[\eta_i(t)-\eta]\rangle,$$
$$\hat{G}_t(x) := \int_{-\infty}^{\infty} d\eta G_t(x,\eta) = \langle \exp[-e^{-x}Z_i(t)]\rangle, \tag{7}$$

Assuming the $Z_i$'s to be independent allows one to write the following evolution equation for $G_t(x,\eta)$:

$$\begin{aligned} G_{t+dt}(x,\eta) &= (1-Jdt)\langle \exp[-e^{-x+\eta_i(t)dt}Z_i(t)]\delta[\eta_i(t+dt)-\eta]\rangle \\ &\quad + Jdt\langle \exp[-e^{-x+q_1}Z_i(t)]\delta[\eta_i(t)-\eta]\rangle \\ &\quad \times \langle \exp[-e^{-x+q_2}Z_j(t)]\rangle^m, \end{aligned} \tag{8}$$

with $q_1 := \log(1-a)$ and $q_2 := \log(a/m)$. The choice in Eq. (2) of an Ornstein-Uhlenbeck process for $\eta$ is particularly simple, since it yields a Markovian equation for $\eta_i(t+dt)$:

$$\eta_i(t+dt) = \eta_i(t) + \left[-\frac{1}{\tau_c}\eta_i(t) + \frac{\sigma}{\tau_c}\xi_i(t)\right]dt, \tag{9}$$

where $\xi$ is a Gaussian white noise. Inserting this into Eq. (8), and expanding to $\mathcal{O}(dt)$, we obtain

$$\begin{aligned} G_{t+dt}(x,\eta) &= \left\langle G_t\left(x, \eta + \frac{\sigma}{\tau_c}\xi_i(t)dt\right)\right\rangle_\xi - JdtG_t(x,\eta) \\ &\quad - \eta dt\partial_x G_t(x,\eta) + \frac{dt}{\tau}\partial_\eta[\eta G_t(x,\eta)] \\ &\quad + JdtG_t(x-q_1,\eta)\hat{G}_t(x-q_2)^m + \mathcal{O}(dt)^2. \end{aligned}$$

Using $\xi_i(t)dt \sim \mathcal{N}(0,dt)$, we now average over $\xi$ and obtain a generalized Fisher-KPP equation for $G$, where the diffusion operator is replaced by the Ornstein-Uhlenbeck operator, involving the additional state variable $\eta$:

$$\begin{aligned} \partial_t G_t(x,\eta) &= \frac{\sigma^2}{2\tau_c^2}\partial_\eta^2 G + \frac{1}{\tau_c}\partial_\eta(\eta G) - \eta\partial_x G \\ &\quad + J[G_t(x-q_1,\eta)\hat{G}_t(x-q_2)^m - G_t(x,\eta)]. \end{aligned} \tag{10}$$

Like the Fisher-KPP equation known from the standard mean-field directed polymer problem [20,21], it gives rise to a front propagating in the $x$ direction. The velocity of this front is precisely the quantity $c$ we are looking for and is fixed by the tail behavior of $G_t$ when $x \to \infty$. In this tail, we make the following ansatz for $G$:

$$G_t(x,\eta) = Q(\eta) - R(\eta)e^{-\gamma(x-ct)} + \cdots \tag{11}$$

with $\int d\eta Q(\eta) = 1$. Inserting this into Eq. (10), one finds, by identifying terms of order 1 and terms of order $e^{-\gamma(x-ct)}$, that $Q(\eta)$ is the stationary Gaussian distribution for the Ornstein-Uhlenbeck process $\eta(t)$ (as it should be), while $R(\eta)$ satisfies

$$\begin{aligned} Rc\gamma &= \frac{\sigma^2}{2\tau^2}\partial_\eta^2 R + \frac{1}{\tau}\partial_\eta(\eta R) + \eta R + Jme^{\gamma q_2}Q\int d\eta R(\eta) \\ &\quad + R(\eta)J(e^{\gamma q_1}-1). \end{aligned} \tag{12}$$

This can be simplified by imposing (without loss of generality) $\int d\eta R(\eta) = 1$ and setting $R = \phi e^{-\eta^2\tau/2\sigma^2}$, $\sigma^2\hat{c} = \gamma c - J(e^{\gamma q_1}-1) - \sigma^2\gamma^2/2$, and $y = \eta/\sigma^2 - \gamma$. One gets the following equation for $\phi$:

$$\begin{aligned} &-\frac{1}{2\sigma^4\tau^2}\phi'' + \frac{1}{2}y^2\phi + \left(\hat{c} - \frac{1}{2\sigma^2\tau}\right)\phi \\ &\quad = \frac{Jme^{\gamma q_2}}{\sigma^2}\frac{e^{-((y+1)^2\sigma^2\tau/2)}}{\sqrt{\pi\sigma^2/\tau}}. \end{aligned} \tag{13}$$

Introducing the harmonic oscillator eigenfunctions $\phi_n(y) = e^{-y^2\sigma^2\tau/2}H_n(y\sigma\sqrt{\tau})$, the solution of the above equation can be written as $\phi(y) = \sum_{n=0}^{\infty} A_n\phi_n(y)$, where the coefficients $A_n$ are given by

$$A_n\left[\frac{n}{\sigma^2\tau} + \hat{c}\right] = \frac{Jme^{\gamma q_2}}{\sigma^2}\frac{e^{-\gamma^2\sigma^2\tau/4}\frac{(-1)^n}{n!}\left(\frac{\sigma\sqrt{\tau}}{2}\right)^n}{\sqrt{\pi\sigma^2/\tau}}. \tag{14}$$

Finally, the condition $\int d\eta R(\eta) = 1$ yields an implicit equation for $c$, valid for arbitrary $\tau$ [22]:

$$1 = Jme^{\gamma q_2 - \gamma^2\sigma^2\tau/2}\sum_{n=0}^{\infty}\frac{(\gamma^2\sigma^2\tau/2)^n}{n!\left[\frac{n}{\tau} + \gamma c - J(e^{\gamma q_1}-1) - \frac{\sigma^2}{2}\gamma^2\right]}. \tag{15}$$

As in the Derrida-Spohn case, the corresponding function $c(\gamma)$ is found to reach a minimum value for a certain $\gamma_{\min}$, that depends on the parameters $J$, $\sigma^2$, $\tau$, $m$. The interpretation of this phenomenon is now standard: only traveling waves with $\gamma \le \gamma_{\min}$ can be sustained and propagate at the speed $c(\gamma)$. A wave front which is "too sharp," i.e., prepared initially with a $\gamma > \gamma_{\min}$, will broaden until it reaches $\gamma = \gamma_{\min}$, and will propagate with the velocity $c(\gamma_{\min})$. In our case, the initial condition $Z = 1$ corresponds to $\gamma = 1$; therefore, either $\gamma_{\min}$ is found to be larger than unity, in which case $c$ is given by the solution of Eq. (15) with $\gamma = 1$, or $\gamma_{\min} \le 1$, in which case $c = c(\gamma_{\min})$. For the directed polymer problem, the first case corresponds to the

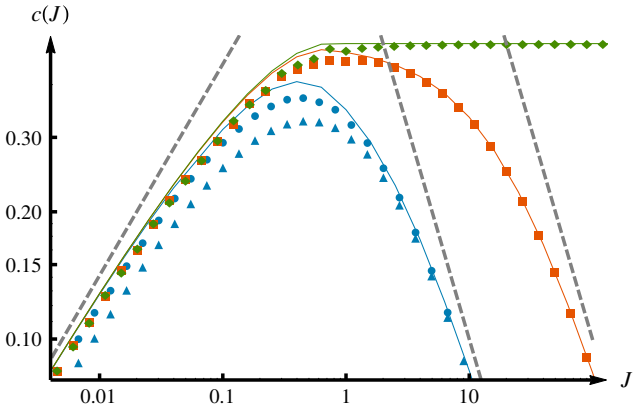


FIG. 2 (color online). Comparison of simulations of Eq. (6) for various $N$ and $\tau$, as a function of the branching (diffusion) rate $J$. Green diamonds, orange squares, and blue circles were obtained from numerical simulation of Eq. (6) for $\tau = 0$, 0.1, and 1 with $N = 2^{20}$. Blue triangles correspond to $\tau = 1$ and $N = 2^8$. In all cases, $\sigma = 1$ and $a = 1/2$, $m = 1$. The solid curves were obtained by numerical solution of Eq. (15) for the corresponding values of $\tau$. The dashed gray lines are the large- and small-$J$ asymptotics.

high-temperature, annealed phase (arising for $J \geq J_c$), while the second case corresponds to a low-temperature, frozen phase (for $J \leq J_c$). In the random growth problems, the latter case corresponds to a localization of the population, wealth, or portfolio on a small number of particularly favorable habitats, individuals, or assets (see the discussion in [4]).

We determine $c(\gamma)$, $\gamma_{\min}$, and $c(\gamma_{\min})$ numerically from Eq. (15), with very good agreement with numerical simulations (see Fig. 2). We see, in particular, that for $\tau = 0$, increasing the migration rate always increases the growth rate, which saturates at a constant value $c = \sigma^2/2$, for all $J \geq J_c$. Therefore, no optimum tradeoff between exploration and exploitation exists in this case—exploring is always favorable or neutral. However, when a finite correlation time $\tau$ is introduced, we see that, as expected, an optimum migration rate indeed appears (cf. Fig. 2) [23]. In particular, we find analytically that for small $J$, $c(J) = \sqrt{2\sigma^2 m J} + \mathcal{O}(J)$ while for large $J$, $c(J) = \sigma^2/2aJ\tau + \mathcal{O}(J)^{-2}$. From the examination of $\gamma_{\min}$ in Eq. (15), one can derive the uniqueness of the maximal speed $c(\gamma_{\min})$, occurring for $\gamma_{\min} = 1$, under the conditions $\tau > 0$, $\sigma > 0$, $0 < a < 1$, and $m \geq 1$ (which is consistent with Eq. (6), where $m$ is the number of new bifurcations). In fact, the large $J$ behavior can be understood heuristically as follows. Clearly, the problem for $\tau > 0$ must be equivalent, for large times, to the standard uncorrelated case ($\tau = 0$), but with a renormalized disorder amplitude. For large $J$ and finite $\tau$, the disorder cannot change the random walk nature of the exploration up to time $\tau$. The walk therefore freely visits $N_{\neq} = \mathcal{O}(J\tau)$ different sites during this time, leading to a preaveraging of the random disorder that reduces the variance $\sigma^2$ by a factor $N_{\neq}$. Since for $\tau = 0$, $c \propto \sigma^2$, the above renormalization immediately leads to $c(J) \sim \sigma^2/J\tau$ at large $J$. [Note that the very same argument leads to $c(J) \sim \sigma^2/\sqrt{J\tau}$ in $d = 1$, as found above, and is also exact in $d = 2$, where logarithmic corrections appear.] Now since $c(J = 0) = 0$ trivially, the decaying behavior of $c(J)$ for large $J$ and finite $\tau$ immediately implies the generic existence of an optimum in the exploration rate, as anticipated above.

We find very similar conclusions [24] for another exactly solvable limit, the fully connected graph where $J_{ij} = J_0/N$, $\forall i, j$, which in fact corresponds (up to minor details) to the limit $a = 1 - (1/N)$ and $m = N$ of the tree model above. Other theoretical methods used to investigate the KPZ or directed polymer problem could also be useful to characterize $c(J)$ in $d + 1$ dimensions or for other geometries, such as mode-coupling theory or the Gaussian variational method. The mapping to interacting bosons in the $1 + 1$ case is also an interesting avenue we are exploring [24]. It would be very interesting to observe the predicted pinning optimum experimentally. One possibility is in superconductors where the hopping rate $J$ is related to the elastic energy of the vortex lattice, which itself depends on the external magnetic field. Changing the temperature is also a way to affect both the hopping constant and the effective pinning strength [25]. Applications of these ideas are numerous, in particular, to quantify how diversified portfolios benefit from a balance between persistence and rebalancing, or to understand how economic growth is impacted by the ability of societies to find a tradeoff between tradition and innovation, or else collapse [26].

We thank G. Biroli, P. Le Doussal, and R. Munos for very helpful insights.

*thomas.gueudre@lpt.ens.fr

[1] J. D. Cohen, S. M. McClure, and A. J. Yu, Phil. Trans. R. Soc. B **362**, 933 (2007).
[2] J. G. March, Organ. Sci. **2**, 71 (1991). Note that it has 11 000 citations at the time of writing.
[3] J. C. Gittins and D. M. Jones, in *Progress in Statistics (European Meeting Statisticians, Budapest, 1972)* (North-Holland, Amsterdam, 1974), p. 241.
[4] J. P. Bouchaud and M. Mézard, Physica (Amsterdam) **282A**, 536 (2000).
[5] D. R. Nelson and N. M. Shnerb, Phys. Rev. E **58**, 1383 (1998).
[6] T. Halpin-Healy and Y.-C. Zhang, Phys. Rep. **254**, 215 (1995).
[7] T. M. Cover, Math. Finance, **1**, 1 (1991).
[8] J.-P. Bouchaud and M. Potters, *Theory of Financial Risks and Derivative Pricing* (Cambridge University Press, Cambridge, 2003).
[9] U. Frisch and J. Bec. Burgulence, in *New Trends in Turbulence Turbulence: Nouveaux Aspects*, edited by

M. Lesieur, A. Yaglom, and F. David (Springer, New York, 2001), p. 341.
[10] J. Bec and K. Khanin, Phys. Rep. **447**, 1 (2007).
[11] J. Krug and H. Spohn, in *Kinetic Roughening of Growing Surfaces in Solids Far from Equilibrium*, edited by C. Godrèche (Cambridge University Press, Cambridge, 1991).
[12] A.-L. Barabasi and H. E. Stanley, *Fractal Concepts in Surface Growth* (Cambridge University Press, Cambridge, 1995).
[13] T. Halpin-Healy, Phys. Rev. E **88**, 042118 (2013).
[14] H. J. Kappen, Phys. Rev. Lett. **95**, 200 (2005).
[15] I. Corwin, Random Matrices Theory Appl. **01**, 1130001 (2012).
[16] B. Maiorov, S. A. Baily, H. Zhou, O. Ugurlu, J. A. Kennison, P. C. Dowden, T. G. Holesinger, S. R. Foltyn, and L. Civale, Nat. Mater. **8**, 398 (2009).
[17] J. Krug and T. Halpin-Healy, J. Phys. I (France) **3**, 2179 (1993).
[18] T. Hwa, P. Le Doussal, D. Nelson, and V. Vinokur, Phys. Rev. Lett. **71**, 3545 (1993).
[19] T. Giamarchi and P. Le Doussal, Phys. Rev. B **53**, 15206 (1996).
[20] B. Derrida and H. Spohn, J. Stat. Phys. **51**, 817 (1988).
[21] J. Cook and B. Derrida, J. Stat. Phys. **57**, 89 (1989).
[22] The infinite sum over $n$ can be rewritten in a integral form that is convenient for an asymptotic analysis of the equation.
[23] Note that the "columnar" limit, where $\tau \to \infty$ [17–19], is not easily approachable through the KPP mapping due to the noncommutativity of the large $t$ and large $\tau$ limits.
[24] T. Gueudré, A. Dobrinevski, and J-P. Bouchaud (to be published).
[25] S. Bustingorry, P. Le Doussal, and A. Rosso, Phys. Rev. B **82**, 140201 (2010).
[26] J. M. Diamond, *Collapse: How Societies Choose to Fail or Succeed* (Penguin, London, 2006).

# 5 An experimental example of stochastic growth

This work was done with Alberto Rosso (LPTMS), as a collaboration with the FAST, at Orsay, and with the tutoring of my PhD advisors.

Up to now, we mentioned theoretical aspects of a benchmark model in the stochastic growth through the KPZ equation. This equation belongs to a robust universality class characterized by anomalous scaling exponents in the diffusion and free energy fluctuation. We gave a detailed analysis of the Directed Polymer statistical properties, under various conditions: other geometries, different disorders, correlations... This toy-model belongs to the large family of *elastic interfaces in disordered medium*. Frequently occurring in Nature, they are the sit of a competition between elasticity and disorder. As a result, they exhibit a complicated, glassy behaviour. We already saw some of these features, but only at equilibrium. And yet, all these elastic structures can be set in motion by applying an external force: one could imagine to pull the extremities of the polymer along the $x$-axis and try to understand how its shape fluctuates, how its move decomposes, how its total energy varies. From the competition between disorder and elasticity, emerges a energy landscape with many metastable states.

## 5.1 Weak and strong pinnings

A characteristic feature of the dynamics of elastic interfaces is the *depinning*. In the presence of disorder, the system remains (more or less) pinned and only polarizes under the action of a small applied force, i.e. moves until it locks on a local minimum of the tilted energy landscape (see Fig.5.1). At a larger drive, the system follows the force $F$ and acquires a non-zero asymptotic velocity $v$.

If the pinning comes from a collective participation of the disorder, it is coined *weak*. To describe it, a fruitful approach, suggested in [147], has drawn much analogy between this depinning transition and critical systems, although the system is now out of equilibrium. A divergent correlation length scale $\xi \propto (F - f_c)^{-\nu}$ exists close to the critical point $F_c$, emphasizing the global mechanism at play. This length is the typical size of avalanches, sudden leaps forwards of the interface. This regime is observed in Barkhausen noise, or fracture of brittle materials (we refer to [148, 85] for more details).

But some systems show a rather different behaviour that can be linked to the statistical properties of the disorder. In those case, the dynamics of the system is concentrated around very few pinning sites, and while being less rough, the interface exhibits large distorted portions, whose shape is purely controlled by elasticity.

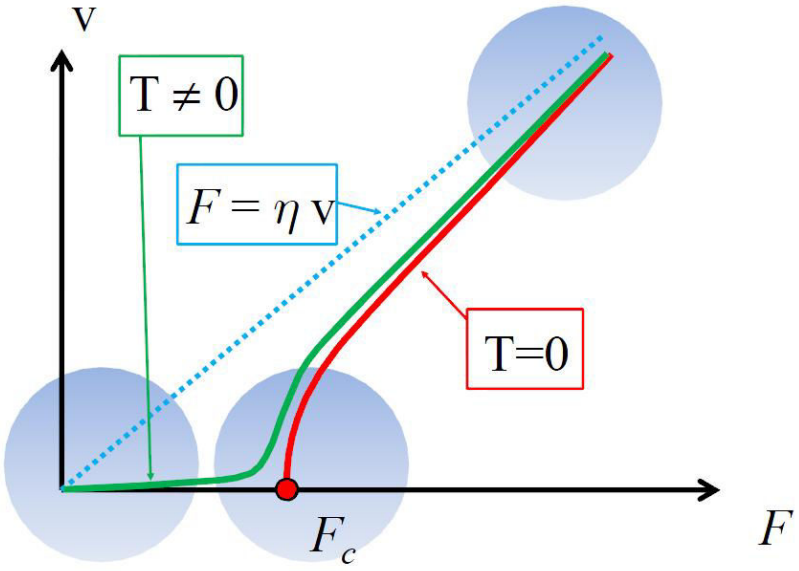


Figure 5.1: (Color online) Velocity of the interface $v$ as a function of the driving force $F$. The curve exhibit a second-order transition at a critical value $F_c$, the depinning force.

The pinning of vortices in superconductors is particularly interesting from that point of view [149]. In an homogeneous system, vortices arrange themselves along a Abrikosov lattice, but in presence of disorder, they pin to defects. This mechanism greatly influences the critical current of the superconductor. While the understanding of the pinning mechanisms are still ongoing research, impressive progress has been made to enhance critical currents using specific inclusions. In the case of weak pins, the *collective pinning theory* provides a reliable tool inspired by the framework developed from disordered systems. On the other hand, the presence of large defects, strongly trapping the vortex, f.e. isotropic and columnar inclusions [150], might be desirable to enhance the critical current. A more thorough theory of this strong pinning regime is currently investigated [151].

In *strong pinning* regime, the system behaviour is simpler, as most of the metastable states in the energy landscape are now dominated by few spots: the glassy properties do not manifest themselves anymore. Yet, much alike we hope for heavy-tailed disorder to probe the emergence of global optimization in Chapter 3, the very same argument for the depinning transition gives us the hope to better understand the role of defects, or how to adapt the analytical tools developed for Gaussian noises (like Replicas or FRG [152]) to cope with large fluctuations.

In this Chapter, we present some experiments about this *strong pinning* regime in a joint collaboration with the FAST about reaction fronts in porous media. We give a stylized, phenomenological model to explain some of their most salient features. The virtue of this approach, that we coin a "Poissonian way of reasoning", is to allow simple computations about the shape of the interface, its energy, some central limit theorems and so on. We stress again that bridging the gap between this modelling and a differential approach would be a great step towards a better understanding of the hydrodynamical limit of a larger class of disordered systems.

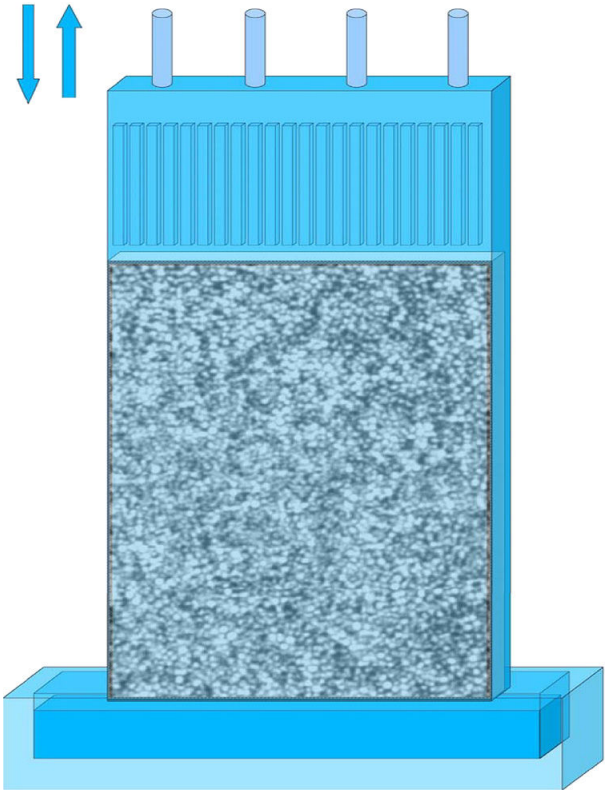

Figure 5.2: (Color online) Picture of the experimental apparatus. From [153].

## 5.2 Front propagation in porous medium

An artificial porous cell is built in a transparent Plexigas cage, filled with beads of two different sizes (1.5 mm and 2 mm) (see Fig.5.2). This prevents any unwanted crystalline structure. The cell width is denoted $L = 100$ mm, while its length in the vertical $y$-direction is $l = 300$ mm, and its depth 4 mm. The bottom is dip in a bath full of auto-catalytic reactants. On top, a set of injectors supply the porous cell with reactive solution and ensure a uniform flow over the whole span. In that configuration, the chemical front without flow field propagates upwards and remains straight. We will consider the case of *adverse* propagation, meaning that the injection of reactive solution goes against the travelling wave.

In the following, we denote $\overline{U}$ the injection rate of reactive solution, with the convention of $\overline{U} > 0$ for adverse flow. $V_\chi$ is the chemical speed of the travelling wave, $l_d$ the correlation length of the porous medium, related to the radius of the beads (see below).

### 5.2.1 Auto-catalytic reactions in advective flow

We mainly follow the presentation given in [154].

A self-sustained reaction presents a positive retroaction loop that allows it to propagate in space and time. The concentration in reactants of such reactions is very well modelled by the FKPP formalism [155]. The chemical reaction used presently, iodate-arsenic acid

is well known:

$$IO_3^- + 5I^- + 6H^+ \rightarrow 3I_2 + 3H_2O$$
$$H_3AsO_3 + I_2 + H_2O \rightarrow H_3AsO_4 + 2I^- + 2H^+$$

The auto-catalyst Iodide has a concentration $C(\mathbf{x}, t)$ obeying:

$$\frac{\partial C}{\partial t} = D_m \Delta C + \alpha C^2 (1 - C)$$

$D_m$ is the diffusion coefficient in water, and $\alpha$ the reaction rate. This reaction develops a propagation front of speed $V_\chi$ and width $l_\chi$ given by:

$$V_\chi = \sqrt{\frac{\alpha D_m}{2}}$$
$$l_\chi = \sqrt{\frac{2D_m}{\alpha}}$$

Because of the underlying velocity flow $\mathbf{U}(x, y)$, one has to amend those fundamental equations by an advection term:

$$\frac{\partial C}{\partial t} + \mathbf{U} \cdot \nabla C = D_m \Delta C + f(C)$$

To distinguish the advection from the self propagation of the chemicals, two dimensionless number, Peclet and Damkohler, are defined by:

$$Pe = \frac{\overline{U} L}{D_m} = \frac{\tau_D}{\tau_A} \quad \text{and} \quad Da = \frac{\alpha L}{\overline{U}} = \frac{\tau_A}{\tau_R}$$

$\tau_A$, $\tau_R$ and $\tau_D$ respectively the advection, diffusion and reaction times, $L$ a characteristic length scale. Different regimes can be distinguished:

- The mixing regime occurs when the diffusion is the dominant mechanism $Pe \ll 1$ and $Da \gg 1$. Reactants diffuse before they react, leading to a blurry front. As a consequence, the front speed is a mere composition of the chemical and flow speed $V_f = \overline{U} + V_\chi$.

- The Eikonal regime corresponds to a reaction speed much greater than the diffusion $Pe \gg 1$ and $Da \gg 1$. The front appears well-defined and sharp. Its speed depends on the curvature, as it locally influences the density of reactants:

$$V_f.\mathbf{n} = V_\chi + U.\mathbf{n} + D_m \kappa \tag{5.1}$$

  with $\kappa$ the front curvature.

The present experiments are all in the Eikonal regime.

### 5.2.2 Statistical properties of porous medium

The disorder is encoded in the velocity field $\mathbf{U}(x, y)$. Indeed, the chemicals are carried by a fluid forced into a porous medium made of beads of different size. The Darcy-Brinkman law relates the pressure $P$ applied to the medium to the average speed of the flow $\overline{U}$. Completed with incompressibility, it characterizes $\mathbf{U}(x, y)$:

$$\nabla \cdot \mathbf{U}(x, y) = 0 \tag{5.2}$$

$$\mathbf{U}(x, y) = -\frac{K(x, y)}{\eta}\nabla P + K(x, y)\Delta\mathbf{U} \tag{5.3}$$

where $P(x, y)$ is the pressure field, $\eta$ the fluid viscosity and $K(x, y)$ the local permeability. Due to the incompressibility, the mean fluid velocity is fixed by the injection rate $\overline{U}$. We are interested in the statistical properties of the velocity field. A common assumption in porous media theory is to implement the effect of the disorder by incorporating a random permeability field $K(\mathbf{r})$, correlated over a distance $\ell_d$. If the permeability is assumed to be Gaussian, $\mathbf{U}(\mathbf{r})$ is well approximated by a log-normal distribution.

Here we can appreciate the relation such an experiment might have with the non-linear stochastic growth. Let us recall that the quenched KPZ (QKPZ) equation is defined by adding a term for preferential growth parallel to the interface slopes, with quenched noise. One can write Eq.5.1 in cartesian coordinates (see [154] for the derivation), to see the KPZ terms appearing, albeit with additional exotic terms whose role has to be cleared. The QKPZ equation is quite a burden to solve analytically: most analytical tools tend to fall apart for quenched disorder, although some attempts have been made to define a proper analytical treatment [156]. Let us add that exact results concerning the coupling of chemical reactions with (potentially turbulent) flow are unsurprisingly scare and most studies rely on numerics [157]. To avoid those hindrances, we tackle the problem from a more phenomenological point of view, allowing us to compute observables of experimental interest.

### 5.2.3 Front freezing in adverse flow

Experiments of auto-catalytic reaction in porous media have been performed before [158, 159]. They indicated that the speed of the front was greatly modified by the presence of disorder. Most notably, they reported the existence of a wide range of injection rates $\overline{U}$ for which the average speed of the front $v_f$ goes to 0. At some threshold, the front undergoes a phenomenon much alike a depinning transition (see Fig.5.3). It was attributed to the existence of stagnation regions, protecting the chemicals from being washed out. The originality of the present device lays in its transparent walls, allowing for a direct observation of the front.

Fig.5.3 reveals a large range of values of $\overline{U}$ for which the front is static, a regime coined $S$. At each extremity, the front displays different shapes. Close to $\overline{U} = -V_\chi$, the flow exactly compensates the chemical speed, and the front is rough. Some works have linked this transition to a percolation threshold [153].

On the contrary, when $\overline{U} \simeq U_{SD}$, the front is deformed into a strongly pinned saw tooth shape (see Fig.5.4) [160]. The pinning points are the stagnation regions expected from

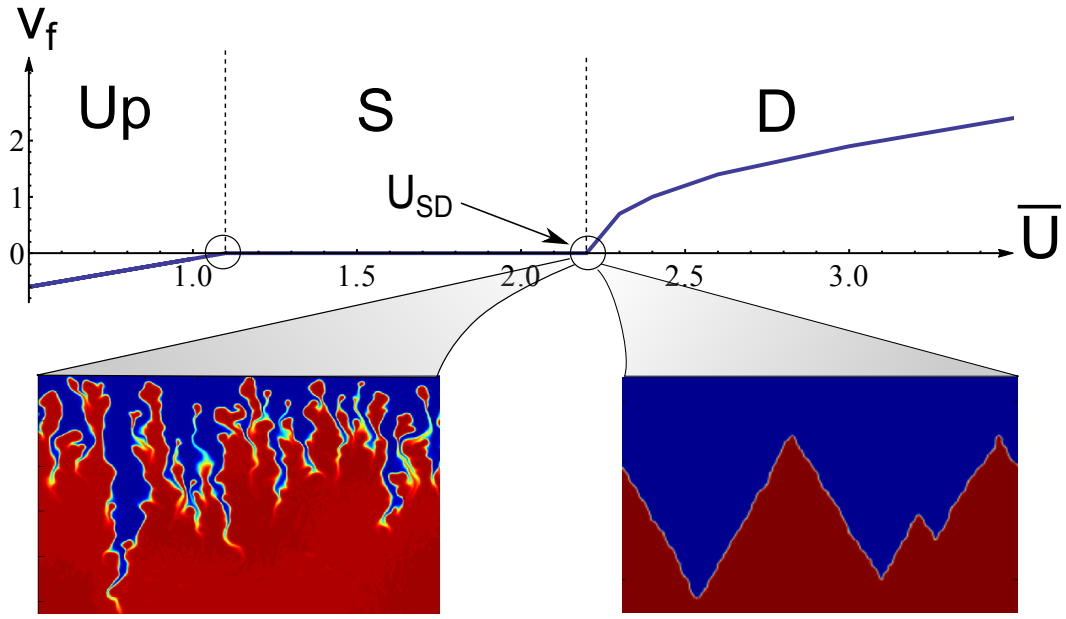


Figure 5.3: (Color online) Average speed of the front $V_f$ as a function of the injection speed $\overline{U}$ (the convention chosen is $\overline{U} > 0$ for an flow from top to bottom of the cell). Depending on the sign of $V_f$, different regimes Up, $S$ and $D$ are defined. For $\overline{U} = U_{SD}$, we observe a transition between a static front ($V_f = 0$) and a downstream front ($V_f > 0$). *Bottom part*: Hydrodynamical simulations of the front, for $\overline{U} \sim U_{SD}$ and for different permeability distributions. Two scenarios are observed: a regular saw-tooth shape (right) or a complicated shape with overhangs (left).

previous experiments. Because $\mathbf{U}(x, y)$ is random, there exists patches with anomalously low speed, despite a rather high $\overline{U}$. A screening effect of the beads protects the Iodide, therefore acting as self-sustained sources of chemicals. Once produced, those red-coloured chemicals are carried by advection and create characteristic cones.

Numerical simulations were performed using a Lattice Boltzmann scheme [161, 162], a robust scheme from microscopic considerations. Some examples are given in the related paper (see also bottom of Fig.5.3). They reveal a surprising fact: depending on the probability distribution of the permeability field $K(x, y)$, the interface exhibits very different geometries for $\overline{U} \sim U_{SD}$ (compare the bottom part of Fig.5.3).

From now on, we thus study the region $\overline{U} \sim U_{SD}$, relevant if one is trying to wash the chemical away by injection. Such strategy might be useful for more general propagation fronts such as flame fronts. Some experimental studies were conducted in the petrol industry [163, 164], as they use porous filters to separate the oil from the other products of extraction. The behaviour of the flame front in the filter, while the latter is sucking the oil out of the sands, may bear some similarities with the problem studied here. The following questions arise:

- Can we always prevent the front from invading the cell, with $\overline{U}$ high enough ?
- Is it possible to wash it completely away ?
- How to characterize the peculiar shape of the front ?

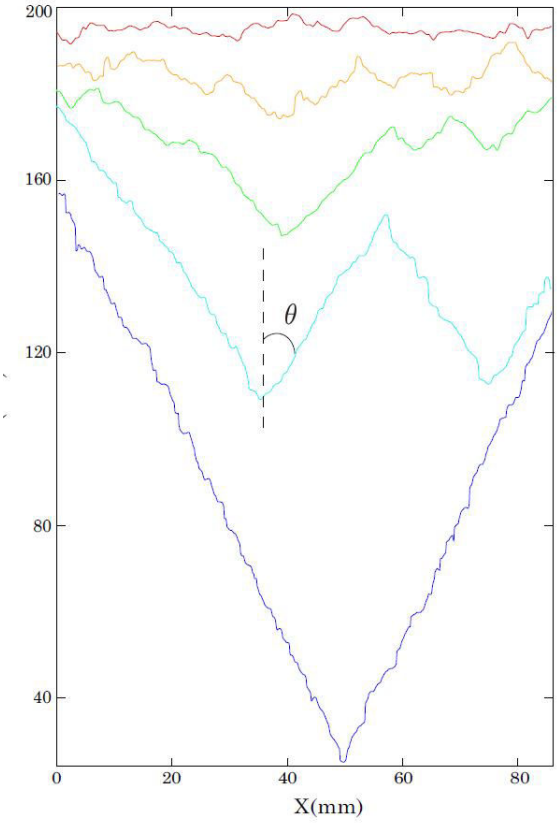


Figure 5.4: (Color online) Front geometries for increasing injection rate $\overline{U}$. The emergence of a triangle is clearly distinguished at large $\overline{U}$ while the small $\overline{U}$ regime is characterized by roughness. Note that the convention chosen in the text for $\theta$ differs by a factor 2.

- How do the details of the disorder matter ?

Mere examination of the shape leads to the intuition that the geometry of the front is controlled by those stagnant patches, whose statistics is related to extremal events of the random field $U(x, y)$ [1]. We are clearly in a *strong pinning* regime. Therefore, we elaborate a stylized model based on those remarks.

### 5.2.4 The Poissonian model of interface

We directly address the question of the statistical properties of the velocity field $\mathbf{U}(x, y)$. It can be seen as a collection of patches of area $l_d^2$. For large $\overline{U}$, $\mathbf{U}(x, y)$ is well approximated by a scalar field: $\mathbf{U} \simeq U\mathbf{e}_y$. On each patch, the random velocity follows a probability distribution of fixed average $\overline{U}$, denoted $P_{\overline{U}}$ with the scaling form:

$$P_{\overline{U}}(U) = \frac{1}{\overline{U}}\phi(U/\overline{U}) \tag{5.4}$$

To quantify the influence of the disorder on the front geometry, we consider two different

[1] The situation is very different for $\overline{U}$ small: although the front is frozen again because of the stagnant regions, those do not obey any extremal statistics.

families. The log-normal distribution is observed most of the time in experiments:

$$\phi(v) = \frac{1}{v\sqrt{2\pi}\sigma} e^{-(\log v)^2/1\sigma^2} \tag{5.5}$$

The second choice, for reasons detailed later, is the Weibull family:

$$\phi(s) = \frac{k}{\lambda}\left(\frac{x}{\lambda}\right)^{k-1} \exp\left(-(x/\lambda)^k\right) \tag{5.6}$$

The stagnation regions are patches of area $l_d^2$, centred at $(x, y)$ where $|U(x, y)| < V_\chi$. Therefore, the probability for a patch to be pinning is:

$$P(|U(x, y)| < V_\chi) = \int_0^{|V_\chi/\overline{U}|} \phi(v)dv = \lambda \tag{5.7}$$

We recall that the front speed is given by Eq.5.1. For a front which is frozen ($V_f = 0$) and straight ($\kappa \simeq 0$), wefining $\theta$ the top edge angle of the cones (see Fig.5.5), we obtain:

$$\sin\left(\frac{\theta}{2}\right) = \left|\frac{V_\chi}{\overline{U}}\right| \tag{5.8}$$

The collection of patches represents a point process, a type of random process for which each realisation consists of a set of isolated points either in time or space. Most of the analytical tools applied to random variables are readily generalized to point processes. In our case, the point process is Poisson: in the continuum limit, the number of pinning points $N(S)$ in a given area $S$ follows a Poisson distribution of parameter $\lambda$:

$$P(N(B) = k) = e^{-\lambda S}\frac{(\lambda S)^k}{k!} \tag{5.9}$$

In particular, $P(N(B) = 0) = e^{-\lambda S} = Q(S)$.

In the experiments, the cell was totally invaded with the reaction before the injection were turned on. Due to no slip boundary conditions, the interface is always pinned on the lateral walls for every $\overline{U}$ (see Fig.5.4). Hence we condition the realizations of the point process to the fact that the walls are pinning. If no stagnant patch is found in the bulk of the cell, the interface acquires a V shape, called the *depinned state* (again see Fig.5.4).

A central quantity for our analysis is $Q(y)$, the probability that, from $y = 0$ to $y$, no stagnant patch is encountered. $Q(y)$ obeys to the differential equation:

$$Q(y + dy) = \left(1 - \lambda dy\left(L - 2\tan(\theta/2)\, y\right)/\ell_d^2\right) Q(y) \tag{5.10}$$

because the probability that no pinning occurs between $y$ and $y + dy$ is $1 - \lambda dy(L - 2\tan(\theta/2)\, y)/\ell_d^2$ in an interval of size $L - 2\tan(\theta/2)\, y$. Hence:

$$Q(y) = e^{-\lambda(Ly - \tan(\theta/2)\, y^2)/\ell_d^2} \tag{5.11}$$

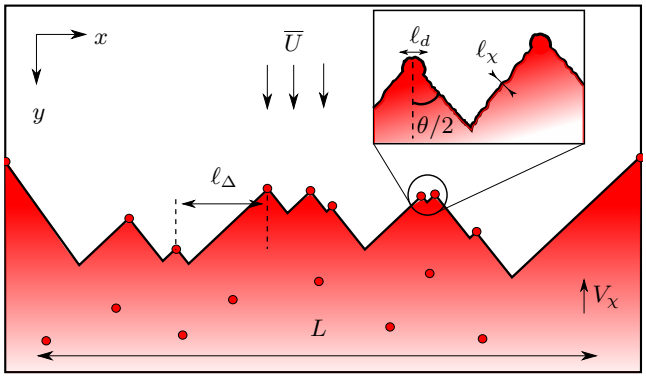


Figure 5.5: (Color online) Sketch of the stylized model: in the thin Eikonal limit $\ell_d \gg \ell_\chi$, the system can be described as a propagating front. Close to $U_{SD}$, the density of stagnant regions becomes small and the interface adopts a *sawtooth* structure.

This formula[2] is valid up to $y_V = \frac{L}{2\tan(\theta/2)}$, value above which the front is in the depinned state.

With Eq.5.11, it is possible to introduce an efficient algorithm to generate the sites pinning the front: with $\epsilon$ a random number uniformly distributed in $(0,1)$, if $\epsilon < Q(y_V)$ the algorithm terminates with a V shape, while if $\epsilon > Q(y_V)$ the height of the first pinning site is $y_1 = Q^{-1}(\epsilon)$ and its position $x_1$ is chosen at random in the segment of length $L - 2\tan(\theta/2)y_1$. This patch divides the segment into two pieces and we recursively apply the algorithm on both pieces until no more stagnant patch is found.

### 5.2.5 A transition to depinning ?

Of experimental interest is the characterization of the threshold $U_{SD}$. From Eq.5.11, the probability that no more pinning sites are encountered by the front at a given injection rate $\overline{U}$ is:

$$Q_{\overline{U}}^{\text{dep}} = \exp\left(-\frac{L^2 \int_0^{|V_\chi|/\overline{U}} \phi(v)dv}{\ell_d^2 \tan(\arcsin(|V_\chi|/\overline{U}))}\right) \tag{5.12}$$

This probability goes to 0 quadratically in $L$ or more generally, in $d$ dimensions, $Q(y_V)$ would decay as $\exp(-L^{-d})$. This explains why washing a propagating front in disordered medium can be surprisingly hard.

$U_{SD}$ diverges with $L$, or equivalently with $l_d \to 0$. Its fluctuations around the mean value are sub-dominant and it leads to a sharp (albeit infinite) threshold speed. At finite size $L$, the full distribution of $U_{SD}$ over the disorder realizations can be computed from $P(U_{SD}) = \partial_{\overline{U}} Q_{\overline{U}}^{\text{dep}}|_{U=U_{SD}}$.

[2]It can be simply recovered from Eq.5.9.

The typical value of $U_{SD}$ is given by the balance:

$$\frac{L^2}{\ell_d^2}\int_0^{|V_\chi|/\overline{U}}\phi(v)dv \sim \frac{|V_\chi|}{\overline{U}} \tag{5.13}$$

The left term measures the statistical depletion of stagnant regions when $\overline{U}$ grows, while the right term comes from the geometrical stretching of the front. The depletion of stagnant regions is strongly dependent of the underlying statistics of the disorder, much alike the Gnedenko-Tippett theorem: in Eq.5.12, only the behaviour of $\phi$ close to 0 matters. Assuming:

$$\phi(v) \sim v^{\delta-1} \quad \text{when} \quad v \to 0$$

Eq.5.12 reduces to:

$$Q_{\overline{U}}^{\text{dep}} = \exp\left(-\frac{L^2}{\ell_d^2}\left(\frac{|V_\chi|}{\overline{U}}\right)^{\delta-1}\right) \quad \text{when } \frac{|V_\chi|}{\overline{U}} \to 0 \tag{5.14}$$

Two scenarios now emerge naturally: if $\delta > 1$, the number of teeth decreases with $\overline{U}$ and the interface always gets depinned, while if $\delta < 1$, the pinning sites proliferate, the front becomes rougher and rougher, the stylized model breaks down and the formation of overhangs is expected. The transition between the two regimes occurs at a critical value $\delta_c = 1$: in that marginal case, the number of teeth remains constant. The interface statistical properties becomes independent of $\overline{U}$.

This prediction is well supported by hydrodynamical simulations of the porous media for different $P_{\overline{U}}(v)$, where a clear transition towards roughening for $\delta < 1$ is observed (see Fig.5.3 bottom). For a log-normal distribution $\phi(v) = (\sqrt{2\pi}v\sigma)^{-1}e^{-(\log v)^2/2\sigma^2}$ with a scale parameter $\sigma = 0.315$ - obtained from direct fit of the velocity distribution close to zero -, a very good agreement with numerics and *no adjusting parameter* is observed. Note that a Log-normal distribution decays to 0 as $v^{-1}\exp(-\log(v)^2)$, faster than the critical case, but not much. Hence, in the experiments, depinning indeed occurs, but it was noticed that, in some cases, the cell was contaminated by the reactants and impossible to wash by injection. This is reminiscent of the above analysis.

The typical size of the triangular structures of the front can be computed as well. One could even access the full distribution $\rho(l_\Delta)$ of the gaps between pins (see Fig.5.5):

$$\begin{aligned}\rho(l_\Delta) &= \frac{1}{\ell_{typ}}\hat{\rho}(r) \text{ with } r = l_\Delta/\ell_{typ}\\ \hat{\rho}(r) &= \frac{2}{\sqrt{\pi}}\left(2\left(e^{-\frac{r^2}{4}} - e^{-r^2}\right) + \right.\\ &\qquad \left.\sqrt{\pi}r\left(\text{erf}\left(\frac{r}{2}\right) - 2\text{erf}(r) + 1\right)\right)\end{aligned} \tag{5.15}$$

and $\ell_{typ} = \sqrt{\tan\theta/\lambda}$. The details of the computation are given in the related paper. It gives finer statistical details about the distortion of the front, for example the width of the interface, even if $\ell_{typ}$ can be easily recovered by a simple scaling argument. The

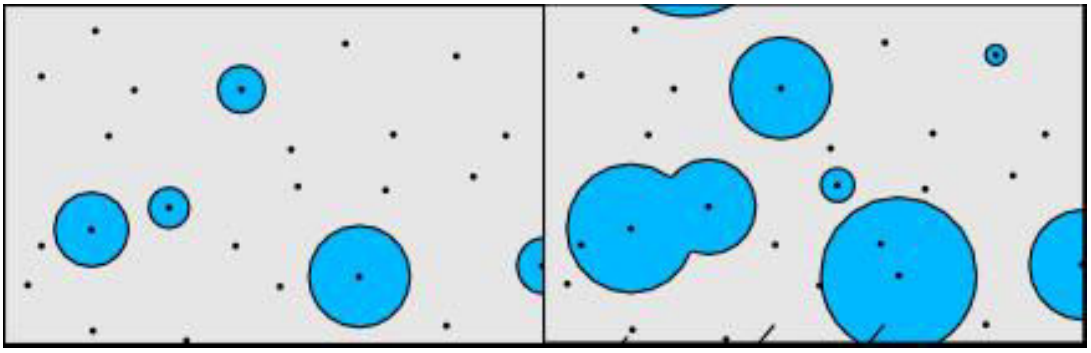

Figure 5.6: (Color online) The Avrami-Kolmogorov model of crystal growth. Seeds are dispersed over the plane, and they randomly act as nucleations of radially growing layers, usually at constant speed. When two layers meet, they merge.

use of those scalings are common in superconductors with strong pinning regimes, as the gap between pins determines the critical current [151]. But it seems that a statistical treatment akin to the model above is still lacking, and would be an interesting extension of the present work.

### 5.2.6 Mapping to growth models

If we consider the vertical $y$-axis as the time $t$-axis and look at the evolution along $t$ of the region of space invaded by the red colouring, the red region behaves as layers whose extremities move at constant speed $v = \tan\theta$. The top of the interface corresponds to the time $\tau$ at which the segment, of size $L$, is totally covered by the layer. This schematic model is a well known model of crystal growth, the Kolmorogov-Avrami model (see Fig.5.6), with a close relation to the Polynuclear Growth model.

This mapping[3] allows to translate many of the known results about the time statistics in Avrami theory to observables in our context: the width of the interface becomes the time needed to cover the entire substrate, and the typical size of the teeth is the distance between nucleation events through time. We feel worthy to mention a version of the Central Limit Theorem (CLT), giving information about the fluctuations of the nucleation events before the end of the process. This maps onto the number of front teeth $N_T$, for a large size $L$. The theorem states that $N_T - E(N_T)/Var(N_T)$ weakly converges to a Normal distribution. Although one may derive this result from the results given in the previous section, a rather elegant proof is given in [165], the CLT refreshingly coming back after so many pages.

## 5.3 Conclusion

In this Chapter, we presented the regime of *strong pinning* and compared its most salient features to the *weak pinning* regime. The analysis of the statistics of the pinning is much

[3]Of course, it holds for models with non-linear geometries, notably for vortices in superconductors with impurities.

eased in that case, because the pinning mechanism relies on few sites. Useful tools for enlightening this situations were illustrated on an experimental collaboration with the FAST, Orsay, about chemical fronts in porous medium.

We did not address the transient behaviour of the the interface, whereas [154] dedicates a large part to that question. Going downwards, the interface exhibits a discontinuous move made of avalanches. A natural question is to explore the critically of those avalanches. Are the sizes distributed with a power-law ? How is it related to other known exponents of avalanches models ? As many interfaces are driven in a disordered landscape, those interrogations are clearly relevant for experiments. Unfortunately, the conclusions from [154] are rather hard to draw, and we do not expect the dynamical exponents to clearly relate to standard critical models, but this is definitely an interesting avenue to pursue.

Very little is known currently about the hydrodynamical coupling between diffusion-reaction and advective flow. And yet it is commonly observed, for example plankton in oceanic currents, or in the ozone hole phenomenon. It has been noticed that this complex interplay greatly modifies the behaviour of the front, usually by enhancing its propagation speed. Although the present analysis is far from solving (or even addressing) those questions, it presents an rather simple “solvable” case of interplay that could be used to benchmark tools developed for a broader context.

PHYSICAL REVIEW E **89**, 041004(R) (2014)

# Strong pinning of propagation fronts in adverse flow

Thomas Gueudré,[1,*] Awadhesh Kumar Dubey,[2] Laurent Talon,[2] and Alberto Rosso[3]
[1]*CNRS-LPT, Ecole Normale Supérieure, 75231 Cedex 05 Paris, France*
[2]*Université Paris-Sud, CNRS, Laboratoire FAST, UMR 7608, Orsay F-91405, France*
[3]*Université Paris-Sud, CNRS, LPTMS, UMR 8626, Orsay F-91405, France*
(Received 14 February 2014; published 18 April 2014)

Reaction fronts evolving in a porous medium exhibit a rich dynamical behavior. In the presence of an adverse flow, experiments show that the front slows down and eventually gets pinned, displaying a particular sawtooth shape. Extensive numerical simulations of the hydrodynamic equations confirm the experimental observations. Here we propose a stylized model, predicting two possible outcomes of the experiments for large adverse flow: either the front develops a sawtooth shape or it acquires a complicated structure with islands and overhangs. A simple criterion allows one to distinguish between the two scenarios and its validity is reproduced by direct hydrodynamical simulations. Our model gives a better understanding of the transition and is relevant in a variety of domains, when the pinning regime is strong and only relies on a small number of sites.

DOI: 10.1103/PhysRevE.89.041004 PACS number(s): 47.54.−r, 82.33.Ln

In the systems separated in distinct phases, the dynamics is controlled by the behavior of the propagating fronts. Those fronts pervade a broad variety of domains in physics, ranging from chemotaxis [1] and plasma physics [2] to flame fronts [3] or epidemics, therefore triggering much activity in their modeling (for a recent review, see [4]). One of the cornerstones in this field is the celebrated Fisher–Kolmogorov-Petrowsky-Piscunov (FKPP) theory, describing the front propagation in reaction-diffusion systems [5]. However, this approach was limited to systems with no advection, i.e., not undergoing any fluid flow, despite its physical importance. Coherent fluidlike motion strongly impacts the dynamics of the fronts [6] and remains a challenging problem, whether because of the appearance of turbulence [7] or because of the influence of a disordered media [8,9]. One natural disordered environment for propagation fronts is a porous medium. Some examples were investigated in the petroleum industry and aeronautics with attempts to address the evolution of a flame front in a gas filter [10,11]. Recently, experiments on self-sustained chemical reactions have allowed a fine and controlled examination of the propagation fronts in a porous medium, revealing some striking features by direct observation [12].

The experimental setup employs an autocatalytic reaction invading a cell filled with a solution of reactants. To reproduce porosity, the cell also contains a mixture of glass spheres of different sizes. The reaction starts at the bottom of the cell and, in the absence of advection flow, develops into an almost flat front propagating upwards with constant chemical speed $|V_\chi| = \sqrt{D_m \alpha/2}$ and width $\ell_\chi = D_m/|V_\chi|$, with $D_m$ being the molecular diffusion constant and $\alpha$ the reaction rate. In the presence of an adverse flow injected from the top at speed $\overline{U}$, the porosity generates a fixed random velocity map of the fluid with short range correlations of characteristic length $\ell_d$. A rich dynamical phase diagram is observed as a function of the flow velocity $\overline{U}$, which is the control parameter of the experiment (see Fig. 1). In particular, the self-sustained fronts can travel downstream along the flow ($D$), remain static over a range of flow rate values ($S$), or move upstream (Up). In all of these phases, the heterogeneities make the front rough and the dynamics proceeds by random jumps called avalanches displaying a free scale statistics.

Here we focus on the transition between the static and the downstream regimes, occurring at the threshold $U_{SD}$ (see Fig. 1). Hydrodynamical simulations show two different scenarios: either the invading chemical reaction is completely washed away for $\overline{U} > U_{SD}$ or some stagnant chemicals remain trapped in the porous media for any $\overline{U}$. In the first case, approaching $U_{SD}$ from below, the front is largely deformed into a sawteeth structure (see Fig. 1, bottom right), while in the second case, the interface adopts a very rough and complicated structure with overhangs (see Fig. 1, bottom left). Experiments typically correspond to the first scenario but the second one has also been observed in very contaminated cells [12].

In this Rapid Communication, we describe the front propagation with a stylized model controlled by two parameters that can be easily measured in experiments. This model gives a simple criterion to discriminate between both scenarios, depending only on the behavior of the disorder distribution close to 0. The critical threshold $U_{SD}$ and the shape of the front can be characterized. Comparison with hydrodynamical *ab initio* simulations using the Darcy equation shows a perfect agreement with our results. Although our approach addresses questions raised by the experiments of [12], the results of this stylized model are much more general and relevant to all systems where the transition between a static and a moving regime is controlled by a small number of pinning sites [13–16].

*From first-principles hydrodynamics to a simple statistical model.* The flow field $\vec{U}(\vec{r})$ can be computed via the Darcy-Brinkman equation:

$$\vec{\nabla} \cdot \vec{U}(\vec{r}) = 0, \tag{1}$$

$$\vec{U}(\vec{r}) = -\frac{K(\vec{r})}{\eta}\vec{\nabla} P + K(\vec{r})\Delta\vec{U}, \tag{2}$$

where $P(\vec{r})$ is the pressure field, $\eta$ is the fluid viscosity, and $K(\vec{r})$ is the local permeability. Due to the incompressibility,

*thomas.gueudre@lpt.ens.fr

 

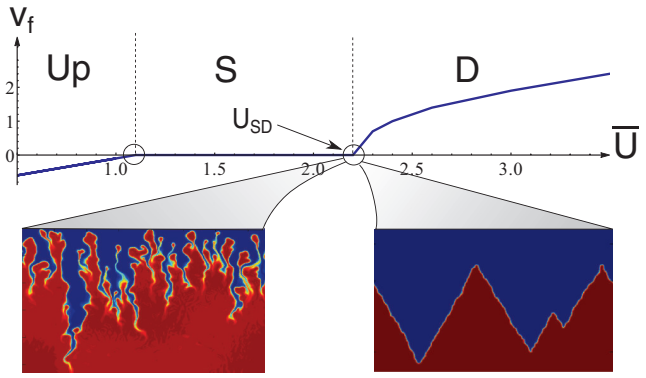


FIG. 1. (Color online) Average speed of the front $V_f$ as a function of the injection speed $\overline{U}$ (the convention chosen is $\overline{U} > 0$ for a flow from top to bottom of the cell). Depending on the sign of $V_f$, the different regimes Up, $S$, and $D$ are defined. For $\overline{U} = U_{SD}$, we observe a transition between a static front ($V_f = 0$) and a downstream front ($V_f > 0$). Bottom part: Hydrodynamical simulations of the front, for $\overline{U} \sim U_{SD}$ and for different permeability distributions. Two scenarios are observed: a regular sawtooth shape (right) or a complicated shape with overhangs (left).

the mean fluid velocity is fixed to the injection rate $\overline{U}$. Once the hydrodynamic problem is solved, the concentration of the chemicals $C(\vec{r},t)$ obeys an advection-diffusion equation (see [17]):

$$\frac{\partial C}{\partial t} + \vec{U} \cdot \vec{\nabla} C = D_m \Delta C + \alpha C^2 (1 - C). \tag{3}$$

The effect of the disorder is incorporated in the permeability $K(\vec{r})$, usually modeled as a random field, correlated over a distance $\ell_d$. Here we study the front geometry for different permeability distributions: the log-normal distribution, often employed to model permeability [18], and the distributions belonging to the Weibull family of parameter $\delta$. Figure 1 displays typical fronts for both log-normal distributed (bottom left) and Weibull distributed (bottom right, with $\delta = 0.8$) permeability fields. Those are generated using a standard method detailed in the Supplemental Material [19]. Both $U(\vec{r})$ and $C(\vec{r},t)$ were solved using a lattice Boltzmann scheme (see [20,21]). We ran the simulations on a square grid of size $L = 512$, up to $N = 2000$ realizations.

In the experimental conditions $\ell_d \gg \ell_\chi$, the front lays in the so-called *thin front eikonal* limit [22,23]. In this limit, at each point of the front, the normal component of the interface velocity satisfies $\vec{V}_f(\vec{r}) \cdot \vec{n} = V_\chi + \vec{U}(\vec{r}) \cdot \vec{n} + D_m \kappa$, where $\vec{n}$ is the unit normal vector and $\kappa$ is the curvature of the front. For $\overline{U} \sim U_{SD}$, $\vec{U}(\vec{r})$ is mainly directed along the $y$ axis, $\vec{U}(\vec{r}) \sim [0, U(\vec{r})]$. It is natural to assume that $U(\vec{r})$ is constant on patches of area $\ell_d^2$ and decorrelated between patches. The velocity of each patch is an independent random variable of average $\overline{U}$, distributed as

$$P_{\overline{U}}(U) = \frac{1}{\overline{U}} \phi(U/\overline{U}), \tag{4}$$

where the scaling function $\phi(v)$ is independent of $\overline{U}$. When $\overline{U} \leqslant U_{SD}$, the front is pinned by the very few stagnant sites where $U(\vec{r}) < |V_\chi|$. Hence the distance $\ell_\Delta$ between

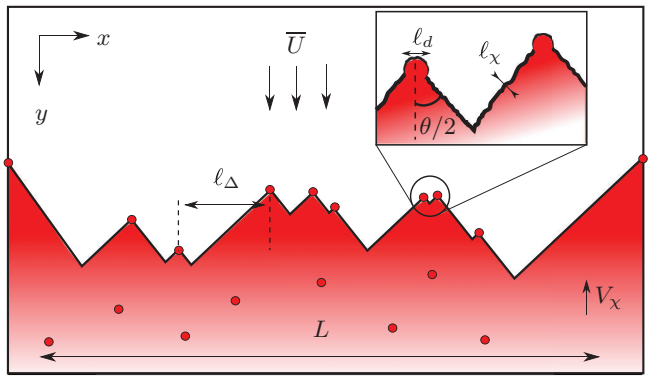


FIG. 2. (Color online) Sketch of the stylized model: in the thin eikonal limit $\ell_d \gg \ell_\chi$, the system can be described as a propagating front. Close to $U_{SD}$, the density of stagnant regions becomes small and the interface adopts a *sawtooth* structure.

them is much larger than $\ell_d$. In the neighborhood of a pinning site, the front has a *sawtooth* shape of angle $\theta$ and the front displays a sawtoothlike structure (see Fig. 2). $\theta$ can be computed observing that, in that regime, $\kappa \simeq 0$, $V_f(\vec{r}) = 0$, and $U(\vec{r}) \simeq \overline{U}$, and thus the eikonal equation becomes [12]

$$V_\chi + \overline{U} \sin(\theta/2) = 0. \tag{5}$$

Therefore, the geometry of the frozen fronts is completely determined by the velocity-dependent angle $\theta$ and by the positions of the pinning sites. In particular, the probability that a given patch of area $\ell_d^2$ is a pinning site is

$$\lambda = \int_0^{|V_\chi|} P_{\overline{U}}(U) dU = \int_0^{|V_\chi|/\overline{U}} \phi(v) dv. \tag{6}$$

For large downstream injection rate $\overline{U} \gg |V_\chi|$, the value of $\lambda$ is controlled only by the behavior of $\phi(v)$ for $v$ close to 0. In [12], it was observed that the fluid velocity vanishes near the wall. To mimic that fact, we always set the interface pinned at the points $\vec{r} = (0,0)$ and $\vec{r} = (L,0)$. Therefore, if no stagnant patch inside the cell pins the front, except at the walls, the interface acquires a V shape that we call the *depinned state*.

A central quantity for our analysis is $Q(y)$, i.e., the probability that, from $y = 0$ to $y$, no stagnant patch is encountered. $Q(y)$ obeys the differential equation,

$$Q(y + dy) = \left\{1 - \lambda dy [L - 2\tan(\theta/2) y]/\ell_d^2\right\} Q(y), \tag{7}$$

because the probability that no pinning occurs between $y$ and $y + dy$ is $1 - \lambda dy[L - 2\tan(\theta/2)y]/\ell_d^2$ in an interval of size $L - 2\tan(\theta/2)\, y$. Hence,

$$Q(y) = e^{-\lambda [Ly - \tan(\theta/2) y^2]/\ell_d^2}. \tag{8}$$

This formula is valid up to $y_V = \frac{L}{2\tan(\theta/2)}$, the value above which the front is in the depinned state. This quantity allows one to introduce an efficient algorithm to generate the sites pinning the front: Note $\epsilon$ as a random number uniformly distributed in (0,1). If $\epsilon < Q(y_V)$, the algorithm terminates with a V shape, while if $\epsilon > Q(y_V)$, the height of the first pinning site is $y_1 = Q^{-1}(\epsilon)$ and its position $x_1$ is chosen at

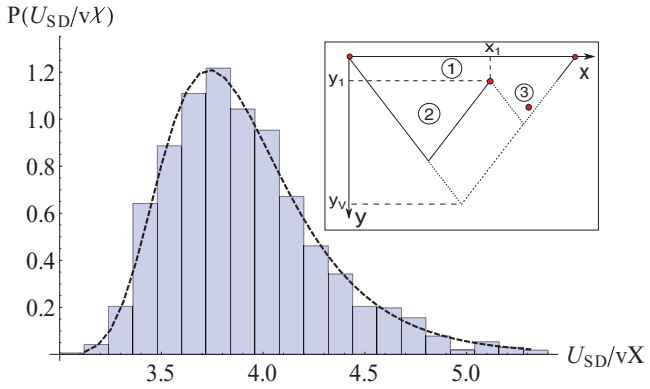


FIG. 3. (Color online) Probability distribution of the velocity threshold $U_{SD}$. The histogram corresponds to the hydrodynamical simulations of $N = 2000$ samples with a log-normal permeability, setting $L = 512$, $V_\chi = 0.0016$, $\overline{U} = 0.0036$, and $\ell_d = 5.0$. The dashed line corresponds to the prediction of the stylized model [Eq. (9)] for a log normal $\phi(v)$ with a scale parameter $\sigma = 0.315$ (see main text). Inset: Sketch of the algorithmic recursive procedure.

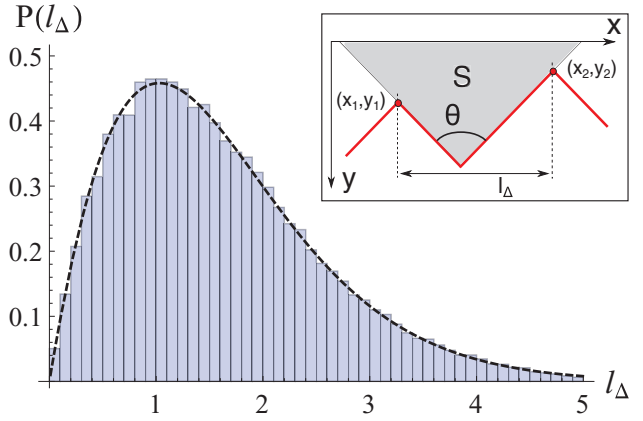


FIG. 4. (Color online) Distribution of $l_\Delta$ for the stylized model with parameters $\lambda = 0.5$ and $\theta = \pi/2$. The system size is $L = 100$ and the simulation is performed over $N = 3000$ samples. The dashed line corresponds to the asymptotic prediction of Eq. (15). Inset: Interface pinned between two adjacent stagnant patches of coordinates $\mathbf{x_1}$ and $\mathbf{x_2}$.

random in the segment of length $L - 2\tan(\theta/2)y_1$. This patch divides the segment into two pieces (see inset of Fig. 3) and we recursively apply the algorithm to both pieces until no more stagnant patch is found.

Moreover, Eq. (8) determines the statistics of the threshold $U_{SD}$. The probability of being in the depinned state for a certain injection rate $\overline{U}$ ($y = y_V$) is given by

$$Q^{\rm dep}_{\overline{U}} = \exp\left\{-\frac{L^2\int_0^{|V_\chi|/\overline{U}}\phi(v)dv}{\ell_d^2\tan[\arcsin(|V_\chi|/\overline{U})]}\right\}. \qquad (9)$$

We note that this probability goes to 0 quadratically in $L$. More generally, in $d$ dimensions, $Q(y_V)$ would decay as $\exp(-L^{-d})$. Hence the effect of the cell size on the transition is very strong and explains why washing a propagating front in disordered medium can be surprisingly hard. With raising $\overline{U}$, Eq. (9) exhibits two competing effects: the stagnant patches get decimated, while the reaction front stretches (namely, $\theta \to 0$) and explores a larger region. Assuming $\phi(v) \sim v^{\delta-1}$ when $v \to 0$, we get

$$Q^{\rm dep}_{\overline{U}} = \exp\left[-\frac{L^2}{\ell_d^2}\left(\frac{|V_\chi|}{\overline{U}}\right)^{\delta-1}\right] \quad \text{when} \quad \frac{|V_\chi|}{\overline{U}} \to 0. \qquad (10)$$

The two scenarios pictured in Fig. 1 now emerge naturally: if $\delta > 1$, the number of teeth decreases with $\overline{U}$ and the interface always gets depinned, while if $\delta < 1$, the pinning sites proliferate and the front becomes rougher and rougher. As the formation of overhangs is expected, the stylized model breaks down. The transition between the two regimes occurs at a critical value $\delta_c = 1$: in that marginal case, the number of teeth remains constant. This prediction is well supported by the hydrodynamical simulations of the porous media for different $P_{\overline{U}}(v)$, where a clear transition towards roughening for $\delta < 1$ is observed. In the experiments, the measured velocity map was fitted to a log-normal distribution, decaying to 0 as $v^{-1}\exp[-\ln(v)^2]$, which is faster than the critical case, but not much. Hence, depinning indeed occurs. Note that the threshold speed $U_{SD}$ is itself random and depends on the realization of the disorder. Its probability distribution $P(U_{SD}) = \partial_{\overline{U}} Q^{\rm dep}_{\overline{U}}|_{\overline{U}=U_{SD}}$ depends on the scaled velocity distribution $\phi(v)$. In Fig. 3, we test the prediction of our model against hydrodynamical simulations for a log-normal permeability. We assume that the velocity of the fluid displays as well a log-normal distribution, $\phi(v) = (\sqrt{2\pi}v\sigma)^{-1}e^{-(\ln v)^2/2\sigma^2}$, with a scale parameter $\sigma = 0.315$ obtained from the direct fit of the velocity distribution close to zero. A very good agreement *with no adjusting parameter* is observed.

To get a better grasp on the front roughness for $\overline{U} \lesssim U_{SD}$, we compute the distance $l_\Delta$ between two adjacent pinning sites. A scaling argument (that can be easily extended to various geometries) extracts the main dependence in $\lambda$ and $\theta$ of the typical distance between stagnant patches: Let us assume the interface pinned at some site and consider its right part (see inset of Fig. 4). The probability of having another pinning is important when the area $S \sim l_\Delta^2/\tan(\theta/2) \sim \lambda^{-1}$, leading to

$$l_\Delta \sim \sqrt{\frac{\tan\theta/2}{\lambda}} = \ell_{\rm typ}. \qquad (11)$$

It turns out that it is possible to compute the whole probability distribution $\rho(l_\Delta)$ in the *sawtooth* geometry. It obeys

$$\rho(l_\Delta) = \int_{\mathcal{D}} d\mathbf{x}_1 d\mathbf{x}_2 P(\mathbf{x}_{12})\delta(l_\Delta - |x_2 - x_1|),$$
$$\mathcal{D} = \left\{0 < x_i < L, 0 < y_i < \min\left(\frac{x_i}{\tan\theta/2}, \frac{L - x_i}{\tan\theta/2}\right)\right\}, \qquad (12)$$

with $i \in \{1,2\}$. $\mathcal{D}$ simply parametrizes the area of the interface in the depinned state. $P(\mathbf{x}_{12})$ is the probability that the interface

is pinned in $\mathbf{x}_1 = (x_1, y_1)$ and $\mathbf{x}_2 = (x_2, y_2)$, with no other nucleation in between:

$$P(\mathbf{x}_{12})d\mathbf{x}_1 d\mathbf{x}_2 = \lambda^2 d\mathbf{x}_1 d\mathbf{x}_2 e^{-\lambda S(x_1,x_2,y_1,y_2)},$$
$$S(x_1,x_2,y_1,y_2) = \frac{\tan(\theta/2)}{4}\left[y_1 + y_2 + \frac{x_2 - x_1}{\tan(\theta/2)}\right]^2 \times H\left(|x_2 - x_1|/\tan(\theta/2) - |y_2 - y_1|\right), \tag{13}$$

with $S$ being the triangular area depicted in the inset of Fig. 4 and $H$ a Heaviside function. Integration over the variables under the constraint that $l_\Delta = |x_2 - x_1|$ leads, in the limit $L \to \infty$, to

$$\rho(l_\Delta) = \frac{1}{\ell_{\text{typ}}}\hat{\rho}(r) \quad \text{with } r = l_\Delta/\ell_{\text{typ}}, \tag{14}$$

$$\hat{\rho}(r) = \frac{2}{\sqrt{\pi}}\left\{2(e^{-\frac{r^2}{4}} - e^{-r^2}) + \sqrt{\pi}r\left[\text{erf}\left(\frac{r}{2}\right) - 2\text{erf}(r) + 1\right]\right\}. \tag{15}$$

The maximum of $\hat{\rho}$ is of the order of 1, recovering the scaling argument given in Eq. (11), and an excellent agreement with the stylized model is observed (see Fig. 4). This distribution gives full information about the fluctuations of the static front in the porous media and allows one, for example, to compute its lateral extension through $\overline{\Delta H} \sim l_\Delta/[2\tan(\theta/2)]$. Finer details about the statistical properties of the interface can be useful, for example, to study fluctuations of the critical currents of a strongly pinned vortex in superconductors [15].

In this Rapid Communication, we presented a general model of pinning for interfaces in random media, when the pinning regime is strong and only relies on a finite number of sites. This, in particular, makes an approach through Poisson processes possible, allowing at the same time efficient numerical simulations and analytical results on the statistical properties of the interface. The essential experimental picture [12] is reproduced and we identified a clear criterium that allows one to discriminate between the possible scenarios shown in Fig. 1. Supported by excellent agreement with *ab initio* simulations used to model the experiments [24], this validates the hypothesis that the depinning transition is controlled by a limited number of events, randomly spread over the medium.

The above model assumes that the interface is in its final state. However, strong pinning phenomena often exhibit avalanches during transient phases, where some stagnant patches temporarily pin the interface before getting suddenly depleted. The temporal critical properties of those systems are not well understood. As a perspective, it would hence be interesting to extend the present work to transient states by introducing the random lifetime of the nucleation events.

We gratefully acknowledge Severine Atis, Pierre Le Doussal, and Dominique Salin for useful discussions.

[1] J. Adler, Science **153**, 708 (1966).
[2] T. J. M. Boyd and J. J. Sanderson, *The Physics of Plasmas* (Cambridge University Press, Cambridge, 2003).
[3] J. Jarosinski and B. Veyssiere, *Combustion Phenomena: Selected Mechanisms of Flame Formation, Propagation and Extinction* (CRC, Boca Raton, FL, 2009).
[4] J. Fort and T. Pujol, Rep. Prog. Phys. **71**, 086001 (2008).
[5] R. A. Fisher, Ann. Eugenics **7**, 355 (1937).
[6] B. F. Edwards, Phys. Rev. Lett. **89**, 104501 (2002).
[7] M. E. Schwartz and T. H. Solomon, Phys. Rev. Lett. **100**, 028302 (2008).
[8] J. Xin, SIAM Rev. **42**, 161 (2000).
[9] I. V. Koptyug, V. Zhivonitko, and R. Sagdeev, J. Phys. Chem. B **112**, 1170 (2008).
[10] A. A. Korzhavin and V. A. Bunev, Combust. Flame **109**, 507 (1997).
[11] K. K. Kuo, R. Vichnevetsky, and M. Summerfield, AIAA J. **11**, 444 (1973).
[12] S. Atis, S. Saha, H. Auradou, D. Salin, and L. Talon, Phys. Rev. Lett. **110**, 148301 (2013).
[13] P. Yang and C. M. Lieber, J. Mater. Res. **12**, 2981 (1997).
[14] B. Maiorov, S. A. Baily, H. Zhou, O. Ugurlu, J. A. Kennison, P. C. Dowden, T. G. Holesinger, S. R. Foltyn, and L. Civale, Nat. Mater. **8**, 398 (2009).
[15] A. E. Koshelev and A. B. Kolton, Phys. Rev. B **84**, 104528 (2011).
[16] D. Dalmas, E. Barthel, and D. Vandembroucq, J. Mech. Phys. Solids **57**, 446 (2009).
[17] N. Jarrige, I. Bou Malham, J. Martin, N. Rakotomalala, D. Salin, and L. Talon, Phys. Rev. E **81**, 066311 (2010).
[18] G. Matheron, *Éléments Pour une Théorie des Milieux Poreux* (Masson et Cie, Paris, 1967).
[19] See Supplemental Material at http://link.aps.org/supplemental/10.1103/PhysRevE.89.041004 for the procedures to generate correlated Gaussian random fields.
[20] L. Talon, J. Martin, N. Rakotomalala, D. Salin, and Y. C. Yortsos, Water Resour. Res. **39**, 1135 (2003).
[21] I. Ginzburg, Phys. Rev. E **77**, 066704 (2008).
[22] M. Leconte, J. Martin, N. Rakotomalala, and D. Salin, Phys. Rev. Lett. **90**, 128302 (2003).
[23] F. Williams, *Combustion Theory*, 2nd ed. (Benjamin/Cummings, New York, 1985).
[24] S. Saha, S. Atis, D. Salin, and L. Talon, Europhys. Lett. **101**, 38003 (2013).

# 6 Summary

The KPZ universality class is currently the simplest and most studied of the non-linear stochastic growth models, describing roughening in experiments. From a more mathematical point of view, it is seen as the best candidate to broaden the applicability of the Central Limit Theorem to strongly correlated random variables. Therefore, recent years have witnessed a large activity from both the physics and mathematics community. From the bridges between both fields has emerged an intricate picture, made of demanding mathematical tools (whose surface we barely scratched) mixed with a sophisticated picture of the physics involved.

In the present Thesis, rather than digging even deeper into this rich structure, we probed the range of the universality with respect to various modifications. They essentially revealed a complex, multi-faceted picture of the KPZ universality, sometimes exhibiting an astonishing robustness, sometimes breaking down completely. The previous Chapters present a set of theoretical tools that could be employed to enlarge the flexibility of those stochastic models, as various as population dynamics, networks of vortices in superconductors or chemical fronts. Integrable systems and Bethe Ansatz, various perturbative approaches, tree geometry and FKPP theory, multi-fractality and multiplicative cascades, Poisson processes... are only a few of the possible routes.

They are many directions in which the present work can be extended, and we chose to give them at the end of each chapter, rather to postpone to the end. From the exact solution of a depinning transition to the link between Anderson localization and optimal growth, new avenues to explore are not lacking, and although stochastic growth is already interdisciplinary, the numerous bridges between various fields of physics are clearly not all built.

We did not address at all the existence of a rough phase in higher dimension, a problem that has resisted twenty years of efforts, and still broadly open. Numerical simulations are progressively ruling out the existence of an upper critical dimension. But a definitive answer would certainly come as a relief. Although it might appear of rather theoretical interest, hopefully an argument about the rough phase holding in every dimension will unravel a more detailed picture of the interplay between disorder and entropy. An in-depth study of the anatomy of the optimal path from a local point of view (for example, the correlations induced between the energies along the polymer) has yet to be performed, while it would allow to characterize the notion of optimality in disordered environment.

The deep analysis of this stochastic model will hopefully broaden the present framework of stochastic calculus. The KPZ equation is one of the simplest Langevin equations with non linearities that could be written down, and yet, it immediately escapes the standard formalism ! It is fair to say that the KPZ equation has nucleated a fast evolution in our understanding of stochastic PDE. Because those systems exhibits intermittency, this class

might be a path to a better quantification of the irregular phases of activity observed in noise-driven physical systems, and the reasons behind. The chaotic character of SPDE is again a field where much remains to explore.

# A Appendix

## A.1 The Ornstein Ulhenbeck process

In this Appendix, we briefly review the properties of the Ornstein-Uhlenbeck process, as it is extensively used for enforcing temporal correlations. This process can be regarded as the simplest temporally correlated process. It is the only process simultaneously Markovian, Gaussian and stationary. Mean-reverting, it drifts towards its mean asymptotically. One can think about it as a Brownian motion with a spring It obeys the Langevin equation[1]:

$$dU_t = -\frac{U_t}{\tau}dt + \frac{\sigma}{\tau}dW_t \tag{A.1}$$

and the following Fokker-Planck equation for its probability density $f(x,t)$:

$$\frac{\partial f}{\partial t} = \frac{1}{\tau}\frac{\partial}{\partial x}(xf) + \frac{\sigma^2}{2\tau}\frac{\partial^2 f}{\partial x^2} \tag{A.2}$$

Mostly everything can be computed for the OU process, from the exact expression for $f(x,t)$:

$$f(x,t) = \sqrt{\frac{\tau}{\pi\sigma^2(1-e^{-t/\tau})}}\exp\left(-\frac{\tau}{\sigma^2}\frac{x^2}{1-e^{-t/\tau}}\right) \tag{A.3}$$

with the initial condition $x(0) = 0$. The stationary limit is readily obtained as $f_s(x) = \sqrt{\frac{\tau}{\pi\sigma^2}}e^{-\frac{\tau x^2}{\sigma^2}}$. It enjoys an Ito integral expression as well:

$$U_t = \frac{\sigma}{\tau}\int_0^t e^{-(t-s)/\tau}dW_s \tag{A.4}$$

from which can be computed $cov(U_t, U_s) = \frac{\sigma^2}{2\tau}e^{-|t-s|/\tau}$.

The knowledge of the transient probability distribution allows for efficient and precise numerical computation. We can follow a procedure much alike a Langevin white noise $\xi_t$, exactly coarse-grained over an interval $dt$ as a Gaussian of variance $\sigma^2 = dt$. Indeed the integrated OU, denoted $V_t$, although not a markovian process, is analytically tractable because it remains Gaussian. Hence the knowledge of the first moments is sufficient. For example:

$$\sigma^2_{V_t} = \sigma^2\tau^3\left(\frac{t}{\tau} - 2(1-e^{-t/\tau} + \frac{1}{2}(1-e^{-2t/\tau}))\right) \tag{A.5}$$

[1]The peculiar scaling of $\sigma$ with $\tau$ stems from the fact that the limit $\tau \to 0$ matches with the standard white noise.

We refer to [137] for the details.

Now, we want to numerically simulate the Langevin equation $\partial_t Z = J\Delta Z + \eta_t(x)Z$ as stated in Chapter 4, discretizing it on a scale $dt$ requires a coarse grained integrated OU on a scale $dt$, that can be exactly updated through:

$$\begin{aligned} U(t+dt) &= U(t)\mu + \sigma_U n_1 \\ V(t+dt) &= U(t) + V(t)\tau(1-\mu) + \left(\sigma_V^2 - \frac{\kappa_{UV}}{\sigma_U^2}\right)^{1/2} n_2 + \frac{\kappa_{UV}}{\sigma_U} n_1 \\ \mu &= e^{-\Delta t/\tau} \\ \sigma_U^2 &= \sigma^2\tau/2(1-\mu^2) \\ \sigma_V^2 &= \sigma^2\tau^3\left(\frac{t}{\tau} - 2\left(1 - e^{-t/\tau} + \frac{1}{2}(1-e^{-2t/\tau})\right)\right) \\ \kappa_{UV} &= \sigma^2\tau^2/2(1-\mu)^2 \end{aligned} \tag{A.6}$$

$n_1$ and $n_2$ being two independent normally distributed variables.

It is much more efficient numerically to sequentially update the noise depending on the chosen $dt$ following the above formula, and *then* apply the scheme chosen for the PDE, as it virtually gets rid of errors done on the stochastic part of the integration. Applications of this procedure in other contexts can be found in [138]. This trick was used for the numerical simulations presented in Chapter 4.

One can check that the limit $\tau \to 0$ naturally recovers the white noise process. Note that that the limit $\tau \to \infty$ allows to recover the columnar noise(or the Brownian, but with a different scaling of $\sigma$ with $\tau$, namely when $dU_t = -U_t/\tau + \sigma dW_t$).

## A.2 A temporal perturbation expansion

In this section we present the perturbation expansion of the KPZ equation for temporally correlated noise, where the perturbative parameter is $\lambda$ the strength of the non-linear growth term $(\nabla h)^2$.

### A.2.1 First order in $J$

Note that the perturbative regime here is associated to high diffusivity, or equivalently to short time. The following rescaling allows us to get rid of other dependencies of $J$:

$$\begin{aligned} h &= \frac{\tilde{h}}{\sqrt{J}} \\ t &= \frac{\tilde{t}}{J} \\ \tau &= \tilde{\tau}/J \end{aligned}$$

leading to the rescaled equation:

$$\partial_{\tilde{t}}\tilde{h} = \Delta\tilde{h} + \frac{(\nabla\tilde{h})^2}{\sqrt{J}} + \eta = \Delta\tilde{h} + \lambda(\nabla\tilde{h})^2 + \eta \tag{A.7}$$

Writing $h = h^{(0)} + h^{(1)} + \dots$ where $h^{(n)} = O(\lambda^n)$, the lowest order is just the Edwards-Wilkinson result, namely in Fourier space:

$$\tilde{h}_q(t) = \int_0^{\tilde{t}} d\tilde{t}' e^{-q^2(\tilde{t}-\tilde{t}')}\tilde{\eta}_q(\tilde{t}') \tag{A.8}$$

$$\begin{aligned}\langle\partial_{\tilde{t}}\tilde{h}_q\rangle &= \lambda\langle(\nabla\tilde{h})^2\rangle \\ &= \lambda\int\frac{dq}{4\pi^2}q^2e^{-2q^2\tilde{t}}\int_0^{\tilde{t}}d\tilde{t_1}d\tilde{t_2}e^{q^2(\tilde{t_1}+\tilde{t_2})}\langle\tilde{\eta}_q(\tilde{t_1})\tilde{\eta}_{-q}(\tilde{t_2})\rangle\end{aligned} \tag{A.9}$$

with the time-rescaled OU correlator ($\tilde{\tau} = \tau J$):

$$\langle\tilde{\eta}_q(\tilde{t_1})\tilde{\eta}_{q'}(\tilde{t_2})\rangle = \frac{2\pi\sigma^2}{2\tilde{\tau}}e^{-|\tilde{t_1}-\tilde{t_2}|/\tilde{\tau}}\delta(q+q') \tag{A.10}$$

It leads to:

$$\begin{aligned}\langle\partial_{\tilde{t}}\tilde{h}\rangle &= \frac{\lambda\sigma^2}{2\pi\tilde{\tau}}\int_q q^2e^{-2q^2\tilde{t}}\int_0^{\tilde{t}}dt_1e^{q^2\tilde{t_1}}\int_0^{\tilde{t_1}}d\tilde{t_2}e^{q^2\tilde{t_2}}e^{-(\tilde{t_1}-\tilde{t_2})/\tilde{\tau}} \\ &\approx \frac{\lambda\sigma^2}{2\pi\tilde{\tau}}\int dq\frac{\tilde{\tau}}{2(1+\tilde{\tau}q^2)} \\ &= \frac{\lambda\sigma^2}{4\sqrt{\tilde{\tau}}}\end{aligned}$$

Introducing the original variables, one obtains:

$$c(J) \simeq \frac{\sigma^2}{4\sqrt{\tau_c J}} \tag{A.11}$$

### A.2.2 Second order in $J$

If we note, always in rescaled variables:

$$h = h_0 + \lambda h_1$$

We obtain the correction to the speed:

$$c = \lambda(\nabla h_0)^2 + 2\lambda^2\nabla h_0\nabla h_1 + \lambda^3(\nabla h_1)^2$$

The second term involves 3-point function of the OU, which vanishes due to Gaussianity. Computing $\langle(\nabla h_1)^2\rangle$ with:

$$h_1(q,t) = \int_0^t e^{-q^2(t-t')}(\nabla h_0)^2(q,t')dt' \tag{A.12}$$

One gets:

$$(\nabla h_1)^2(q,t) = \frac{-1}{2\pi}\int_{q'} q'(q-q')h_1(q',t)h_1(q-q',t)$$
$$= \frac{1}{2\pi}\int_{q'} q'^2 h_1(q',t)h_1(-q',t) \tag{A.13}$$

as only the mode $q=0$ will remain.

And so, writing down the complete expression of $h_1(q,t)$:

$$h_1(q,t) = \int_0^t e^{-q^2(t-t')}\int_{q'} q'(q-q')h_0(q',t')h_0(q-q',t')$$
$$= \int_{t'=0}^t \int_{q'} e^{-q^2(t-t')}q'(q-q')$$
$$\int_{t_1,t_2} e^{-q'^2(t'-t_1)}e^{-(q-q')^2(t'-t_2}\eta_{q'}(t_1)\eta_{q-q'}(t_2)$$

Expanding $\langle h_1(q,t)h_1(-q,t)\rangle$ leads to the 4 point function of OU (with the time variables being integrated):

$$\langle \eta_{q'}(t_1)\eta_{q-q'}(t_2)\eta_{q''}(t_3)\eta_{-q-q''}(t_4)\rangle \tag{A.14}$$

The Wick theorem gives only two (symmetrical) contributions for $q' = -q''$ and $q' = q-q''$ with a factor of $\left(\frac{\sigma^2\pi}{\tau}\right)^2$:

$$\langle h_1(q,t)h_1(-q,t)\rangle = 2\left(\frac{\sigma^2\pi}{\tau}\right)^2$$
$$\int_{q'}\int_{(t',t'')<t}\int_{(t_1,t_2)<t',(t_3,t_4)<t''} e^{-2q^2t^2}e^{(q^2-q'^2-(q-q')^2)(t'+t'')}$$
$$e^{q'^2(t_1+t_3)}e^{(q-q')^2(t_2+t_4)}q'^2(q-q')^2e^{-|t_3-t_1|/\tau}e^{-|t_4-t_2|/\tau}$$

So basically, from the 2-times integral, ones obtains:

$$\int_{t_1,t_3} e^{q'^2(t_1+t_3)}e^{-|t_3-t_1|/\tau} = \tau^2 f(T',T'',q') \tag{A.15}$$

$$f(T',T'',Q') = \int_{T_1=0}^{T'}\int_{T_3=0}^{T''} e^{Q'^2(T_1+T_3)-|T_3-T_1|} \tag{A.16}$$

that we can symmetrize and which has an explicit (but not really user-friendly) expression. However, its scaling is easily extracted in the dimensionless variables $T = t/\tau$ and $Q = \sqrt{\tau}q$. At the end, it boils down to:

$$\tilde{c} = \frac{\lambda^3\sigma^4}{\tau^{2+3+1-6}}\int_{Q,Q',T',T''} Q^2Q'^2(Q-Q')^2$$
$$e^{-2Q^2T^2}e^{(Q^2-Q'^2-(Q-Q')^2)(T'+T'')}f(T',T'',Q')f(T',T'',Q-Q')$$

with the following counting in $\tau$: 2 from the OU correlator, 3 from the $Q^2$ factors, 1 from the $dQ, dQ'$, 6 from all the $dT$. Finally, reintroducing the original variables:

$$\begin{aligned} c = \sqrt{J}\tilde{c} &\sim \sqrt{J}\lambda^3\sigma^4 \\ &\sim \frac{\sigma^4}{J} \end{aligned} \tag{A.17}$$

Hence the next term is $\tau$ independent.

## A.3 A small correlations expansion

It turned out that on a tree, the speed can be exactly computed for arbitrary large values of $\tau$. However, it relies on the ability to properly guess the limiting form of the generating function $g$ defined in Eq.4.2.2.2. A more systematic approach is possible through perturbations in $\tau$. For small $\tau$, the noise is "almost" white, and Eq.4.30 can be expanded in fast and slow modes. The details of the general procedure can be found in [166].

Let us first rescale $\eta =: V/\sqrt{\tau}$ and rewrite Eq.4.30 as

$$\begin{aligned} \partial_t G_t(x,\eta) =& \frac{1}{\tau} L_1 G_t(x,V) + \frac{1}{\sqrt{\tau}} L_2 G_t(x,V) \\ &+ \lambda G_t(x-q_1,V)\hat{G}_t(x-q_2) - \lambda G_t(x,V), \end{aligned} \tag{A.18}$$

where the operators $L_1$ and $L_2$ are defined as

$$L_1 f := \frac{\sigma^2}{2}\partial_V^2 f + \partial_V(Vf), \tag{A.19}$$

$$L_2 f := -V\partial_x f \tag{A.20}$$

We also define the projector $P$ on the stationary distribution $P_0$ of $V$

$$Pf_t(x,V) := P_0(V)\int_{V_2} f_t(x,V_2) = P_0(V)\hat{f}_t(x) \tag{A.21}$$

$$P_0(V) = \frac{1}{\sqrt{\pi\sigma^2}}\exp\left(-\frac{V^2}{\sigma^2}\right). \tag{A.22}$$

The projector $P$ and the operators $L_1$, $L_2$ satisfy, among others, the relations $PL_1 = L_1P = 0$ and $PL_2P = 0$. Let us now decompose the solution $G_t(x,V)$ in a slow part $v_t$ and a fast part $w_t$ , defined as

$$v_t(x,V) := PG_t(x,V) = P_0(V)\hat{G}_t(x) \tag{A.23}$$

$$w_t(x,V) := (1-P)G_t(x,V) = G_t(x,V) - v_t(x,V) \tag{A.24}$$

Inserting this into Eq.A.18 we obtain a system of coupled equations for $w, v$:

$$\begin{aligned}\partial_t v_t(x,V) =& \frac{1}{\sqrt{\tau_c}} P L_2 w_t(x,V) + \lambda v_t(x-q_1,V)\hat{G}_t(x-q_2) \\ & - \lambda v_t(x,V), \qquad \text{(A.25)} \\ \partial_t w_t(x,V) =& \frac{1}{\tau_c} L_1 w_t(x,V) + \frac{1}{\sqrt{\tau_c}}(1-P) L_2 w_t(x,V) \\ & + \frac{1}{\sqrt{\tau_c}} L_2 v_t(x,V) + \lambda w_t(x-q_1,V)\hat{G}_t(x-q_2) \\ & - \lambda w_t(x,V). \qquad \text{(A.26)}\end{aligned}$$

Comparing the leading-order term $\frac{1}{\tau_c} L_1 w_t(x,V)$ for small $\tau$ in the second equation with the source term $\frac{1}{\sqrt{\tau_c}} L_2 v_t(x,V)$ shows that $w$ is of order $\sqrt{\tau}$, i.e. small. This means that $v$ and $w$ can be expanded in powers as follows:

$$\begin{aligned} w =& \sqrt{\tau}\, w^{(0)} + \tau\, w^{(1)} + \tau^{3/2}\, w^{(2)} + \mathcal{O}(\tau)^2, \qquad \text{(A.27)} \\ v =& v^{(0)} + \sqrt{\tau}\, v^{(1)} + \tau\, v^{(2)} + \mathcal{O}(\tau)^{3/2}. \qquad \text{(A.28)}\end{aligned}$$

Note that the ansatz for $v$ implies an anologous expansion for $\hat{G}$:

$$\hat{G} = \hat{G}^{(0)} + \sqrt{\tau}\, \hat{G}^{(1)} + \tau\, \hat{G}^{(2)} + \mathcal{O}(\tau)^{3/2}. \qquad \text{(A.29)}$$

Inserting this into Eq.A.25 and solving it order by order in $\tau$, one obtains after some algebra expressions for the fast modes $w^{(i)}$ in terms of the slow modes $v^{(i)}$, $\hat{G}^{(i)}$:

$$\begin{aligned} w^{(0)}(x,V) =& - L_1^{-1} L_2 v^{(0)}(x,V), \\ w^{(1)}(x,V) =& - L_1^{-1}(1-P) L_2 w^{(0)}(x,V) - L_1^{-1} L_2 v^{(1)}(x,V), \\ w^{(2)}(x,V) =& - L_1^{-1}\Big[-\partial_t w^{(0)}(x,V) + \lambda w^{(0)}(x-q_1,V)\hat{G}^{(0)}(x-q_2) \\ & \quad -\lambda w^{(0)}(x,V)\Big] \\ & - L_1^{-1}(1-P) L_2 w^{(1)}(x,V) - L_1^{-1} L_2 v^{(2)}(x,V).\end{aligned}$$

This allows evaluating the source terms in (A.25), which are driving the slow modes $v^{(i)}, \hat{G}^{(i)}$:

$$\begin{aligned} P L_2 w^{(0)}(x,V) =& P_0(V)\frac{\sigma^2}{2}\partial_x^2 \hat{G}^{(0)}(x) \\ P L_2 w^{(1)}(x,V) =& P_0(V)\frac{\sigma^2}{2}\partial_x^2 \hat{G}^{(1)}(x) \\ P L_2 w^{(2)}(x,V) =& P_0(V)\frac{\sigma^2}{2}\Big\{\partial_x^2 \hat{G}^{(2)}(x) \\ & -\partial_t \partial_x^2 \hat{G}^{(0)}(x) + \frac{\sigma^2}{2}\partial_x^4 \hat{G}^{(0)}(x) \\ & +\lambda \partial_x\Big[(\partial_x \hat{G}^{(0)}(x-q_1))\hat{G}^{(0)}(x-q_2) - \partial_x \hat{G}^{(0)}(x)\Big]\Big\}.\end{aligned}$$

Inserting these expressions into (A.25), one obtains closed equations for the slow modes $\hat{G}^{(i)}$. After cancelling the $P_0(V)$ factors and combining the different orders in $\tau$, one finds

the following equation for $\hat{G}(x) = \hat{G}^{(0)}(x) + \sqrt{\tau}\hat{G}^{(1)}(x) + \tau\hat{G}^{(2)}(x) + \mathcal{O}(\tau)^2$:

$$\begin{aligned}\partial_t\hat{G}(x) =& \frac{\sigma^2}{2}\partial_x^2\hat{G}(x) + \lambda\left[\hat{G}(x-q_1)\hat{G}(x-q_2) - \hat{G}(x)\right] \\ &+ \frac{\sigma^2}{2}\tau\left\{-\partial_t\partial_x^2\hat{G}(x) + \frac{\sigma^2}{2}\partial_x^4\hat{G}(x)\right. \\ &\left.+ \lambda\partial_x\left[(\partial_x\hat{G}(x-q_1))\hat{G}(x-q_2) - (\partial_x\hat{G}(x))\right]\right\} \\ &+ \mathcal{O}(\tau)^2. \end{aligned} \tag{A.30}$$

From this last expression, now only depending on $x$, the same analysis than in the white-noise case can be performed, to extract the lowest order dependence of the dispersion relation similar to Eq.4.25 with $\tau$. This leads as well to the existence of an optimum.

# Bibliography


[1] John Terborgh. Mixed flocks and polyspecific associations: costs and benefits of mixed groups to birds and monkeys. *American Journal of Primatology*, 21(2):87–100, 1990.

[2] Mile Gu, Christian Weedbrook, Álvaro Perales, and Michael A. Nielsen. More really is different. *Physica D: Nonlinear Phenomena*, 238(9–10):835 – 839, 2009.

[3] Jun-ichi Wakita, Hiroto Itoh, Tohey Matsuyama, and Mitsugu Matsushita. Self-affinity for the growing interface of bacterial colonies. *Journal of the Physical Society of Japan*, 66(1):67–72, 1997.

[4] Kazumasa A. Takeuchi, Masaki Sano, Tomohiro Sasamoto, and Herbert Spohn. Growing interfaces uncover universal fluctuations behind scale invariance. *Sci. Rep.*, 1, July 2011.

[5] Dubois-Violette, E., de Gennes, P.G., and Parodi, O. Hydrodynamic instabilities of nematic liquid crystals under a. c. electric fields. *J. Phys. France*, 32(4):305–317, 1971.

[6] Michael J. Stephen and Joseph P. Straley. Physics of liquid crystals. *Rev. Mod. Phys.*, 46:617–704, Oct 1974.

[7] KazumasaA. Takeuchi and Masaki Sano. Evidence for geometry-dependent universal fluctuations of the kardar-parisi-zhang interfaces in liquid-crystal turbulence. *Journal of Statistical Physics*, 147(5):853–890, 2012.

[8] Kazumasa A. Takeuchi and Masaki Sano. Universal fluctuations of growing interfaces: Evidence in turbulent liquid crystals. *Phys. Rev. Lett.*, 104:230601, Jun 2010.

[9] Tomohiro Sasamoto and Herbert Spohn. One-dimensional kardar-parisi-zhang equation: An exact solution and its universality. *Phys. Rev. Lett.*, 104:230602, Jun 2010.

[10] Gideon Amir, Ivan Corwin, and Jeremy Quastel. Probability distribution of the free energy of the continuum directed random polymer in 1 + 1 dimensions. *Communications on Pure and Applied Mathematics*, 64(4):466–537, 2011.

[11] Pierre Le Doussal and Pasquale Calabrese. The kpz equation with flat initial condition and the directed polymer with one free end. *Journal of Statistical Mechanics: Theory and Experiment*, 2012(06):P06001, 2012.

[12] V. Dotsenko. Bethe ansatz derivation of the tracy-widom distribution for one-dimensional directed polymers. *EPL (Europhysics Letters)*, 90(2):20003, 2010.

[13] A. M. Somoza, M. Ortuno, and J. Prior. Universal distribution functions in two-dimensional localized systems. *Physical Review Letters*, 99(11):116602, September 2007.

[14] BL Altshuler, VE Kravtsov, and IV Lerner. Distribution of mesoscopic fluctuations and relaxation processes in disordered conductors. *Mesoscopic Phenomena in Solids. Elsevier Science Publishers B. V, P. O. Box 211, Amsterdam, 1000 AE, Netherlands, 1991.*, pages 449–521, 1991.

[15] Yuli V. Nazarov and Yaroslav M. Blanter. *Quantum Transport: Introduction to Nanoscience*. Cambridge University Press, May 2009.

[16] Reinhard Lipowsky and Michael E. Fisher. Wetting in random systems. *Phys. Rev. Lett.*, 56:472–475, Feb 1986.

[17] Benoit B. Mandelbrot. *The Fractal Geometry of Nature*. Henry Holt and Company, 1983.

[18] Benoit B. Mandelbrot and James R. Wallis. Noah, joseph, and operational hydrology. *Water Resources Research*, 4(5):909–918, 1968.

[19] Benoit B. Mandelbrot, Dann. E. Passoja, and Alvin J. Paullay. Fractal character of fracture surfaces of metals. *Nature*, 308(5961):721–722, April 1984.

[20] Paul Meakin. The growth of rough surfaces and interfaces. *Physics Reports*, 235(4–5):189 – 289, 1993.

[21] S. F. Edwards and D. R. Wilkinson. The surface statistics of a granular aggregate. *Proceedings of the Royal Society of London. A. Mathematical and Physical Sciences*, 381(1780):17–31, August 1982.

[22] Modeling and rendering of metallic patinas. `http://www.cescg.org/CESCG97/spatzek/index4.html`. Accessed: 2010-09-30.

[23] Mehran Kardar, Giorgio Parisi, and Yi-Cheng Zhang. Dynamic scaling of growing interfaces. *Physical Review Letters*, 56(9):889–892, March 1986.

[24] Dieter Forster, David R. Nelson, and Michael J. Stephen. Large-distance and long-time properties of a randomly stirred fluid. *Physical Review A*, 16(2):732–749, August 1977.

[25] Erwin Frey and Uwe Claus Täuber. Two-loop renormalization-group analysis of the burgersˇkardar-parisi-zhang equation. *Phys. Rev. E*, 50:1024–1045, Aug 1994.

[26] David A. Huse, Christopher L. Henley, and Daniel S. Fisher. Huse, henley, and fisher respond. *Physical Review Letters*, 55(26):2924–2924, December 1985.

[27] Jurgen Gartner and Wolfgang Konig. The parabolic anderson model. In Jean-Dominique Deuschel and Andreas Greven, editors, *Interacting Stochastic Systems*, pages 153–179. Springer Berlin Heidelberg, 2005.

[28] J.M. Burgers. *The Non-Linear Diffusion Equation: Asymptotic Solutions and Statistical Problems*. Springer, December 1974.

[29] C. H. Su and C. S. Gardner. Korteweg de vries equation and generalizations iii. derivation of the korteweg de vries equation and burgers equation. *Journal of Mathematical Physics*, 10(3):536–539, 1969.

[30] Kai Nagel. Particle hopping models and traffic flow theory. *Phys. Rev. E*, 53:4655–4672, May 1996.

[31] U. Frisch and J. Bec. Burgulence. In M. Lesieur, A. Yaglom, and F. David, editors, *New trends in turbulence Turbulence: nouveaux aspects*, volume 74 of *Les Houches - Ecole d'Ete de Physique Theorique*, pages 341–383. Springer Berlin Heidelberg, 2001.

[32] David A. Kessler, Herbert Levine, and Yuhai Tu. Interface fluctuations in random media. *Phys. Rev. A*, 43:4551–4554, Apr 1991.

[33] Ernesto Medina, Terence Hwa, Mehran Kardar, and Yi-Cheng Zhang. Burgers equation with correlated noise: Renormalization-group analysis and applications to directed polymers and interface growth. *Physical Review A*, 39(6):3053–3075, March 1989.

[34] Timothy Halpin-Healy and Yi-Cheng Zhang. Kinetic roughening phenomena, stochastic growth, directed polymers and all that. aspects of multidisciplinary statistical mechanics. *Physics Reports*, 254(4–6):215 – 414, 1995.

[35] T. Halpin-Healy. Extremal paths, the stochastic heat equation, and the three-dimensional kardar-parisi-zhang universality class. *Phys. Rev. E*, 88:042118, 2013.

[36] Jeffrey Kelling and Géza Ódor. Extremely large-scale simulation of a kardar-parisi-zhang model using graphics cards. *Phys. Rev. E*, 84:061150, Dec 2011.

[37] Vladimir G. Miranda and Fábio D. A. Aarão Reis. Numerical study of the kardar-parisi-zhang equation. *Phys. Rev. E*, 77:031134, Mar 2008.

[38] Francesca Colaiori and M. A. Moore. Upper critical dimension, dynamic exponent, and scaling functions in the mode-coupling theory for the kardar-parisi-zhang equation. *Phys. Rev. Lett.*, 86:3946–3949, Apr 2001.

[39] Mehran Kardar. Replica bethe ansatz studies of two-dimensional interfaces with quenched random impurities. *Nuclear Physics B*, 290(0):582–602, 1987.

[40] Kurt Johansson. Shape fluctuations and random matrices. *Communications in Mathematical Physics*, 209(2):437–476, 2000.

[41] Pasquale Calabrese and Pierre Le Doussal. Exact solution for the kardar-parisi-zhang equation with flat initial conditions. *Phys. Rev. Lett.*, 106:250603, Jun 2011.

[42] Takashi Imamura and Tomohiro Sasamoto. Replica approach to the kpz equation with the half brownian motion initial condition. *Journal of Physics A: Mathematical and Theoretical*, 44(38):385001, 2011.

[43] P. Calabrese, P. Le Doussal, and A. Rosso. Free-energy distribution of the directed polymer at high temperature. *EPL (Europhysics Letters)*, 90(2):20002, 2010.

[44] Victor Dotsenko and Boris Klumov. Bethe ansatz solution for one-dimensional directed polymers in random media. *Journal of Statistical Mechanics: Theory and Experiment*, 2010(03):P03022, 2010.

[45] Craig A. Tracy and Harold Widom. Level-spacing distributions and the airy kernel. *Physics Letters B*, 305(1–2):115 – 118, 1993.

[46] CraigA. Tracy and Harold Widom. Level-spacing distributions and the airy kernel. *Communications in Mathematical Physics*, 159(1):151–174, 1994.

[47] Romain Allez, Jean-Philippe Bouchaud, and Alice Guionnet. Invariant beta ensembles and the gauss-wigner crossover. *Phys. Rev. Lett.*, 109:094102, Aug 2012.

[48] Jose Ramirez, Brian Rider, and Balint Virag. Beta ensembles, stochastic airy spectrum, and a diffusion. *Journal of the American Mathematical Society*, 24(4):919–944, 2011.

[49] Percy Deift. Universality for mathematical and physical systems. *arXiv:math-ph/0603038*, March 2006. arXiv: math-ph/0603038.

[50] Sylvain Prolhac and Herbert Spohn. The one-dimensional kpz equation and the airy process. *Journal of Statistical Mechanics: Theory and Experiment*, 2011(03):P03020, 2011.

[51] T Imamura, T Sasamoto, and H Spohn. On the equal time two-point distribution of the one-dimensional kpz equation by replica. *Journal of Physics A: Mathematical and Theoretical*, 46(35):355002, 2013.

[52] Victor Dotsenko. Two-point free energy distribution function in (1+1) directed polymers. *arXiv:1304.6571 [cond-mat, physics:math-ph]*, April 2013. arXiv: 1304.6571.

[53] Patrik L Ferrari. Slow decorrelations in kardar parisi zhang growth. *Journal of Statistical Mechanics: Theory and Experiment*, 2008(07):P07022, 2008.

[54] Malte Henkel, Jae Dong Noh, and Michel Pleimling. Phenomenology of aging in the kardar-parisi-zhang equation. *Phys. Rev. E*, 85:030102, Mar 2012.

[55] J. Krug and H. Spohn. *Kinetic roughening of growing surfaces in Solids Far from Equilibrium*. C. Godrèche, Cambridge University Press, 1991.

[56] Thomas Kriecherbauer and Joachim Krug. A pedestrian's view on interacting particle systems, kpz universality and random matrices. *Journal of Physics A: Mathematical and Theoretical*, 43(40):403001, 2010.

[57] I. Corwin. The Kardar-Parisi-Zhang equation and universality class. *Random Matrices: Theory and Applications*, 01(01):1130001, 2012.

[58] Ivan Corwin and Alan Hammond. KPZ line ensemble. *arXiv:1312.2600 [cond-mat, physics:math-ph]*, December 2013. arXiv: 1312.2600.

[59] Dmitry Chelkak and Stanislav Smirnov. Universality in the 2d ising model and conformal invariance of fermionic observables. *Inventiones mathematicae*, 189(3):515–580, 2012.

[60] Martin Hairer. Introduction to regularity structures. *arXiv:1401.3014 [math-ph]*, January 2014. arXiv: 1401.3014.

[61] F.C. Klebaner. *Introduction to Stochastic Calculus with Applications*. Imperial College Press, 2012.

[62] Erwin Bolthausen. A note on the diffusion of directed polymers in a random environment. *Communications in Mathematical Physics*, 123(4):529–534, 1989.

[63] Philippe Carmona and Yueyun Hu. Strong disorder implies strong localization for directed polymers in a random environment. *arXiv:math/0601670*, January 2006. arXiv: math/0601670.

[64] Francis Comets and Nobuo Yoshida. Directed polymers in random environment are diffusive at weak disorder. *The Annals of Probability*, 34(5):pp. 1746–1770, 2006.

[65] Pierre Le Doussal. Crossover from droplet to flat initial conditions in the KPZ equation from the replica bethe ansatz. *arXiv:1401.1081 [cond-mat, physics:math-ph]*, January 2014. arXiv: 1401.1081.

[66] B. Derrida and O. Golinelli. Thermal properties of directed polymers in a random medium. *Phys. Rev. A*, 41:4160–4165, Apr 1990.

[67] J. Cook and B. Derrida. Polymers on disordered hierarchical lattices: A nonlinear combination of random variables. *Journal of Statistical Physics*, 57(1-2):89–139, 1989.

[68] Joachim Krug, Paul Meakin, and Timothy Halpin-Healy. Amplitude universality for driven interfaces and directed polymers in random media. *Phys. Rev. A*, 45:638–653, Jan 1992.

[69] Timothy Halpin-Healy and Yuexia Lin. Universal aspects of curved, flat, and stationary-state kardar-parisi-zhang statistics. *Phys. Rev. E*, 89:010103, Jan 2014.

[70] S. Bustingorry, P. Le Doussal, and A. Rosso. Universal high-temperature regime of pinned elastic objects. *Phys. Rev. B*, 82(14):140201, 2010.

[71] Herbert Spohn. KPZ scaling theory and the semi-discrete directed polymer model. *arXiv:1201.0645 [cond-mat]*, January 2012. arXiv: 1201.0645.

[72] Yi-Kuo Yu, Ning-Ning Pang, and Timothy Halpin-Healy. Concise calculation of the scaling function, exponents, and probability functional of the edwards-wilkinson equation with correlated noise. *Physical Review E*, 50(6):5111–5114, December 1994.

[73] Thomas Nattermann and Lei-Han Tang. Kinetic surface roughening. i. the kardar-parisi-zhang equation in the weak-coupling regime. *Phys. Rev. A*, 45:7156–7161, May 1992.

[74] Yi-Cheng Zhang. Replica scaling analysis of interfaces in random media. *Phys. Rev. B*, 42:4897–4900, Sep 1990.

[75] Yi-Cheng Zhang. Directed polymers with complex amplitudes. *EPL (Europhysics Letters)*, 9(2):113, 1989.

[76] Thimothée Thiery and Pierre Le Doussal. Log-gamma directed polymer with fixed endpoints via the replica bethe ansatz. *arXiv:1406.5963 [cond-mat]*, June 2014. arXiv: 1406.5963.

[77] Pasquale Calabrese, Marton Kormos, and Pierre Le Doussal. From the sine-gordon field theory to the kardar-parisi-zhang growth equation. *arXiv:1405.2582 [cond-mat, physics:hep-th, physics:math-ph]*, May 2014. arXiv: 1405.2582.

[78] Alexei Borodin and Ivan Corwin. Macdonald processes. *Probability Theory and Related Fields*, 158(1-2):225–400, 2014.

[79] Nicolas Allegra, Jean-Yves Fortin, and Malte Henkel. Boundary crossover in semi-infinite non-equilibrium growth processes. *Journal of Statistical Mechanics: Theory and Experiment*, 2014(2):P02018, 2014.

[80] N Oelkers, M T Batchelor, M Bortz, and X-W Guan. Bethe ansatz study of one-dimensional bose and fermi gases with periodic and hard wall boundary conditions. *Journal of Physics A: Mathematical and General*, 39(5):1073, 2006.

[81] Jean-Sébastien Caux and Pasquale Calabrese. Dynamical density-density correlations in the one-dimensional bose gas. *Phys. Rev. A*, 74:031605, Sep 2006.

[82] Elliott H. Lieb and Werner Liniger. Exact analysis of an interacting bose gas. i. the general solution and the ground state. *Phys. Rev.*, 130:1605–1616, May 1963.

[83] Pasquale Calabrese and Jean-Sebastien Caux. Dynamics of the attractive 1d bose gas: analytical treatment from integrability. *Journal of Statistical Mechanics: Theory and Experiment*, 2007(08):P08032, 2007.

[84] Ernesto Medina and Mehran Kardar. Nonuniversality and analytical continuation in moments of directed polymers on hierarchical lattices. *Journal of Statistical Physics*, 71(5-6):967–980, 1993.

[85] Alexander Dobrinevski. Field theory of disordered systems – avalanches of an elastic interface in a random medium. *arXiv:1312.7156 [cond-mat]*, December 2013. arXiv: 1312.7156.

[86] Éric Brunet and Bernard Derrida. Probability distribution of the free energy of a directed polymer in a random medium. *Phys. Rev. E*, 61:6789–6801, Jun 2000.

[87] V.E. Korepin. Calculation of norms of bethe wave functions. *Communications in Mathematical Physics*, 86(3):391–418, 1982.

[88] Craig A. Tracy and Harold Widom. On orthogonal and symplectic matrix ensembles. *Communications in Mathematical Physics*, 177(3):727–754, 1996.

[89] Anna Galluccio and Martin Loebl. On the theory of pfaffian orientations. i. perfect matchings and permanents. *Electron. J. combin*, 6(1):R6, 1999.

[90] Pierre Le Doussal and Thomas Gueudre. The directed polymer with a hard wall via replica bethe ansatz. *To be published*, 2014.

[91] Patrik L Ferrari and Herbert Spohn. A determinantal formula for the goe tracy–widom distribution. *Journal of Physics A: Mathematical and General*, 38(33):L557, 2005.

[92] T. Sasamoto and T. Imamura. Fluctuations of the one-dimensional polynuclear growth model in half-space. *Journal of Statistical Physics*, 115(3-4):749–803, 2004.

[93] G. J. Heckman and E. M. Opdam. Yang's system of particles and hecke algebras. *Annals of Mathematics*, 145(1):pp. 139–173, 1997.

[94] Yi-Cheng Zhang. Growth anomaly and its implications. *Physica A: Statistical Mechanics and its Applications*, 170(1):1–13, December 1990.

[95] J. Krug and H. Spohn. Anomalous fluctuations in the driven and damped sine-gordon chain. *EPL (Europhysics Letters)*, 8(3):219, February 1989.

[96] Yi-Cheng Zhang. Non-universal roughening of kinetic self-affine interfaces. *Journal de Physique*, 51(19):2129–2134, 1990.

[97] Sergey V. Buldyrev, Shlomo Havlin, Janos Kertész, H. Eugene Stanley, and Tamas Vicsek. Ballistic deposition with power-law noise: A variant of the zhang model. *Physical Review A*, 43(12):7113–7116, June 1991.

[98] Chung-Kang Peng, Shlomo Havlin, Moshe Schwartz, and H. Eugene Stanley. Directed-polymer and ballistic-deposition growth with correlated noise. *Phys. Rev. A*, 44:R2239–R2242, Aug 1991.

[99] V K Horvath, F Family, and T Vicsek. Dynamic scaling of the interface in two-phase viscous flows in porous media. *Journal of Physics A: Mathematical and General*, 24(1):L25, 1991.

[100] Chi-Hang Lam and Leonard M. Sander. Exact scaling in surface growth with power-law noise. *Phys. Rev. E*, 48:979–987, Aug 1993.

[101] Chi-Hang Lam and Leonard M. Sander. Surface growth with power-law noise. *Phys. Rev. Lett.*, 69:3338–3341, Dec 1992.

[102] Joachim Krug. Kinetic roughening by exceptional fluctuations. *Journal de Physique I*, 1(1):9–12, January 1991.

[103] Giulio Biroli, Jean-Philippe Bouchaud, and Marc Potters. Extreme value problems in random matrix theory and other disordered systems. *Journal of Statistical Mechanics: Theory and Experiment*, 2007(07):P07019, 2007.

[104] S. Kida. Asymptotic properties of Burgers turbulence. *Journal of Fluid Mechanics*, 93:337–377, July 1979.

[105] J.-P. Bouchaud and M. Mézard. Universality classes for extreme-value statistics. *J. Phys. A: Math. Gen.*, 30(23):7997, December 1997.

[106] P. Le Doussal. Exact results and open questions in first principle functional RG. *Annals of Physics*, 325:49–150, 2009.

[107] M. Bauer and D. Bernard. Sailing the deep blue sea of decaying burgers turbulence. *J. Phys. A: Mathematical and General*, 32(28):5179, 1999.

[108] Ya. G. Sinai. The limiting behavior of a one-dimensional random walk in a random medium. *Theory of Probability & Its Applications*, 27(2):256–268, January 1983.

[109] Ya.G. Sinai. Statistics of shocks in solutions of inviscid burgers equation. *Commun. Math. Phys.*, 148(3):601–621, September 1992.

[110] P. Le Doussal and K.J. Wiese. Size distributions of shocks and static avalanches from the functional renormalization group. *Phys. Rev. E*, 79:051106, 2009.

[111] D. J. Daley and P. Hall. Limit laws for the maximum of weighted and shifted i.i.d. random variables. *The Annals of Probability*, 12(2):571–587, 1984.

[112] D. Bernard and K. Gawedzki. Scaling and exotic regimes in burgers turbulence. *Journal of Physics. A*, 31(44):8735–8743, 1998.

[113] I. V. Kolokolov and S. E. Korshunov. Optimal fluctuation approach to a directed polymer in a random medium. *Phys. Rev. B*, 75:140201, Apr 2007.

[114] I. V. Kolokolov and S. E. Korshunov. Explicit solution of the optimal fluctuation problem for an elastic string in a random medium. *Phys. Rev. E*, 80:031107, Sep 2009.

[115] I. V. Kolokolov and S. E. Korshunov. Universal and nonuniversal tails of distribution functions in the directed polymer and kardar-parisi-zhang problems. *Phys. Rev. B*, 78:024206, Jul 2008.

[116] Gregory Schehr. Extremes of n vicious walkers for large n: Application to the directed polymer and kpz interfaces. *Journal of Statistical Physics*, 149(3):385–410, 2012.

[117] Gregorio Moreno Flores, Jeremy Quastel, and Daniel Remenik. Endpoint distribution of directed polymers in 1 + 1 dimensions. *Commun. Math. Phys.*, 317(2):363–380, January 2013.

[118] Ben Hambly and James B. Martin. Heavy tails in last-passage percolation. *Probab. Theory Relat. Fields*, 137(1-2):227–275, January 2007.

[119] Antonio Auffinger and Oren Louidor. Directed polymers in a random environment with heavy tails. *Communications on Pure and Applied Mathematics*, 64(2):183–204, 2011.

[120] Nikolaos Zygouras and Partha Dey. personal communication.

[121] Francis Comets and Vincent Vargas. Majorizing multiplicative cascades for directed polymers in random media. *arXiv:math/0510525*, October 2005. arXiv: math/0510525.

[122] Jacques G. Amar, Pui-Man Lam, and Fereydoon Family. Surface growth with long-range correlated noise. *Phys. Rev. A*, 43:4548–4550, Apr 1991.

[123] Dietrich E. Wolf and Lei-Han Tang. Inhomogeneous growth processes. *Phys. Rev. Lett.*, 65:1591–1594, Sep 1990.

[124] J Krug and P Meakin. Universal finite-size effects in the rate of growth processes. *Journal of Physics A: Mathematical and General*, 23(18):L987, 1990.

[125] L. Bertini, N. Cancrini, and G. Jona-Lasinio. The stochastic burgers equation. *Communications in Mathematical Physics*, 165(2):211–232, 1994.

[126] Lorenzo Bertini and Giambattista Giacomin. Stochastic burgers and kpz equations from particle systems. *Communications in Mathematical Physics*, 183(3):571–607, 02 1997.

[127] Martin Hairer. Solving the KPZ equation. *arXiv:1109.6811 [math-ph]*, September 2011. arXiv: 1109.6811.

[128] M. Hairer. A theory of regularity structures. *Inventiones mathematicae*, pages 1–236, 2014.

[129] M. Hairer. Rough stochastic PDEs. *Communications on Pure and Applied Mathematics*, 64(11):1547–1585, November 2011.

[130] Martin Hairer. Singular stochastic PDEs. *arXiv:1403.6353 [math]*, March 2014. arXiv: 1403.6353.

[131] Jean-Philippe Bouchaud and Marc Mézard. Wealth condensation in a simple model of economy. *Physica A: Statistical Mechanics and its Applications*, 282(3–4):536 – 545, 2000.

[132] Takashi Ichinomiya. Bouchaud-mézard model on a random network. *Phys. Rev. E*, 86:036111, Sep 2012.

[133] Feng-Rung Hu. On the ratio processes induced from the mean-field bouchaud-mezard model. *WSEAS Trans. Math.*, 7(6):406–416, June 2008.

[134] Franti šek Slanina. Inelastically scattering particles and wealth distribution in an open economy. *Phys. Rev. E*, 69:046102, Apr 2004.

[135] Marco Patriarca, Anirban Chakraborti, and Kimmo Kaski. Statistical model with a standard $\gamma$ distribution. *Phys. Rev. E*, 70:016104, Jul 2004.

[136] P. R. Freeman. The secretary problem and its extensions: A review. *International Statistical Review / Revue Internationale de Statistique*, 51(2):pp. 189–206, 1983.

[137] Daniel T. Gillespie. Exact numerical simulation of the ornstein-uhlenbeck process and its integral. *Phys. Rev. E*, 54:2084–2091, Aug 1996.

[138] Ivan Dornic, Hugues Chaté, and Miguel A. Muñoz. Integration of langevin equations with multiplicative noise and the viability of field theories for absorbing phase transitions. *Phys. Rev. Lett.*, 94:100601, Mar 2005.

[139] B. Derrida and H. Spohn. Polymers on disordered trees, spin glasses, and traveling waves. *J Stat Phys*, 51(5-6):817–840, 1988.

[140] Éric Brunet and Bernard Derrida. Exactly soluble noisy traveling-wave equation appearing in the problem of directedpolymers in a random medium. *Phys. Rev. E*, 70:016106, Jul 2004.

[141] E. Brunet, B. Derrida, A. H. Mueller, and S. Munier. Noisy traveling waves: Effect of selection on genealogies. *EPL (Europhysics Letters)*, 76(1):1, 2006.

[142] Daniel S. Fisher and David A. Huse. Directed paths in a random potential. *Phys. Rev. B*, 43:10728–10742, May 1991.

[143] René Carmona and Stanislav A. Molchanov. *Parabolic Anderson Problem and Intermittency*. American Mathematical Soc.

[144] Igor Arsenin, Timothy Halpin-Healy, and Joachim Krug. Competing effects of point versus columnar defects on the roughening of directed polymers in random media. *Phys. Rev. E*, 49:R3561–R3564, May 1994.

[145] Joachim Krug and Timothy Halpin-Healy. Directed polymers in the presence of colununar disorder. *Journal de Physique I*, 3(11):2179–2198, November 1993.

[146] Remco van der Hofstad, Wolfgang König, and Peter Mörters. The universality classes in the parabolic anderson model. *Communications in Mathematical Physics*, 267(2):307–353, 2006.

[147] Daniel S. Fisher. Sliding charge-density waves as a dynamic critical phenomenon. *Phys. Rev. B*, 31:1396–1427, Feb 1985.

[148] T. Giamarchi, A.B. Kolton, and A. Rosso. Dynamics of disordered elastic systems. In M.Carmen Miguel and Miguel Rubi, editors, *Jamming, Yielding, and Irreversible Deformation in Condensed Matter*, volume 688 of *Lecture Notes in Physics*, pages 91–108. Springer-Verlag, 2006.

[149] G. Blatter, M. V. Feigel'man, V. B. Geshkenbein, A. I. Larkin, and V. M. Vinokur. Vortices in high-temperature superconductors. *Rev. Mod. Phys.*, 66:1125–1388, Oct 1994.

[150] C. V. Varanasi, J. Burke, H. Wang, J. H. Lee, and P. N. Barnes. Thick yba2cu3o7 basno3 films with enhanced critical current density at high magnetic fields. *Applied Physics Letters*, 93(9):–, 2008.

[151] A. E. Koshelev and A. B. Kolton. Theory and simulations on strong pinning of vortex lines by nanoparticles. *Phys. Rev. B*, 84:104528, Sep 2011.

[152] Pierre Le Doussal. Exact results and open questions in first principle functional {RG}. *Annals of Physics*, 325(1):49 – 150, 2010. January 2010 Special Issue.

[153] Sandeep Saha, Severine Atis, Dominique Salin, and Laurent Talon. Phase diagram of sustained wave fronts opposing the flow in disordered porous media. *EPL (Europhysics Letters)*, 101(3):38003, 2013.

[154] Severine Atis. *Propagation de fronts d'onde en ecoulement desordonne*. Unpublished, January 2013.

[155] V. Volpert and S. Petrovskii. Reaction–diffusion waves in biology. *Physics of Life Reviews*, 6(4):267 – 310, 2009.

[156] Maria Chiara Angelini, Giorgio Parisi, and Federico Ricci-Tersenghi. Ensemble renormalization group for disordered systems. *Phys. Rev. B*, 87:134201, Apr 2013.

[157] Willem Hundsdorfer and Jan G. Verwer. *Numerical Solution of Time-Dependent Advection-Diffusion-Reaction Equations*. Springer Science & Business Media, January 2003.

[158] I. V. Koptyug, V. Zhivonitko, and R. Sagdeev. Advection of chemical reaction fronts in a porous medium. *The Journal of Physical Chemistry B*, 112(4):1170–1176, January 2008.

[159] J. Xin. Front propagation in heterogeneous media. *SIAM Rev.*, 42(2):161–230, June 2000.

[160] Severine Atis, Sandeep Saha, Harold Auradou, Dominique Salin, and Laurent Talon. Autocatalytic reaction fronts inside a porous medium of glass spheres. *Phys. Rev. Lett.*, 110:148301, Apr 2013.

[161] L. Talon, J. Martin, N. Rakotomalala, D. Salin, and Y.C. Yortsos. Lattice BGK simulations of macrodispersion in heterogeneous porous media. *Water Resour. Res.*, 39:1135–1142, 2003.

[162] I. Ginzburg. Consistent lattice boltzmann schemes for the brinkman model of porous flow and infinite chapman-enskog expansion. *Physical Review E (Statistical, Nonlinear, and Soft Matter Physics)*, 77:066704, 2008.

[163] A. A. Korzhavin and V. A. Bunev. Dynamics of gaseous combustion in closed systems with an inert porous medium. *Combustion and Flame*, (4):507–520, 1997.

[164] K.K. Kuo, R. Vichnevetsky, and M. Summerfield. Theory of flame front propagation in porous propellant charges under confinement. *AIAA Journal*, 11(4):444–451, April 1973.

[165] S.N. Chiu. A central limit theorem for linear kolmogorov's birth-growth models. *Stochastic Processes and their Applications*, 66(1):97 – 106, 1997.

[166] CW Gardiner. *Stochastic methods*. Springer-Verlag, Berlin–Heidelberg–New York–Tokyo, 1985.